The Role of Telomeric Proteins in Regulating the Metazoan DNA Damage Response

Benjamin Peter Wetherall

Thesis Submitted for the Degree of Doctor of Philosophy

Institute for Cell and Molecular Biosciences
Faculty of Medical Sciences
Newcastle University
September 2019

Abstract

Both telomere regulation and the repair of DNA damage are essential processes for maintaining genomic stability in eukaryotes. Distinctions between these processes have become harder to make as we further our understanding of their governing pathways and the overlap of proteins involved.

The CST complex was originally discovered in budding yeast, it is the capping complex that ensures telomeric deoxyribonucleic acid (DNA) is appropriately replicated and protected. In 2009 the CST complex was identified in humans, but the role of the human CST complex has been found to extend beyond the telomere.

Here I report that whilst loss of the CTC1-STN1-TEN1 (CST) complex component CTC1 in human cells does result in telomere mis-regulation, it also induces a rapid compromise to genomic stability unrelated to its telomeric function. My data suggest *CTC1*Δ human cells are failing to correctly repair DNA damage. I also show that *STN1*, another CST complex component, can significantly compromise genomic stability when overexpressed. This instability may be due to the fact that a high level of STN1 appears capable of suppressing homology-directed repair (HDR) whilst promoting non-homologous end joining (NHEJ). Human *STN1* mRNA, like the budding yeast homologue, appears to be degraded by nonsense-mediated decay (NMD), perhaps as a mechanism for NMD and the stress response to regulate repair pathways via STN1.

Finally, I report that the recently proposed critical role for the nuclease/helicase Dna2 at the telomeres of budding yeast appears to be conserved in the nematode *C. elegans*.
The overlap in proteins that regulate the telomere and those that play an active role in the repair of DNA damage continues to grow. The human CST complex was originally characterised as a regulator of the telomere but appears to also play a significant role in the DNA damage response. Telomere regulation and DNA damage repair play key roles in both the ageing processes and cancer development, and the data presented in this thesis link *STN1* regulation and NMD to these processes.

Acknowledgements

I would like to thank my supervisor David Lydall for the opportunity to undertake this project in his lab, and for his guidance and advice along the way. I would also like to thank my co-supervisor Niall Kenneth for his help with tissue culture and his willingness to let me bounce questionable ideas off of him. Thank you to Carolyn Price for providing the inducible *CTC1*-knockout cell line, and Anton Gartner for providing the *C. elegans* strains. Thank you to the members of Alan Morgan's lab for the significant amount of time they spent teaching me how to work with *C. elegans*.

Thank you to members of the Papamichos Chronakis lab as well as Laura Maringele and Cameron Robertson for your feedback and advice in lab meetings, and for tolerating sharing lab space with me. I owe a great deal of thanks to the Perkins lab (members past and present) for the use of antibodies, inhibitors and other reagents, as well as being a great source of advice and friendship.

Thank you to everyone at The Town Mouse where a significant portion of this thesis was written, for being a surprisingly productive writing retreat and putting up with me sitting in the corner and abusing your free WiFi.

Finally, I would like to thank my friends and family who have supported me these past four years, in particular Catherine Park. I would not have made it this far without you all.

Contents

List of Figures

List of Tables

Species-specific nomenclature			
Species	Wild-type gene	Protein	Mutant allele
Human	Fully capitalised and italicised Eg. *CTC1*	Fully capitalised and non-italic Eg. CTC1	Specific changes to nucleotides or amino acids are described as appropriate
S. Cerevisiae	Fully capitalised and italicised Eg. *CDC13*	First letter capitalised and non-italic Eg. Cdc13	Recessive mutant alleles are lower case, italicised, and followed by a dash and number Eg. *cdc13-1*
C. elegans	Lower case italicised letters followed by a dash and number Eg. *fncm-1*	Fully capitalised and non italic Eg. FNCM-1	Alleles are given unique alphanumeric identifier following gene in brackets Eg. *fncm-1(tm3148)*

Table 1. Species-specific nomenclature

Index of Abbreviations

ALT	alternative lengthening of telomeres
ANOVA	analysis of variance
APC	anaphase promoting complex
ATP	adenosine triphosphate
BCA	bicinchoninic acid
BER	base excision repair
BIR	break-induced repair
BLAST	basic local alignment search tool
BSA	bovine serum albumin
CDK	cyclin-dependent kinase
cDNA	complementary DNA
CIP	calf intestinal alkaline phosphatase
CMG	Cdc45 Mcm2-7 GINS
CMV	cytomegalovirus
CST	CTC1-STN1-TEN1
Ct	cycle threshold
CTD	C-terminal domain
DAPI	4',6-diamidino-2-phenylindole
DDK	Dbf4/Drf1-dependent kinase
DDR	DNA damage response
DMSO	dimethyl sulfoxide
DNA	deoxyribonucleic acid
dNTP	deoxynucleoside triphosphates
DPBS	Dulbecco's phosphate buffered saline
DRGFP	direct repeat green fluorescent protein
DSB	double strand break
dsDNA	double-stranded DNA
ECL	enhanced chemiluminescence
EJC	exon junction complex
FBS	foetal bovine serum
FISH	fluorescent in situ hybridisation
GINS	*go-ichi-ni-san*

HDR	homology-directed repair
HRP	horseradish peroxidase
IF	immunofluorescence
LB	lysogeny broth
LB+AMP	LB with ampicillin
LED	light-emitting diode
LINE	long interspersed nuclear element
loxP	locus of x-over P1
MCM	minichromosome maintenance protein complex
MMEJ	microhomology-mediated end joining
MMR	mismatch repair
mRNA	messenger RNA
NCBI	national centre for biotechnology information
NER	nucleotide excision repair
NGM	nematode growth medium
NHEJ	non-homologous end joining
NMD	nonsense-mediated decay
NP-40	nonyl phenoxypolyethoxylethanol
OB	oligonucleotide/oligosaccharide binding
OD	optical density
ORC	origin recognition complex
ORF	open reading frame
PBS	phosphate buffered saline
PBST	phosphate buffered saline with tween-20
PCR	polymerase chain reaction
PIC	pre-initiation complex
PIKK	phosphatidylinositol 3-kinase-related kinase
PNA	peptide nucleic acid
PTC	premature termination codon
PVDF	polyvinylidene difluoride
qPCR	quantitative PCR

RCF	relative centrifugal force
RFC	replication factor C
RNA	ribonucleic acid
ROS	reactive oxygen species
RPM	rotations per minute
rRNA	ribosomal RNA
RT-PCR	reverse transcriptase PCR
SAC	spindle-assembly checkpoint
SDS	sodium dodecyl sulphate
SDS-PAGE	sodium dodecyl sulfate - polyacrylamide gel electrophoresis
SINE	short interspersed nuclear element
siRNA	small interfering RNA
snRNP	small nuclear ribonucleoprotein
SOC	super-optimal broth with catabolite repression
SSA	single-strand annealing
SSB	single-strand break
ssDNA	single-stranded DNA
TAE	tris-acetate-EDTA
TBE	tris-borate-EDTA
TBST	tris-buffered saline with tween 20
TE	tris-ethylenediaminetetraacetic acid
TERRA	telomeric-repeat-containing RNA
TIF	tagged image format
tRNA	transfer RNA
UFB	ultra-fine bridge
uORF	upstream open reading frame
UPF	up-frame suppressor
UTR	untranslated region
UV	ultraviolet

Index of Human Proteins

53BP1	tumour protein 53 binding protein 1
9-1-1	Rad9-Rad1-Hus1
APLF	aprataxin and PNK-like factor
Apollo	5′ exonuclease Apollo (DNA cross-link repair 1B)
ATF4	activating transcription factor 4
ATM	ataxia telangiectasia-mutated
ATR	ATM and rad3-related
ATRX	alpha thalassemia/mental retardation syndrome X-linked
BLM	Bloom syndrome
BRCA1	breast cancer 1
BRCA2	breast cancer 2
CDC25	cell division cycle 25
CDC25A	cell division cycle 25A
CDC25C	cell division cycle 25C
CFTR	cystic fibrosis transmembrane conductance regulator
c-MYC	cellular avian myelocytomatosis viral oncogene homologue
CDK1	cycin-dependent kinase 1
CDK2	cycin-dependent kinase 2
CDK4	cycin-dependent kinase 4
CDK6	cycin-dependent kinase 6
CHK1	checkpoint kinase 1
CHK2	checkpoint kinase 2
CTC1	conserved telomere maintenance component 1
CtIP	CTBP-interacting Protein
DNA-PKcs	DNA-dependent protein kinase core subunit
DNA2	DNA replication ATP-dependant helicase/nuclease 2
eIF2-alpha	eukaryotic initiation factor 2 alpha
eIF4A-III	eukaryotic initiation factor 4A III

ER	estrogen receptor
eRF3	ETS-related gene
EXO1	exonuclease 1
FANCM	Fanconi anemia complementation group M
FEN1	flap endonuclease 1
GEN1	group G endonuclease 1
GFP	green fluorescent protein
H2AX	H2A histone family member, X
Ku70	Lupus Ku autoantigen protein p70
Ku80	Lupus Ku autoantigen protein p80
MAGOH	Mago Nashi Homolog
MAPK14	mitogen-activated protein kinase 14
MCM10	minichromosome maintenance protein 10
MRN	Mre11, RAD50 and Nbs1
mTOR	mammalian target of rapamycin
ORCL	Lowe oculocerebrorenal syndrome protein
p21	cyclin-dependant kinase inhibitor 1
p38	mitogen-activated protein kinase
p53	tumour protein p53
PABPC1	poly(A) binding protein cytoplasmic 1
PARP	poly (ADP-ribose) polymerase
PCNA	proliferating cell nuclear antigen
PIF1	petite integration frequency 1
PNKP	polynucleotide kinase 3′-phosphatase
POLD3	DNA polymerase delta subunit 3
POLD4	DNA polymerase delta subunit 4
POT1	protector of telomere 1
RAD1	radiation sensitive 1
RAD51	radiation sensitive 51
RAD52	radiation sensitive 52
RBM8A	RNA-binding protein 8A
RBP1	retinol-binding protein 1

RIF1	Rap-1 interacting factor 1 homologue
RnaseH1	ribonuclease H1
RNPS1	RNA-binding protein with serine-rich domain 1
RPA	replication protein A
RPL13A	ribosomal protein L13a
RTEL1	regulator of telomere elongation helicase 1
SLX1	structure-specific endonuclease subunit 1
SLX4	structure-specific endonuclease subunit 4
SMG1	suppressor with morphological effect on genitalia 1
SMG5	suppressor with morphological effect on genitalia 5
SMG6	suppressor with morphological effect on genitalia 6
SMG7	suppressor with morphological effect on genitalia 7
STN1	suppressor of cdc thirteen
TBP	TATA-binding protein
TEN1	telomeric pathways with STN1 protein
TERC	telomerase RNA component
TERT	telomerase reverse transcriptase
TFIIB	transcription factor II B
TFIID	transcription factor II D
TFIIE	transcription factor II E
TFIIF	transcription factor II F
TPP1	TINT1 PTOP PIP1 1
TRF1	telomere repeat binding factor 1
TRF2	telomere repeat binding factor 2
TRRAP	transformation/transcription domain associated protein
UPF1	up-frameshift suppressor 1
UPF2	up-frameshift suppressor 2
UPF3b	up-frameshift suppressor 3b
WEE1	Wee1-like protein kinase
WRN	Werner syndrome ATP-dependent helicase

XLF	XRCC4-like factor
XRCC4	X-Ray repair cross-complementing protein 4

Index of *S. cerevisiae* Proteins

Cdc13	cell division control protein 13
Chk1	checkpoint kinase 1
Dna2	DNA replication ATP-dependant helicase/nuclease 2
Esp1	extra spindle pole bodies 1
Mec1	mitosis entry checkpoint 1
Mph1	mutator phenotype 1
Pds1	precocious dissociation of sisters 1
Rad53	radiation sensitive 53
Rad9	radiation sensitive 9
Stn1	suppressor of cdc thirteen 1
Ten1	telomeric pathways with Stn1 protein

Index of *C. elegans* Proteins

DNA-2	DNA replication ATP-dependant helicase/nuclease 2
FNCM-1	Fanconi anemia complementation group M 1
MRT-2	mortal germline 2

1 Introduction

1.1 The Eukaryotic Cell

The Eukaryotic cell consists of a nucleus, surrounded by a membrane, inside a cytoplasm-filled outer membrane. Within the cytoplasm exists organelles that carry out specialised cellular functions, such as the Golgi apparatus and mitochondria. The surrounding of organelles in membranes is what separates eukaryotes from prokaryotes [1]. The genomic content of the nucleus consists of one or more linear chromosomes; DNA wrapped tightly around histones to form a nucleoprotein structure called chromatin [2]. Eukaryotes can be single or multi-cellular, with cells specialising into structures of different cell types called tissues.

The eukaryotes are composed of four kingdoms: animalia, plantae, fungi, and protista. The development of molecular phylogenetic technologies highlighted the complex phylogenetic relationships between eukaryotes, producing wildly different trees depending on the genes analysed, and the specifics of the analytical approaches. The broad consensus now is the eukaryote phylogenetic tree consists of 5 supergroups: opisthokonta (containing animals, fungi, and some protists), amoebozoa, excavata, archaeplastida (plantae), and SAR (stramenopiles, alveolates, and rhizaria) [3]. The main three organisms discussed in this thesis are *Homo sapiens* (humans), *Saccharomyces cerevisiae* (budding yeast) and *Caenorhabditis elegans* (a nematode). The latter two being common model organisms from the fungi and animalia kingdoms respectively.

1.2 The Structure of DNA

DNA is the carrier molecule of genetic information in the cell, consisting of two polynucleotide strands. The polynucelotides are chains of four different monomers known as nucleotides. Each nucleotide consists of a phosphate group; a deoxyribose sugar; and one of 4 nuclear bases, adenine (A), thymine (T), guanine (G) or cytosine (C). The two strands of DNA are held together by hydrogen bonds between adenine and thymine or guanine and cytosine. The two strands are considered antiparallel, running in opposite directions (determined by the orientation of the phosphate-sugar backbone) and complimentary; adenine always opposite thymine and guanine always opposite cytosine [4]. The human genome consists of 3.2 billion base pairs [5], and is estimated to contain around 21 thousand protein coding genes [6]. Protein-coding sequences account for only approximately 1.5% of the genome [7], the rest is regulatory elements, introns, long interspersed nuclear element (LINE)s, short interspersed nuclear element (SINE)s, DNA specifying non-coding ribonucleic acid (RNA), and DNA yet to be functionally determined. The human nuclear genome is split between 46 chromosomes [8].

DNA strands are wrapped around histones to form nucleosomes and the nucleoprotein

complex chromatin. The chromatin can supercoil and compact to varying degrees during the cell cycle [9]. This compaction of DNA allows it to be sorted during mitosis and meiosis. The human genome consists of two copies of each chromosome, one of paternal origin and one of maternal origin. Human somatic cells have 22 autosomal chromosome pairs and one pair of sex chromosomes, X and Y for males and two X chromosomes for females.

1.3 The Cell Cycle and DNA Replication

The basic purpose of every living organism, the driving force of natural selection, is the propagation of genetic information. Evolution describes the process by which an organism adapts and changes so that it is more likely to succeed in producing offspring and passing on its genetic to the next generation. DNA replication is therefore obviously a crucial process. The process is largely semi-conservative, DNA must be copied accurately enough that the offspring is essentially the same organism, but with enough variation that allows the species to evolve and adapt to its environment.

Human cells (along with most members of the animalia kingdom) are diploid, they have two copies of each chromosome (one that was maternally inherited and one that was paternally inherited). When our cells replicate they must produce a copy of every chromosome and then equally divide them between two daughter cells. In somatic cells this process is mitosis, where a 2N cell copies its genome to become 4N, which is then evenly divided into two 2N daughter cells.

1.3.1 The Cell Cycle

Somatic cells divide by a process called mitosis, but germline cells can also use a second process called meiosis . During mitosis one diploid cell replicates its genome then divides once, producing two diploid daughter cells. During meiosis a diploid cell replicates its genome, but then goes through two rounds of cell division (meiosis I and meiosis II) to produce four haploid daughter cells [10]. During meiosis I a high degree of genetic crossover occurs between maternal and paternal chromosomes [11], contributing to genetic diversity of offspring. Meiosis is used by germline cells to produce haploid gametes for use in sexual reproduction. The vast majority of cell divisions in a multicellular organism are not meiotic but mitotic, as mitosis is how somatic cells replicate and contribute to the growth and repair of tissues.

The mitotic cell cycle can be broken down into five stages (Fig. 1). S-phase is the stage of the cell cycle in which DNA is replicated. In humans the 46 chromosomes (23 maternal origin and 23 paternal origin) are each copied to produce 92 chromosomes. At the end of S-phase, once various checkpoints are satisfied that replication has successfully completed, the cell moves into the G_2-phase. In G_2 cells rapidly grow and produce proteins so that

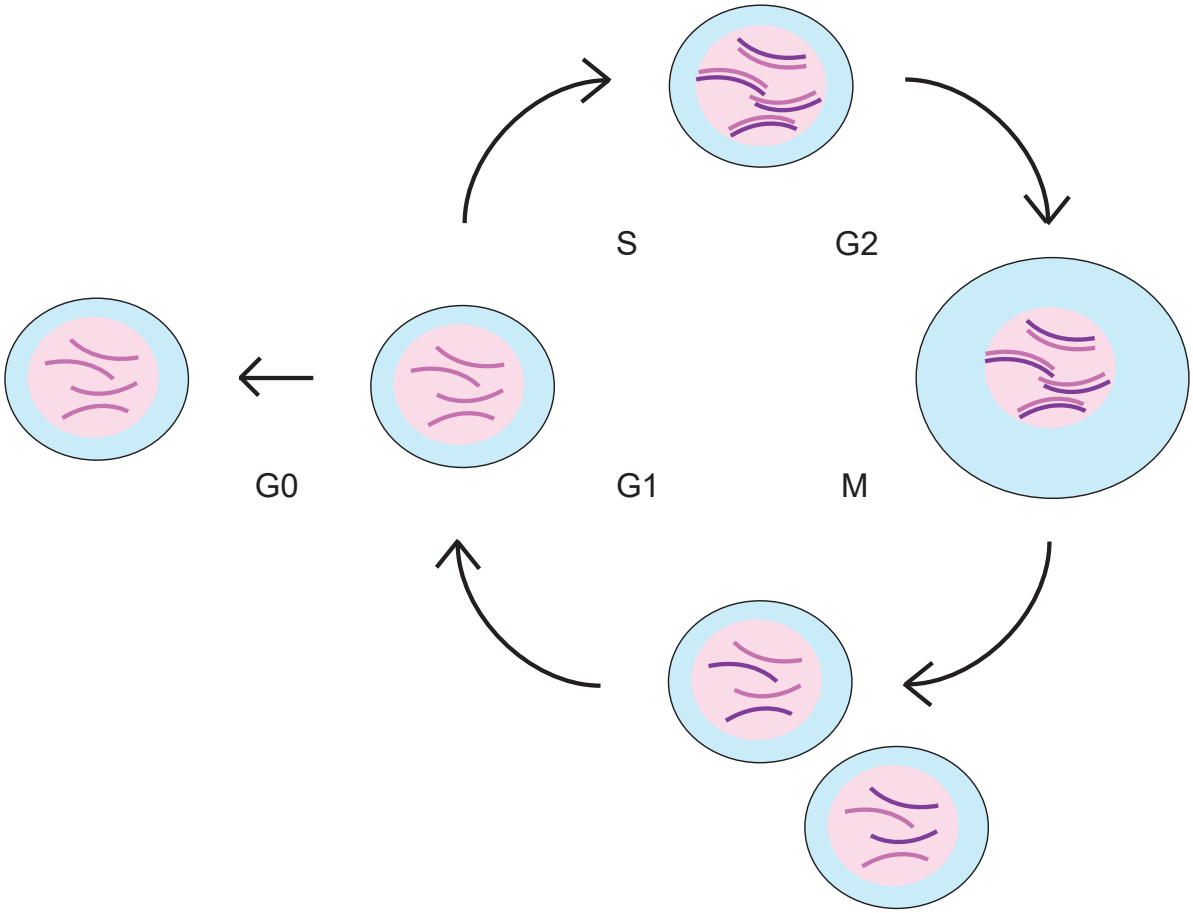

Figure 1. Overview of the mitotic cell cycle. Diploid cells replicate their genome to become tetraploid in S-phase. After S-phase cells grow and produce proteins to be able to divide (G_2 phase). The large tetraploid cell divides in two, giving each daughter cell one copy of the genome during M-phase. The diploid daughters have an intermediate phase (G_1) before re-entering S-phase for another round of replication and division. Alternatively they can exit the cell cycle into G_0.

it is large enough to divide. The G_2/M checkpoint ensures there is no lingering DNA damage before allowing the cell to progress into mitosis (M-phase) [12]. During mitosis the DNA content of the cell becomes highly condensed to allow its easy segregation. The nuclear membrane breaks down and the chromosomes are pulled towards opposite poles. The cell then divides into two daughter cells, each with one complete copy of the genome. Once mitosis has completed the cell is now in G_1, the intermediate phase between cell division and the restart of the replication process [13]. Some cells exit the cell cycle and remain in G_1 indefinitely. These cells are referred to as being in G_0.

The major cell cycle controlling proteins are cyclins and CDKs. Specific cyclin-CDK complexes are formed at different stages of the cell cycle, phosphorylating a range of downstream targets to promote or suppress cell cycle progression (table 6). Whilst CDK levels remain relatively consistent throughout the cell cycle, cyclin levels rise and fall during different phases [14].

CDK	**Cyclins**	**Cycle Phase**
CDK4	D1, D2, D3	G_1
CDK6	D1, D2, D3	G_1
CDK2	E	G_1/S
CDK2	A	S
CDK1	A	G_2/M
CDK1	B	M

Table 6. Complexes of Cyclins and CDKs Present Throughout The Cell Cycle

Inhibition of cell cycle progression is an important function of the DNA damage response (DDR). Up to ten thousand DNA lesions can occur in a single cell in one day, of which DSBs are the most genotoxic [15]. Damage to DNA can interfere with various stages of the cell cycle with catastrophic effects on genome integrity. It is often important that the cell is able to recognise and repair such damage before moving into the next phase of the cell cycle. As such the DDR is a major upstream inhibitor of CDK activity. It has been shown that a single DSB is capable of triggering a robust DDR and arresting the cell cycle [15].

1.3.2 DNA Replication

The process of DNA replication is highly conserved across all domains of life. A replication fork moves along as a bubble in double-stranded DNA (dsDNA), one strand being copied and synthesised in the same direction as the replication fork, and one strand in the opposite direction. The 'leading' strand that is synthesised in the same direction as the travelling replication fork is produced in one continuous strand, whilst the anti-parallel

strand is produced as a series of fragments called Okazaki fragments [16]. Each individual fragment is synthesised in the opposite direction as the replication fork, however each subsequent fragment is started upstream of the previous fragment, and as such the net synthesis of 'lagging' strand DNA is in the direction of the replication fork.

Assembly of the replisome can be split into four stages (Fig. 2) [17]. First the origin recognition complex (ORC) recruits two MCM hexamers to the site of the replication origin, the two MCM hexamers form a symmetrical double-hexamer, enclosing DNA [18]. The second step is the Dbf4/Drf1-dependent kinase (DDK) and CDK driven recruitment and assembly of a number of factors. Here the *go-ichi-ni-san* (GINS) complex, a heterotetrameric ring-like complex tightly interacting with Pol-ϵ, is loaded onto the replisome [19][20]. The third stage of replisome assembly is the separation of the two MCM hexamers to form two diverging replication forks, separating the dsDNA to form a bubble of single-stranded DNA (ssDNA) strands. This step is catalysed by MCM10 and RPA [21][22], and the MCM complex is rearranged to form an active helicase. The final step is the binding of RPA to the ssDNA generated, which forms a binding site for Pol-α to prime DNA synthesis.

The leading strand replicase consists of the Cdc45 Mcm2-7 GINS (CMG) helicase and Pol-ϵ. Evidence suggests the MCM core travels along the leading strand ssDNA, unravelling the dsDNA ahead of it in a 3′-5′ direction [23][24]. The helicase is adenosine triphosphate (ATP) dependent, hydrolysis of which confers conformational changes to the complex [25][26]. Once the DNA is unwound the leading strand is replicated by Pol-ϵ (Fig. 3a). The N-terminal domain of Pol-ϵ is responsible for DNA polymerisation, essentially replacing the now-displaced lagging strand with identical DNA. The N-terminal domain also has exonucleolytic activity, through which it proofreads and removes erroneously placed mismatching bases [27][28].

Whilst both leading strand and lagging strand DNA synthesis are primed by Pol-α, lagging strand synthesis is largely carried out by Pol-δ and not Pol-ϵ. For each fragment DNA synthesis by Pol-α is terminated after 20-30 nucleotides, at which point Pol-δ takes over [29]. The switch from Pol-α to Pol-δ appears to be driven by the loading of PCNA by replication factor C (RFC) [30][31]. The PCNA sliding clamp significantly increases the processivity of Pol-δ [32]. When the 3′ end of the Okazaki fragment extends and reaches the 5′ end of the proceeding fragment, the 3′ end of the synthesised fragment displaces a

---

Figure 2 . Assembly of the replisome. The assembly of the eukaryotic DNA replisome can be broken down into 4 stages. 1) Recruitment of the minichromosome maintenance protein complex (MCM) complex by the ORC. 2) Assembly of the pre-initiation complex. 3) Rearrangement of the MCM to form an active helicase. 4) Priming of DNA replication by Pol-α before extension by Pol-ϵ. Figure adapted from Burgers and Kunkel (2017) [17].

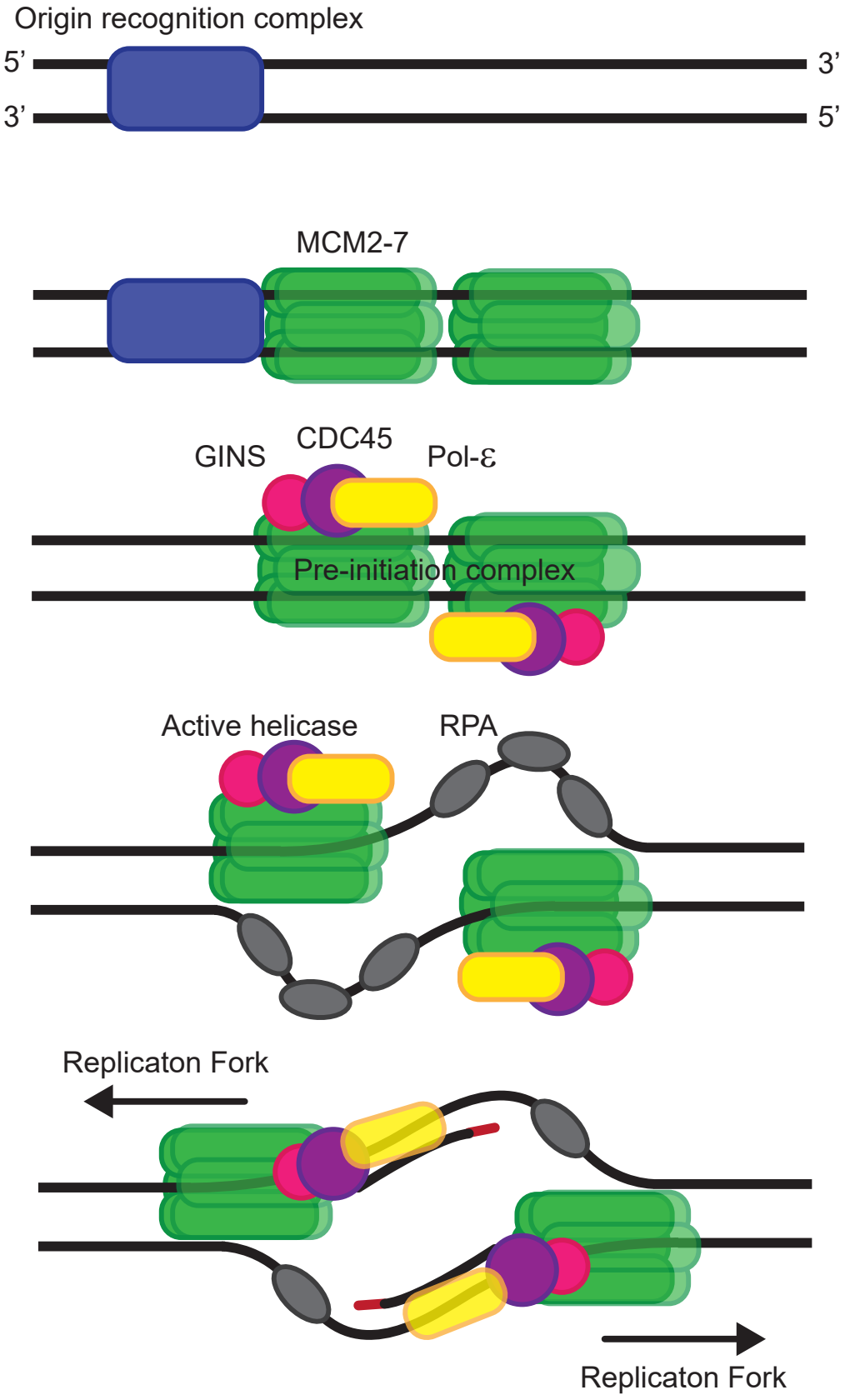
Origin recognition complex
5’
3’
3’
5’
MCM2-7
GINS
CDC45
Pol-ε
Pre-initiation complex
Active helicase
RPA
Replicaton Fork
Replicaton Fork

small flap of the proceeding fragment (Fig. 3b). Pol-δ is capable of $3'$ exonucleolytic activity that resects the new fragment back to the position at which it meets the proceeding fragment [33]. FEN1 is responsible for the excision of any $5'$ flaps that are nonetheless generated [34], although FEN1 is not competent at resecting particularly long flaps that are prone to secondary structures or RPA coating. These long flaps are resected by the nuclease/helicase Dna2 [35]. Finally the remaining nick is ligated by DNA ligase I [36] to complete the synthesis of continuous dsDNA.

Figure 3 . Replication of The Leading and Lagging Strand. (A) The structure of the replisome as it moves with the replication fork. The leading strand is copied continuously by Pol-ϵ whilst the lagging is copied in short sections called Okazaki fragments by Pol-δ. (B) Completion of the lagging strand by the joining of Okazaki fragments. Newly synthesised Okazaki fragments often displace part of the proceeding fragment, generating a flap that must be processed by Dna2 and FEN1. The fragments are then ligated together by DNA ligase I. Figure adapted from Burgers and Kunkel (2017) [17].

A

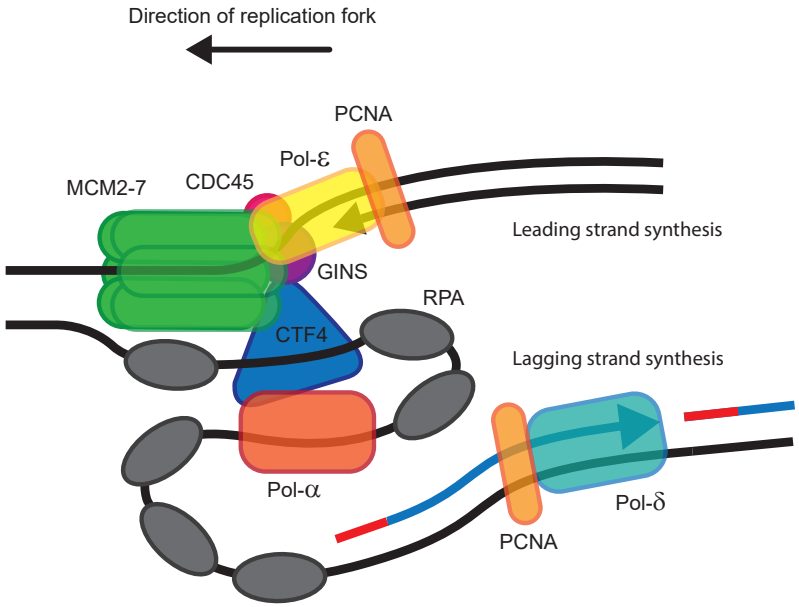
Direction of replication fork
PCNA
Pol-ε
MCM2-7
CDC45
Leading strand synthesis
GINS
RPA
CTF4
Lagging strand synthesis
Pol-α
Pol-δ
PCNA

B

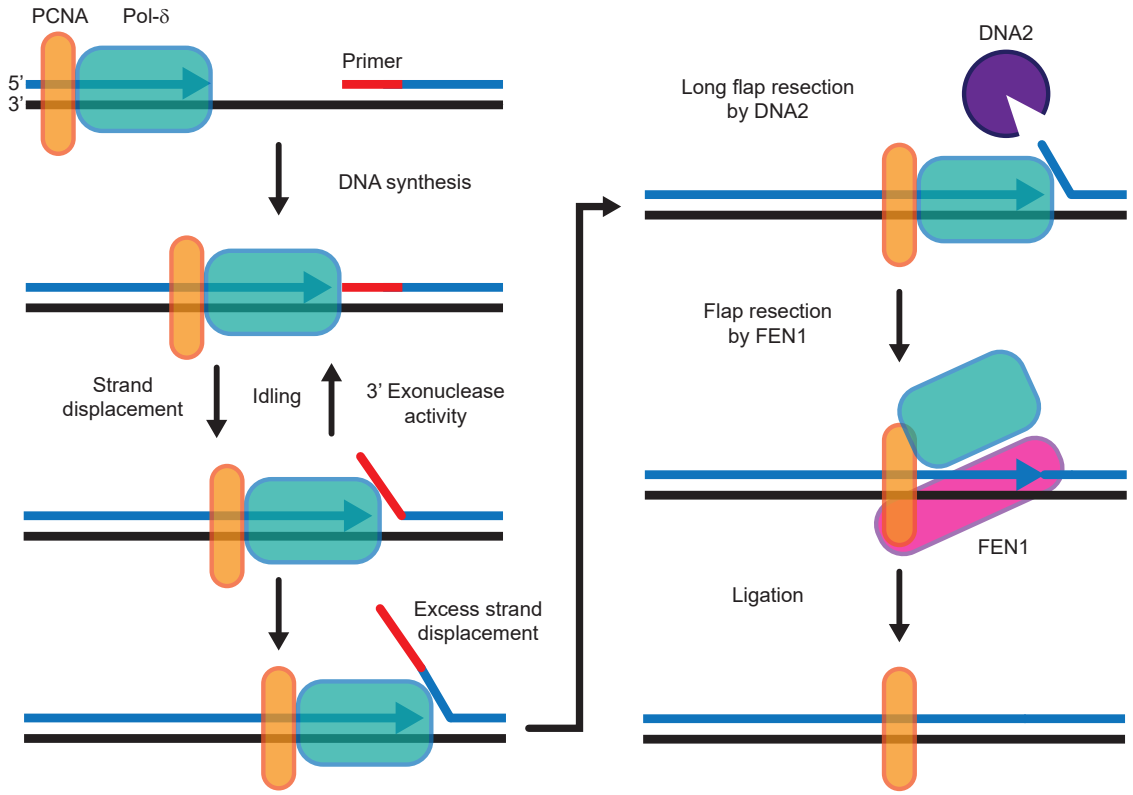
PCNA
Pol-δ
5'
3'
Primer
DNA synthesis
Strand displacement
Idling
3' Exonuclease activity
Excess strand displacement
DNA2
Long flap resection by DNA2
Flap resection by FEN1
FEN1
Ligation

1.3.3 Mitosis

Mitosis is the process by which eukaryotic cells replicate asexually. The eukaryotic cell copies its genome then divides into two daughter cells, each with one full copy of the genome. The process of mitosis can be separated into seven stages (Fig. 4).

The first stage, prophase, sees the chromosomes condense by supercoiling to form individually distinguishable chromosomes, with the help of specialised proteins called condensins [38]. The two condensed copies of each chromosome are held together at the centre by a region called the centromere. As the chromosomes become more and more condensed transcription is shut down as transcription factors are displaced [39]. By the end of prophase the nucleolus has dispersed, and the nuclear envelope will begin to break down [40]. Microtubules and microfilaments in the cytoplasm largely lose their stability and break down [41], but some new microtubules begin to form what will become the mitotic spindle at the two centrosomes.

During the second stage, prometaphase, the mitotic spindle further develops and extends from each centrosome pole into the centre of the cell. The nuclear envelope rapidly breaks down into small vesicles within the cytoplasm. Chromosomes engage with the spindle via large multiprotein structure called the kinetochore [42]. The kinetochore contains fibrous proteins that bind microtubule walls, and motor proteins that generate the forces used to spatially organise chromosomes. Kinetochore-microtubule binding occurs stochastically and often only transiently. This release and re-binding allows incorrectly bound kinetochores (ones which would segregate chromatids incorrectly) to be corrected [43][44]. Kinetochore components have kinase activities that control the spindle-assembly checkpoint (SAC), prolonging the phase until correct assembly is determined to have been reached (thought to be in response to microtubule attachment and tensioning [45]).

Chromosomes that are attached to the mitotic spindle begin to migrate to the centre of the spindle, forming the metaphase plate. This third stage of mitosis, known as metaphase, is the point at which all chromosomes are assembled at the equator of the cell.

If the SAC is satisfied that every chromosome kinetochore is correctly attached to the spindle, then the metaphase state is short-lived and the cell progresses into the fourth stage of mitosis, anaphase. Separase cleaves the Cohesin rings that hold sister chromatids together, and the chromatids are pulled towards the centrosomes at opposite poles [46]. This is achieved by decreasing the distance of each centromere from the centrosome it is attached to (anaphase A), and the increasing in the distance between the two centrosome poles (anaphase B). These two mechanisms are performed by some cells simultaneously, whilst other cells might perform them in series or only perform one. Anaphase A is achieved by the shortening of kinetochore microtubules (through the loss of tubulin subunits) at one or both ends of the microtubule [47][48]. Anaphase B in contrast is characterised by the sliding apart of overlapping microtubules at the spindle. The sliding apart is thought to be driven by a 'pushing' force of kinesin motors, and a 'pulling'

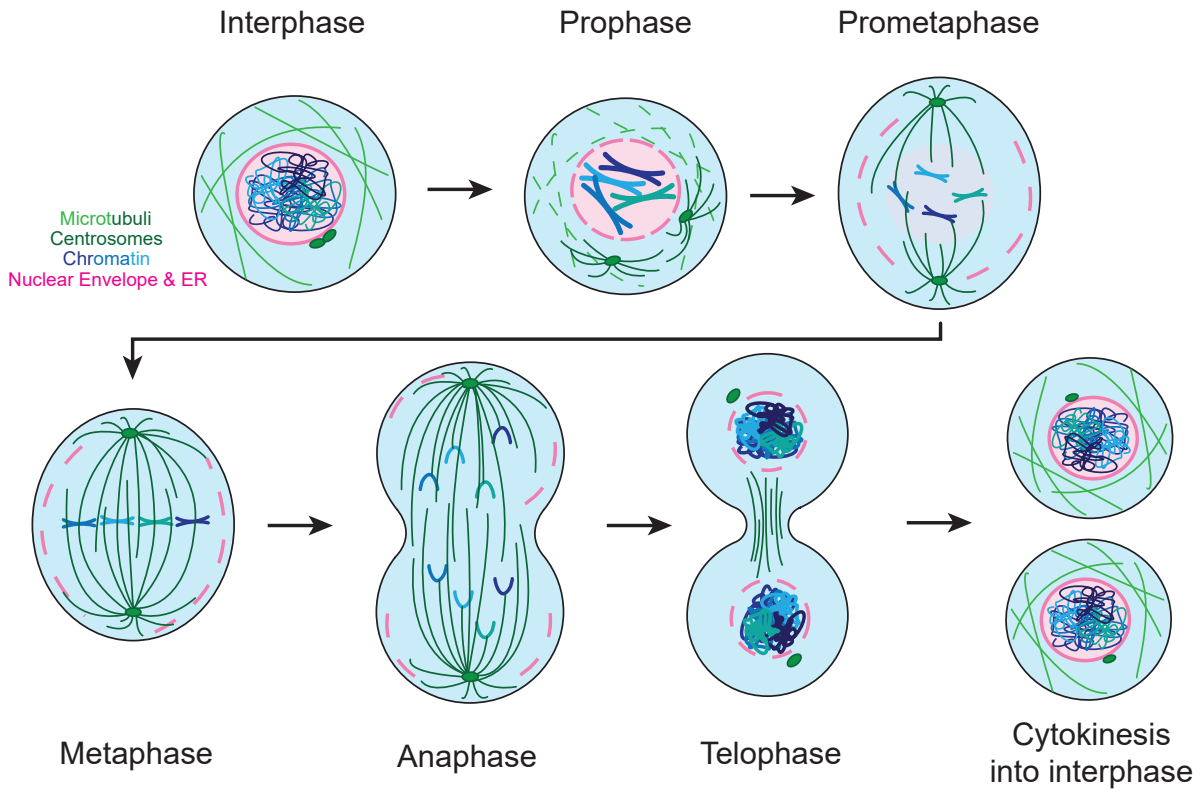

Figure 4. The stages of mitosis. Mitosis is the process by which eukaryotic cells asexually divide, sharing identical copies of their genome between two daughter cells. The process can be broken into 6 stages. In prophase chromosomes start to condense and the nuclear membrane begins to break down. In prometaphase the nuclear membrane breaks down completely and chromosomes begin to assemble on the encroaching mitotic spindle. The cell reaches metaphase when all chromosomes are correctly attached and assembled on the metaphase plate. In anaphase sister chromatids are pulled towards opposite poles. The cell then starts to pinch in at the centre and build a new nuclear envelope around the two groups of chromosomes in telophase. Finally the cell initiates cytokinesis and splits into two daughter cells, now in interphase. Figure adapted from Schellhaus et al. (2016) [37].

force driven by both the breakdown of astral (beyond the centrosome) microtubules, and dynein motors that exert a pulling force on those astral microtubules [49].

The next stage, telophase, involves the reforming of the nuclear envelope around the two groups of chromosomes. Condensin activity peaks a second time to further condense chromosomes, thought to help the separation of chromatids and capture within the new nuclei [50]. Inner nuclear envelope proteins begin to associate with and encapsulate the condensed chromosomes, eventually nuclear pore complexes are reintegrated and the nucleoplasm-cytoplasm boundary is restored. Following that chromosome decondensation begins, transcription restarts, and the nucleolus reforms.

Once the nuclear content of the two daughter cells-to-be has been spatially separated into two nuclei the cell must perform cytokinesis. This requires the assembly and constriction of a contractile ring of filamentous proteins at the equator of the cell [51]. The contractile ring constricts, pinching the centre of the cell, forming the cleavage furrow after anaphase. After telophase contraction of the centre of the cell continues, eventually resulting in scission of the membrane, and completing cytokinesis to produce two daughter cells [51]. The daughter cells are now in interphase, the intermediate stage between rounds of mitosis comprising G_1, S-phase, and G_2.

1.3.4 Cell Cycle Checkpoints

At many points during the cell cycle there are checkpoints that must be satisfied before the cell will progress to the next phase. Some checkpoints are activated in response to DNA damage, others are related to phase-specific activities such as DNA synthesis or cell growth. Mutations in genes that take part in these checkpoints often result in oncogenesis as cell proliferation becomes unchecked [52]. Generally speaking cell cycle checkpoints can be split into four main points, G_1/S, intra-S, G_2/M, and Spindle Assembly (Fig. 5).

The G_1/S checkpoint, referred to as the restriction point in mammalian cells, is the point at which the cell commits to replication. The primary purpose of the G_1/S checkpoint is to ensure the DNA replication process is not started whilst DNA damage persists. Intra-G_1 cyclin-CDK complexes D-4 and D-6 are inhibited by DNA damage sensing pathways via p53 and p21. The p53 pathway and the CHK1/CHK2 pathways inhibit the G_1/S transition cyclin-CDK complexs E-2 and A-2 [53][54]. These inhibitory pathways are activated downstream of the DDR kinases ATM and ATR [55][56]. The cell will be unable to progress into S-phase until the G_1/S checkpoint is satisfied DNA damage is not going to interfere with faithful replication of the genome.

The DNA damage-activated kinases ATM and ATR are key players throughout the majority of the cell cycle, inhibiting the cell from progressing to the next stage whilst DNA damage persists. ATR in particular is also essential for sensing ssDNA and replication stress during S-phase, and activating the intra-S checkpoint [57]. This intra-S checkpoint is dependant on the WEE1 kinase as turnover of p21 is exceptionally high during S-phase

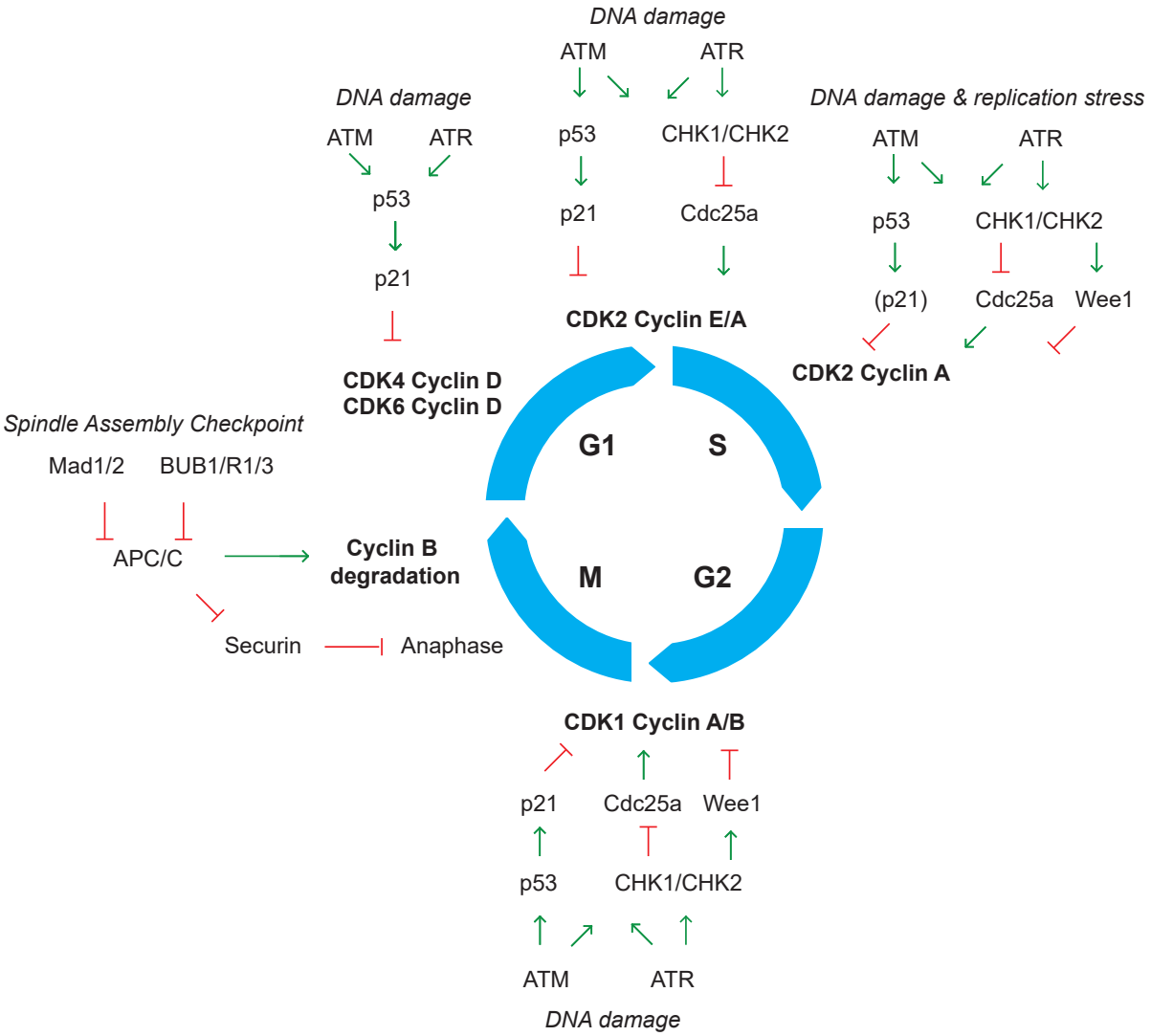

Figure 5. Checkpoint control throughout the cell cycle. Cyclin-CDK complex formation is controlled to form checkpoints throughout the cell cycle. At many points these checkpoints respond to DNA damage (primarily via the kinases ATM and ATR), but also respond to stage-specific factors such as replication stress or mitotic chromosome-spindle assembly.

[58][59]. Once replication has completed the cell will continue to grow through G_2. Here the ATM and ATR kinases are again capable of triggering DNA damage-induced cell cycle arrest. Evidence suggests this checkpoint is also controlled by cell size, ensuring the cell is physically capable of dividing into two daughter cells [59][60].

During mitosis cell cycle progression is controlled by the SAC (Fig. 6), chromosome kinetochores must be connected to the mitotic spindle and correctly orientated so as to allow equal division of genomic content [61][62]. Once the SAC is satisfied then cleavage of the Cohesin subunit Kleisin by Separase allows sister chromatids to separate, and degradation of Cyclin B signals the transition into G_1 [63][64].

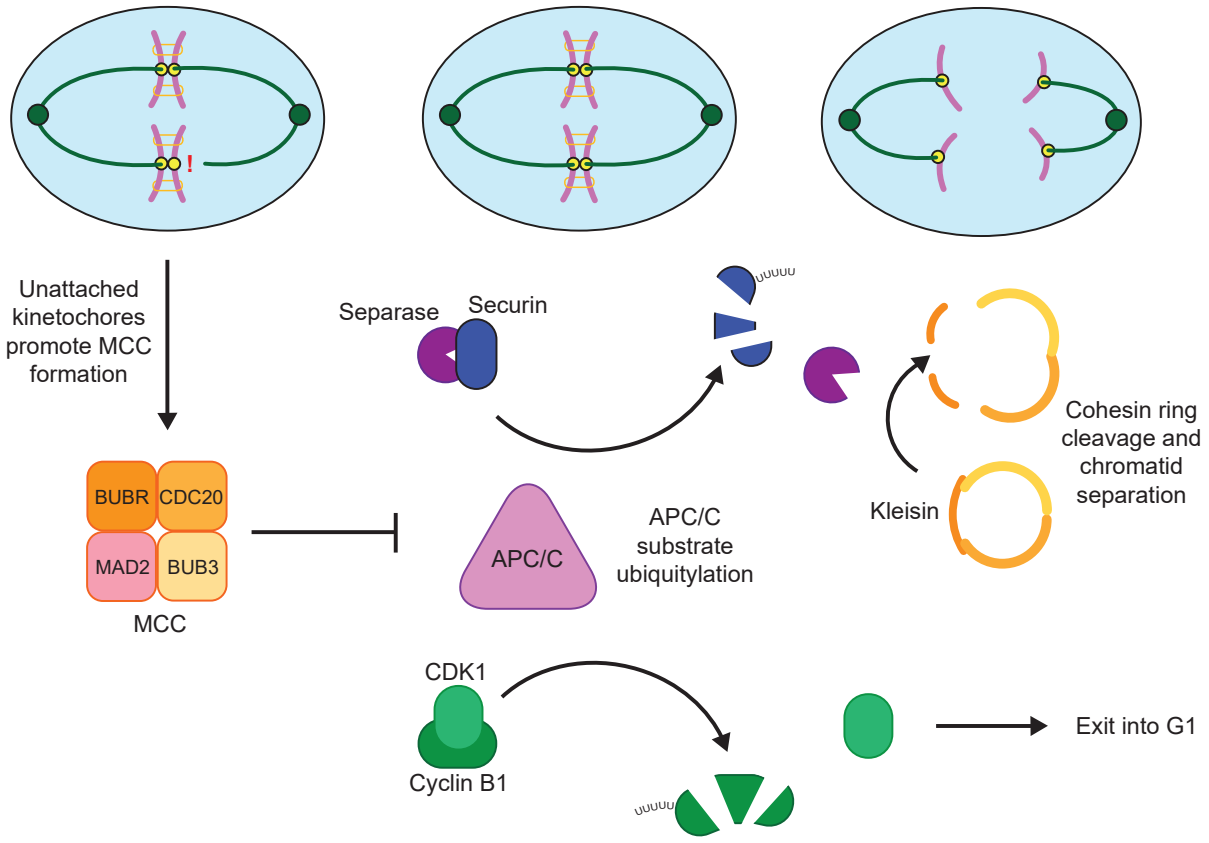

Figure 6. The Spindle Assembly Checkpoint. Incorrectly attached kinetochores result in the formation of the MCC complex, which blocks anaphase promoting complex (APC) activation. APC activation is necessary to A) allow sister chromatids to physically separate by cleavage of Cohesin and B) degrade Cyclin B and trigger entry into G_1. Figure adapted from Lara-Gonzalez et al. 2012 [63].

1.4 The DNA Damage Response

Damage to DNA is a frequently occurring event in the cell. Damage can be induced by a wide range of factors such as ionising and non-ionising radiation, reactive oxygen species (ROS), chemical agents, or viruses. This damage can take the form of breaks in one or both strands of DNA, or chemical modifications to nucleotides. When DNA damage is detected the cell must activate the appropriate pathway for repair. If the amount of damage is above a certain threshold then the cell cycle is arrested and not restarted until the damage has been repaired. Unrepaired DNA damage can result in permanent exit from the cell cycle (senescence) or apoptosis. Damage to DNA repair genes can result in a positive feedback loop of greater and greater genomic instability and rearrangement, this alongside damage to genes that regulate cell growth results in the unchecked proliferation of cells that constitutes cancer.

The cell has specialised pathways for the different forms of DNA damage that can occur. Base excision repair (BER) repairs relatively small DNA adducts that have a minimal effect on the tertiary structure of DNA, such as damage from oxidation, deamination and alkylation, and single-strand breaks. Nucleotide excision repair (NER) is responsible for the repair of larger, bulky adducts such as oxidation-induced endogenous lesions and thymine dimers. Small mutations, insertions and deletions can be repaired by the mismatch repair (MMR) pathway.

DSBs in DNA are repaired by one of four pathways (Fig. 7). The most frequently used pathways are NHEJ and HDR. HDR, the most accurate form of DSB repair, uses a template strand of DNA (such as from a sister chromatid in S-phase and G_2) and strand invasion to accurately replace the damaged DNA. NHEJ on the other hand does not use a template strand for repair, and is capable of ligating blunt/near-blunt ends of DNA together at the cost of accuracy (NHEJ can result in deletions, insertions, or even chromosome fusions). The decision whether to use HDR or NHEJ is determined by cell cycle stage and competing protein factors. The other two mechanisms for DSB repair are microhomology-mediated end joining (MMEJ) and single-strand annealing (SSA), both of which can occur at ssDNA overhangs and are relatively mutagenic.

The key controlling event that commits a cell to HDR instead of NHEJ is the resection of the $3'$ strand [65]. Once resection has been initiated the DNA end is no-longer an effective substrate for the major NHEJ pathway proteins Ku70 and Ku80. The Ku complex and MRN/CtIP compete for binding at DSBs. If MRN and CtIP bind without Ku they are able to perform initial resection which is followed by extensive resection by EXO1 and DNA2. Ku is a barrier to resection by EXO1 and DNA2 [66], but may be removed by MRN-CtIP [67]. BRCA1 plays a major role in promoting HDR through the recruitment of HDR factors to DSBs, competing with 53BP1 which recruits NHEJ factors [68][69]. Loss of either BRCA1 or 53BP1 effectively switches off their respective pathways, but HDR can be restored in BRCA1-mutant cells through loss of 53BP1 [70].

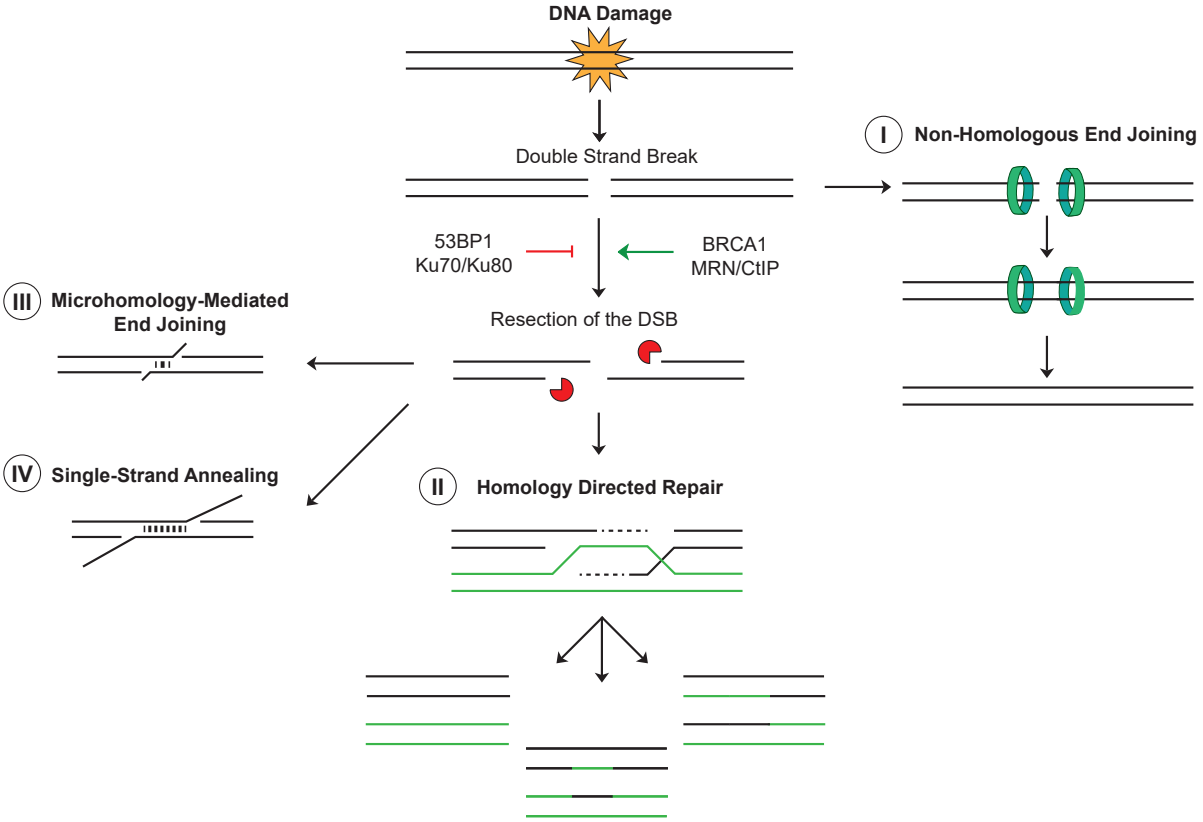

Figure 7. An overview of DSB repair pathways. When a DSB forms the most common route of repair is NHEJ (I). Ku proteins rapidly localise to the break, then recruit other NHEJ factors to process and re-ligate the blunt end. Particularly in S-phase or G_2 the cell may use HDR instead (II). For HDR to occur the DNA ends must be ssDNA overhangs, typically produced by the activity of nucleases. These overhangs are used for strand invasion into template DNA, and the template strand is copied to replace the damaged DNA. How the strands are resolved affects whether permanent crossover of DNA strands occurs. After end resection the two ends may be re-ligated by MMEJ (III) or SSA (IV) instead of HDR. MMEJ uses 1-16 bp of homology to attach the ssDNA strands, whilst SSA uses larger stretches of repetitive DNA. MMEJ and in particular SSA result in significant deletions of DNA.

1.4.1 Non-Homologous End Joining

The first step of NHEJ is the recognition of the DSB by the Ku70/Ku80 heterodimer [71], which has a very high affinity to DNA ends. The heterodimer forms a ring-like structure that slides onto the ends of the dsDNA [72], binding to the sugar backbone. The Ku proteins act as a scaffold, recruiting other NHEJ factors including DNA-PKcs, XRCC4, DNA ligase IV, XLF, and APLF [73–76]. DNA-PKcs is a phosphatidylinositol 3-kinase-related kinase (PIKK) family protein, the kinase activity of which is activated upon its localisation to DNA ends. XRCC4 acts as an additional scaffolding protein, recruiting processing enzymes such as DNA polymerase-μ and the WRN helicase [77][78].

The Ku70/Ku80 heterodimer is responsible for more than just recruitment of other NHEJ factors, it also protects the exposed DNA ends from non-specific processing. It has been demonstrated that the Ku heterodimer can physically hold the two ends of a DSB together [79]. DNA-PKcs and the XRCC4-XLF complex appear to also play a role in physically bridging the two DNA ends [80][81].

The DNA ends must often be processed first before they can be ligated. This can include resection, fill-in of DNA, and the removal of blocking end groups. PNKP is responsible for the addition or removal of phosphate groups at the exposed backbone ends [82], and Aprataxin removes adenylate groups from 5′ phosphate ends [83]. Artemis, WRN, and APLF are responsible for the resection of DNA ends. Artemis has 5′ to 3′ exonucleolytic and endonucleolytic activity that produces blunt duplex DNA [84]; WRN acts as a 3′ to 5′ exonuclease [85]; and APLF acts as an endonuclease and 3′ to 5′ exonuclease [86].

After the DNA ends have been processed, the final step is the ligation of DNA by DNA ligase IV. XRCC4 stimulates DNA ligase IV, which can ligate incompatible DNA ends and across gaps [87][88]. The release of DNA-PKcs is mediated by its autophosphorylation [89], but it is not known if it happens immediately before or after ligation. Once ligation is complete the Ku70/Ku80 heterodimer is polyubiquitylated and degraded by the proteasome [90].

Figure 8 . The Ku70/Ku80 complex rapidly recognises and binds to DSBs, recruiting DNA-PKcs, other scaffolding proteins, processing factors, and DNA ligase IV. The DNA ends are processed by nucleases or modified by kinases and phosphatases to prime them for ligation. DNA ligase IV joins the blunt ends and DNA-PKcs dissociates from the complex, followed by the remaining recruited NHEJ factors.

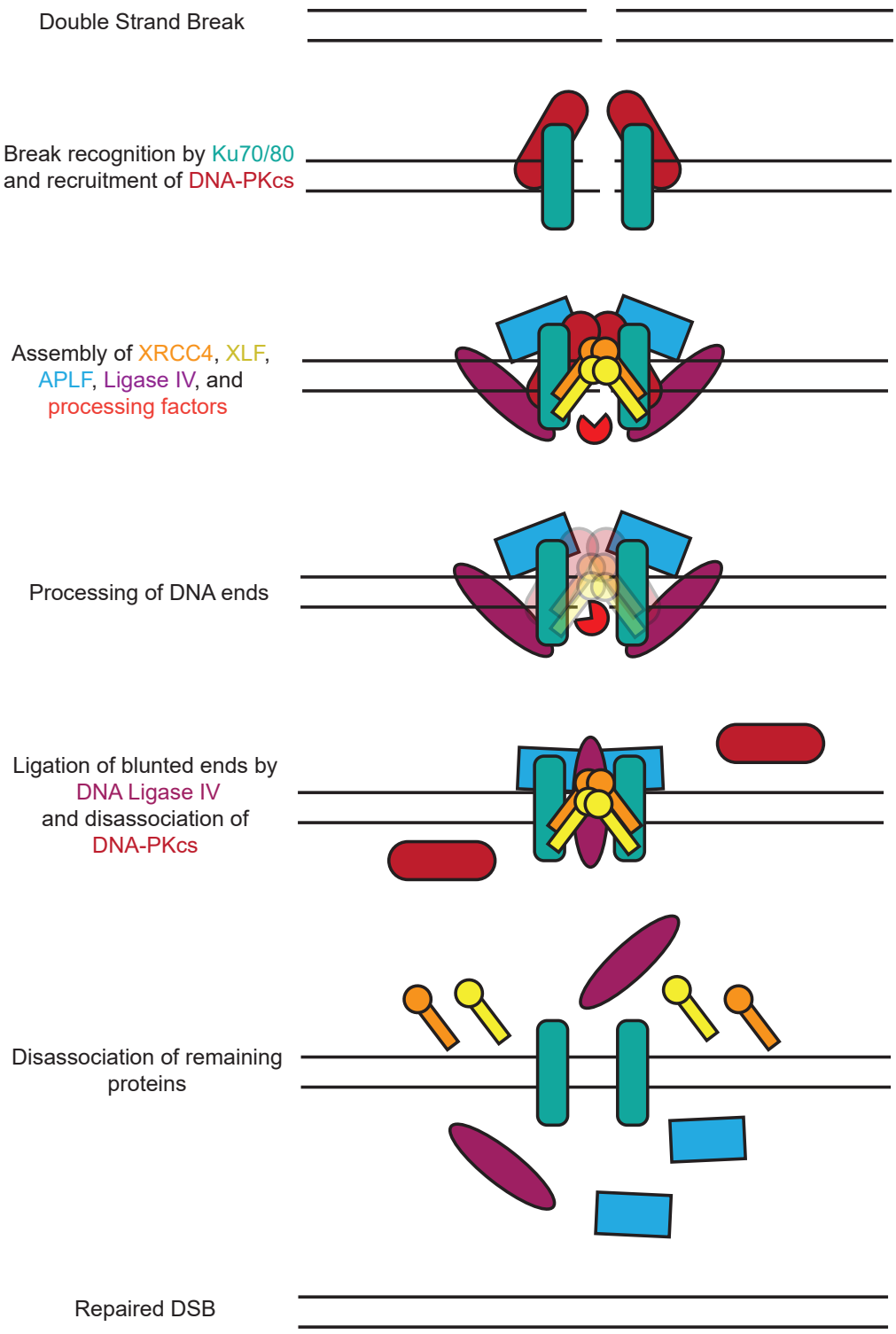
Double Strand Break
Break recognition by Ku70/80
and recruitment of DNA-PKcs
Assembly of XRCC4, XLF,
APLF, Ligase IV, and
processing factors
Processing of DNA ends
Ligation of blunted ends by
DNA Ligase IV
and disassociation of
DNA-PKcs
Disassociation of remaining
proteins
Repaired DSB

1.4.2 Homology Directed Repair

Unlike NHEJ, HDR requires a 3′ ssDNA overhang. This overhang is generated by initial resection of the 5′ strand of DNA by the MRN complex and CtIP [91], promoted by BRCA1 [69]. Then further resection is performed by EXO1 or DNA2 [92] (Fig. 9). The ssDNA overhang produced is coated by RPA, the key ssDNA sensing protein that activates the ATR/ATM PIKK pathways.

RAD51 is a DNA-binding ATPase necessary for the next step of HDR that must replace the RPA bound to the ssDNA overhang. This replacement of RPA with RAD51 is facilitated by BRCA2 in mammals and suppresses SSA [93][94][95]. The recruitment of BRCA2 is promoted by BRCA1, but this role of BRCA1 does not appear to be essential to HDR, unlike its role in initiating resection [96]. The RAD51 coated 3′ ssDNA filament then undergoes strand invasion, invading the dsDNA of the template DNA (such as that of the sister chromatid) forming a D-loop (Fig. 10).

New DNA synthesis occurs, using the undamaged second copy of the locus as a template to replace the DNA that was damaged and resected. This invading DNA strand now has a number of potential fates, resulting in crossovers and non-crossovers [97][98]. In mitotic cells the BLM helicase and others function to resolve the strand invasion intermediates without producing crossovers of DNA that result in large transfers of genetic material from one chromatid to another [99]. A primary pathway of resolution that results in non-crossover events in mitotic cells is dissociation of the newly extended 3′ overhang from the D-loop and re-annealing with its original partner strand (Fig. 10a). If the D-loop captures the second strand and forms a double-Holliday junction this can result in crossover events (this process is biased towards crossover in meiosis) (Fig. 10b). However these double-Holliday junctions can be resolved by BLM-mediated branch migration to be resolved without a crossover (Fig. 10c). If the intermediate escapes BLM the intermediates may also be targeted by other resolvases such as GEN1 which may or may not result in a crossover (Fig. 10d). Once the strand invasion intermediate has been resolved HDR is complete, having accurately repaired the DSB.

Figure 9 . Resection of DSBs for HDR. MRN is responsible for initiating resection of DSBs and activating the ATM PIKK pathway. MRN-CtIP resection is followed by further EXO1 or DNA2 resection, extensive RPA binding and activation of the ATR PIKK pathway. ATM and ATR phosphorylate a wide spectrum of downstream signalling proteins coordinating cell cycle arrest and apoptosis such as CHK1 and CHK2. Figure adapted from Symington and Gautier (2011) [100]

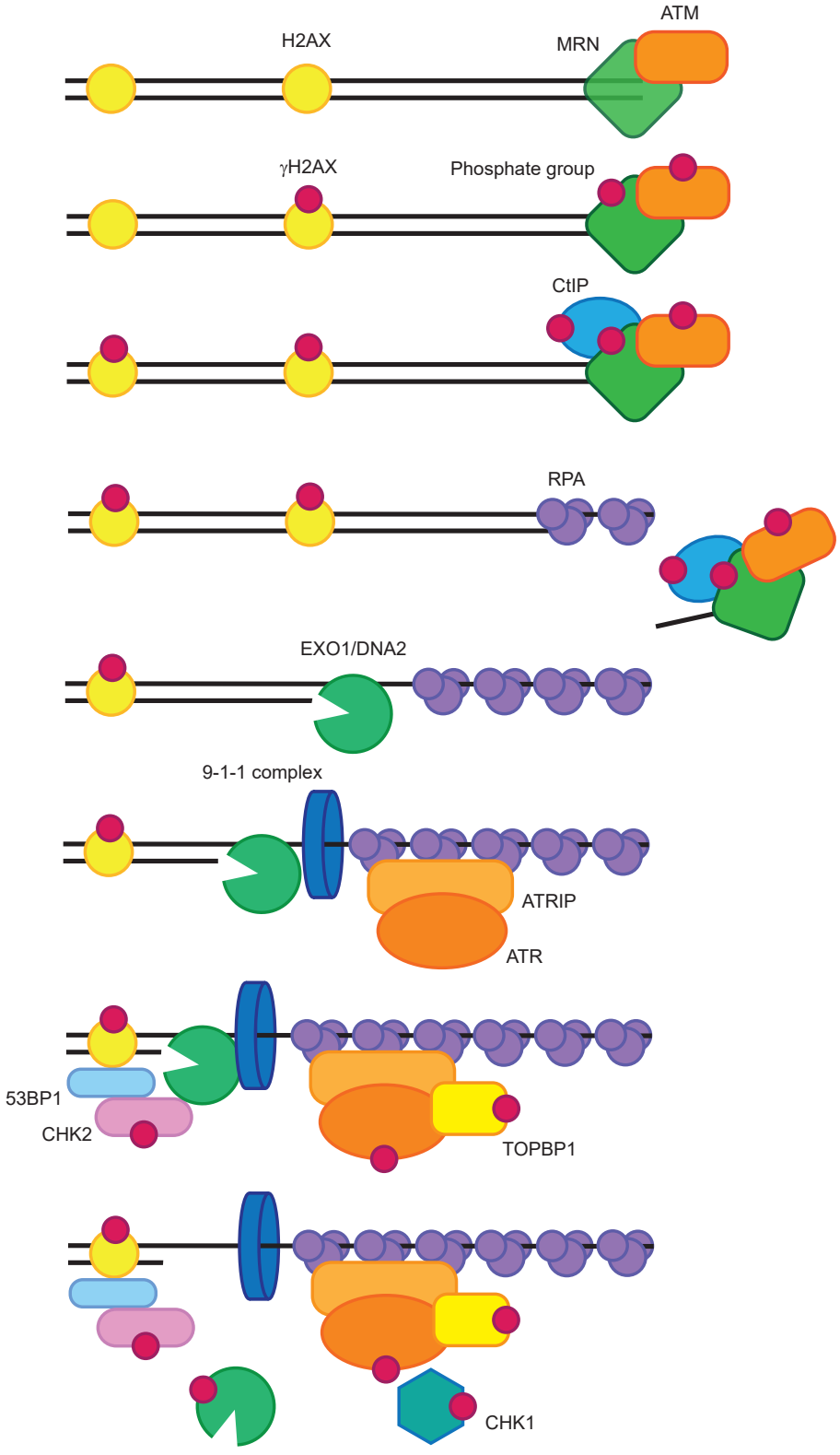

MRN recruits ATM to DSB ends.

ATM phosphorylates MRN and histone H2AX.

CtIP is recruited and activated.

Resection initiation clips MRN/ATM/CtIP from the break and generates the RPA-substrate ssDNA overhang.

Extensive resection by EXO1/DNA2.

ssDNA-bound RPA recruits ATRIP-ATR.

ATR activation by ATRIP requires TOPBP1 and the 9-1-1 complex. ATR and 53BP1-dependent CHK2 autophosphorylation.

CHK2-dependant phosphorylation inhibits EXO1. CHK1 is phosphorylated by ATR.

.

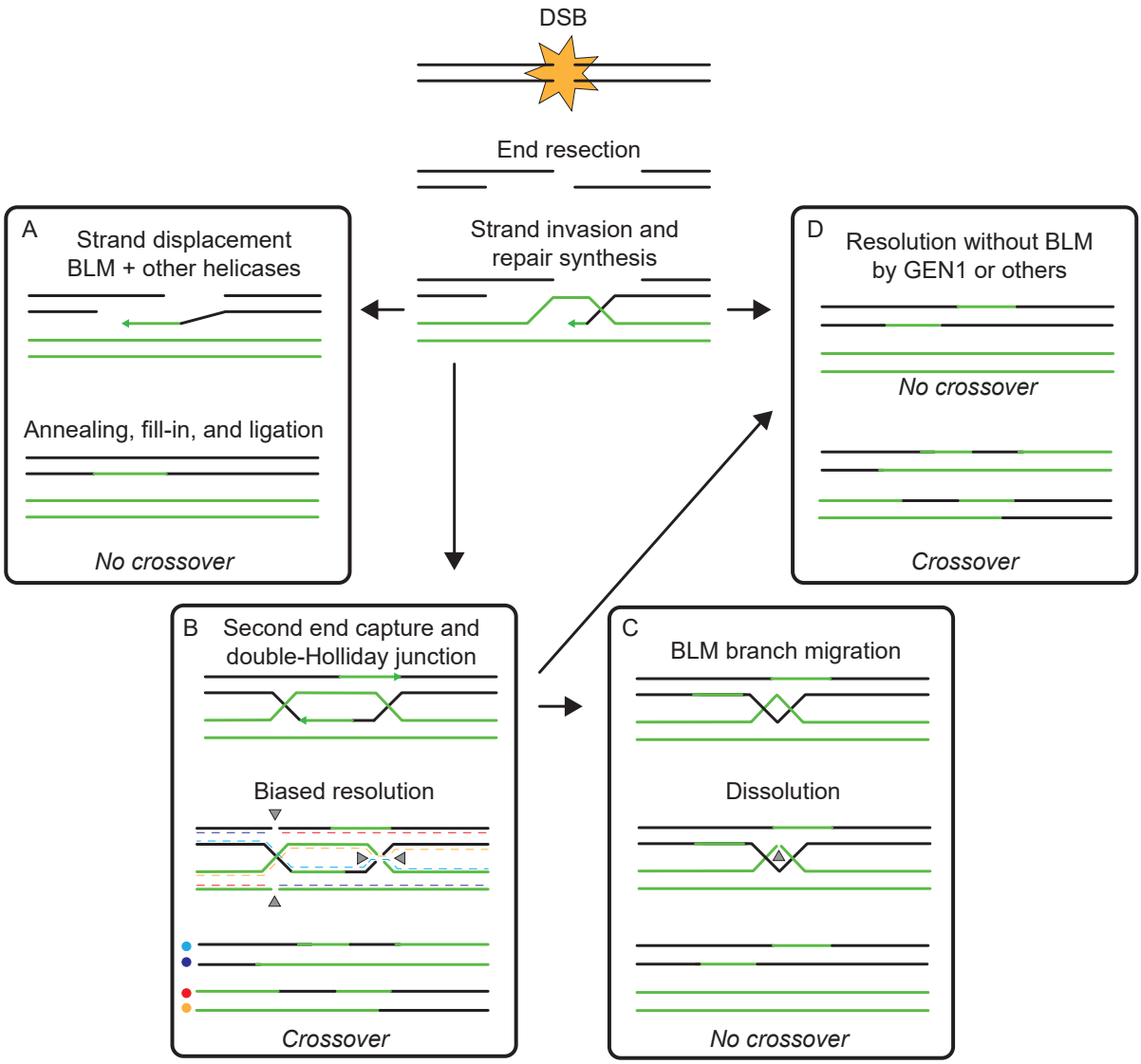

Figure 10. Resolution of HDR intermediates. (A) strand displacement and annealing with the help of BLM is the simplest route of resolution and does not result in a crossover. (B) Capture of the other strand end by the D-loop produces a double-Holliday junction. In meiotic cells this is biased to resolve into a crossover. (C) Branch migration by BLM allows double-Holliday junctions to be resolved by topoisomerase without a crossover event. (D) The strand invasion intermediate escapes BLM and is resolved randomly by other resolvases including GEN1. Figure adapted from Jasin and Rothstein (2013) [99]

.

1.4.3 PIKKs

The human PIKK family of kinases includes six proteins that play a vast range of signalling roles within the cell. ATM and ATR play key signalling roles in the DDR, predominantly activating in response to DSBs and ssDNA respectively. DNA-PKcs is important in the orchestrating of NHEJ and immune system V(D)J recombination. SMG1 is part of the NMD pathway of PTC detection and degradation of mRNA. mTOR controls the translation machinery in response to nutrient and amino acid availability, whilst TRRAP is an essential cofactor for c-MYC and the E2F transcription factor family pathways.

ATM, ATR, and DNA-PKcs play a crucial role in the cellular response to DNA damage, coordinating DDR factors and cell-cycle arrest. Mutations in these pathways are frequently associated with cancer.

ATM exists as a multimer until its autophosphorylation (at serine 1981 in humans) activates it and initiates disassociation of the homodimer [101]. ATM is recruited to DSBs by the MRN complex [102]. ATM is then able to phosphorylate histone H2AX which recruits ubiquitin ligases, facilitating chromatin changes that enable the assembly of large multiprotein complexes [103]. ATM is responsible for the activation through phosphorylation of HDR components such as CtIP which resect the DNA end. Following its activation, ATM plays a major role in cell cycle regulation, particularly through the checkpoint kinase CHK2 and p53 [104][105]. Activation of CHK2 induces phosphorylation and inhibition of CDC25A, which is responsible for activating CDKs. Thus ATM activation induces cell cycle arrest [106]. Failure to rapidly repair DNA results in the phosphorylation and stabilisation of p53 (both directly by ATM and by CHK2) which upregulates transcription of the CDK inhibitor p21. This typically results in persistent cell-cycle arrest and apoptosis.

ATR is involved in DSB repair, but is also crucial in the regulation of DNA replication in S-phase, the primary activator of ATR being ssDNA [107]. The best characterised target of ATR is CHK1, which is phosphorylated at serines 317 and 345 [108][109]. CHK1 regulates replication integrity in S-phase [110], and plays a crucial role in the regulation of cell-cycle progression. CHK1 slows progression through S-phase via CDC25 mediated CDK inhibition, and also prevents cells from entering mitosis with damaged DNA. During HDR a distinct switch from ATM to ATR activation occurs, as the blunt ATM-attracting end is resected and replaced with an ATR-activating RPA-bound ssDNA overhang [111]. CHK1 initiates sequestration of CDC25C into the cytoplasm and the degradation of CDC25A, which maintains inactive CDK1, resulting in G_2/M arrest [112][113].

1.5 The Telomere

The linear nature of eukaryotic chromosomes comes at a cost. The natural breaks in DNA at the end of these chromosomes would be indistinguishable from deleterious DNA damage if it were not for an elaborate nucleoprotein complex that hides them from the

DDR. This terminal DNA is the telomere and consists of many kilobases of TTAGGG repeats in humans. At birth the human telomere averages 11 kilobases [114], but this can be reduced to less than 4 kilobases in the elderly [115].

The telomere consists of double stranded DNA that ends with a G-rich, 3' ssDNA overhang of 35 to 600 nucleotides in length [116]. This ssDNA is looped back and invades the upstream telomeric dsDNA, forming a structure called the T-Loop [117] (Fig. 11). This structure, combined with the specialist telomere capping complexes Shelterin and CST [118][119], serves to effectively hide the end of the telomere from DDR factors.

The telomere also solves an additional problem; the standard DNA replication machinery is incapable of fully replicating the very end of the chromosome. As the replisome moves along the chromosome, the replication fork consists of a leading and lagging strand. The lagging strand is built out of short stretches of DNA called Okazaki fragments [120], but this process is unable to extend to the very end of the chromosome. As such the last few bases of DNA for this strand are not replicated. Telomeres solve this issue in two ways. The first is that they provide a buffer of non-coding DNA that can be eroded without compromising any genetic information, and the second is providing a substrate for telomerase, a protein that is able to extend the telomeric overhang [118].

Shelterin is a six-subunit complex that binds both dsDNA and ssDNA at the telomere [118]. The members of the Shelterin complex are also able to function as smaller subsets that bind either ssDNA or dsDNA, but together bridge the ds-ssDNA junction and suppress activation of the DDR. They are thought to do this by suppressing RPA binding to ssDNA (and therefore activating the ATR DDR pathway) [121], and assisting in the formation of the T-Loop structure [122][123] (which inhibits end recognition by the MRN complex and activation of the ATM DDR pathway [124]). Inappropriate targeting of the telomere by the DDR can result in cell cycle arrest [125], telomere degradation and even fusions [126] which have a catastrophic effect following replication. Shelterin is also responsible for recruiting telomerase to the telomere, thereby promoting extension of the 3' overhang [127].

The second telomeric complex is the CST complex. Comprising the 3 proteins CTC1, STN1 and TEN1 in mammals [119], the CST complex's role is assisting in the replication of both the telomere and telomere-like regions of the genome. STN1 and TEN1 are highly conserved between humans and *S. cerevisiae*, together forming an RPA-like structure with multiple oligonucleotide/oligosaccharide binding (OB) folds [128]. CTC1 on the other hand shares little to no sequence homology with its budding yeast homologue Cdc13, but was identified due to its structural similarity to Cdc13 and its interaction with STN1/TEN1 [119].

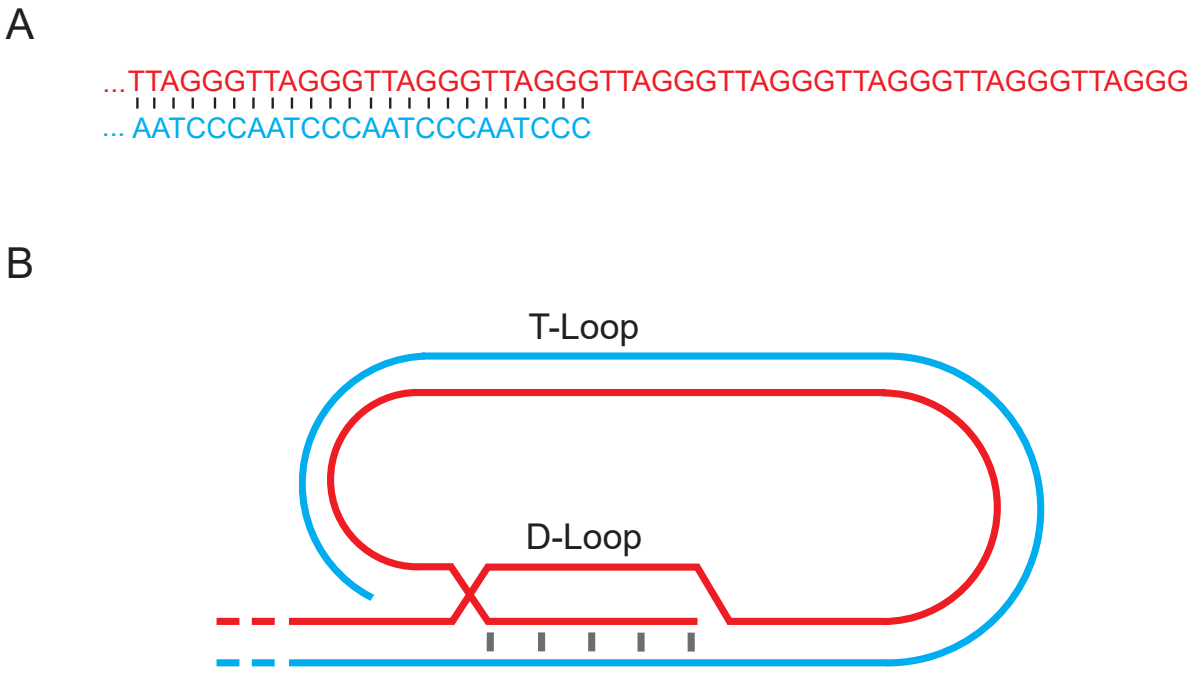

Figure 11. The structure of human telomeric DNA. (A) Human telomeres consist of TTAGGG repeats for multiple kilobases. The majority of the telomere is duplex DNA, but it terminates in an overhang of 3′ G-rich ssDNA. (B) The ssDNA overhang loops back and re-enters the upstream duplex DNA by strand invasion. The bubble of DNA at the site of strand invasion is referred to as the D-Loop, whilst the overall structure is referred to as a T-Loop.

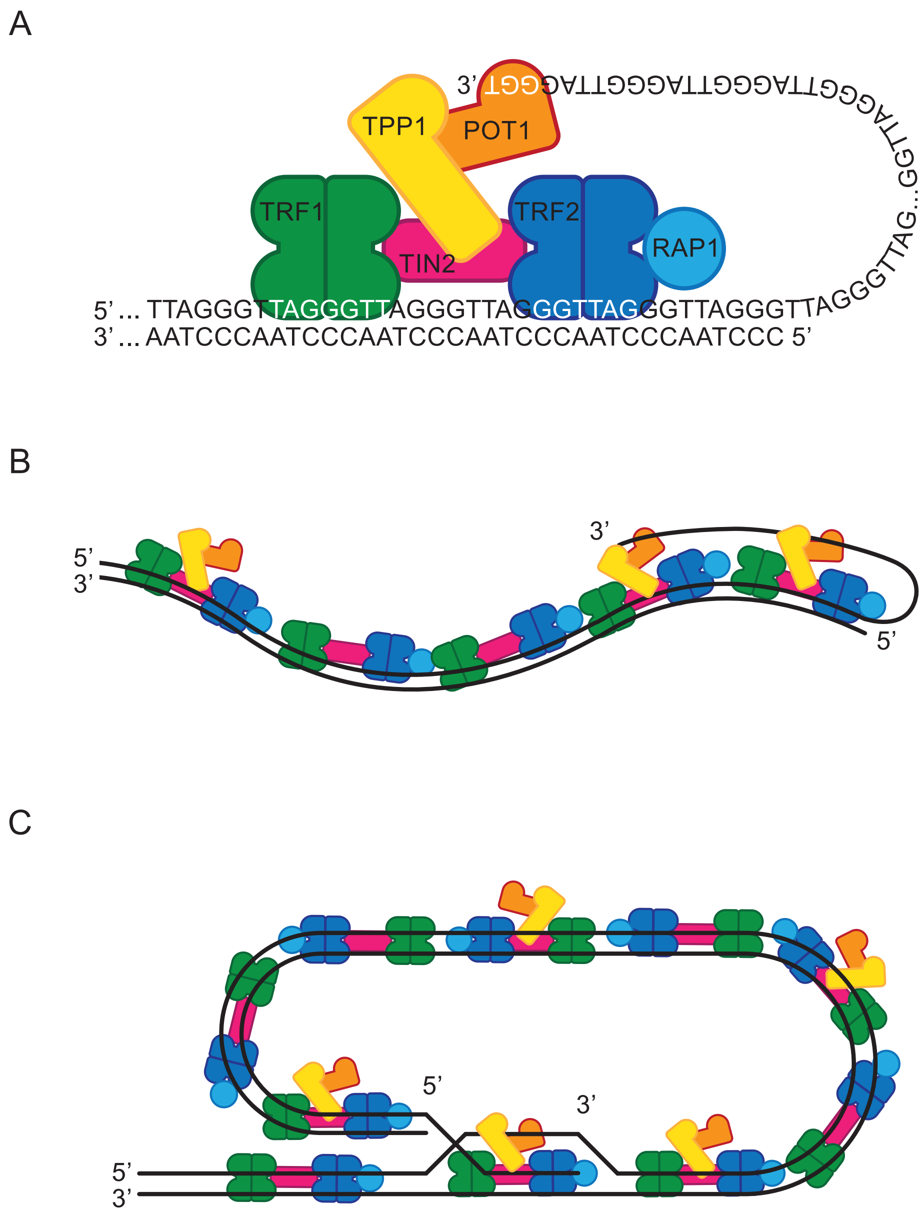

Figure 12. The structure of the Shelterin complex. (A) The subunits of the Shelterin complex; TRF1 and TRF2 interact with dsDNA whilst POT1 interacts with ssDNA. (B) The interaction of Shelterin complexes with a linear telomere. (C) The interaction of Shelterin with the T-loop and D-loop telomere structures. Figure adapted from de Lange (2018) [129].

1.5.1 Semiconservative Telomere Replication

Whilst budding and fission yeast telomere replication is initiated late in S-phase [130], the majority of telomeres in mammalian cells are replicated throughout S-phase [131]. Timing of replication origin firing and replication stress-inducing obstacles both affect telomere length homeostasis [132][133]. Telomere replication typically occurs unidirectionally, moving away from the centromere and towards the end of the chromosome [134]. Telomeric DNA poses a challenge to the replication machinery, behaving like fragile sites that are prone to fork stalling and collapse [135]. Factors that inhibit replication fork progression at the telomere include secondary structures of G-rich DNA called G-quadruplexes; R-loop DNA-RNA hybrids; T-loop structures; and telomere compaction/topological restrictions [136–139].

Stabilised by a monovalent cation, four guanines associating through Hoogsteen bonds can form a planar G-quartet. G-quartets can stack and form a G-quadruplex structure. The replication or transcription of G-rich loci can be inhibited by the ssDNA forming these structures. At the telomere G-quadruplexes present a barrier to both replication forks and telomerase, inhibiting the replication of the telomere [140]. It has been suggested that G-quadruplexes may also act to protect the ssDNA overhang from deleterious processing [141]. Unwinding of these G-quadruplex structures is performed by the RecQ family of helicases, as well as the RecQ-like WRN and BLM helicases [142][143]. Cells lacking WRN lose G-rich telomere strands [144], and BLM knockout induces the fragile telomere phenotype [135]. The RTEL1 helicase resolves G-quadruplexes and interacts with PCNA, and its knockout induces fragile telomeres. It is therefore believed that RTEL1 is recruited to the replisome to aid the replication of the telomere [145].

T-loops are formed when the 3′ ssDNA overhang invades the upstream dsDNA of the telomere, resulting in a closed circle. T-loops are an important part of protecting the end of the chromosome but also present an obstacle for replication forks. Therefore T-loops must be disassembled in order for the telomere to be replicated. The RTEL1 helicase is involved in this process [138], mediated through interaction with TRF2 [146]. In the absence of RTEL1 T-loops are resolved by the SLX1-SLX4 nuclease which results in the excision of the T-loop from the telomere and the production of free circularized telomeric DNA called a T-circle [138]. In vitro evidence suggests D-loop (and therefore T-loop) disassembly might also be performed by other RecQ and RecQ-like helicases [147][148].

In many eukaryotes, including humans, telomeric DNA is transcribed to produce telomeric-repeat-containing RNA (TERRA) [149]. These RNA molecules are capable of annealing to their genomic template and forming DNA-RNA hybrids called R-loops [150]. R-loops themselves are a barrier to replication fork progression, but additionally the displaced ssDNA (if it is the G-rich strand) is capable of forming G-quadruplexes. RnaseH1 is the major enzyme involved in R-loop resolution, degrading the RNA molecule [151]. Other proteins associated with R-loop suppression are the chromatin remodeler ATRX, UPF1,

and the helicase PIF1 [149][152][153].

One way that shelterin acts to protect the telomere is through mediating telomere compaction and topology, forming compact globular chromatin structures that occlude members of the DDR [154][155]. Furthermore, human telomeres are anchored to the nuclear matrix through shelterin and lamins [156]. This compaction and anchoring by shelterin acts as a barrier to replication. Conversely, shelterin component TRF2 (along with the 5′-exonuclease Apollo and Topoisomerase 2α) is necessary for the removal of superhelical/topological constraints and allowing decompaction [139].

1.5.2 Telomerase

The bulk of the telomere is replicated semiconservatively by the canonical replication machinery. As this machinery is incapable of replicating the very end of the lagging strand, telomeres would progressively shorten with each cell cycle. Telomerase is a specialised polymerase that overcomes the end replication problem by adding TTAGGG repeats to the end of the 3′ overhang [157].

Telomerase activity was first discovered in 1985 in *T. thermophila* [158] before being identified in the human HeLa cell-line [157]. Outside of cancers human telomerase activity is widespread only in early development, largely limited to embryonic stem cells [159]. The reactivation of telomerase is a requirement of most human tumourigenesis [160]. Without telomerase activity the cancerous cells' telomeres would progressively shorten with each cell division, eventually inducing an anti-proliferative signal.

Human telomerase is a ribonucleoprotein, comprising a catalytic core of the reverse-transcriptase component TERT and an RNA primer component TERC. Catalytically active telomerase in humans exists as a dimer, with two copies of TERT, TERC, and Dyskerin [161].

1.5.3 Alternative Lengthening of The Telomere

Tumourigenesis requires the bypass of the Hayflick limit, a limit on the number of divisions a cell can go through before becoming senescent due to the progressive shortening of telomeres. In approximately 90% of cancers this bypass is achieved by the reactivation of telomerase [162]. The remaining minority (but still a substantial number) of cancers must use a different method of telomere extension, referred to as alternative lengthening of telomeres (ALT) [163].

ALT appears to be facilitated by homologous recombination between telomeres. The first direct evidence for homologous recombination of telomeres in ALT cells was the copying of a neomycin resistance marker from one telomere into others in an ALT cell line [164]. Such behaviour is not seen in non-ALT cells. ALT cells exhibit an abundance of C-circles (C-rich T-circles), suggesting increased intra-telomeric recombination events [165].

Whilst ALT cells exhibit increased homologous recombination events at the telomere, there appears to be no effect on general homologous recombination throughout the rest of the genome, suggesting the pathway is telomere-specific [166].

Recent evidence suggests there are two break-induced repair (BIR) ALT pathways, one RAD52-dependent, and one RAD52-independent but requiring BLM and BIR proteins POLD3 and POLD4 [167]. BIR repair at telomeres requires a ssDNA end to invade and capture template telomeric DNA, RAD52 appears important for facilitating this annealing of ssDNA in the presence of RPA. This differs from RAD51 which is known to promote D-loop formation but requires the presence of BRCA2 to overcome RPA [168] [169]. How the RAD52-independent pathway operates is less clear, but it is this pathway that is responsible for C-circle formation in ALT cells [167].

1.6 The CST Complex

The telomeres of higher order eukaryotes are protected from the DDR by the six-protein complex Shelterin. The telomeres of the fission yeast *S. pombe* are protected by a Shelterin-like complex, but the telomeres of the budding yeast *S. cerevisiae* are capped by the trimeric RPA-like CST complex (comprising Cdc13, Stn1, and Ten1). Shelterin and CST were believed to be mutually exclusive systems, until the homologues of the budding yeast CST complex were discovered in plants and mammals in 2009; *Arabidopsis* first then mammals including mice and humans [128][119]. Whilst the budding yeast CST complex plays a dual role in telomere protection and replication [170], it appears the Shelterin complex in humans is largely responsible for the exclusion of DDR factors, whilst the CST complex is concerned with telomere replication and regulation.

Mammalian and plant STN1 and TEN1 share sequence homology with their budding yeast orthologues. A potential *Arabidopsis* STN1 orthologue was identified bioinformatically, then confirmed by *in vitro* studies of STN1 knockouts. ArTEN1 was soon afterwards identified based on sequence homology. CTC1 shares no sequence homology with Cdc13, but was identified in *Arabidopsis* in 2009 in a genetic screen for telomere defects. Structural predictions suggested CTC1 formed multiple OB folds homologous to RPA70. The sequence of ArCTC1 was then used in database searches to find the vertebrate homologue [119]. Since its discovery the human CST complex has been shown to regulate the ssDNA overhang of the telomere [171][172]; support the replication of the telomere and telomere-like DNA throughout the genome [173][174]; and promote ssDNA overhang fill-in at DSBs [175]. Mutations in CST complex components are associated with Coats Plus syndrome [176][177].

1.6.1 The Roles of The Human CST Complex in DNA Replication

Throughout our lifespan the telomeres in our somatic cells shorten. This is due to the end replication problem, the lagging strand during DNA replication cannot be replicated

to the very end by the replisome. The lagging strand is replicated in short fragments that are primed by polymerase-α primase, but the last stretch of DNA cannot be replicated as there is no more upstream DNA for the primer to bind to. Telomeres are allowed to erode with each cell division, and when they become critically short the cell becomes senescent and ceases dividing, contributing to the ageing process. By enforcing a replicative limit on cells the organism as a whole is protected from cancerous over-proliferation. As previously discussed, this telomere erosion is avoided in stem cells and the germline by the action of telomerase, a DNA polymerase that extends the 3′ G-rich ssDNA overhang [178][179]. In human somatic cells TERT is expressed at very low levels, if at all [180].

The activity of telomerase is not completely unchecked in cells with telomerase expression, the extension of the overhang must be appropriate to allow continuous proliferation, but not generate excessive ssDNA that might erroneously attract DDR factors such as RPA. Processive extension of the 3′ overhang of the telomere by telomerase is enabled by the Shelterin components POT1 and TPP1. POT1-TPP1 slows telomerase primer dissociation and promotes translocation on the polymerase [127][181]. The CST complex restricts telomerase-mediated telomere extension to a single extension event [171]. CST appears to bind to newly extended ssDNA and block the interaction of POT1-TPP1 with telomerase (Fig. 13a).

The CST complex also limits the length of the 3′ ssDNA overhang by promoting the extension of the C-rich strand [182]. This contributes to the overall extension of the telomere, whilst minimising the amount of ssDNA exposed to DDR factors. Before CTC1 was identified as the third member of the human CST complex it was identified as a protein that interacted and precipitated with polymerase-α-primase [183][119]. It is therefore hypothesised that the CST complex promotes the 5′ to 3′ polymerase activity of Polymerase-α through direct interaction with the primase (Fig. 13a).

The CST complex promotes progression of replication forks through the telomere, but also plays a role in replication outside the telomere [173]. CST has been shown to rescue GC-rich stalled forks in situations of replication stress, and is suggested to facilitate the firing of new origins of replication [184]. CST recruits RAD51 to GC-rich stalled forks in an ATR dependant manner [185], which protects ssDNA at stalled forks from nuclease activity [186]. It is unclear if the restart of stalled forks is in part due to the interaction between CST and Pol-α-primase; Pol-α is an important part of the replisome but proteomics studies indicate Pol-α is not enriched at stalled forks [187]. As the CST complex binds G-rich ssDNA that is prone to forming secondary structures such as G-quadruplexes, it has been suggested that the CST complex might resolve (or inhibit) secondary structures that can block replication [185].

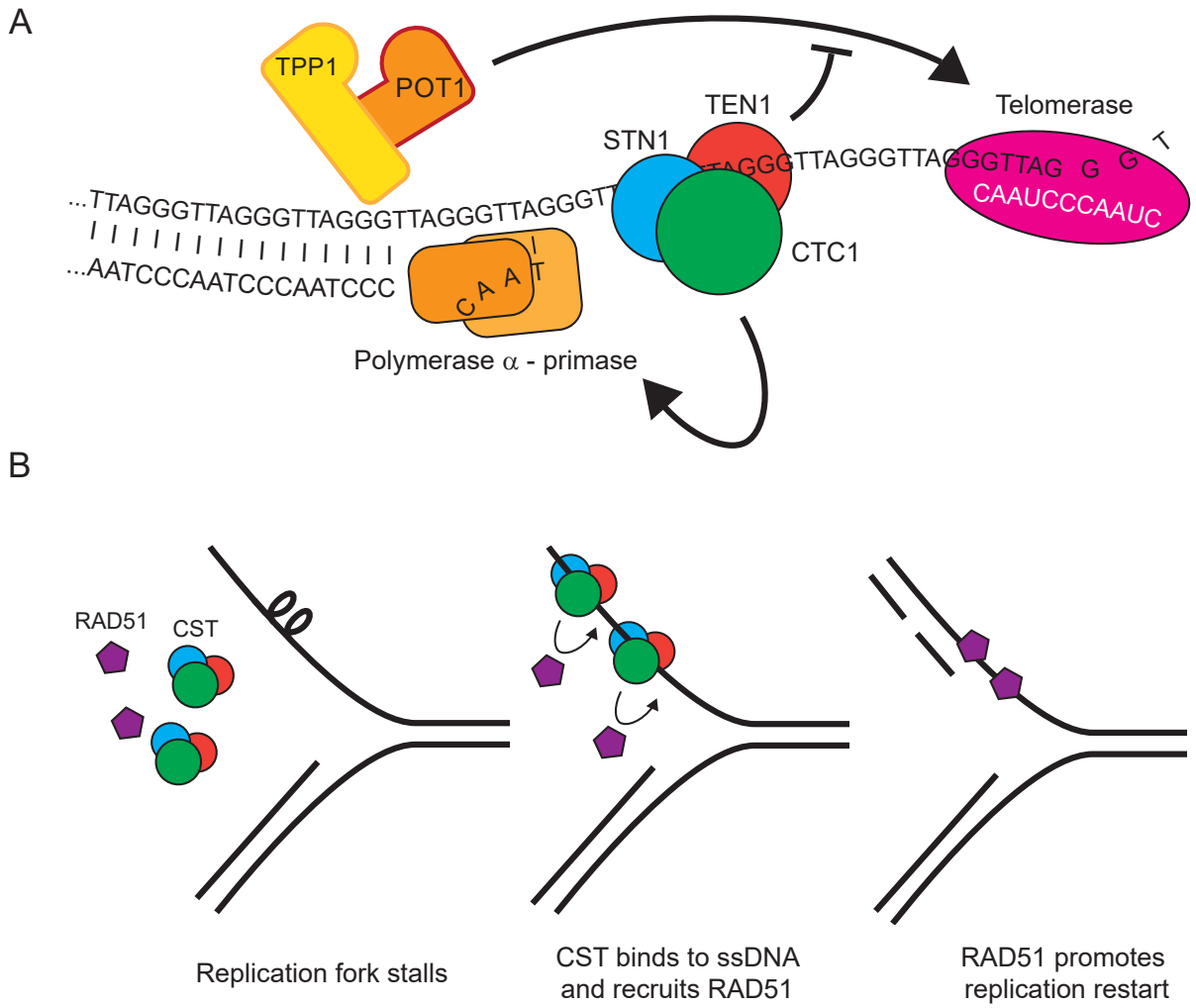

Figure 13. The CST complex regulates telomere ssDNA overhang length and promotes replication restart at stalled telomeric forks. (A) CTC1 interacts directly with Polymerase-α primase to promote its activity at the telomere. Polymerase-α fills-in the C-strand, extending the duplex DNA and shortening the ssDNA overhang. The CST complex also inhibits the action of telomerase on the G-rich strand beyond a single cycle of extension, preventing the build up of a long ssDNA overhang. (B) The CST complex binds to telomeric and telomere-like (GC-rich) ssDNA at stalled replication forks, possibly resolving secondary structures. By binding to the stalled fork the CST complex recruits RAD51, necessary for the restart of replication.

1.6.2 The Influence of The CST Complex on Double Strand Break Repair

Loss of BRCA1 function is common in many cancers, as it effectively eliminates the accurate HDR DSB repair pathway, forcing the cell to use the error-prone NHEJ pathway. Loss of BRCA1 results in unimpeded 53BP1 binding to DSBs, resulting in the recruitment of NHEJ factors and the exclusion of nucleases necessary to initiate resection and HDR [68–70]. BRCA1 deficient cancers are frequently treated with PARP inhibitors. PARP is necessary for the repair of single-strand breaks (SSBs) by BER, therefore PARP inhibition induces many DSBs within the cell as ssDNA breaks are not repaired and become DSBs at replication forks. BRCA1-proficient non-cancer cells are able to use the accurate HDR to repair these breaks, but BRCA1 deficient cells are not able to do so. PARP inhibitor-treated BRCA1-deficient cancer cells therefore experience targeted lethality as (unlike non-cancerous cells in the body) they are either unable to repair the damage at all, or rely on extensive error-prone NHEJ and the mutagenesis of the NHEJ pathway eventually triggers apoptosis.

Some BRCA1-deficient cells gain resistance to PARP inhibitors through the reactivation of the HDR pathway. This can be achieved by loss of NHEJ promoting factors such as 53BP1 [188]. ssDNA overhangs are once again able to be produced and maintained, providing a substrate necessary for HDR. Recently, loss of CST complex members *CTC1* or *STN1* were identified in a CRISPR/Cas9 knockout screen as conveying PARP inhibitor resistance in BRCA1-deficient cancers [175]. This resistance involved the rescue of the resection defect of the BRCA1-deficient cells, therefore allowing them to perform HDR. It has since been shown that CST-Pol-α recruitment to resected DSBs is performed by the 53BP1-RIF1-Shieldin complex [189]. CST promotes the activity of Pol-α, filling-in resected DNA and eliminating the ssDNA overhang.

PARP inhibitor sensitivity of BRCA1-deficient cells therefore relies on the CST complex to fill-in resected DSBs and block HDR (Fig. 14II). When the CST complex is lost in BRCA1 deficient cells this fill in does not occur and the overhang persists, enabling HDR. The role of the CST complex in DSB fill-in has been hypothesised to exist in order to limit excessive hyper-resection, which can promote the mutagenic SSA pathway of DSB repair (Fig. 14I) [175].

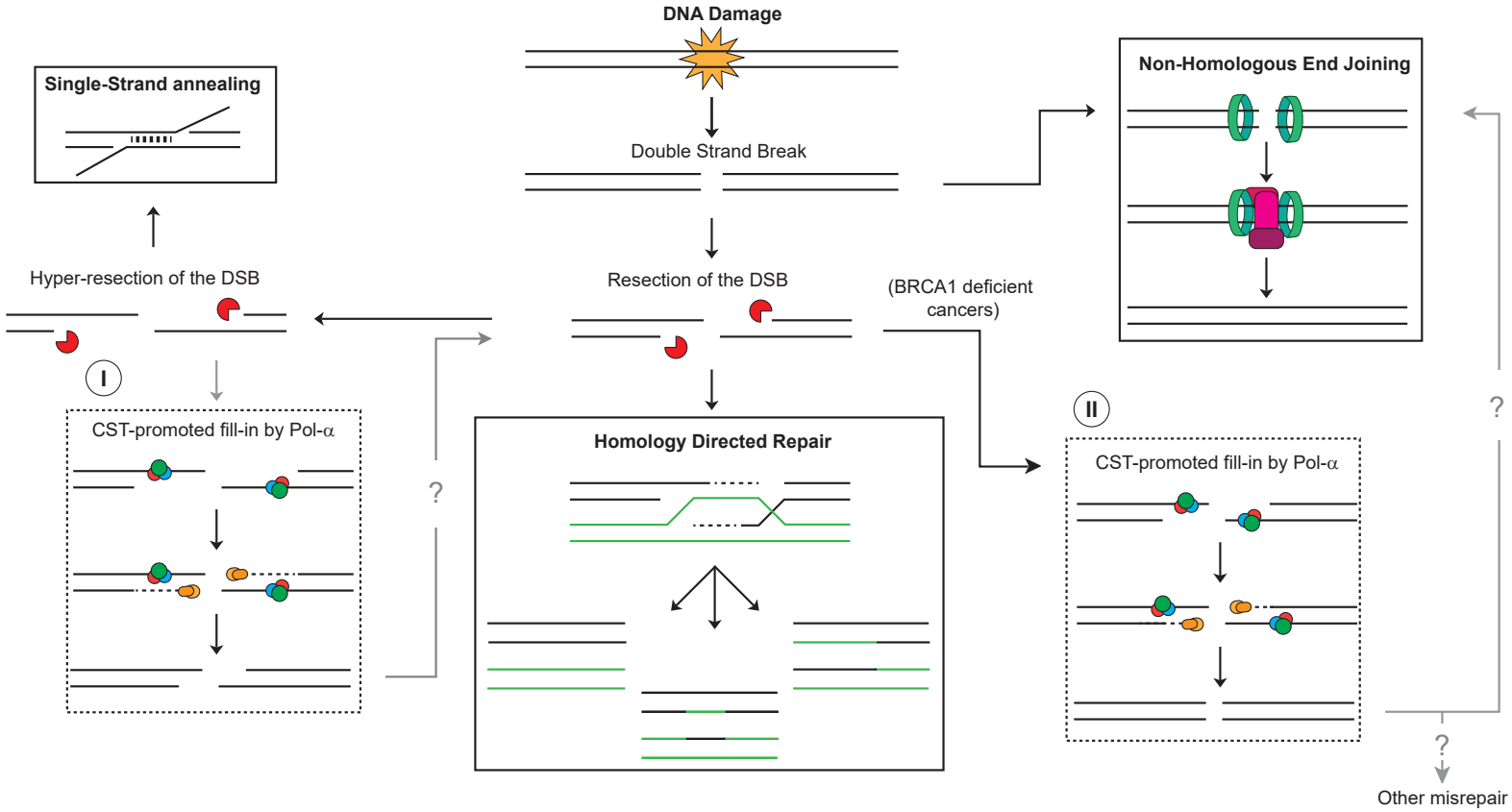

Figure 14. The CST complex promotes fill-in at DSBs. DSBs in DNA can be repaired by a variety of pathways, HDR requires the generation of ssDNA overhangs in order to use strand invasion to generate a Holliday junction. NHEJ does not require an overhang, acting on blunt (or near-blunt) ends. The CST complex is recruited to DSB overhangs by 53BP1/Shieldin/RIF1 and promotes the activity of Pol-α. (I) This fill-in is hypothesised to prevent hyper-resection inducing erroneous SSA which can be highly mutagenic. (II) In BRCA1 deficient cancers the CST complex is proposed to inhibit HDR by reducing/eliminating the ssDNA overhang. This HDR inhibition could result in misrepair of the DSB.

1.7 Transcription and Translation

The cell cycle, telomeres, and the DNA damage response are parts of a complex system that serves a basic purpose: the accurate transmission of genetic information in the form of DNA from one generation to the next. The central dogma of molecular biology is that DNA is transcribed to make RNA, and RNA is translated to make proteins. RNA polymerases in the nucleus 'read' the locus of DNA containing a gene to produce pre-mRNA. Pre-mRNA is processed in various ways, after which the finished product (mRNA) leaves the nucleus and is read by the ribosome. The ribosome uses the mRNA as instructions for assembling individual amino acids to form polypeptides. The polypeptide chains fold to form secondary and tertiary structures, and functional proteins.

Not all RNA produced is mRNA that is read to produce a protein. These non-coding RNAs can have specialised functions such as TERC, the RNA component of telomerase, or transfer RNA (tRNA) which is involved in the translation process at the ribosome.

1.7.1 Transcription

Pre-mRNA, the RNA required for protein production, is synthesised by the polymerase RNA Polymerase II [190]. Transcription is initiated at the promoter of a gene, a specialised region of DNA upstream of the coding sequence which attracts and assembles the RNA polymerase enzyme and transcription factors [191].

The transcription machinery is assembled at the promoter, starting with the TFIID transcription factor (Fig. 15). TFIID comprises TBP and TBP-associated factors [192]. TFIIB is responsible for locating the start of the gene, which binds then undergoes a conformational change with TFIID. The result is the bending of the DNA double-helix, initiating melting (separating hydrogen bonds between strands) and exposing ssDNA [193]. Once this happens TFIIF and RNA Pol II are recruited, forming the pre-initiation complex (PIC) [194]. The final step is the recruitment of TFIIE and TFIIF to complete the transcription initiation complex [190].

Phosphorylation of the CTD of RNA Pol II initiates transcription, at which point most transcription factors can dissociate. The RNA polymerase travels along the template strand in the $3'$ to $5'$ direction, assembling an RNA copy of the opposite 'coding' strand [195][196]. RNA is built using 3 of the 4 bases that DNA uses, A, C, and G, but RNA uses U (uracil) instead of T (thymidine). RNA nucleotides bind to the template strand by hydrogen bonding. The sugar phosphate backbone is connected to that of the proceeding nucleotide (by the RNA Pol II subunit RBP1) and the newly assembled nucleotide is released from the template DNA, now part of the mRNA strand [190]. At the start of transcription a methyl-cap is added at the $5'$ end of the pre-mRNA molecule. This is performed by a triphosphatase, a guanyl transferase, and a methyl transferase, which add seven methyl groups to the triphosphate A $5'$ terminus of the transcript [197].

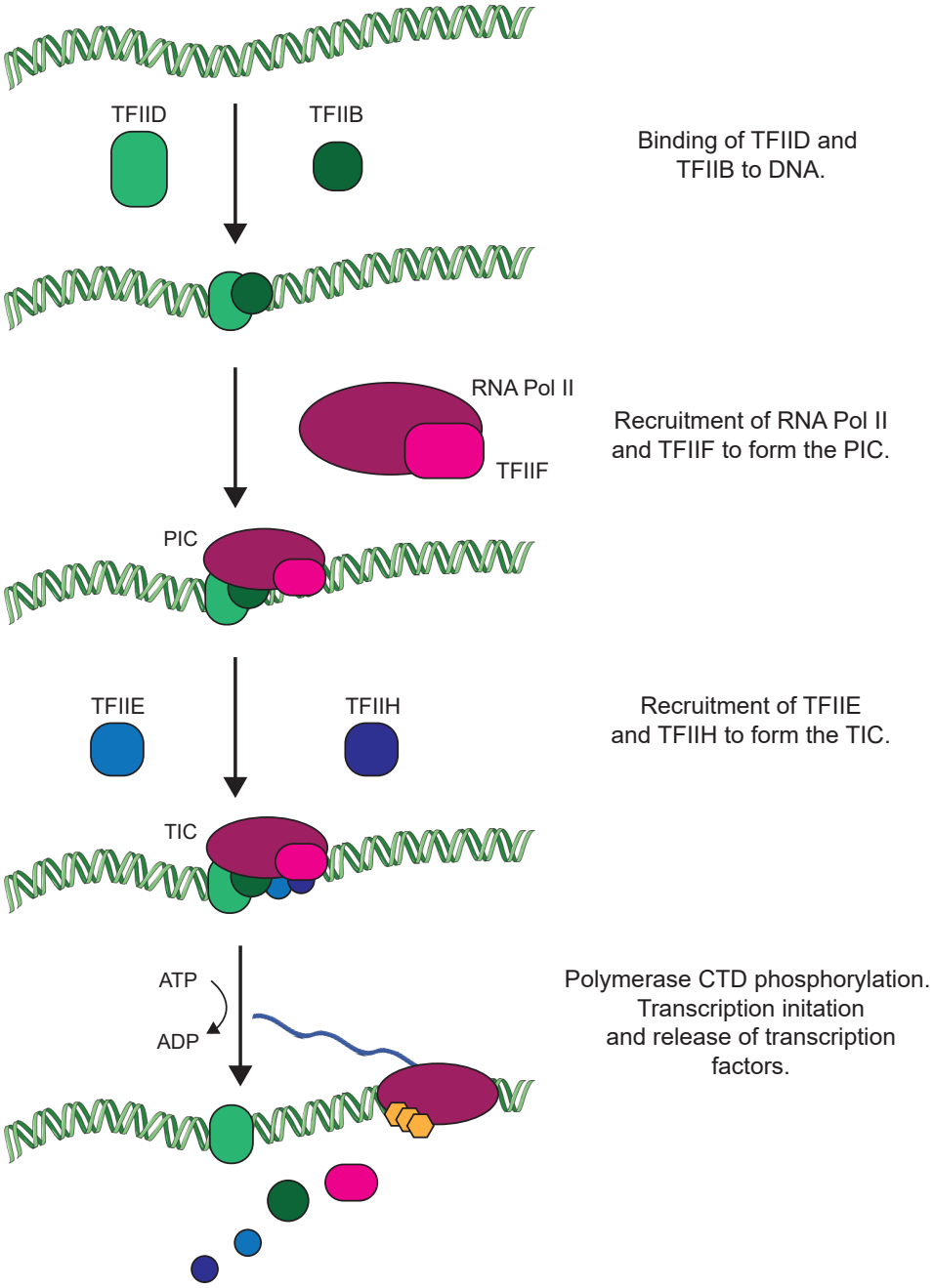

Figure 15. Recruitment of RNA polymerase II and transcription initiation. Transcription factors TFIID and TFIIB bind to the promoter region of a gene and recruit TFIIF-bound RNA Pol II to form the Pre-Inititation Complex. Transcription is initiated after the binding of TFIIE and TFIIH (forming the Transcription Initiation Complex), and the phosphorylation of the RNA Pol II C-terminal domain (CTD).

Transcription continues beyond the promoter region, through the body of the gene. The elongation stage of transcription is regulated by elongation factors and chromatin remodelling complexes [198]. The transcriptome continues partially past the end of the coding region of the gene before terminating. Multiple adenines are added to the 3′ end of the pre-RNA molecule to prevent degradation, after which it is released. The transcriptome dissociates from DNA, allowing the ssDNA bubble to close [199][200].

1.7.2 RNA Processing

Addition of the 5′ methyl cap and the 3′ Poly-(A) tail is not the only processing that RNA goes through before translation. The genes of higher level eukaryotes are typically split into introns and exons [201]. Introns are non-coding sequences that must be removed from mRNA before it can be translated, whilst exons are the coding sequences of DNA that are translated. Introns are removed by a process called splicing. Not all exons are necessarily included in the final RNA product, some can be removed during the splicing process to produce variations in protein functionality (Fig. 16). The range of different mRNA products that originated from one gene are called splice variants. Alternative splicing is thought to happen to 95-100% of human genes [202]. The mRNA splicing process appears to generally occur co-transcriptionally. Assembly of the spliceosome at an exon-intron junction can start before the downstream intron has even finished being transcribed [203].

Alternative splicing patterns fall within one of five categories: (1) cassette exons, which may be either selected or skipped; (2) mutually exclusive exons; (3) intron retention; (4) alternative donor, and (5) acceptor sites which alter the length of exons [204]. Recognition of splice sites is regulated by sequences that enhance or suppress splicing, present within both exons and introns [205].

The spliceosome is a multiprotein complex that cleaves RNA at intron-exon boundaries and ligates two exons. The spliceosome comprises five small nuclear ribonucleoprotein (snRNP)s (U1, U2, U4, U5 and U6) and over one hundred different polypeptides [206] (Fig. 17). The spliceosome is thought to assemble at recognised splice sites, remove the RNA sequence between two exons by a double-cleavage process, ligate the ends of two exons together, then largely dissociate as many components are recycled for another splicing event elsewhere [207]. After splicing completes the EJC (comprising eIF4A-III, MAGOH, and RBM8A) binds to each exon-exon junction site [208].

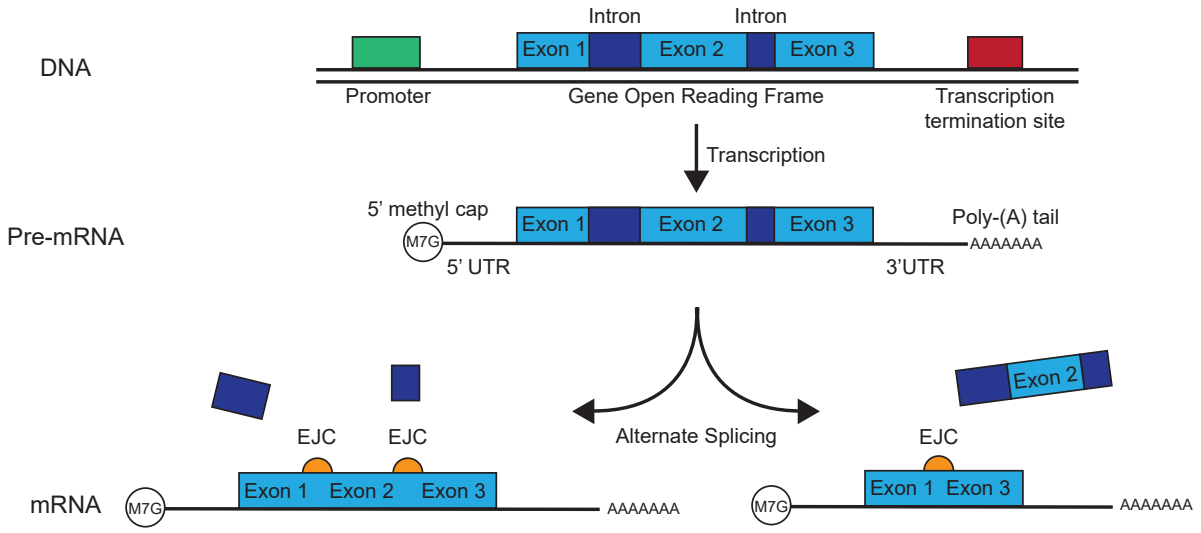

Figure 16. Alternate splicing of pre-mRNA. Pre-mRNA is produced by the transcription of a gene locus. The pre-mRNA contains an untranslated region (UTR) at both ends, a methyl-cap at the $5'$ end and a Poly-(A) tail at the $3'$ end. Different combinations of introns and exons can be removed from one pre-mRNA to produce multiple mRNAs that code for different proteins by a process called alternate splicing. Once splicing is complete the exon junction complex (EJC) is left bound to the mRNA at sites of exon-exon joining.

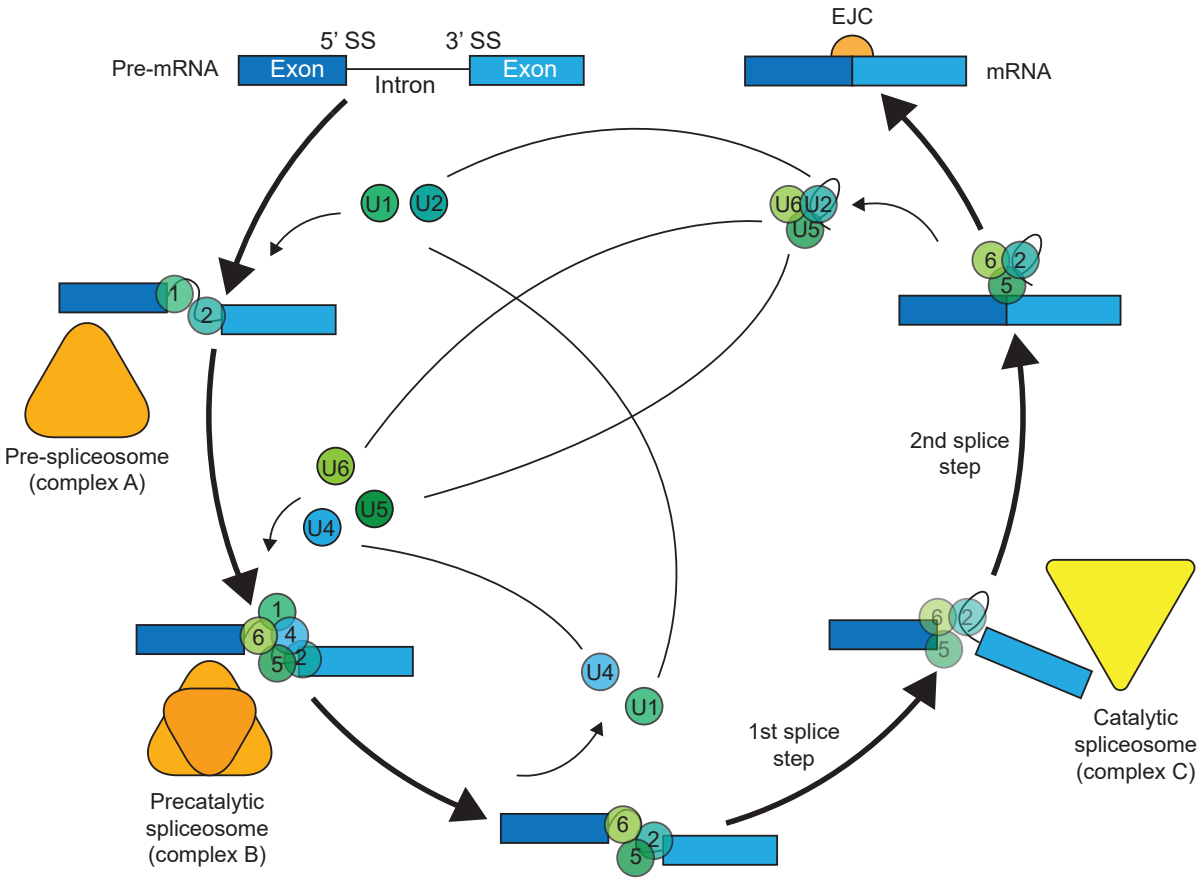

Figure 17. The splicing process. Introns (and some exons) are removed from pre-mRNA by splicing. The U1, U2, U4, U5 and U6 snRNPs recognise 5′ and 3′ splice sites and mediate the 2-step excision of introns from mRNA, before being released and recycled. After splicing occurs the EJC binds to the sequence of exon-exon junction. Figure adapted from Lee and Rio (2015) [207].

1.7.3 Translation

mRNA is exported from the nucleus to be translated into proteins. RNA codons are decoded into amino acid chains using tRNAs. Codons of three bases redundantly code for one of the twenty amino acids used in protein synthesis. For example AUG (ATG on DNA) codes for a methionine, whilst AGU codes for serine but so does AGC. tRNAs specifically bind to amino acids and act as carriers, bringing amino acids to the translation machinery for polypeptide synthesis. This is performed at the endoplasmic reticulum by the ribosome. The eukaryotic ribosome comprises four ribosomal RNAs (rRNAs) and approximately 80 proteins. The ribosome has two major subunits, the 60S (large) subunit is made of rRNAs 28S, 5.8S and 5S plus 49 proteins, whilst the 40S (small) subunit comprises 18S rRNA and 33 proteins [209–211].

The mRNA molecule is bound by the ribosome and read. When the ribosome reaches a 'start' codon (which codes for a methionine) it can begin translation. A start codon is necessary but not sufficient for translation initiation. Likelihood of translation initiation in eukaryotes is determined by the similarity of start-adjacent bases to the Kozak consensus sequence ((gcc)gccRcc**AUG**G) [212]. Translation is initiated with a methionine-bound tRNA, the next mRNA codon is read and a tRNA carrying the appropriate amino acid brought into proximity with the methionine. A peptide bond is created between the two amino acids [213]. The mRNA is moved through the ribosome which progressively assembles the protein polypeptide. The polypeptide folds to produce the secondary and tertiary structures of the final protein, and the ribosome has been shown to participate in the folding process [214]. When the ribosome reaches a stop codon (TAA, TAG, or TGA) translation is terminated and the polypeptide released. The ribosome components may then disengage the mRNA molecule and re-enter the pool for use on a new mRNA, but in some cases ribosome components continue scanning along the mRNA and are able to re-initiate translation at a second start codon downstream [215]. This re-initiation of translation is necessary for mRNAs with open reading frame (ORF)s in the $5'$ UTR, upstream of the main gene reading frame.

1.8 Nonsense Mediated Decay

1.8.1 Detection of Premature Termination Codons

Mutation of a gene that changes a non-stop codon to a stop codon terminates translation prematurely and produces truncated proteins (Fig. 18b). Mutations that insert or delete bases frequently introduce a premature termination codon as they shift the reading frame, changing how all downstream codons are read. The truncated protein may be unable to perform the necessary functions of the wild-type protein. Furthermore, the mutant protein product may be a dominant negative, interfering with the function of the remaining wild-type allele. Therefore stopping the mRNA from being translated is often a better option

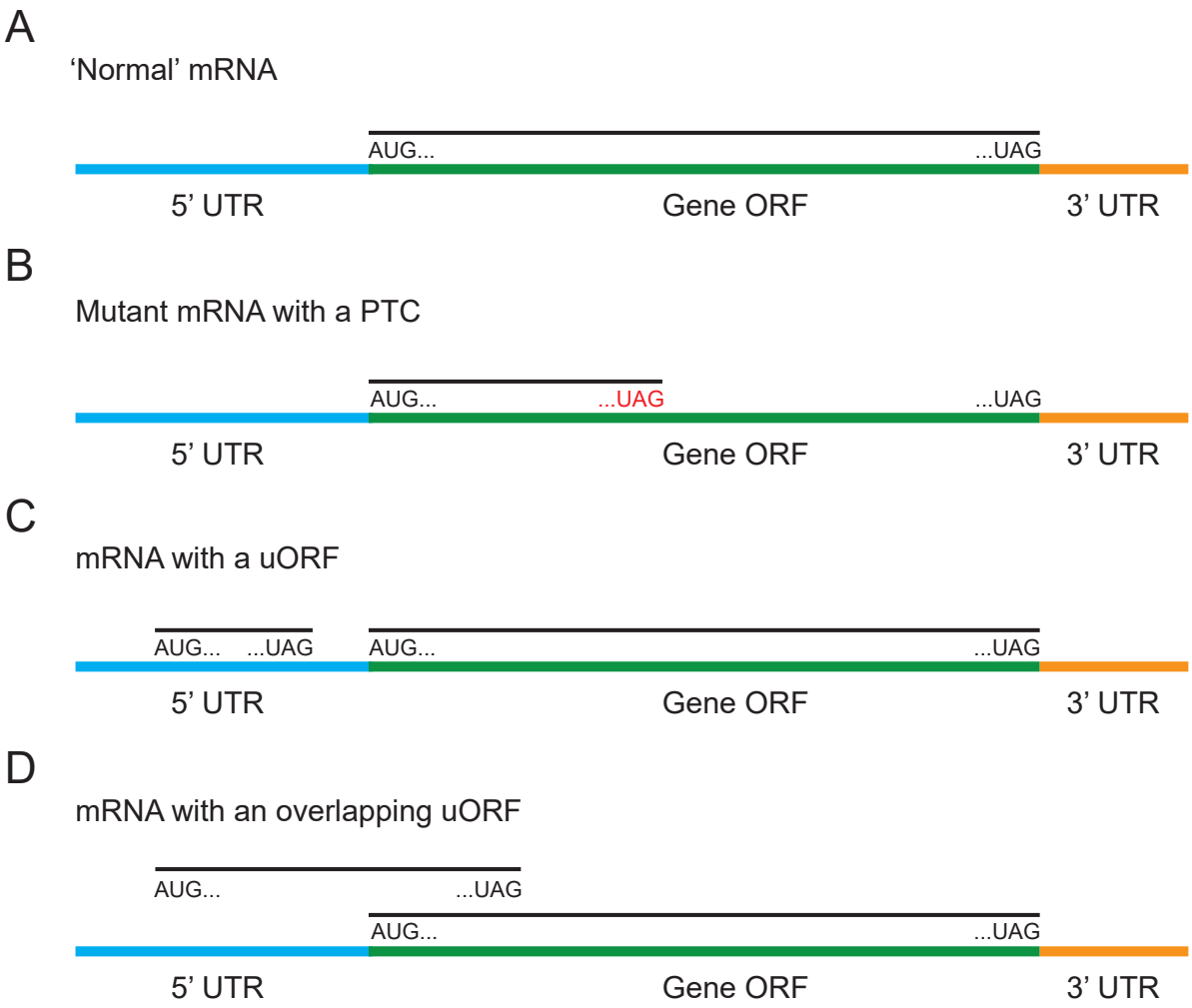

Figure 18. mRNA Open Reading Frames. (A) A typical mRNA transcript with a single ORF which encodes the gene. (B) A mutant mRNA transcript with a PTC. (C) An mRNA transcript with a upstream open reading frame (uORF) that starts and ends in the 5′ UTR. (D) An mRNA transcript with a uORF that starts in the 5′ UTR and partially overlaps with the main ORF, terminating at a stop codon within (but out of frame with) the main ORF.

for the cell than allowing a truncated version of the protein to be synthesised.

The machinery used to detect and eliminate mRNA with these PTCs is NMD. In mammals NMD is largely linked to premRNA splicing and translation, with detection of stop codons more than 50-55 nucleotides upstream of the final EJC inducing mRNA degradation [216][217]. In contrast budding yeast NMD is exon-junction independent, with PTC definition based on distance from the 3′ end [218]. The EJC remains associated with mRNA until it is displaced by the translation machinery [219].

The central component of the NMD pathway is UPF1, an RNA helicase. Prevailing models of NMD propose the recruitment of UPF1 and the PIKK SMG1 to the terminating ribosome by interaction with the stop codon marker eRF3 [220][221]. Phosphorylation of UPF1 is performed by SMG1 upon interaction of UPF1 with a downstream EJC-bound UPF2 and UPF3b [222] [223]. This phosphorylation of UPF1 activates the NMD complex of UPF1, UPF2 and UPF3b, translocating it from the 5′ end of the EJC to the 3′ end. Subsequent to this translocation the NMD complex interacts with and activates SMG5, SMG6, and SMG7. SMG6 is an endonuclease that cleaves the mRNA whilst SMG5 and SMG7 catalyse the de-capping and de-adenylation of the mRNA leaving it exposed to the action of exonucleases [224–226]. Consequently the mRNA containing a PTC is degraded after a single round of translation.

It should be noted that stop codon distance from the poly-(A) tail can sometimes also function as an alternative activator of NMD in mammalian cells. This is thought to be due to the lack of interaction between the terminating ribosome and PABPC1 which is bound to the tail. If PABPC1 does not interact with eRF3 at the ribosome then the terminating ribosome will stall, allowing activation of UPF1 [227].

Figure 19 . EJC-dependant degradation of mRNA with PTCs by NMD. (A) On a normal transcript the ribosome begins translation at the start codon of an mRNA, then moves along the mRNA producing a polypeptide chain and displacing EJCs. When the ribosome reaches the stop codon translation is terminated and the ribosome displaced. (B) If an mRNA contains a PTC upstream of an EJC then NMD is activated. UPF1 interacts with stop-codon-bound ribosomes, and when UPF1 is brought into proximity and interacts with EJC-bound UPF2 and UPF3b it is phosphorylated by SMG1. Phosphorylation of UPF1 results in SMG5, SMG6 and SMG7 activation. SMG6 is an endonuclease that acts on the mRNA, whilst SMG5-SMG7 initiates deadenylation and decapping (exposing the mRNA to exonucleases).

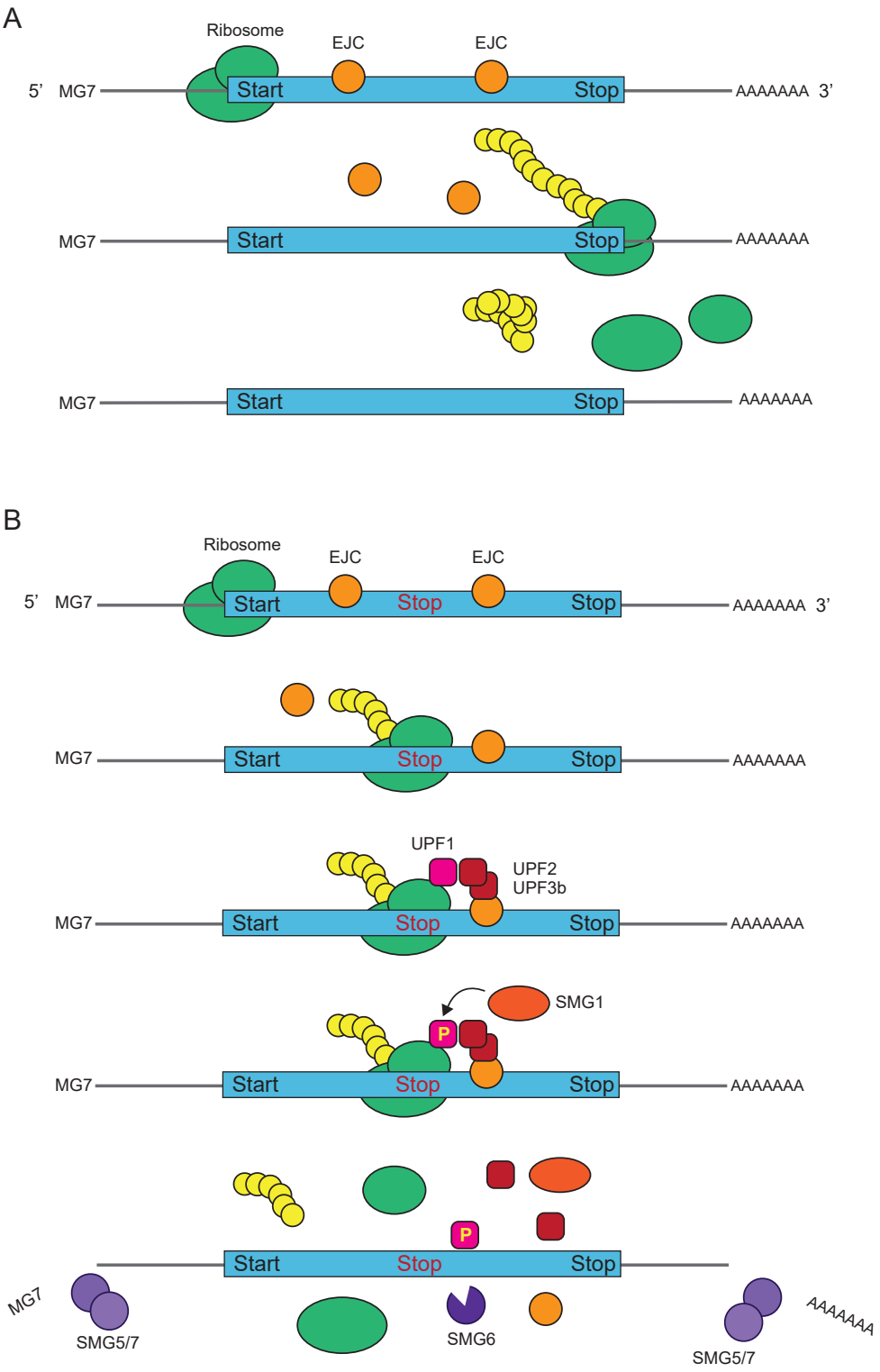
A
Ribosome
EJC
EJC
5’
MG7
Start
Stop
AAAAAAA
3’
MG7
Start
Stop
AAAAAAA
MG7
Start
Stop
AAAAAAA
B
Ribosome
EJC
EJC
5’
MG7
Start
Stop
Stop
AAAAAAA
3’
MG7
Start
Stop
Stop
AAAAAAA
UPF1
UPF2
UPF3b
MG7
Start
Stop
Stop
AAAAAAA
SMG1
P
MG7
Start
Stop
Stop
AAAAAAA
P
Start
Stop
Stop
MG7
SMG5/7
SMG6
SMG5/7
AAAAAAA

1.8.2 Open Reading Frames and Nonsense Mediated Decay

Whilst NMD primarily targets deleterious mutation-induced PTCs in mRNA, it also targets some natural transcripts, affecting approximately 10% of the budding yeast transcriptome [228]. It remains unclear why the cell regulates some genes through the NMD pathway, but key features in mRNA that can attract the action of NMD are well characterised.

Whilst the role of EJC location plays a major role in the direction of NMD, the mammalian NMD pathway can also use distance from the poly-(A) tail as an indicator of a PTC. Some wild-type mRNAs with long 3′ UTRs are consequently also degraded by NMD [218]. Another feature of an mRNA that can activate NMD is an overlapping-uORF. Some transcripts contain ORFs that start before the main gene-coding ORF and do not code for a functional protein. These uORFs can terminate upstream or downstream of the gene's true AUG start codon (Fig. 18c,d). uORFs that overlap with the main ORF are referred to as overlapping-uORFs. If translation is initiated on the uORF then logically it will be terminated at the uORF's stop codon. This termination site will typically be far from the 3′ UTR/poly-(A) tail of the mRNA and upstream of many EJCs, both of which are factors that promote degradation by NMD. Examples of human genes with uORFs that trigger NMD include CFTR and SMG5 [229][230].

NMD affects Stn1 levels in *S. cerevisiae* because of the uORF that overlaps with the main *STN1* ORF [231]. Budding yeast *STN1* mRNA also has a second uORF that does not overlap with the main ORF, but loss of this uORF did not increase Stn1 levels when removed [231]. The overlapping uORF introduces a stop codon within the body of the gene just two nucleotides after the main ORF start codon, this close proximity of the overlapping uORF codon to the main *STN1* start codon is key to the suppression of *STN1*, as extension of the overlapping uORF further into the gene (moving the stop codon 72 amino acids downstream) increased *STN1* mRNA and protein levels. This raised expression was not increased further after NMD inactivation [231]. This suggests that NMD in budding yeast affects *STN1* mRNA and protein levels due to the close proximity of an overlapping uORF stop codon to the *STN1* start codon. The human *STN1* homologue mRNA contains three overlapping uORFs, in frame with each other, terminating at a stop codon that overlaps the *STN1* start codon (Fig. 20). The similar presence of uORFs suggests regulation of *STN1* by NMD is possible. Data published by Torrance and Lydall using part of the 5′ UTR of human *STN1* in a luciferase expression assay indicate that the sequence was capable of suppressing downstream protein expression [231], however this only included two of the three uORFs in reported *STN1* mRNA transcripts. It remains unknown if NMD targets endogenous *STN1* transcripts in human cells.

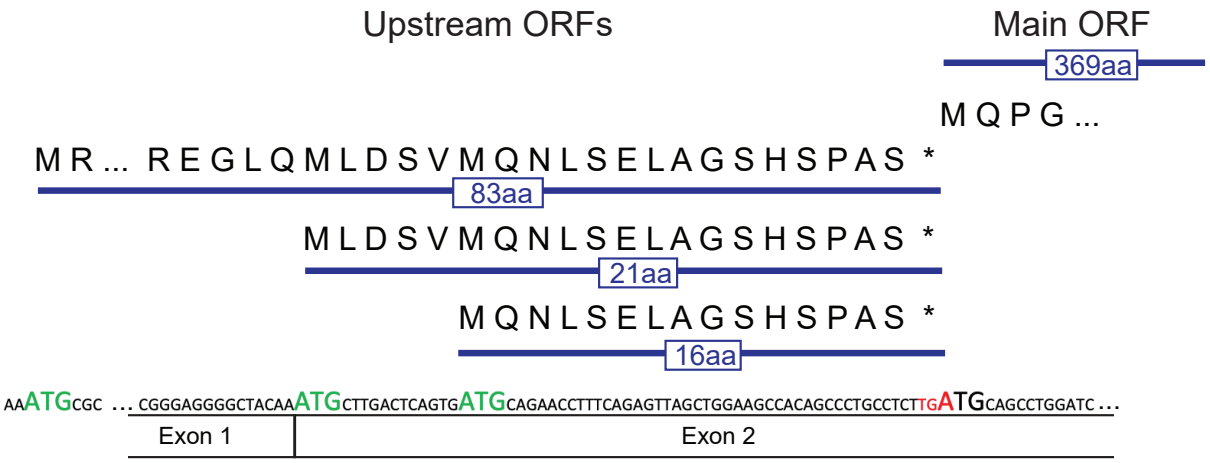

Figure 20. The uORFS of human *STN1*. *STN1* mRNA has 3 overlapping-uORFs. All three are in frame and terminate at a stop codon that overlaps the start codon of the main gene ORF. Figure adapted from Torrance and Lydall (2018) [231].

1.8.3 The Regulation of NMD

NMD activity varies between cell types and tissues [221]. Cellular levels of EJC peripheral factor RNPS1 have been correlated with NMD activity [232]. NMD targets a number of components of the NMD pathway itself, thus acting as a negative feedback loop regulating its own activity [233].

In response to stress the cell activates a wide range of pathways that make large changes to gene expression in an attempt to alleviate that stress. In a number of stress conditions such as hypoxia or nutrient deprivation NMD is downregulated [234]. This reduction in NMD, which is at least partially due to phosphorylation of eIF2-alpha, raises the expression level of NMD targets and helps to support the stress response [235][236]. It was recently reported that cells arrested in G_0 that have persistent DNA damage (damage that persisted for four days) deactivate NMD in a p38 (MAPK14)-dependant manner [237].

2 Aims

The principle hypothesis of this project is that the CST complex (and its appropriate regulation) is essential for maintaining genomic stability beyond the telomere. The CST complex was, until 2009, believed to be budding yeast specific, with vertebrates dependant on the Shelterin complex for telomere capping and regulation. The telomere-specific role of the CST complex in *S. cerevisiae* has been well established, controlling ssDNA overhang length and protecting the telomere from the DDR. Since its discovery the mammalian CST complex has been shown to not only play a role in telomere regulation, but to also support replication throughout the genome and promote polymerase-α activity at DSBs. Interestingly the reported effects of CST complex component knock-down vary significantly depending on the degree to which expression was inhibited, implying tight regulation of CST component levels is very important. This project focusses on the role CST complex components play in maintaining genome stability beyond their roles at the telomere, and how levels of those components are regulated.

Specific aims include:

1) Establish the *CTC1*$^{lox/lox}$ HCT116 cell line in our lab as a model system, and confirm the reported effect of *CTC1* loss on telomere regulation.

2) Examine the impact of *CTC1* loss on genome stability that is separate from its role at the telomere.

3) Investigate the regulation of STN1 levels and the impact loss of regulation has on the cell, particularly on the response to DNA damage.

4) Perform preliminary experiments to determine if an essential telomeric role for Dna2 is conserved from *S. cerevisiae* to metazoans.

The hallmark of cancer is an increase in cellular proliferation, usually fueled by an increase in mutagenesis and genomic instability. Through its role at the telomere and at DSBs the CST complex can directly affect both proliferation and genome stability. It is becoming more and more likely that the CST complex could play a significant role in a range of disease pathogenesis beyond Coats Plus syndrome, including ageing related diseases and cancer. Furthering our understanding of the role and regulation of the CST complex may ultimately result in improved disease prognosis and treatment.

3 Materials and Methods

3.1 Mammalian Cell Culture

3.1.1 Cell Lines

HCT116
The predominant cell line used in experiments was HCT116. HCT116 cells are near diploid, with polyploids reported at a frequency of 6.8% . The HCT116 cell line was derived from an adult male colorectal carcinoma [238].

Three variations of the HCT116 cell line were used during this project, each provided by the lab of Carolyn Price (University of Cincinnati):

- *CTC1*$^{lox/lox}$ HCT116 cells containing *loxP* sites flanking exon 5 of *CTC1*, as well as a Cre-recombinase expression cassette (which also conveys resistance to puromycin). Exposure of this cell line to tamoxifen induces deletion of *CTC1* exon 5 and the subsequent knockout of *CTC1* [182].
- The above *CTC1*$^{lox/lox}$ Cre-recombinase HCT116 cells that also contain a *CTC1* expression cassette that constitutively expresses *CTC1* even after knockout of endogenous *CTC1* by tamoxifen exposure.
- HCT116 cells that do not induce *CTC1* deletion upon exposure to tamoxifen.

U-2 OS
U-2 OS cells are a highly altered hypertriploid adherent human cell line derived in 1964 from a sarcoma of the tibia of a 15-year-old girl. The cell population typically contains chromosomal rearrangements involving chromosomes 1, 7, 9 and 11 [239]. This cell line was used as it is highly transfectable and sensitive to the NMD inhibitor NMDI14.

RPE-1
RPE-1 cells are the only non-cancer derived cell line used, they are derived from human retinal epithelial cells that have been immortalised with exogenous hTERT expression [240]. These cells were selected for use in experiments requiring non-cycling cells as there is a strong growth inhibition when these cells are confluent in culture [237].

3.1.2 Cell Culture Conditions

HCT116 cells were cultured in McCoy's 5A medium with L-Glutamine (Lonza: BE12-688F) supplemented with 10% sterile-filtered foetal bovine serum (FBS) (Gibco: 10270), Penicillin, Streptomycin, and L-Glutamine (Corning: 30-006-Cl). Cells were kept in a humidified incubator at 37°C with 5% CO_2.

U-2 OS and RPE-1 cells were maintained in Dulbecco's Modified Eagle's Medium (DMEM) with 4.5g/L Glucose and with L-Glutamine (Lonza: 12-604F), but otherwise grown in the same conditions as HCT116 cells.

For passage, cells were washed with calcium/magnesium-free Dulbecco's phosphate buffered saline (DPBS) (Lonza: BE17-512F) and dissociated from the culture vessel by incubation with Trypsin-Versene (Lonza BE02-007E) (made up from 10X in DPBS) at 37°C for 5-10 minutes. Trypsin was inactivated by addition of an equal volume of fresh culture medium, and cells were resuspended into a single-cell suspension before counting or direct reseeding. For passage cells were split between 1:5 and 1:8 after reaching 70-80% confluency. Cells were primarily maintained in T75 culture flasks with filter lids (TPP: 90076), however 10cm and 15cm plates (TPP: 93100/93150) were used in some circumstances.

When necessary, single cell suspensions were centrifuged at 125 relative centrifugal force (RCF) for 8 minutes and the supernatant removed before resuspension in culture media.

3.1.3 Frozen Cell Storage

Cells were washed with calcium/magnesium-free DPBS (Lonza: BE17-512F) and dissociated from the culture vessel by incubation with Trypsin-Versene (Lonza BE02-007E) (made up from 10X in DPBS) at 37°C for 5-10 minutes. Trypsin was inactivated by addition of an equal volume of fresh culture medium, and cells were pelleted by centrifugation at 125 RCF for 8 minutes. Supernatant was removed, and cells were resuspended at $1x10^6$ cells/ml in 4°C culture media with 5% dimethyl sulfoxide (DMSO) (Sigma: D2650). 1 ml of cell suspension was aliquoted per cryovial, which were then incubated on ice for 10-45 minutes. Cryovials were placed inside a Nalgene Mr. Frosty (Sigma-Aldrich: C1562) containing isopropanol (pre-chilled to 4°C) and stored at -80°C.

To thaw cells, cryovials were removed from -80°C storage and placed in a 37°C water-bath with gentle agitation for 1-2 minutes until fully thawed. 1 ml of cell suspension was then added to 9 ml of pre-warmed culture media before pelleting at 125 RCF for 8 minutes. The supernatant was removed, and the cell pellet resuspended in 10 ml of pre-warmed media. The 10 ml suspension was then placed into a T25 flask (TPP: 90026), and incubated under standard conditions for 24 hours, at which point the media was changed to remove dead cells and residual DMSO. Cells were regularly monitored over the following week to ensure healthy recovery.

3.1.4 Drug Treatments

Small molecule drug treatments were used at otherwise standard cell culture conditions. Drugs in DMSO were suspended at working concentration in fresh media prior to replacement of old culture media. Control culture media was replaced at the same time, supplementing with the vector DMSO to the appropriate concentration.

Mammalian Cell Drug treatments			
Target	**Drug**	**Concentration**	**Source**
CHK1	CCT245737	0.2-5 μM	SelleckChem: CCT245737
SMG7-UPF1	NMDI14	5 μM	Sigma-Aldrich: SML1538

Table 7. Mammalian Cell Drug Treatments

3.1.5 Mycoplasma Contamination

Cells were tested for mycoplasma using the MycoAlert detection kit (Lonza: LT07-218) following the manufacturers protocol. Mycoplasma positive HCT116 cells were treated with Plasmocin (Lonza: VZA-1012) following the manufacturer's protocol to eliminate mycoplasma, and all cell lines were retested periodically. All experiments were performed following mycoplasma elimination.

3.2 *CTC1* Knockout Induction

Exon 5 of both copies of *CTC1* in the edited HCT116 cell line from Carolyn Price (henceforth identified as HCT116$^{lox/lox}$) are flanked by locus of x-over P1 (loxP) sites. loxP sites are recognised by the Cre-recombinase topoisomerase which is capable of recombining the two sites, looping out and eliminating the genetic information between them [241]. These HCT116$^{lox/lox}$ cells constitutively express Cre-recombinase fused to a ligand binding domain of the human oestrogen receptor. As a result, the recombinase is shuttled into the nucleus only in the presence of tamoxifen [242]. The integrated Cre-recombinase expression cassette includes a puromycin resistance marker, as such the HCT116$^{lox/lox}$ cells were grown in media containing 1 μg/ml puromycin (Cambridge Bioscience: CAY13884) to ensure the locus was not silenced.

In order to induce the deletion of *CTC1*, tamoxifen was added to the culture media at a concentration of 10 nM. Extensive *CTC1* deletion was detectable after 2 days. Tamoxifen stock is dissolved in ethanol at 10 mM for long term storage, further diluted in ethanol to 20 μM for a working stock and added 1:2000 to the media for a final concentration of 10 nM. Subsequently, ethanol was added 1:2000 to control cells.

3.3 Protein Analysis

3.3.1 Protein Extraction

Protein extraction of whole-cell lysates was performed using urea lysis buffer: 8M urea, 300 mM NaCl, 0.5% v/v nonyl phenoxypolyethoxylethanol (NP-40) substitute (Sigma-

Aldrich: 74385), 50 mM Na_2HPO_4, 50 mM Tris (pH 8.0). 10 ml of lysis buffer was supplemented with 1 PhosSTOP phosphatase inhibitor cocktail tablet (Roche: 04906837001). To harvest lysates cells were washed with DPBS before lysis buffer was added (200 μl for cells in 6-well plate, 500 μl for 10cm dish). Cells were scraped before collection in Eppendorf tubes, snap frozen on dry ice and stored at -80°C (if not immediately used). Samples were sonicated to reduce viscosity using an MSE Soniprep 150. Sonication was performed at an amplitude of 4 microns for 2 cycles of 30 seconds on, 30 seconds off.

3.3.2 BCA Assay

Protein lysates in urea lysis buffer were analysed by bicinchoninic acid (BCA) assay to determine protein concentration. The Pierce BCA Protein Assay Kit (Thermofisher: 23227) was used following the manufacturers protocol.

3.3.3 Sample Preparation

Samples were made up to uniform concentration in loading buffer. Loading buffer was diluted to 1x from 5x stock. Samples in loading buffer were heated to 95°C for 2-3 minutes immediately before use to ensure suspension of sodium dodecyl sulphate (SDS).

3.3.4 SDS-PAGE

Sodium dodecyl sulfate - polyacrylamide gel electrophoresis (SDS-PAGE) was performed using 4-15% or 7.5% Bio-Rad Mini-Protein TGX Precast Gels (Bio-Rad: 4561086/4561026). Combs were removed, and the gels assembled in the running cassette of a Bio-Rad Mini-Protein Tetra Vertical Electrophoresis cell (Bio-Rad: 1658004). The tank and cassette chamber were filled with running buffer. 5 μl of PageRuler Plus Protein ladder (Thermofisher: 26620) was loaded into lane 1 followed by 12 μl of protein samples in subsequent wells. Samples were run at 100V (Bio-Rad: 1645050) until the dye front reached the bottom of the gel.

3.3.5 Western Blot

Proteins were transferred onto a polyvinylidene difluoride (PVDF) membrane using the Bio-Rad Trans-Blot Turbo Transfer system (Bio-Rad: 1704150) and the Trans-Blot Turbo RTA Mini LF PVDF Transfer Kit (Bio-Rad: 1704275) following the manufacturer's instructions and using the 1 Mini Gel transfer pre-set. Membranes were blocked in blocking buffer at room temperature for 1 hour, washed 3 times in tris-buffered saline with tween 20 (TBST) for 5 minutes, then incubated in 5 ml primary antibody solution at 4°C overnight or for 1 hour at room temperature. After primary antibody incubation, membranes were washed 3 times in TBST before incubation in 10-20 ml horseradish peroxidase (HRP)-tagged secondary antibody solution for 1 hour at room temperature. Membranes were washed again 3 times in TBST. All incubation and washing steps were performed

Buffers for Western blot	
Buffer	Ingredients
5x loading Buffer	0.2M Tris-HCl pH 6.8, 40% v/v glycerol, 8% SDS and 20% β-mercaptoethanol, bromophenol blue to dye
Running Buffer	90% MQ H2O, 10% 10x TGS buffer (Bio-Rad: 161-0732)
Transfer Buffer	20% Trans-Blot Turbo 5x Transfer Buffer (Bio-Rad: 10026938), 20% ethanol, 60% MQ H_2O
TBST	20 mM Tris-HCl pH 7.6, 120 mM NaCl, and 0.1% Tween20 (Sigma-Aldrich: P7949)
Blocking Buffer	4% w/v Marvel Skimmed Milk Powder in TBST
Primary Antibody Solution	2% bovine serum albumin (BSA) (Sigma: A9647) in TBST

Table 8. Buffers for Western Blot

with gentle agitation on a rocker or roller. Membranes were then treated with enhanced chemiluminescence (ECL) substrate following the manufacturers protocol. Membranes were placed in glossy plastic document sleeves and imaged using a FujiFilm LAS4000 luminescence imager taking incremental length exposures. Images were thresholded and saved in the tagged image format (TIF).

3.3.6 Signal Quantification

8-bit TIF files were imported into the FIJI distribution of ImageJ [243]. Individual lanes were assigned using the "Select First Lane" and "Select Next lane" commands. Lane density curves were plotted using the "Plot Lanes" command. Curves were closed using the line tool as necessary, and the area under the curve measured using the wand tool. GraphPad Prism software was used for calculation of statistical significance between groups using analysis of variance (ANOVA) tests, correcting for multiple comparisons using Sidak's or Tukey's method depending on the comparisons being made.

3.4 DNA Electrophoresis

Agarose gel electrophoresis was used for analysis of DNA fragment size as well as quantitative PCR (qPCR) primer validation. Depending on the size of the band expected, 0.8-2% agarose gels (Bioline: BIO-41025) were made up in 0.5x tris-borate-EDTA (TBE) buffer or 1x tris-acetate-EDTA (TAE) buffer. The suspension was heated to boiling point by microwave until all agarose had dissolved and then allowed to cool briefly. SYBR safe dsDNA stain (Thermofisher: S33102) was then added to the still molten agarose 1:10,000

Primary Antibodies					
Target	Concentration	Host	Source	Catalogue No.	Clonality
Total β-actin	1:10,000	Mouse	Sigma-Aldrich	A5441	Monoclonal
Total CHK1	1:1000	Mouse	Cell Signaling	2360	Monoclonal
P-CHK1 (s298)	1:1000	Rabbit	Cell Signaling	2349	Polyclonal (Lot 7)
Total STN1	1:1000	Mouse	Abcam	ab89250	Polyclonal (Lot GR129845-10)
Total p53	1:1000	Mouse	Cell Signaling	9282	Monoclonal
P-p53 (s15)	1:1000	Rabbit	Cell Signaling	9284	Polyclonal (Lot 21)
p21	1:1000	Rabbit	Cell Signaling	2947	Monoclonal

Table 9. Primary Antibodies for Western Blot

HRP-conjugated Secondary Antibodies				
Target	Concentration	Source	Catalogue No.	Clonality
Mouse Ig	1:5000	Dako	P0447	Polyclonal (Lot 35941)
Rabbit Ig	1:5000	Dako	P0448	Polylonal (Lot 25020)

Table 10. Secondary Antibodies for Western Blot

before the gel was poured and allowed to set. Gels were submerged in TBE or TAE in a Bio-Rad Wide Mini-Sub Cell GT electrophoresis cell (Bio-Rad: 1704405). 6x DNA loading buffer was added to the DNA samples, and the samples loaded into wells in the gel. DNA ladder solution was loaded into one well for band size comparison. Gels were then run at 70-150V depending on band size and desired resolution for 0.5-2 hours. Bands were imaged using a Syngene G:Box.

Buffers for DNA electrophoresis	
Buffer	Ingredients
0.5x TBE Buffer	Diluted 1:20 from 10x stock (Bio-Rad: 1610770)
1x TAE Buffer	40 mM Tris, 0.1% v/v Glacial Acetic Acid, 1 mM EDTA pH8
6x DNA Loading Buffer	30% Glycerol, Bromophenol blue dye
DNA Ladder Solution	1:6 6x Loading buffer, 10% 1Kb Plus DNA ladder (Thermofisher: 10787018)

Table 11. Buffers for DNA Electrophoresis

3.5 Plasmid Cloning

3.5.1 Generating Competent *E. coli*

5 ml of lysogeny broth (LB) was inoculated with TOP10 *E. coli* and grown overnight in a shaking incubator at 37°C. 1 ml of the overnight culture was used to inoculate 100 ml of LB in a 1L flask. This culture was then grown at 37°C until an optical density $(OD)_{600}$ of 0.5-0.6 was achieved. The next steps were all performed on ice in a cold room, and all pipetting was performed very gently. 25 ml fractions of the *E. coli* culture was aliquotted into 50 ml falcon tubes. Cells were centrifuged at 1000 RCF at 4°C for 10 minutes. The supernatant was removed, and each pellet resuspended in 5 ml of ice cold 100 mM $MgCl_2$ by swirling. Cells were pelleted again at 1000 RCF for 10 minutes at 4°C, and the supernatant removed. The pellets were resuspended in 1 ml of ice cold 100 mM $CaCl_2$ by swirling. The bacterial suspensions were left on ice for 2 hours before being combined into a single 15 ml falcon tube. 1 ml of 100% glycerol was added to the suspension, and the tube gently swirled to mix. The suspension was then aliquotted 100 μl at a time into pre-chilled Eppendorf tubes and immediately transferred to a -80°C freezer.

3.5.2 Bacterial Transformation

For transformation of bacteria with very low plasmid concentration (such as following the ligation step when cloning): Competent TOP10 derived *E. coli* were removed from -80°C

storage and thawed on ice for 10 minutes. 5 μl of typical ligation reaction was added to 100 μl of *E. coli* in a 1.5 ml Eppendorf tube and left on ice for 30 minutes. The *E. coli* DNA mix was then heat shocked at 42°C for 45 seconds before immediately placing back on ice for 2 minutes. 900 μl of super-optimal broth with catabolite repression (SOC) was added to the tube, and the suspension incubated on a rotating wheel at 36°C for 2 hours. Cells were pelleted at 2700 RCF for 3 minutes, before 800 μl of supernatant was removed and the pellet resuspended in the remaining 200 μl. Cell suspension was then plated out onto a 10cm LB with ampicillin (LB+AMP) plate and incubated overnight at 37°C.

For transformation of bacteria with high plasmid copy number (such as when expanding a plasmid from a miniprep stock): Competent TOP10 derived *E. coli* bacteria were removed from -80°C storage and thawed on ice for 10 minutes. 1 μl of standard miniprep elute was added to 50 μl of *E. coli* in a 1.5 ml Eppendorf tube and left on ice for 30 minutes. The *E. coli* DNA mix was then heat shocked at 42°C for 45 seconds before immediately placing back on ice for 2 minutes. 450 μl of SOC was added to the cell suspension, and 20 μl of suspension streaked onto a 10cm LB+AMP plate. The plate was then incubated at 37°C overnight.

3.5.3 Plasmid Isolation

Using a sterile pipette tip, a single *E. coli* colony was picked from LB+AMP plates the day after transformation. 1-5 ml of liquid LB+AMP was inoculated with the picked colony. For isolation of approximately 10 μg of plasmid DNA in 30 μl of TE, the *E. coli* suspension was incubated on a rotating wheel at 36°C overnight before the plasmid was extracting using the Qiagen Plasmid Mini Kit (Qiagen: 12125) following the manufacturer's protocol. For isolation of approximately 100 μg of plasmid DNA in 50 μl of tris-ethylenediaminetetraacetic acid (TE), the *E. coli* suspension was incubated on a rotating wheel at 36°C for 8 hours as a starter culture. 25 ml of liquid LB+AMP was inoculated with 25 μl of the starter culture and incubated with vigorous shaking at 37°C overnight. The next day the plasmid was extracted using the Qiagen Plasmid Midi Kit (Qiagen:12143) following the manufacturer's protocol.

3.5.4 Restriction Enzyme Digestion

Restriction enzyme digestions were performed in volumes of 20 μl. All restriction enzymes were supplied by New England Biolabs (NEB). Approximately 2 μg of miniprepped plasmid DNA in TE (8 μl) was digested in a reaction containing 10-20 units of restriction enzyme (typically 0.1-2μL) and 2 μl of NEB 10x restriction enzyme buffer (2.1, 3.1 or Cutsmart depending on the enzyme(s) used). Digestions were performed at 37°C or 65°C depending on the restriction enzyme for at least an hour. Many digestions required optimisation of component concentrations or duration to achieve optimal results. If the

linearised plasmid was to be used as a vector, 1 unit of calf intestinal alkaline phosphatase (CIP) (NEB: M0290S) was added directly to the digestion reaction and incubated at 37°C for a further 30 minutes.

3.5.5 Gel Purification

4 μl of loading buffer was added to each 20 μl digestion reaction tube and the entire reaction was loaded into a 1% agarose gel with SYBR Safe for electrophoresis as previously described. The agarose gel was then run at a low voltage (60-80V) for as long as possible for optimal band resolution. Once the band(s) had sufficiently resolved, the desired fragment was cut from the gel using a fresh scalpel blade and an Invitrogen Safe Imager transilluminator (Invitrogen: S37102). Care was taken to excise the minimum amount of gel and to minimise exposure of the DNA fragment to ultraviolet (UV) light. The excised gel fragment was placed in a pre-weighed Eppendorf tube. The tube was then weighed again in order to estimate the volume of gel inside. DNA extraction was then performed using the QIAquick polymerase chain reaction (PCR) Purification Kit (Qiagen: 28106) per the manufacturer's instructions.

3.5.6 Fragment Ligation

Ligation reactions were performed in volumes of 10 μl. When ligating a linearised vector with a desired insert, vector-only and insert-only controls were performed. Sticky-end ligations were performed at 16°C for 1 hour using the volumes outlined in table 6. The volumes of purification elutions in table 6 were usually sufficient and appropriate, however some volume optimisation was occasionally necessary to achieve a vector:insert molar ration of approximately 1:3. Blunt end ligations were performed overnight. Following ligation, 5 μl of each ligation reaction was used to transform 100 μl of competent *E. coli* as described previously. If many colonies were present on only the Vector + Insert plate then the transformation was likely to have worked, and 4 colonies were picked, miniprepped, and sequenced.

3.5.7 Gibson Assembly

In instances where traditional cloning methods proved ineffective and sequence overlap between vector and insert fragments was present, Gibson Assembly was used. Blunt-end vector and insert fragments were produced by digestion reactions and gel purified as described previously then ligated using the Gibson Assembly Cloning Kit (NEB: E5510S) according to the manufacturer's protocol. 5 μl of the reaction was then transformed into 100 μl of competent TOP10 *E. coli* as described previously.

Typical Ligation Reaction Volumes			
Component	Vector-Only Control	Insert-Only Control	Vector and Insert
Water	6 μl	2 μl	0 μl
T4 Ligase (NEB: M0202S)	1 μl	1 μl	1 μl
10x T4 Buffer (Supplied with Ligase)	1 μl	1 μl	1 μl
Gel-Purified Vector	2 μl	0 μl	2 μl
Gel-Purified Insert	0 μl	6 μl	6 μl

Table 12. Typical Ligation Reaction Volumes

3.6 Transient Transfection of Mammalian Cells

Transient transfection was used for assays requiring (over)expression of a specific protein or proteins for a short period of time. Mammalian expression vector plasmids carrying the gene of interest were prepared in TE at high concentration (0.5-2 μg/μl) by Qiagen midiprep or maxiprep as described above. 1x10^6 HCT116 or U-2 OS cells were transfected with up to 2 μg of DNA using the Amaxa Cell Line Nucleofector kit V (Lonza: VCA-1003) following the manufacturer's protocol.

3.7 Generation of Stable-Expression Clonal Cell Lines

3.7.1 Antibiotic Kill-Curve

HCT116 cells were grown in culture media containing G418 (Cambridge Bioscience: 1557) at 0, 50, 100, 200, 400, 600, 800 and 1000 μg/ml for 10 days. Cell viability was assessed by light microscopy. The lowest concentration with 100% cell death after 10 days was used for resistance selection. G418 stock concentration was adjusted for potency directed by manufacturer's datasheet. Typical G418 potency was approximately 70%.

U-2 OS cells were grown in culture media containing puromycin at 0, 1, 2, 3, 4, and 5 μg/ml for 10 days. Cell viability was assessed by light microscopy. The lowest concentration with 100% cell death after 10 days was used for resistance selection.

3.7.2 *STN1* Overexpression

HCT116 cells were transfected with a pcDNA3-STN1 mammalian expression plasmid using the Amaxa Nucleofector as described previously. 48 hours following transfection the cells were passaged (1:10, 1:50, 1:100, 1:200, each in duplicate) into 10cm plates containing 10 ml culture media with 400 μg/ml G418. Media containing G418 was refreshed every

4 days. 16 days later large colonies had formed and the culture media was removed and the cells gently rinsed with 10 ml warm DPBS. After removing the DPBS, small sterile disks of blotting paper (made by holepunch and autoclaved) were soaked in warm Trypsin-Versene and placed individually onto each clonal colony. Colonies were incubated at 37°C for 5 minutes, during which time the cells dissociated from the plate surface but adhered to the cloning disk. Using fine-nosed tweezers 48 cloning disks and associated cells were moved to individual wells of 2 24-well plates (TPP: 92024). The disks were lightly shaken once in the 24-well plate well so as to dislodge cells. When each well of the 24-well plate became near-confluent, cells were passaged 1:2 in duplicate into a well of a 6-well plate (TPP: 92006). Once 70-80% confluent, one of the wells of each clone was harvested for STN1 expression analysis by Western blot using urea lysis buffer (as described previously), whilst the other was frozen down in cryovials for temporary storage at -80°C (as described previously).

3.7.3 DRGFP Reporter Expression

Generation of U-2 OS DRGFP stable cells was performed by transfection of 2 μg pDRGFP as described previously. 48 hours after transfection cells were passaged 1:1 into media with 4 μg/ml puromycin in a 10cm dish. Cells were maintained in 4 μg/ml puromycin for 14 days as a heterogenous population of stable integrations. Cells were trypsinised as described previously to generate a single cell suspension, counted by haemocytometer and plated out in 10cm plates at a density of 50, 250, 500, 1000 and 2000 cells per plate. Media was changed every 3-4 days until large clonal colonies of cells had formed. 48 colonies were picked using cloning disks as described previously. Once the clones were near confluent in the 24-well plates the media was removed and the cells rinsed with DPBS. 100 μl of Trypsin-Versene was added to each well and incubated at 37°C for 5-10 minutes. 50% of the Trypsin single-cell suspension was transferred into an Eppendorf tube, and 200 μl of culture media with 10% DMSO was added to the remaining cells in the well. The plate was then sealed in parafilm, wrapped extensively in paper towel and placed in a -80°C freezer. The Trypsin-Versene in the Eppendorf tubes was neutralised with 50 μl of culture media before being centrifuged at >20,000 RCF for 30 seconds. The supernatant was removed and the cell pellets snap-frozen on dry ice before transfer to a -80°C freezer for storage. Cell pellets were later used for RNA extraction and analysis by qPCR.

3.8 Genotyping

3.8.1 Crude Genomic DNA Lysates

Cells were grown in 6-well plates before scraping and collecting in a 1.5 ml Eppendorf tube. Cells were then pelleted at >14,000 RCF for 30 seconds before the supernatant was removed and the pellet snap frozen on dry ice. DirectPCR (Tail) Lysis reagent (Viagen:

102-T) was supplemented with 0.4 mg/ml Proteinase K (Sigma-Aldrich: P4850). Each cell pellet was resuspended in 50 μl lysis reagent and incubated at 56°C for 16 hours. Proteinase K was inactivated by heating to 95°C for 10 minutes, and lysates were stored at -20°C.

3.8.2 Genomic DNA Extraction for qPCR

For extraction of genomic DNA for qPCR, a higher quality DNA sample was required than the crude lysate produced by DirectPCR lysis reagent. For this mammalian cells were grown, scraped and pelleted as described previously. Genomic DNA was extracted using the Qiagen DNeasy Blood & Tissue kit (Qiagen: 69504) following the manufacturer's protocol.

3.9 mRNA Analysis

3.9.1 Harvesting Cells for mRNA Extraction

Cells were grown to 70-80% confluence in a 6-well plate or 10cm dish. The culture media was removed and the cells rinsed with DPBS before scraping into an Eppendorf tube. Cells were then pelleted at >14,000 RCF for 30 seconds, the remaining DPBS supernatant removed and the pellet snap-frozen on dry ice. Pellets were stored at -80°C if not used immediately.

3.9.2 Extraction of RNA

The Qiagen RNeasy Mini Kit (Qiagen: 74106) was used for extraction of RNA from cultured human cells. RNA was extracted following the manufacturer's protocol, using a needle and syringe for the lysate homogenisation step.

3.9.3 RNA Concentration and Quality Analysis

The concentration and quality of RNA eluted from the RNeasy Mini Kit was measured by Thermo Scientific NanoDrop 2000C spectrophotometer (Thermofisher: ND-2000C), blanked using RNase-free H_2O. The 260/280 nM wavelength absorbance ratio was used to calculate nucleic acid purity compared to aromatic amino acids, and 260/230 nM wavelength absorbance was used to calculate purity compared to other contaminants. Acceptable ratios were 1.8-2.2 and >1.7 respectively.

3.9.4 Production of cDNA from mRNA by Reverse Transcription

Complementary DNA (cDNA) was produced from up to 1 μg of RNA by reverse transcription using the QuantiTect Reverse Transcription Kit from Qiagen (Qiagen: 205311)

PCR Primers		
Target	Forward Primer	Reverse Primer
RPL13A mRNA	CCT GGA GGA GAA GAG GAA AGA GA	TTG AGG ACC TCT GTG TAT TTG TCA A
CTC1 mRNA	TTT CTG TTC CCC CGT TGG AG	TGA GCT TGT TTC TGA GCC TGA
CTC1 DNA exon 5	CAC AGT AAG GCC CTA TTT CTA C	ACC TGG CTG GGA GTC TAG TT
STN1 mRNA	GAG ATT CAT GCC ACC GCT TAC	GCG CCT GGA TTG CTT AGT G
TEN1 mRNA	AAG AAA TCC GAG GAC CGG C	GAA TTC CTC AGG GGA AGG GC
ATF4 mRNA	ACA ACA GCA AGG AGG ATG CC	CCA ACG TGG TCA GAA GGT CA
ORCL mRNA	GGC AGC AGA TGA AAT CTG AA	TCC AGA ATG TGA TTT TTG CAG
Ribosomal 18S RNA	AAA CGG CTA CCA CAT CCA AG	CGC TCC CAA GAT CCA ACT AC
DRGFP DNA	GGG ATC ACT CTC GGC ATG G	TAT GTT TCA GGT TCA GGG GGA G

Table 13. qPCR Primers

following the manufacturer's protocol, which included a genomic DNA contamination elimination step.

3.9.5 Primer Design and Validation

When well established primers were not found in the literature, primers were designed using the national centre for biotechnology information (NCBI) primer basic local alignment search tool (BLAST), choosing an optimal melting temperature of 60.0°C, a product length of 120-180 nucleotides and ensuring primers span an exon-exon junction. Primers were checked for specificity using the NCBI reference sequence database. Primers were custom ordered from Sigma-Aldrich and suspended at 200 μM in TE before storage at -20°C. Optimal melting temperature was assessed by performing PCR with a range of annealing temperatures and running the products on an agarose gel, checking for a single strong band. Primer efficiency was performed by qPCR and assessing deviation from a standard curve of cDNA concentrations.

3.9.6 Quantitative PCR

20 μl reactions were performed in triplicate in 0.1 ml 96-well reaction plates (Applied Biosystems: 4346907). 5 μl of typical cDNA suspension (Produced by Quantitect reverse transcriptase PCR (RT-PCR) kit and further diluted 1:20 in DNase/RNase-free H_2O) or genomic DNA (Extracted by Qiagen DNeasy Blood & Tissue Kit and diluted 1:20 with DNase/RNase-free H_2O) was combined with 15 μl of master mix (4 μl 5x GoTaq Colourless Reaction Buffer, 3 μl 25 mM $MgCl_2$, 2.5 μl 2.5 mM deoxynucleoside triphosphates (dNTP) mix, 0.2 μl GoTaq G2 DNA Polymerase, 0.5 μl 10 μM primer mix, 0.2 μl SYBR Green (1:200 in DMSO) (Promega: M7845)). qPCR was performed in an Applied Biosystems StepOnePlus Real-Time PCR system with the following reaction: 1 cycle: 95°C 10 minutes; 40 cycles: 95°C 30 seconds, 60°C 30 seconds, 72°C 30 seconds. The reaction was terminated with a final stage of gradual temperature increase to produce a melt curve. Cycle threshold (Ct) values were taken at the exponential amplification phase and exported for analysis. Each gene master mix was tested with water in place of template DNA to ensure no master mix contamination.

3.9.7 Relative mRNA Abundance Analysis

Relative RNA abundance between treated and untreated samples was calculated from cDNA $\Delta\Delta$Ct values, using *RPL13A* and ribosomal 18S as endogenous control genes. Melt curve data were analysed to ensure a single PCR product was present in each reaction, confirming primer specificity and a lack of contamination.

3.10 Locus Copy-Number Estimation

For rough estimation of locus copy number between clones, the Ct value of a genomic qPCR product of the locus in question was compared to the Ct value of a PCR product of identical size from a locus of known copy number. For identification of clones with single pDRGFP integrations in hypertriploid U-2 OS cells, the clones with a DRGFP PCR product signal 25% - 33% the magnitude of a *CTC1* PCR product (which U-2 OS cells have 3-4 copies of) likely carried single integrations. In support of these clones having single integrations there were no clones with significantly lower DRGFP locus PCR product abundance.

3.11 Fluorescent Microscopy

3.11.1 Fixing Asynchronous Cells

$0.3x10^6$ cells were seeded onto a 19mm round glass coverslip (VWR: 631-0156) in a 6-well plate well containing 3 ml of culture media. 48 hours later the culture media was removed, and the cells washed with 3 ml DPBS. Cells were fixed in 2% formaldehyde

(Sigma: F8775) in DPBS for 10 minutes. Formaldehyde was removed, and the coverslips washed in 3 ml DPBS 3 times for 5 minutes. Fixed coverslips were stored at 4°C in DPBS for up to 2 weeks.

3.11.2 Preparing Metaphase Chromosome Spreads

$0.3x10^6$ cells were seeded into onto a 19mm round glass coverslip (VWR: 631-0156) in a 6-well plate well containing 3 ml of culture media. 48 hours later 0.1 μg/ml Colcemid (Thermofisher: 15210040) was added to the culture media for 3 hours. The media was gently removed (so as not to dislodge mitotic cells) and replaced with room temperature hypotonic buffer (0.2% KCl, 0.2% $Na_3C_6H_5O_7$) for 15 minutes. Coverslips were placed face-up on glass microscope slides, clipped into inserts for a Shandon Cytospin 3, and spun at 1000 rotations per minute (RPM) for 5 minutes. Immediately after centrifugation the coverslips were removed from the cytospin inserts and placed in 2% formaldehyde DPBS for 10 minutes. After fixation the coverslips were washed 3 times for 5 minutes each in 3 ml DPBS and stored in DPBS at 4°C.

3.11.3 Staining Cells for Immunofluorescence

Fixed coverslips were permeabilised in 1% Triton X-100 (Sigma: T8787) in phosphate buffered saline with tween-20 (PBST) for 12-15 minutes at room temperature, which was then removed and the coverslips washed once in PBST. The coverslips were then blocked by incubation in 5% w/v BSA PBST at room temperature for 45 minutes. Primary antibody was diluted as appropriate in 5% w/v BSA PBST, and the coverslips placed face down onto a 100 μl droplet of antibody solution. The coverslips were incubated at room temperature for >1.5 hours in a humidified chamber. The coverslips were washed for 5 minutes 3 times in PBST before incubation with secondary antibody diluted as appropriate in 5% w/v BSA PBST in a humidified chamber at room temperature for 1 hour. After incubation the coverslips were washed 3x in phosphate buffered saline (PBS) for 5 minutes before rinsing with MQ H_2O to remove salts and allowed to air dry for 5-10 minutes. Coverslips were then placed face down on a droplet of Prolong Gold Antifade Mountant with 4',6-diamidino-2-phenylindole (DAPI) (ThermoFisher: P36941) on a glass slide. Slides were cured at room temperature in the dark for 24 hours before the edges were sealed with nail varnish. Once the nail varnish was dry, slides were stored at -20°C.

3.11.4 Staining Cells for Co-Immunofluorescence/Fluorescent In Situ Hybridisation

Cytospun metaphase spread coverslips were permeabilised in PST-Triton buffer for 10 minutes before blocking in co-IF/FISH antibody dilution buffer for 15 minutes at 37°C. Coverslips were then incubated for 1.5 hours with primary antibody in Co-IF/FISH antibody dilution buffer (face down on a 100 μl droplet in a humidified chamber). Coverslips

PNA probes			
Target	Nucleotide Sequence	Conjugated Fluorophore	Catalogue No.
Telomere C-rich strand	TTA GGG TTA GGG TTA GGG	Cy5	PN-TG055-005
Centromere	AAA CTA GAC AGA AGC ATT	Alexa488	PN-CN060-005

Table 14. Eurogentec PNA probe details

Primary Antibodies					
Target	Concentration	Host	Source	Catalogue No.	Clonality
G-Quadruplex DNA	1:400	Mouse	Merck Millipore	MABE1126	Monoclonal
γH2AX	1:800	Rabbit	Cell Signaling	2577	Polyclonal (Lot: 11)

Table 15. Primary Antibodies for Immunofluorescence

were washed 3 times in PBST for 5 minutes then incubated with secondary antibody in Co-IF/FISH antibody dilution buffer for 30 minutes (face down on a 100 μl droplet in a dark humidified chamber). Coverslips were washed 3 times in PBST for 5 minutes before antibodies were fixed in 4% formaldehyde PBS for 10 minutes at room temperature. After rinsing the coverslips twice with MQ H_2O, the cells were dehydrated with an ethanol series at 4°C (70%, 90%, then 100% for 2 minutes each). A hotblock was heated to 90°C then covered in a wet sheet of paper towel. A 40 μl droplet of 200 nM PNA probe (Table 14) in preheated hybridization buffer was placed on a preheated glass slide, and the fixed coverslips placed face down on the droplet. The slide and coverslip were then incubated on the damp hotblock for 3 minutes loosely covered with tin foil. Slides were then moved to a dark humidified chamber, allowing the probe to anneal at room temperature for 2 hours. Coverslips were then washed twice in wash buffer A for 5 minutes, then twice in wash buffer B for 5 minutes. After briefly rinsing with MQ H_2O, coverslips were air dried and mounted in a droplet of Prolong Gold Antifade Mountant with DAPI on a glass slide. Slides were cured at room temperature in the dark for 24 hours before the edges were sealed with nail varnish. Once the nail varnish was dry, slides were stored at -20°C.

Co-IF/FISH solutions		
Solution	Ingredients	Notes
PBS	10 mM Na_2HPO_4, 1.8 mM KH_2PO_4, 137 mM NaCl, 2.7 mM KCl	
PBST	0.1% Tween-20 in PBS	
PST-Triton Buffer	120 mM KCl, 20 mM NaCl, 10 mM Tris pH 7.5, 0.1% Triton X-100	
Co-IF/FISH Antibody Dilution Buffer	20 mM Tris pH 7.5, 2% w/v BSA, 0.2% fish gelatine (Sigma: G7765), 150 mM NaCl, 0.1% Triton X-100, 100 μg/ml RNase A	
PNA Hybridisation Buffer	10 mM Tris-HCl pH 7.2, 70% formamide (Promega: H5052), 1% blocking reagent (1:10 from 10% stock)	Made fresh, filter sterilised.
Blocking Reagent 10% stock	10% w/v Blocking reagent (Sigma-Aldrich: 11096176001) in maleic acid buffer	Autoclaved and stored at 4°C.
Maleic Acid Buffer	100 mM maleic acid, 150 mM NaCl	Adjusted to pH 7.5 with NaOH.
Wash Buffer A	70% formamide, 10 mM Tris pH 7.5, 0.1% w/v BSA	
Wash Buffer B	50 mM Tris pH 7.5, 300 mM NaCl, 0.8% Tween-20	

Table 16. Co-IF/FISH solutions

Fluorophore Conjugated Secondary Antibodies						
Target	Concentration	Host	Conjugated Fluorophore	Source	Catalogue No.	Clonality
Mouse Ig	1:200	Goat	DyLight 650	Thermo-Fisher	84545	Polyclonal (Lot: R1240430)
Mouse Ig	1:200	Goat	DyLight 550	Thermo-Fisher	84540	Polyclonal (Lot: PD195111)
Rabbit Ig	1:200	Goat	DyLight 550	Thermo-Fisher	84541	Polyclonal (Lot: 84541)
Rabbit Ig	1:200	Goat	AlexaFluor 488	Thermo-Fisher	A-11008	Polyclonal (Lot: 1797971)

Table 17. Secondary Antibodies for Immunofluorescence

3.11.5 Microscopy

Slides were removed from -20°C storage and allowed to reach room temperature before cleaning with lens cleaning paper. Microscopy was performed on a Zeiss AxioImager (illuminated by Colibri light-emitting diode (LED) system) or Nikon Eclipse 50i (illuminated by metal halide lamp) widefield microscopes. Multichannel fluorescent images were captured in Zeiss Zen software or Jentopik ProgRes software respectively. Sample exposure to fluorescent light was kept to a minimum in order to avoid bleaching.

3.11.6 Scoring Micronuclei

Images captured at 20x objective lens magnification were scored blind using the Filename Randomizer macro from Tiago Ferreira [244]. Total nuclei in the DAPI channel were counted using a custom written macro. Micronuclei frequency was scored by eye. Micronuclei were defined as an approximately round DNA body distinctly separate from the main nucleus, and no larger than 1/3 the size of the main nucleus. "Micronuclei frequency (%)" represents the frequency of nuclei with adjacent micronuclei and does not distinguish between nuclei with a single micronucleus or multiple micronuclei.

3.11.7 Scoring Chromatin Bridges

Images captured at 40-100x objective lens magnification were scored blind. DAPI channel nuclei were automatically counted by ImageJ macro, and chromatin bridges counted by eye. A chromatin bridge was defined as a bridge of DNA connecting two distinct interphase

nuclei. “Chromatin bridge frequency (%)” is defined as number of bridges per 100 nuclei.

3.11.8 Scoring Nuclear γH2AX Foci

Images of interphase nuclei were captured at 40x objective lens magnification. γH2AX foci frequency was scored using a custom ImageJ macro using the DAPI channel to define individual nuclei. Foci in the γH2AX antibody channel were counted using the find maxima tool.

3.11.9 Measurement of Telomere Length

C-strand telomere length was measured by PNA probe fluorescence. Cy5-labelled PNA probes specific to the C-rich strand of human telomeres were annealed to metaphase spreads as described previously. Telomere C-strand length and fluorescent signal intensity are linearly proportional. Images were captured at 40-100x objective lens magnification by widefield microscopy. Signal intensity was scored automatically using the FIJI distribution of ImageJ.

3.11.10 Localisation of Telomeres and γH2AX

Multichannel fluorescent images were captured of co-IF/FISH stained metaphase chromosome spreads. Images were captured at 60-100x objective lens magnification by widefield microscopy. The images were scored blind using the FIJI distribution of ImageJ for overlapping telomeric PNA probe signal and γH2AX foci.

3.11.11 Measuring Relative G-Quadruplex Abundance

G-quadruplex abundance was measured by IF staining of interphase nuclei with a G-quadruplex specific antibody. Images were captured at 40x objective lens magnification by widefield microscopy. Nuclear signal intensity was scored automatically using a custom ImageJ macro.

3.11.12 Statistical Analysis

All statistical analysis of microscopy quantification was performed using the GraphPad Prism software. Statistical significance was calculated by one or two-way ANOVA correcting for multiple comparisons using Sidak or Tukey’s method as appropriate. Three biological repeats were performed on separate days and fixed. Replicates were stained and imaged together for consistency of fluorescent staining.

3.12 Homology Directed Repair Analysis by DRGFP Reporter

Clonal populations of U-2 OS cells that had integrated 1-2 copies of the DRGFP reporter cassette (determined as described previously) were assessed for GFP expression. pDRGFP was a gift from Maria Jasin (Addgene plasmid 26475) [245]. Clones with <0.2% baseline GFP expression (assayed by fluorescent microscopy) were chosen and transfected with 0.5 μg of pDNA3-SceI to transiently express the SceI endonuclease. 48 hours after transfection cells were assessed for GFP expression again. A clone was chosen that significantly increased GFP expression after transfection with pcDNA3-SceI. To assay the impact of *STN1* overexpression on HDR, an *STN1* mammalian expression plasmid was co-transfected with pcDNA3-SceI, and the frequency of GFP positive cells scored 48 hours later. Empty pcDNA3 expression vector was used as a negative control, and total amount of DNA transfected was consistent between samples.

3.13 Cell Growth

3.13.1 Cell Counting

Measurement of cell population size was performed using a haemocytometer. Once a single cell suspension was achieved following trypsinisation, 15 μl of cell suspension was placed on a glass haemocytometer and counted in at least duplicate. For long term population growth assays cells were counted before passage every 2 days. The number of population doublings between timepoints was calculated using the following formula:

$$log_2(\frac{\text{cell count timepoint } x}{\text{cell count timepoint } x-1}) = \text{Population doublings}$$

3.13.2 PrestoBlue Assay of Cell Viability

Cell viability was measured indirectly using PrestoBlue Cell Viability Reagent (ThermoFisher: A13261). 8 replicates of 2500 cells per well were plated in a 96-well plate with 200 μl of culture media. 24 hours after seeding, culture media was temporarily replaced with 10% PrestoBlue media for 60 minutes. The PrestoBlue media was removed and absorbance measured at 570nm to take a baseline measurement of population size. Cells were then treated per the specific experiment for 24-72 hours before being incubated in PrestoBlue media again for 60 minutes. Relative viable cell count was inferred from the final absorbance value, correcting for seeding variation using the initial pre-treatment reading.

3.13.3 Senescence-Associated β-Galactosidase Assay

Cellular senescence was measured by staining for senescence-associated β-galactosidase activity. Mammalian cells were cultured in 6-well plates until 70-80% confluent before

washing with PBS and fixing in 1% formaldehyde PBS for 15 minutes at room temperature. The cells were then washed twice with PBS before incubating in 1 ml of β-galactosidase assay buffer (38.6 mM citric acid pH6, 38.6 mM NaH_2PO_4 pH 6, 145 mM NaCl, 1.93 mM $MgCl_2$, 46 mM $K_4[Fe(CN)_6]\cdot 3H_2O$, 46 mM $K_3[Fe(CN)_6]$, 0.29 mg/ml X-Gal) for 20 hours in the dark at 37°C (with atmospheric CO_2). Assay buffer was removed, and the cells preserved in 70% glycerol at 4°C. Images of the cells were captured using a widefield visible light microscope, and the frequency of blue stained cells (considered to be senescent) was scored blind in the FIJI distribution of ImageJ.

3.13.4 Trypan Blue Exclusion Assay

Dead mammalian cells were identified by addition of Trypan blue (ThermoFisher: 15250061) to a single cell suspension. 0.4% Trypan Blue solution was added 1:1 to a cell suspension before counting by haemocytometer. Blue stained cells were scored as dead as they were unable to exclude the dye, and unstained cells were scored as alive.

3.14 *Caenorhabditis elegans*

***C. elegans* strains**	
Strain	Genotype
Bristol N2	Wild Type
NB320	*dna-2*(jh115)/mln1[*dpy-10*(e128) *mls14*(*GFP*) II
Unassigned *fncm-1* mutant	*fncm-1*(tm3148)
CB5348	*mrt-2*(e2663)

Table 18. *C. elegans* Strains

3.14.1 Maintaining Stock Populations

C. elegans were maintained on nematode growth medium (NGM) plates at 20°C in sealed containers to preserve humidity. Plates were propagated by picking approximately 5 adult worms twice a week. NGM plates were seeded with 50 μl of an OP50 *E. coli* culture the day before use, allowing the bacterial lawn to grow overnight. All strains were maintained as homozygotes except NB320, which was maintained as a mixed population of homozygotes and heterozygotes, using the GFP balancer chromosome to distinguish genotype.

Solutions for maintenance of *C. elegans* strains	
Solution	Ingredients
NGM with Agar	51 mM NaCl, 62.5 mg/ml Peptone (Formedium: PEP03), 20 mg/ml Agar (Formedium: STDA01), 1 mM $CaCl_2$, 1 mM $MgSO_4$, 25 mM KH_2PO_4, 0.1% cholesterol solution.
Cholesterol Solution	0.5 mg/ml cholesterol (Sigma-Aldrich: C8667) in ethanol.
M9 Buffer	5 mg/ml NaCl, 3 mg/ml KH_2PO_4, 6 mg/ml Na_2HPO_4, 1 mM $MgSO_4$
Worm Freezing Solution	5.85 mg/ml NaCl, 6.8 mg/ml KH_2PO_4, 5.6 mM NaOH, 3 mM $MgSO_4$, 30% glycerol.

Table 19. Solutions Used in the Maintenance of *C. elegans* Strains

3.14.2 Freezing *C. elegans*

An overgrown (but not dauer) plate that has been starved for approximately 1 day, containing many L1/L2 larvae, was chosen. The plate was flooded with 2.5 ml sterile M9 buffer and gently swirled to dislodge the larvae. The buffer containing suspended larvae was pipetted off and added to an equal volume of freezing solution. The solution was vortexed and aliquotted into 4 cryovials. The cryovials were wrapped in paper towel and placed in a -80°C freezer.

3.14.3 Crossing Strains

3 early adult stage hermaphrodites were picked and placed on a 6cm NGM plate with a small OP50 colony (seeded from 20 μl overnight liquid culture) at the centre, alongside 15 adult males. 5 days after plating, the plates were checked for male frequency. If the plate contained many males, the cross was considered to have been successful. Adult hermaphrodites or males were picked depending on requirement (under fluorescent stereoscope if discerning balancer chromosome absence/presence was necessary). Picked adults were plated individually into 6 well plates containing NGM, and after 2-3 days (when L1-L2 offspring were abundant but had not reached the L3 stage yet) the adults were removed for genotyping by single-worm PCR. Once the adult genotypes were known, plates containing offspring of the desired adult were taken forward.

3.14.4 Single-Worm PCR

Individual worms were picked and placed in a 200 μl PCR tube containing 10 μl 1 mg/ml Proteinase K in 1x GoTaq Colourless Reaction Buffer. Tubes were then snap-frozen at -80°C for a minimum of 10 minutes. Lysis was carried out in an Applied Biosystems Veriti

96-well thermocycler, heating to 65°C for 90 minutes before proteinase K inactivation at 95°C for 15 minutes. Lysed worms were stored at -80°C before being used directly in GoTaq PCR reactions as described previously.

3.14.5 Genotyping with Restriction Digestion

The *mrt-2* mutation in strain CB5348 is a single base change that introduces a PTC. This change cannot be detected by running a PCR product directly on an agarose gel. The mutant allele can however be detected by attempting to digest a PCR product of the locus with the endonuclease BstNI, as this mutation destroys a BstNI restriction site. The mutant locus was amplified in a 20 μl PCR reaction as described previously, then 5 μl of the PCR product was added to a 20 μl digestion reaction (1 μl BstNI (NEB: R0168S), 1 μl NEB 3.1 buffer, 13 μl H_2O) and digestion was carried out at 65°C for 1 hour. The digestion reaction product was then run on a 2% agarose gel for analysis.

3.14.6 Embryo Development Rate

Homozygous L1 worms were grown at 16°C, 20°C or 25°C for 3 days (5 days for 16°C). Adult worms were picked to fresh NGM plates and allowed to lay eggs for 3 hours. The adults were removed, and the embryos grown at the same temperature. Embryo hatching was scored by visible light stereoscope every 6 hours for 36 hours. For worm strains carrying the *dna-2* mutation, homozygous -/- worms grown from the L1 stage at 16°C, 20°C or 25°C were the first generation progeny from *dna-2*(+/-) heterozygotes.

3.15 Representation of Statistical Significance

P values were calculated throughout using the Graphpad Prism software, using the appropriate statistical method (such as ANOVA or t-test) and correcting for multiple comparisons as described previously. Data were considered statistically significant (and the null hypothesis rejected) if a calculated P value was smaller than 0.05. Asterisks are used to indicate P values. * = P<0.05, ** = P<0.01, *** = P<0.001, **** = P<0.0001.

4 The Effect of *CTC1* Loss on Human Cell Growth and Telomere Homeostasis

Much of the following work was performed using an HCT116 cell line modified by the laboratory of Carolyn Price to carry an inducible homozygous deletion of *CTC1*. The aim of this chapter was to establish this cell line as a model for *CTC1* deletion in our laboratory, confirming preliminary data characterising the effect of *CTC1* loss on the telomere and cell growth conveyed to us by Carolyn Price. The inducible *CTC1* deletion in the HCT116 cell line uses the (ER)Cre-lox system. Introns flanking exon 5 of *CTC1* were edited to include loxP sites. loxP sites are 34bp sequences originating from the bacteriophage P1 that are capable of being recombined by the Cre recombinase. Recombination results in the looping out and deletion of the DNA tract between the two sites [241]. In HCT116 $CTC1^{lox/lox}$ cells deletion of the DNA tract results in the loss of exon 5 as well as the formation of a premature termination codon. Cre recombinase is constitutively expressed in these cells, but it is fused to a ligand-binding domain of the human oestrogen receptor. As a result the Cre recombinase is retained in the cytoplasm, but enters the nucleus upon interaction with the ER-binding drug tamoxifen. Knockout of *CTC1* can be achieved simply by exposing the $HCT116^{lox/lox}$ cells to 10 nM tamoxifen in the culture media.

To confirm the deletion of the *CTC1* exon 5 locus by the Cre-loxP system cells were exposed to 10 nM tamoxifen for 0 to 8 days, before the locus was assayed by PCR using primers that flanked one of the loxP sites. The PCR products were run on an agarose gel and the successful deletion of the locus confirmed (Fig. 21a). Whilst some PCR product is still detectable at days 2-8 (indicating incomplete deletion of *CTC1* in the population), this method is only semi-quantitative. Band intensity of tamoxifen-free samples is likely to be limited due to exhaustion of the PCR reaction, and the true frequency of locus retention in tamoxifen-treated samples lower than appears. To address this, non-recombined *CTC1* mRNA level at day 2 was assayed by qPCR using primers that were specific to the boundary of exon 4 and exon 5. Full *CTC1* mRNA was determined to be reduced by greater than 90% (Fig. 21b). In conclusion, deletion of *CTC1* is efficient and highly penetrative.

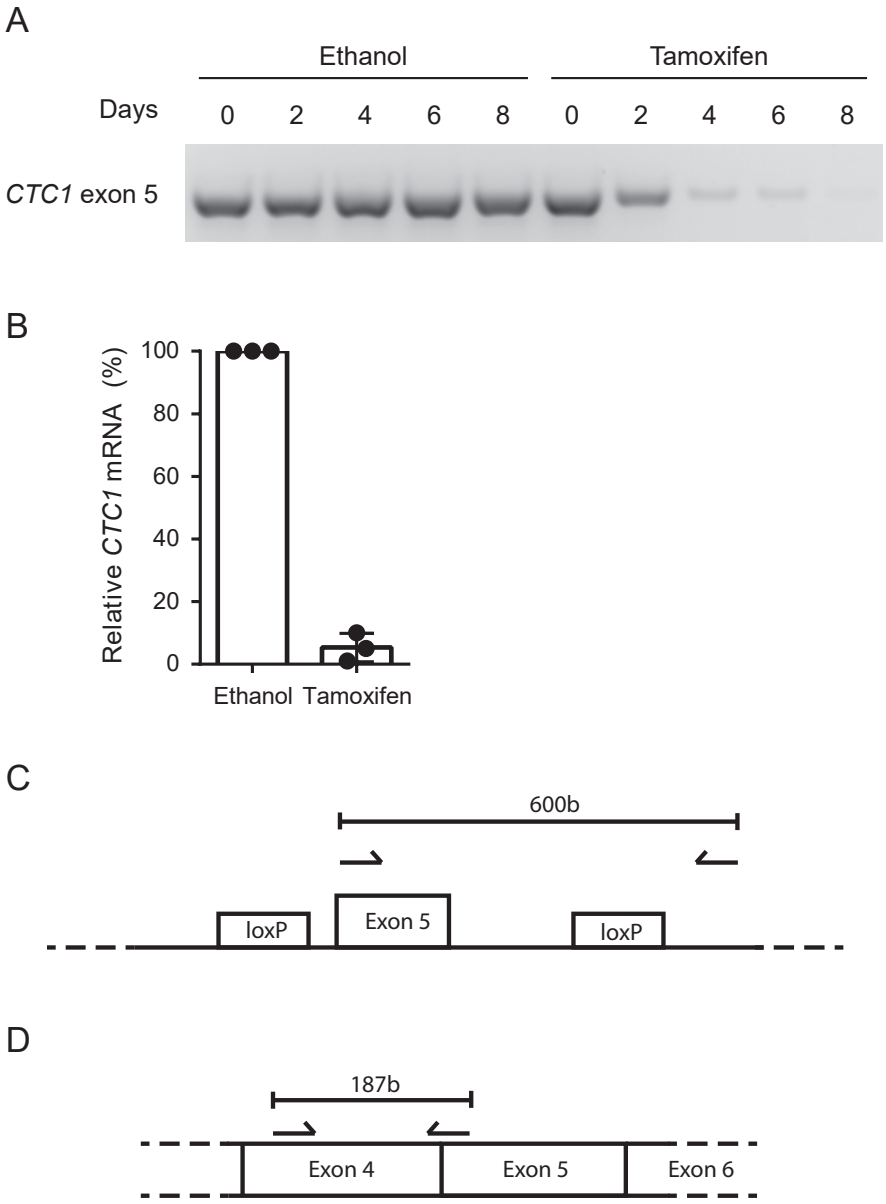

Figure 21. Knockout of *CTC1* in *CTC1*$^{lox/lox}$ HCT116 cells by 10 nM tamoxifen exposure (1:2000 ethanol was used as a vector control). (A) Deletion of the loxP-flanked *CTC1* exon 5 locus was semi-quantitatively assayed by PCR. (B) Relative *CTC1* mRNA levels after 2 days exposure to 10 nM tamoxifen was measured by qPCR. Bars represent standard deviation between 3 separate experiments (Biological repeats collected separately and analysed simultaneously). (C) Diagram of *CTC1* exon 5 locus and intronic loxP sites with forward and reverse PCR primer locations indicated as used in (A). (D) Diagram of *CTC1* mRNA exon 4/5/6 locus with forward and reverse primer locations indicated as used in (B). The forward primer was located within exon 4 and the reverse primer was located across the exon4/5 boundary.

4.1 Loss of *CTC1* Results in a Growth Defect

The Price lab reported a strong, albeit delayed, growth defect in HCT116 cells after *CTC1* knockout by addition of tamoxifen. In order to confirm this effect, 10 nM tamoxifen was added to the HCT116 *CTC1*$^{lox/lox}$ culture media. Tamoxifen is a common endocrine therapeutic agent used in cancer treatments that is capable of blocking oestrogen receptors and affecting cell growth. HCT116 cells do not express ER-α, but do express ER-β. However, no effect of oestrogen on HCT116 cell growth rate has been reported [246]. In order to be sure the loss of *CTC1* was the controlling growth factor and not the presence of tamoxifen, a control HCT116 cell line that did not contain loxP sites were exposed to tamoxifen. As ethanol was used as the vector for tamoxifen, both cell lines were also exposed to 1:2000 ethanol as an additional control. Cells were counted and passaged every 2-3 days.

A slight decline in population doubling rate in the tamoxifen treated HCT116$^{lox/lox}$ cell line was detectable by day 6 (Fig. 22). This decline continued until day 12, at which point growth between time points became very limited. In contrast, neither the ethanol treated *CTC1*$^{lox/lox}$ or either of the wild-type *CTC1* cell line cultures demonstrated any growth defect. These data are congruent with that reported by the Price lab [182].

4.2 *CTC1* Deletion Induces Telomere C-strand Shortening

Following the DNA replication process the telomere's 3′ G-rich strand is extended by telomerase, and the C-rich strand is potentially resected by exonucleases. This ssDNA overhang can attract DDR factors. In order to maintain the dsDNA structure of the majority of the telomere, and to limit the production of ssDNA, data from the Price lab suggest that a major role of CTC1 in human cells is in telomeric C-strand fill-in. They report knockout of *CTC1* results in gradual loss of telomeric C-rich DNA. As *CTC1* is known to interact with polymerase α-primase [247], they propose the role of CTC1 is in the promotion of C-rich strand fill-in.

CTC1 deletion was induced and the abundance of C-rich telomeric DNA was measured after 10 days by PNA probe FISH. 10 days was chosen as the timepoint to maximise the impact of *CTC1* deletion before cell growth became severely limited and metaphase spread generation would become more difficult (with fewer cells in mitosis). Fluorophore-tagged PNA probes bind to their target DNA highly efficiently and with linear proportionality. As such target abundance can be inferred directly from fluorescent microscopy of PNA probe signal intensity. Telomeric C-rich DNA 10 days after *CTC1* knockout-induction was reduced significantly (Fig. 23).

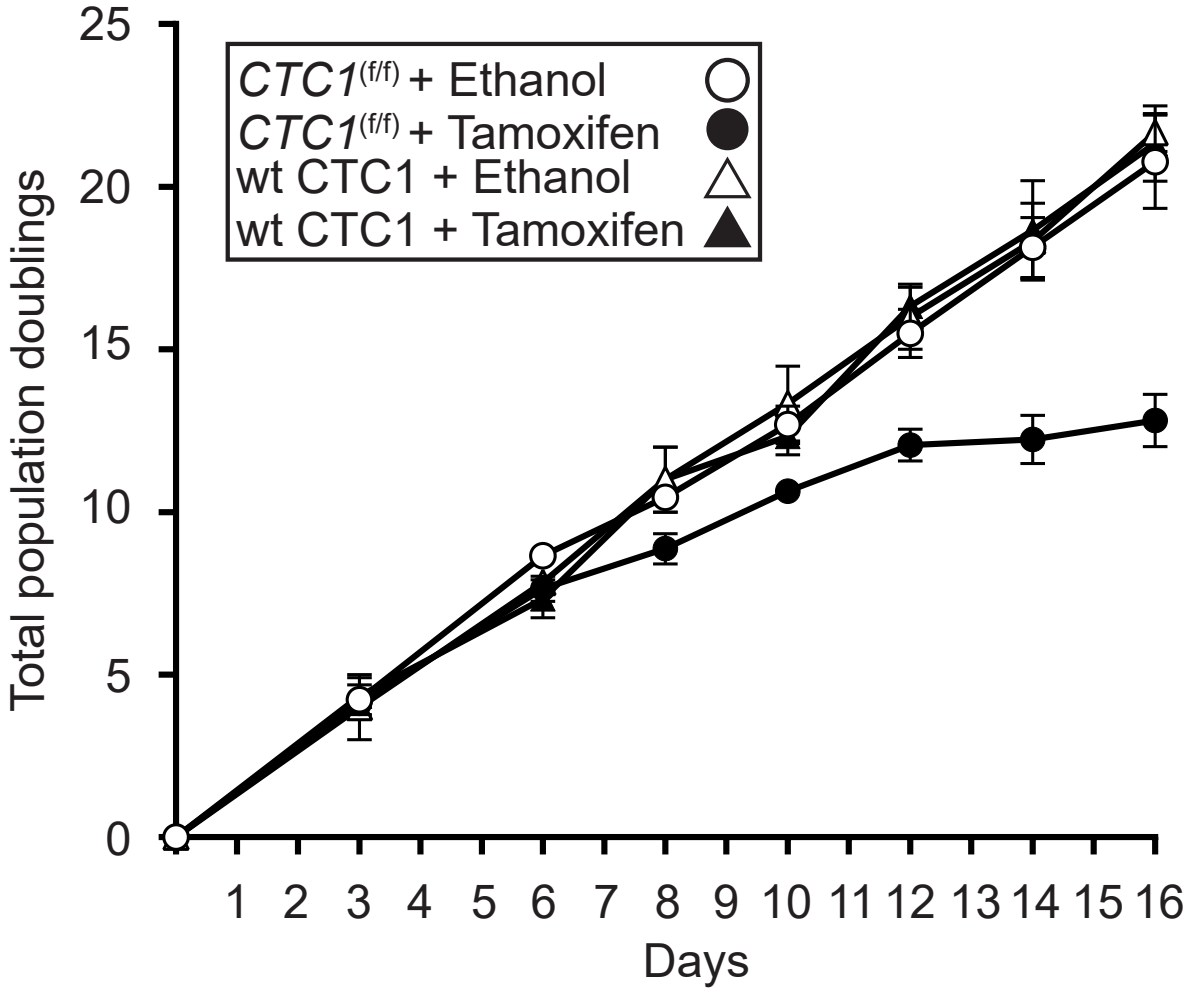

Figure 22. Growth defect after deletion of *CTC1*. Deletion of *CTC1* from $CTC1^{lox/lox}$ HCT116 cells was induced by addition of 10 nM tamoxifen to the culture media (1:2000 ethanol used as a vector control). Cells were counted and passaged after 2-3 days. HCT116 cells without *loxP* sites were also treated with 10 nM tamoxifen as a control. Bars represent standard deviation between 3 experimental repeats.

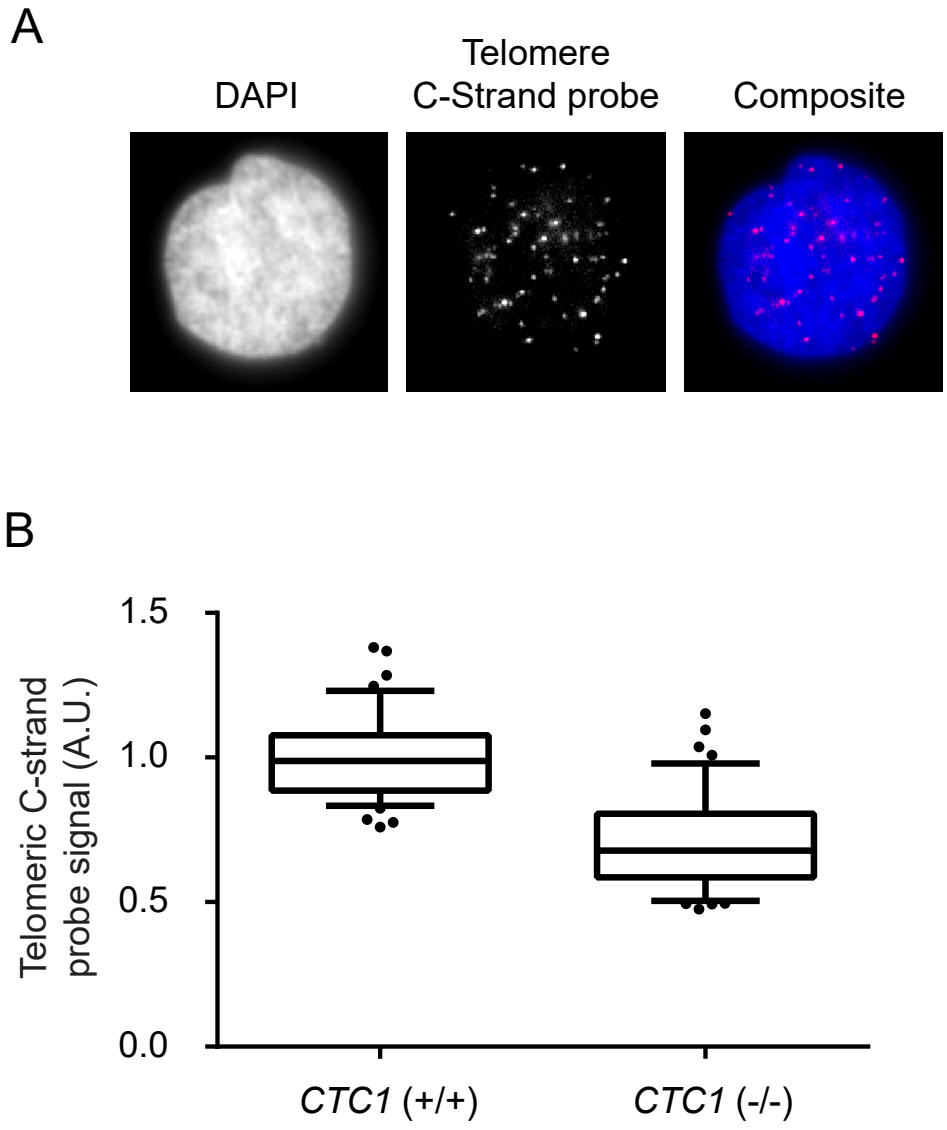

Figure 23. Reduction in telomeric C-strand signal 10 days after *CTC1* knockout. Deletion of *CTC1* from $CTC1^{(lox/lox)}$ HCT116 cells was induced by addition of 10 nM tamoxifen to the culture media (1:2000 ethanol used as a vector control). Total telomeric signal per nucleus was measured by PNA-probe FISH at day 10. (A) Representative fluorescent images of a $CTC1^{+/+}$ HCT116 cell. (B) Quantification of telomeric C-strand probe signal per nucleus. n >350 nuclei per sample.

4.3 Discussion

This chapter confirms pre-publication data reported to us by the Price lab, ensuring that the model cell-line that was to be worked with behaved as expected. The Price lab data are now published as of May 2017 [182]. The cells were received with a mycoplasma infection, and as such it was particularly important to replicate the reported *CTC1*Δ phenotypes after mycoplasma elimination.

The deletion of the exon 5 locus of *CTC1* quickly achieved high penetrance in the population under these conditions as indicated in figure 21. Tamoxifen is a chemotherapeutic ER ligand that inhibits ERα and ERβ activation and the subsequent proliferative or anti-proliferative (respectively) signal by blocking the receptor binding sites. HCT116 cells, being colorectal carcinomas, express ERβ but not ERα. Consequently 10 nM tamoxifen, were it to have any effect on cell proliferation at all, would likely promote cell growth and not inhibit it. Oestrogen has however been reported to not effect HCT116 cell growth, even at significantly higher concentrations than used here [246]. Despite this, it was important to ensure that tamoxifen was not affecting the growth of HCT116 cells in a way that might be enhancing or masking a growth defect. As shown in figure 22, 10 nM tamoxifen did not affect cell growth in control cells. In contrast, cells containing the *CTC1*$^{\text{lox/lox}}$ system had the gradually increasing growth defect described by the Price lab. From this we can be confident that the growth defect is induced by the loss of *CTC1*. The gradual development of the growth defect is consistent with a telomeric defect, as genome-protective cellular senescence becomes more and more frequent as the telomeres of cells in the population shorten.

The Price lab reported a shortening of of the C-rich strand of the telomere after *CTC1* knockout in the HCT116 *CTC1*$^{\text{lox/lox}}$ cell-line. They proposed the essential role of *CTC1* was in C-strand fill in, based on the gradual loss of the C-strand and the previously reported interaction of *CTC1* with polymerase-α primase. Here those data are replicated, showing the average amount of telomeric C-strand signal per nucleus is reduced significantly 10 days after the *CTC1* knockout was initiated. Combined with the growth data, the *CTC1* inducible knockout cell line appears to be an effective and consistent model for examining the function of *CTC1*.

5 Investigating the Effect of *CTC1* Deletion on Genomic Stability and Checkpoint Activation

What has become clear is that the roles of the CST complex and its components extend beyond the telomere and into the wider genome. For example STN1 has been demonstrated to support replication restart at stalled forks during DNA replication [173] (albeit limited to GC-rich regions) through the recruitment of RAD51 [185]. Distinguishing telomeric impacts of *CTC1* loss from genome-wide impacts however is not straightforward. It has been reported that loss of *CTC1* in *Arabidopsis* induces chromatin bridges [119] (a marker of genomic instability). This appears to be a result of telomere uncapping as *CTC1* loss in *Arabidopsis* induces frequent telomere fusions, a precursor of chromatin bridge formation. Additionally, inhibition of telomere fusions in *ctc1* mutant *Arabidopsis* (by eliminating end-joining pathways) restores normal plant growth [248]. In contrast to this, whilst chromatin bridges have been reported in *CTC1* partial knockdown human cell lines [173], very few chromosome fusions were reported in *CTC1*$^{-/-}$ cells [182]. An additional complicating factor is that previously reported phenotypes of *CTC1* depletion appear to differ significantly depending on the efficiency of the knockdown and whether the knockdown was stable or acute [173] (For example acute knockdown of *CTC1* by small interfering RNA (siRNA) in HeLa S3 cells increased the frequency of chromosomes with telomere signal-free ends, but this was not seen in sh*CTC1* or sh*STN1* HeLa clones). The goal of this chapter is to examine the nature of the genomic instability observed in *CTC1*$^{-/-}$ HCT116 cells in order to elucidate telomeric from non-telomeric impacts of the loss of *CTC1*.

5.1 Loss of *CTC1* Induces Genomic Instability

One marker for genomic instability is the presence of micronuclei [249]. Micronuclei are small nuclei outside of the main nucleus of the cell. They contain DNA that was not incorporated into one of the two daughter nuclei formed during cell division. The root cause of micronuclei formation is typically one of three events: a chromosome failed to correctly attach to the mitotic spindle and was subsequently not pulled into one of the two new daughter nuclei (Fig. 24a); incorrectly repaired DNA DSBs generated a dicentric chromosome and a centromere-free chromosome fragment that cannot attach to the mitotic spindle (Fig. 24b); or telomeric fusions result is a dicentric chromosome that is pulled in two directions simultaneous, trapping DNA in the cytoplasmic space between the daughter nuclei (Fig. 24c) [250]. All three pathways mean a complete and accurate copy of the genome is not transferred to both daughter cells of the division. If the daughter cells survive the event this can result in a wide spectrum of diseases, from developmental disorders (due to chromosome aneuploidy) to cancers (due to loss or gain of function mutations in tumour suppressors and oncogenes). Micronuclei are a simple

marker for a catastrophic failure in the maintenance of a cell's genomic integrity.

To assess whether the loss of *CTC1* increases micronuclei frequency in HCT116 cells, deletion of *CTC1* was induced. Four days after *CTC1*$^{lox/lox}$ knockout induction micronuclei frequency increased approximately 3 fold (Fig. 26). This change was suppressed in the exogenous *CTC1*-rescue cell line. These data imply an important role for *CTC1* in maintaining genomic integrity in human cells.

The *CTC1* knockout micronuclei phenotype shows a significant compromise to genomic stability after the loss of *CTC1*. What remained unclear is the nature of the micronuclei formation; micronuclei could be indicative of a chromosome-spindle assembly error, telomeric fusions, or DSB repair errors/failure [250]. As shown in Fig. 24, the different pathways of micronuclei formation produce distinguishable patterns of chromatin bridges and telomere/centromere segregation. Spindle binding errors can produce micronuclei by proceeding through anaphase with a kinetochore connected to both spindle poles (referred to as a merotelic kinetochore), which as a result lags behind the other chromosomes. This produces no chromatin bridges, but does produce a micronucleus containing both centromeric and telomeric DNA (Fig. 24a). Incorrect repair of DSBs can result in the production of dicentric and acentric chromosomes (Fig. 25). If this happens then during anaphase the dicentric chromosome is pulled in two directions simultaneously, producing a (non-telomeric) chromatin bridge. The acentric chromosome is pulled towards neither pole, and subsequently forms a micronucleus containing telomeres but not centromeres (Fig. 24b). Additional micronuclei may form when the chromatin bridge is broken, but these will contain no telomeric or centromeric signal. The production of micronuclei by telomere fusion-induced dicentric chromosomes can be distinguished from the above pathways by identifying the presence of their precursor, chromatin bridges that contain telomeric signal. These telomere-positive chromatin bridges will form telomeric (but not centromeric) micronuclei when they break and leave DNA trapped outside the daughter nuclei (Fig. 24c).

To assess the origin of *CTC1* knockout-induced micronuclei, *CTC1* knockout was induced in HCT116 cells and the micronuclei/chromatin bridges produced were probed for telomeric and centromeric content by PNA probe FISH. The predominant class of micronucleus present both before and after *CTC1* knockout contained telomeric but not centromeric DNA (Fig. 27). At 4, 8 and 12 days post *CTC1* knockout approximately 15% of all nuclei had adjacent micronuclei containing only telomeric signal (Fig. 27b). This is an approximately 6-fold change compared to 2.5% of nuclei at day 0. Micronuclei containing only centromeric probe signal were very rare and the was no significant change in their frequency (Fig. 27c). Micronuclei containing both telomeric and centromeric DNA were 10-fold less frequent than micronuclei with only telomeric signal, but there was a significant increase in their frequency from approximately 0.4% of nuclei at day 0 to 1.5% at day 12 (Fig. 27d). Micronuclei containing neither telomeric nor centromeric signal were also significantly increased at days 4 and 12, but again at a much lower frequency than

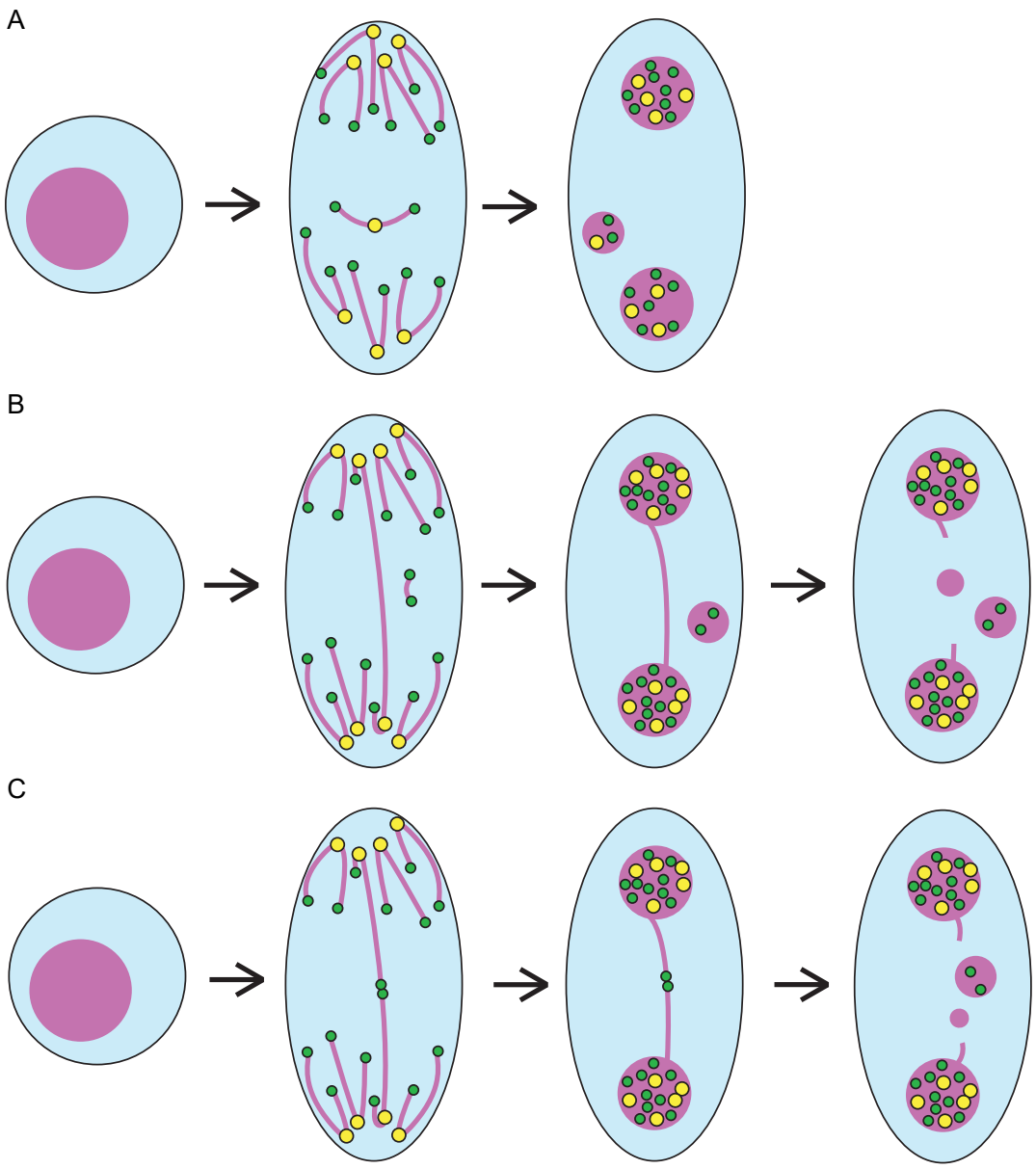

Figure 24. Pathways of Micronucleus and Chromatin Bridge Formation. Telomeres are indicated in green, centromeres are indicated in yellow. (A) A chromosome is inappropriately attached to the mitotic spindle (such as being attached to both spindle poles) and lags behind the group of correctly attached chromosomes during anaphase. (B) Incorrect repair of DSBs can produce dicentric and acentric chromosomes (as shown in figure 25). The acentric chromosome is unable to attach to the mitotic spindle and as such is not pulled towards either pole during anaphase. Consequently it is not integrated into either of the daughter nuclei. The dicentric chromosome is pulled towards both poles simultaneously and as such produces a chromatin bridge. This bridge can also form additional micronuclei if/when the bridge is broken. (C) The fusion of telomeres can produce a multi-centric chromosome that is pulled towards both poles simultaneously during anaphase, forming a chromatin bridge. This chromatin bridge is discernible from the kind described in *B* as it contains telomeric DNA. As above, breakage of this telomeric chromatin bridge can produce micronuclei. Figure adapted from Fenech et al., 2011 [250].

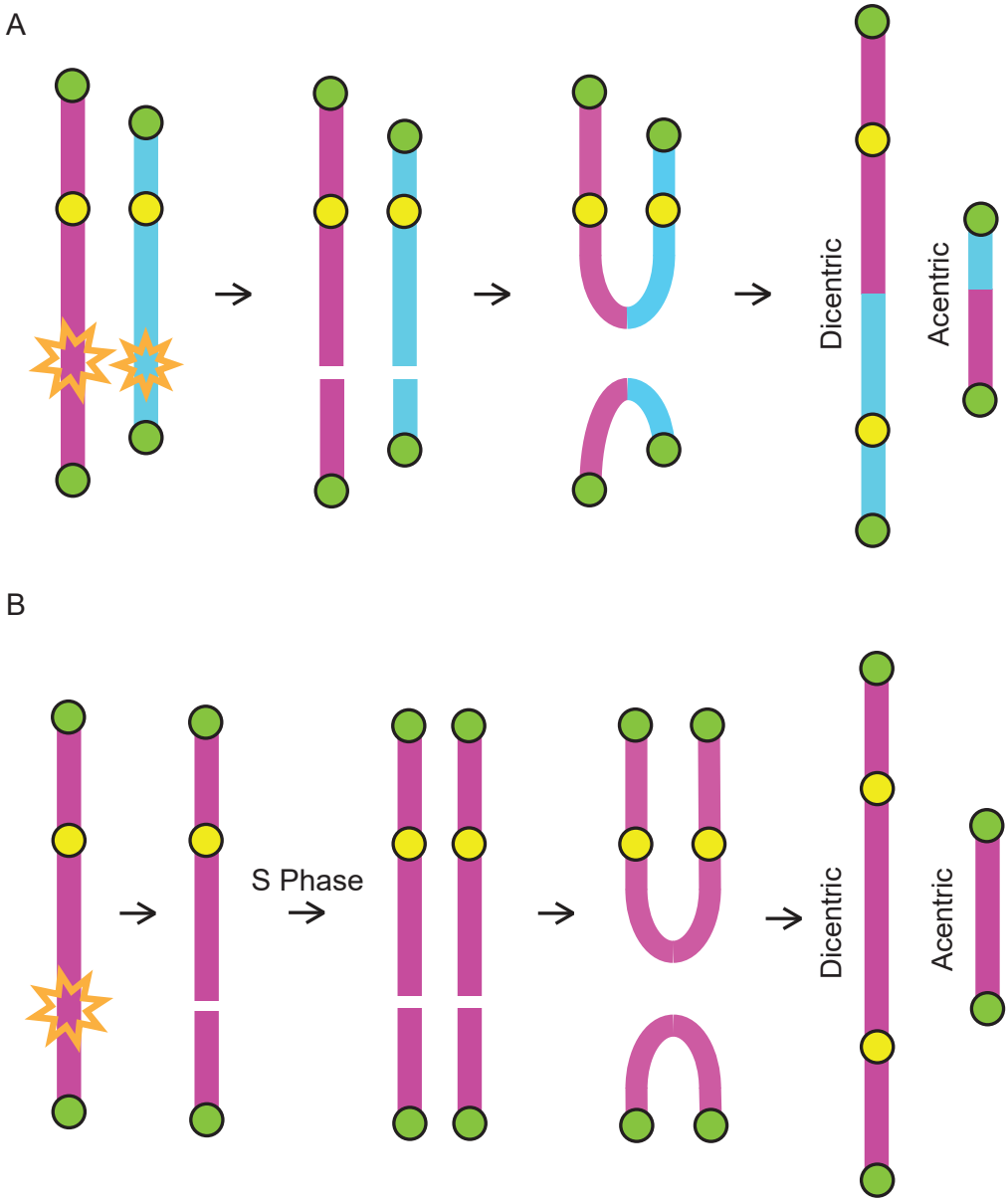

Figure 25. Formation of Dicentric and Acentric Chromosomes from DSB Repair Errors. When DSBs occur the two ends of the break must be re-ligated. (A) If an error-prone repair mechanism is used to repair multiple blunt breaks simultaneously the the fusion of chromosomes is possible. (B) If a cell with a single DSB fails to arrest and enters S-phase, then one broken chromatid becomes two broken chromatids, and these sister chromatids may be inappropriately ligated together. Telomeres are indicated in green, centromeres are indicated in yellow. Figure partially adapted from Fenech et al., 2011 [250].

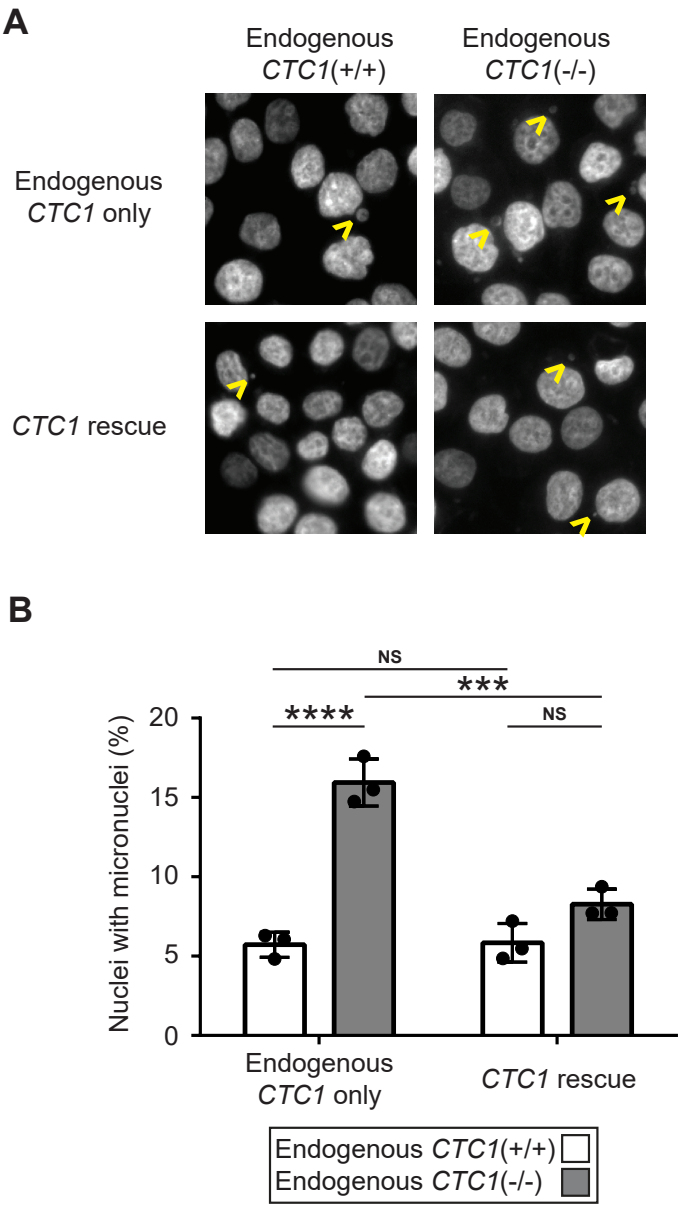

Figure 26. Formation of micronuclei following *CTC1* knockout in HCT116 cells. Deletion of *CTC1* from HCT116 cells was induced by addition of 10 nM tamoxifen to the culture media (1:2000 ethanol used as a vector control). After 4 days cells were fixed on coverslips and stained with DAPI. Micronuclei frequency was scored blind from 20x magnification widefield fluorescent microscopy images. (A) Representative fluorescent images of micronuclei in HCT116 cells. Yellow arrowheads indicate micronuclei. (B) Quantification of the frequency of micronuclei. Bars represent standard deviation between three experimental repeats. Statistical significance was performed by two-way ANOVA correcting for multiple comparisons (Tukey's method).

telomere-only micronuclei (Fig. 27e).

The dominant presence of micronuclei with only telomeric signal from day 4 suggests the primary cause of micronuclei in *CTC1*$^{-/-}$ cells is either a global DSB repair defect, or telomeric fusions. The Price lab reported an insignificant effect of *CTC1* knockout on telomere fusion frequency [182] which suggests the former pathway is likely the cause. This can be confirmed by examining chromatin bridge frequency and content. The increase in micronuclei containing neither telomeric nor centromeric DNA could be explained by either telomere fusions or DSB repair errors as they are a product of chromatin bridge breakage. Despite representing only a small portion of total micronuclei, the approximately 3-fold change in the frequency of micronuclei containing both telomeric and centromeric DNA was significant. Mis-segregation of whole chromosomes means the SAC failed to ensure all chromosomes are attached to the mitotic spindle correctly before entering anaphase. This suggests that whilst spindle assembly errors are very rare in HCT116 cells, *CTC1* knockout does negatively impact the ability of the SAC to control chromosome segregation.

The main impact of *CTC1* knockout on genomic stability appears to involve DSB repair failure rather than telomere fusions (based on the logic above), but in order to rule out telomere fusions, chromatin bridges in *CTC1*$^{-/-}$ HCT116 cells were probed for telomeric DNA. As expected from the micronuclei data, 4 days after knockout induction the frequency of telomeric signal-free chromatin bridges increased from approximately 1 bridge per 100 nuclei to more than 5 bridges per 100 nuclei (Fig. 28). A more than 5-fold increase. The frequency of telomeric chromatin bridges at this time-point was effectively 0 in both control and *CTC1*$^{-/-}$ cells. 10 days after *CTC1* knockout induction chromatin bridges staining positive for telomeric signal occurred approximately 1.5 times per 100 *CTC1*$^{-/-}$ nuclei scored. These data suggest loss of *CTC1* in human cells can induce telomere fusions (as telomeric signal appears to be located between two centromeres on a dicentric chromosome, see figure 24b), however these fusions appear at a relatively low frequency. The telomeric bridges also do not appear until relatively late compared to the bulk of *CTC1*$^{-/-}$-induced chromatin bridges and micronuclei. From this data we can conclude the bulk of the genomic instability induced by loss of *CTC1*, particularly at early time-points, is most likely a result of global DNA repair errors and not a telomere-specific phenotype.

Figure 27 . Telomeric and centromeric DNA in *CTC1*-deletion induced micronuclei. Deletion of *CTC1* from HCT116 cells was induced by addition of 10 nM tamoxifen to the culture media (1:2000 ethanol used as a vector control). After 4, 8 or 12 days cells were fixed on coverslips and probed with telomeric C-strand and centromere specific PNA probes. Micronuclei content was scored blind from 60x magnification widefield fluorescent microscopy images. (A) Representative fluorescent images of a *CTC1*$^{-/-}$ (day 12) HCT116 nucleus. White arrowhead indicates micronucleus containing both telomeric and centromeric DNA. (B) Quantification of the frequency of micronuclei containing telomeric but not centromeric DNA. (C) Quantification of the frequency of micronuclei containing centromeric but not telomeric DNA. (D) Quantification of the frequency of micronuclei containing both telomeric and centromeric DNA. (E) Quantification of the frequency of micronuclei containing neither telomeric nor centromeric DNA. Bars represent standard deviation between three experimental repeats. Statistical significance was performed by two-way ANOVA correcting for multiple comparisons (Sidak's method).

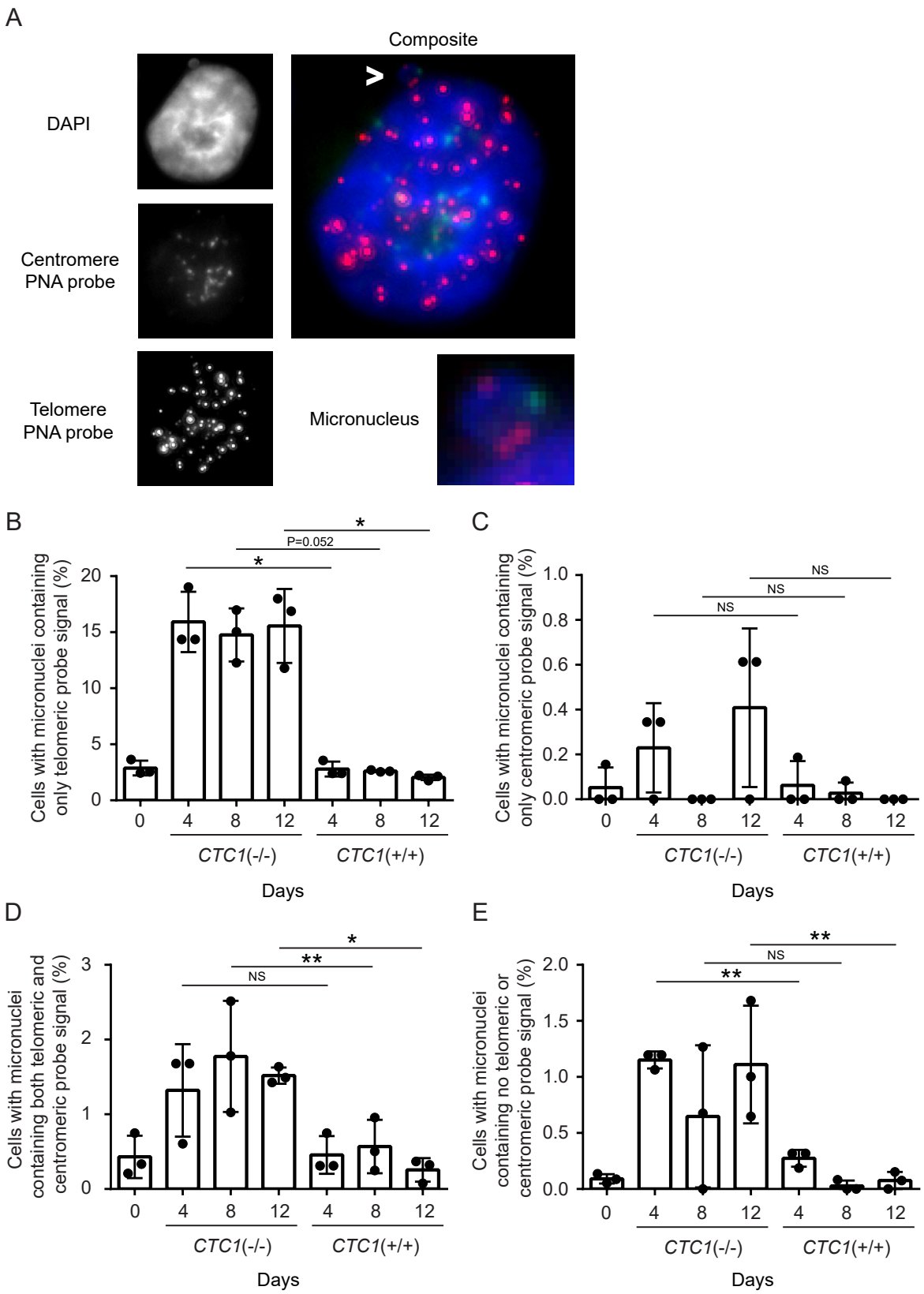
A
Composite
DAPI
Centromere PNA probe
Telomere PNA probe
Micronucleus
B
Cells with micronuclei containing only telomeric probe signal (%)
P=0.052
*
0
4
8
12
CTC1(-/-)
CTC1(+/+)
Days
C
Cells with micronuclei containing only centromeric probe signal (%)
NS
D
Cells with micronuclei containing both telomeric and centromeric probe signal (%)
**
E
Cells with micronuclei containing no telomeric or centromeric probe signal (%)

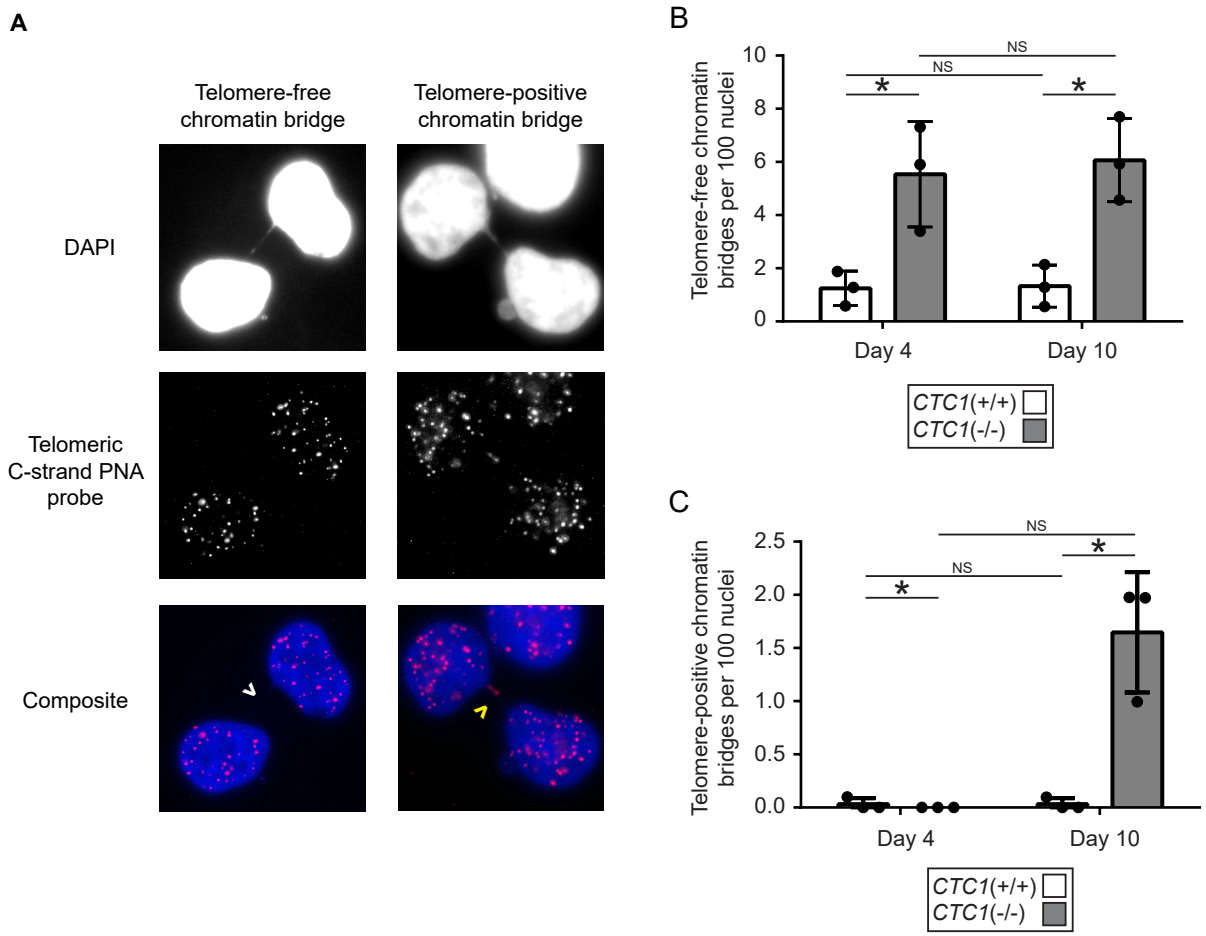

Figure 28. Telomeric chromatin bridges in *CTC1*$^{-/-}$ HCT116 cells. Deletion of *CTC1* from HCT116 cells was induced by addition of 10 nM tamoxifen to the culture media (1:2000 ethanol used as a vector control). After 4 or 10 days cells were fixed on coverslips and probed with a telomeric C-strand specific PNA probe. Telomere signal on chromatin bridges was scored blind from 60x magnification widefield fluorescent microscopy images. (A) Representative fluorescent images of *CTC1*$^{-/-}$ (day 10) HCT116 nuclei. The white arrowhead indicates a non-telomeric chromatin bridge. The yellow arrowhead indicates a telomeric chromatin bridge. (B) Quantification of the frequency of non-telomeric chromatin bridges at day 4 and day 10. (C) Quantification of the frequency of telomeric chromatin bridges at day 4 and day 10. Bars represent standard deviation between three experimental repeats. Statistical significance was performed by two-way ANOVA correcting for multiple comparisons (Tukey's method).

5.2 Checkpoint Activation after Knockout of Human *CTC1* Differs from Checkpoint Activation by *cdc13-1* in *Saccharomyces cerevisiae*

S. cerevisiae CTC1 homologue *CDC13* has a well-characterised mutant allele *cdc13-1*. *cdc13-1* is a temperature sensitive mutant, at the non permissive temperature (>30°C) ssDNA accumulates and a checkpoint-dependant G2/M arrest is induced [251]. This arrest can be bypassed for multiple cell cycles by the deletion of *CHK1* [252]. Telomere damage induced by *cdc13-1* activates the Mec1 kinase (homologue of human ATR) which, via the adapter protein Rad9, results in the phosphorylation of Chk1 [253][254] (Rad9 also activates Rad53, the budding yeast homologue of CHK2, which inhibits degradation of the uncapped telomere [255]). Activated Chk1 mediates cell-cycle arrest via phosphorylation of Pds1 [256]. In human cells ATR is activated like Mec1 in response to ssDNA, which phosphorylates (both directly and indirectly) CHK1. The primary effect of CHK1 phosphorylation is the phosphorylation of CDC25, resulting in its inhibition and degradation. Inhibition of CDC25 leads to increased inhibitory phosphorylation of CDK-cyclin complexes and cell cycle progression is stopped [257]. It has been reported that populations of $CTC1^{-/-}$ cells have a slight increase in G2 cells after 20 days [182], which suggests Chk1-mediated arrest seen in budding yeast might be mirrored in human $CTC1^{-/-}$ cells.

In order to determine if a bypass of human CTC1 dependence could be achieved by inhibiting CHK1, *CTC1* knockout was induced and six days later the relative population size was compared to that of a $CTC1^{+/+}$ culture. Six days was chosen as it is the first time-point at which a statistically significant change in growth rate can be detected. Cells were exposed simultaneously to CHK1 inhibitor CCT245737 ranging from 0 to 5 μM, covering the range of concentrations CCT245737 has been reported to be effective at in cell culture [258] and including the concentration at which CCT245737 appeared

---

Figure 29 . Checkpoint protein CHK1 is not activated after loss of *CTC1*. 4, 8 or 12 days after *CTC1* knockout by addition of 10 nM tamoxifen the culture media (or 1:2000 ethanol as a vector control), whole cell protein lysates were collected from HCT116 cells. CHK1 total levels and serine 296 phosphorylation status was assayed by Western blot. Histone H3 was used as a loading control. (A) Representative Western blot of CHK1 total levels and serine 296 phosphorylation status. 3 mM Hydroxyurea (6 hours) was used as a positive control for detection of CHK1 phosphorylation. (B) Quantification of P-CHK1 (s296) signal normalised to loading control histone H3 and day 0. (C) Quantification total CHK1 signal normalised to loading control histone H3 and day 0. Bars represent standard deviation between three experimental repeats. Quantifications were performed using the FIJI distribution of ImageJ analysis software. Statistical significance was performed by two-way ANOVA correcting for multiple comparisons (Sidak's method).

A

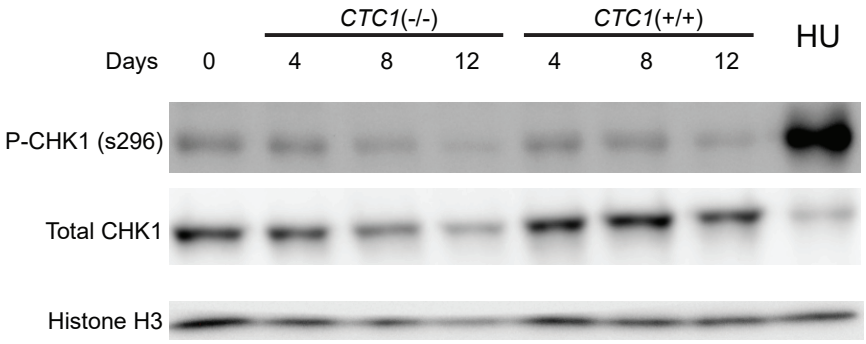
CTC1(-/-)
CTC1(+/+)
HU
Days
0
4
8
12
4
8
12
P-CHK1 (s296)
Total CHK1
Histone H3

B

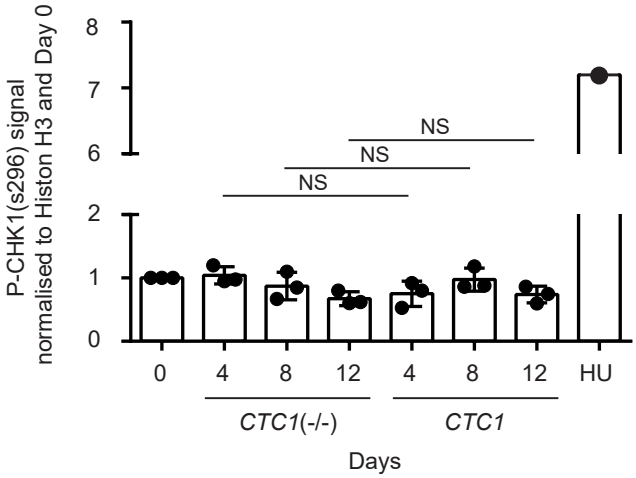
P-CHK1(s296) signal
normalised to Histon H3 and Day 0
8
7
6
2
1
0
NS
NS
NS
0
4
8
12
4
8
12
HU
CTC1(-/-)
CTC1
Days

C

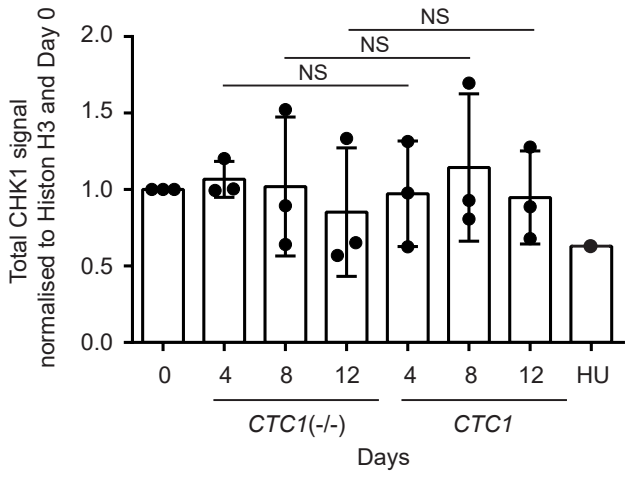
Total CHK1 signal
normalised to Histon H3 and Day 0
2.0
1.5
1.0
0.5
0.0
NS
NS
NS
0
4
8
12
4
8
12
HU
CTC1(-/-)
CTC1
Days

effective in inhibiting P-CHK1(s296) accumulation in response to etoposide (Fig. 30c). In contrast to what is seen in *S. cerevisiae*, inhibition of CHK1 was not able to rescue the growth defect of *CTC1*$^{-/-}$ cells (Fig. 30). Human CHK1 has an essential function in normal mitotic progression that can be uncoupled from the DDR [259], unlike in *S. cerevisiae* which can be completely knocked-out without stopping cell cycle progression [252]. In this sense it is perhaps unsurprising that inhibition of CHK1 in human cells is not able to positively impact cell cycle progression.

To further rule out any role CHK1 may have in the response to loss of *CTC1*, CHK1 phosphorylation at serine 296 (the autophosphorylation site of CHK1) was assayed by Western blot 4, 8 and 12 days after *CTC1* knockout. In concordance with the inability of a CHK1 inhibitor to rescue the *CTC1*$^{-/-}$ growth defect, no increase in phosphorylation of CHK1(s296) was detectable after *CTC1* knockout (Fig. 29). Taken together these data imply that unlike *cdc13-1* in budding yeast, cell cycle arrest after human *CTC1* knockout is CHK1 independent.

Whilst activation of CHK1 by ATR is necessary for the G2/M DNA damage checkpoint, ATR can also induce cell cycle arrest by activating the p53-p21 pathway [260], predominantly (but not strictly) at G1/S [261]. As *CTC1*$^{-/-}$ induced growth arrest appears CHK1-independent, the p53-p21 pathway presented a second potential candidate.

p21 is a potent inhibitor of cyclin-CDK2/CDK1/CDK4/CDK6 complexes [262][263], mediating cell cycle progression and promoting senescence. The expression of p21 can be induced in p53 dependent and independent manners (although the expression of p21 is clinically considered a marker for wild-type p53 expression [263]). To determine if the *CTC1*$^{-/-}$ growth defect involved p21, p21 protein level was assayed by Western blot. 4, 8 and 12 days after *CTC1* knockout induction whole-cell protein lysates were collected

---

Figure 30 . Treatment with CHK1 inhibitor does not rescue the growth defect of *CTC1* knockout cells. 6 days after *CTC1* knockout with 10 nM tamoxifen (the first timepoint at which the knockout growth defect is statistically significant), viable population size was measured by PrestoBlue assay. The effect of a range of concentrations of CHK1 inhibitor CCT245737 on relative viable cell count was assayed. (A) Quantification of relative viability of both *CTC1*$^{+/+}$ and *CTC1*$^{-/-}$ HCT116 cells whilst exposed to a range of concentrations of CCT245737. Bars represent standard deviation between three experimental repeats. (B) Quantification of *CTC1*$^{-/-}$ cell viability relative to *CTC1*$^{+/+}$ cells at each concentration. Bars represent standard deviation between three experimental repeats, statistical significance calculated by one-way ANOVA, correcting for multiple comparisons using Dunnett's method. (C) Western blot of CHK1 phosphorylation at serine 296 to confirm efficacy of CHK1 inhibitor CCT245737 in HCT116 cells. Cells were exposed in duplicate to 1 μM CHK1 inhibitor and/or 10 μM etoposide for 6 hours.

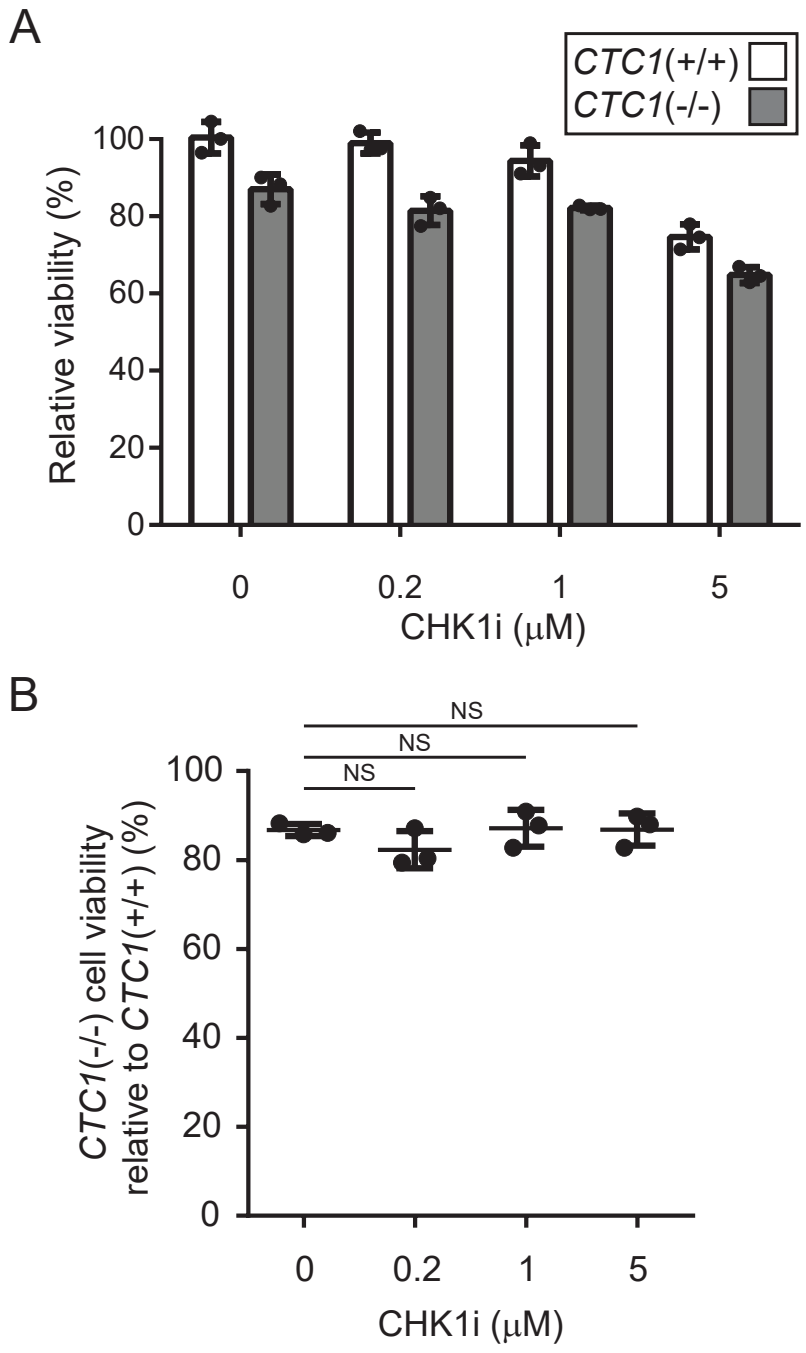
A
CTC1(+/+)
CTC1(-/-)
Relative viability (%)
100
80
60
40
20
0
0
0.2
1
5
CHK1i (μM)
B
NS
NS
NS
CTC1(-/-) cell viability relative to CTC1(+/+) (%)
100
80
60
40
20
0
0
0.2
1
5
CHK1i (μM)
C
Etoposide - - + + + +
CHK1i - - - - + +
P-CHK1 (s296)
Histone H3

from HCT116 cells and p21 expression was assayed. An increase in p21 was statistically significant by day 8, and particularly strong by day 12 (Fig. 31b). The conclusion drawn from this is that the growth defect of *CTC1* knockout is most-likely p21 mediated.

p21 can be activated in a p53 dependant and p53 independent manner; to determine if p53 was activated after *CHK1* knockout, p53 serine 15 phosphorylation and total p53 abundance was also assayed by Western blot. Like p21, p53 stabilisation was significantly increased at day 12 after *CTC1* knockout (Fig. 31d), as was its phosphorylation (Fig. 31c). These data suggest the growth defect in $CTC1^{-/-}$ cells is due to the activation of p53, promoting the expression of p21 and inhibiting CDKs.

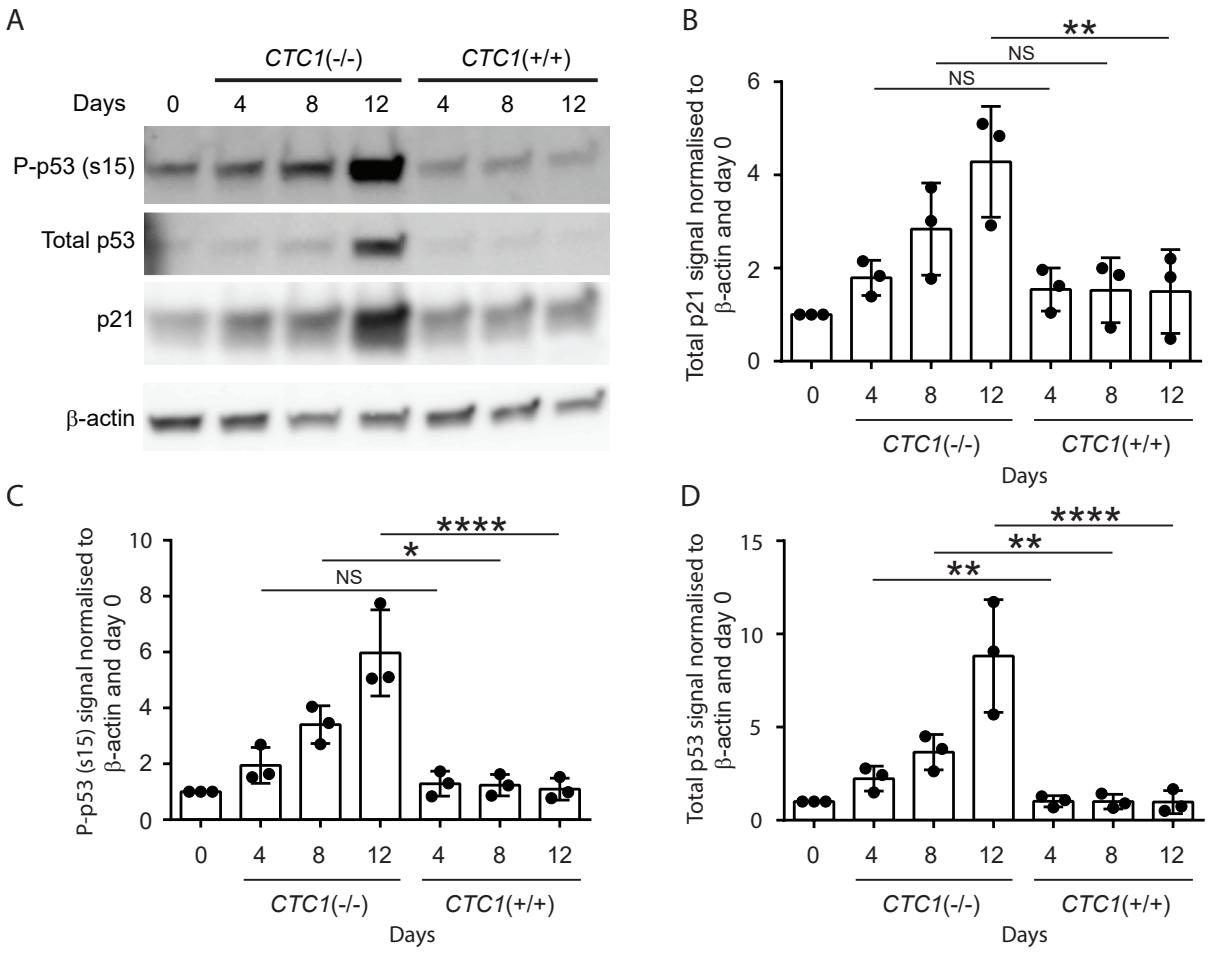

Figure 31. p53 and p21 are activated after loss of *CTC1*. 4, 8 or 12 days after *CTC1* knockout by addition of 10 nM tamoxifen the culture media (or 1:2000 ethanol as a vector control), whole cell protein lysates were collected from HCT116 cells. Total p21, total p53 and p53 s15 phosphorylation was assayed by Western blot. β-actin was used as a loading control. (A) Western blot representative of three experimental repeats. (B) Quantification of total p21 relative to β-actin. (C) Quantification of phosphorylated p53(s15). (D) Quantification of total p53. Bars represent standard deviation between three experimental repeats. Statistical significance was calculated by two-way ANOVA using Sidak's correction for multiple comparisons.

5.3 Inhibition of G-Quadruplex DNA Structures by CTC1

The human CST complex facilitates recruitment of RAD51 to GC-rich stalled replication forks, promoting fork restart [185]. It was hypothesised that this might be at least partly due to the suppression of DNA secondary structures by the CST complex. G-Quadruplexes are secondary structures formed by G-rich tracts of DNA. They can be formed by 1, 2 or 4 separate strands of oligonucleotides, but all forms rely on Hoogsteen hydrogen bonds between guanine bases of DNA or RNA [264]. G-quadruplexes occur naturally throughout the genome, particularly on the G-rich telomere strand [140]. These secondary structures have been demonstrated to inhibit the action of telomerase, polymerases, and helicases at the telomere [140].

To determine if the CST complex might be inhibiting the formation of (and/or resolving) G-quadruplex structures, G-quadruplex DNA abundance in *CTC1*$^{-/-}$ cells was assayed by immunofluorescence. *CTC1* knockout was induced and 4 days later cells were fixed and probed with anti-G4 monoclonal antibody 1H6 [265]. Interphase nuclei of *CTC1*$^{-/-}$ HCT116 cells contained an average of approximately 40% more G-quadruplex signal than *CTC1*$^{+/+}$ control cells. These data suggest than the CST complex is able to either inhibit the formation of, or resolve, G-quadruplex DNA structures. Assisting the unimpeded progression of replication forks through G-rich DNA by eliminating G4 structures is an obvious benefit to the cell, but the telomeric impacts are perhaps more nuanced. G-quadruplexes have been demonstrated to inhibit the activity of telomerase [140], but the CST complex is also a telomerase inhibitor. The CST complex is responsible for ensuring overextension of telomeric 3′ ssDNA does not occur [171], as this can attract DDR factors. In a similar way, G-quadruplexes may be one of many important balancing factors necessary for maintaining telomere homeostasis through their inhibition of telomerase, polymerases and helicases.

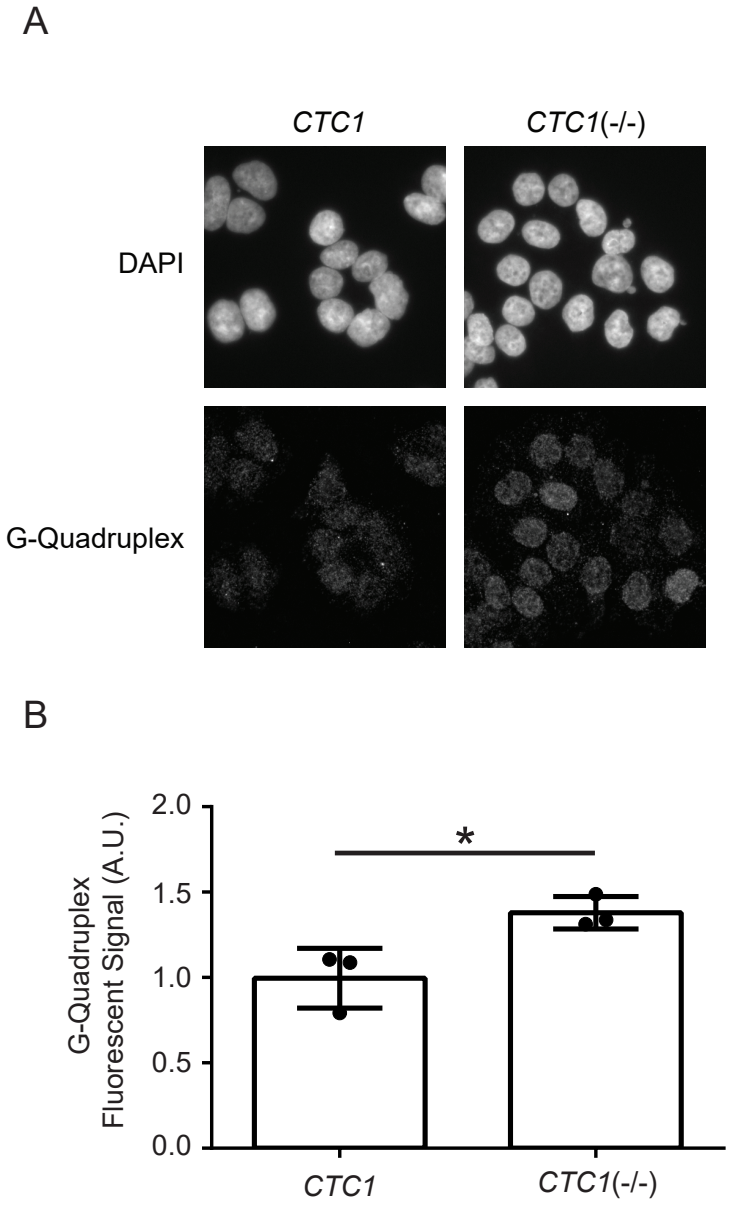

Figure 32. Increased G-Quadruplex DNA secondary structures after *CTC1* knockout. 4 days after *CTC1* knockout by addition of 10 nM tamoxifen the culture media (or 1:2000 ethanol as a vector control), HCT116 cells were fixed and stained for immunofluorescence. Images were captured by widefield fluorescent microscopy and signal quantification was performed using the FIJI distribution of ImageJ. (A) Representative fluorescent images of G-Quadruplex signal in HCT116 cells. (B) Quantification of G-Quadruplex immunofluorescent signal. Bars represent standard deviation between 3 experimental repeats. Significance calculated by student's t-test.

5.4 Discussion

This chapter uses the inducible *CTC1* knockout HCT116 cell-line to address the roles of CTC1 and the CST complex beyond the promotion of polymerase-α activity at the telomere. Non-telomeric roles for the CST complex have been previously identified by others, such as recruiting RAD51 to stalled replication forks [185]. When replicating the HCT116 *CTC1* knockout data from the Price lab, the rapid increase in micronuclei abundance was surprising; all other reported *CTC1*$^{-/-}$ phenotypes such as telomere shortening, γH2AX foci, and growth-rate decline gradually accumulated over more than 10 days. Micronuclei on the other hand were strongly apparent from as early as day 2, maintaining a consistent frequency of 15-20% after that point. The disparity in time-frames between the micronuclei and the telomeric phenotypes pointed towards separate destabilising pathways.

A small fraction of chromatin bridges and micronuclei present 10 days after *CTC1* knockout do appear to be due to telomere fusions (1 in 5 chromatin bridges contain telomeric signal (Fig. 28). Telomere fusions are typically produced by activation of the DDR at uncapped telomeres, resulting in NHEJ being used to attach the ends of two separate chromatids/chromosomes. It appears that whilst compromise to telomere homeostasis in *CTC1*$^{-/-}$ cells is inducing some genomic instability at day 10, the bulk of the instability induced by *CTC1* loss is telomere independent. At earlier time-points this non-telomeric destabilisation appears to be responsible for effectively all micronuclei formed due to the loss of *CTC1*. The high frequency of micronuclei with telomeric signal but not centromeric signal (Fig. 27), and the low frequency of telomere-positive chromatin bridges (Fig. 28) points to a DSB-repair issue (as explained in figures 24 & 25) [250]; either more DNA damage is occurring after *CTC1* knockout, or the same amount of damage is occurring but a larger portion of it is being repaired incorrectly. Loss of *CTC1* has been reported to not affect non-telomeric γH2AX frequency [266] (these data are also replicated in chapter 6), which suggests the latter could be true. *CTC1*$^{-/-}$ HCT116 cells appear to have compromised DSB repair.

Interestingly, there is a significant increase of micronuclei containing whole chromosomes in *CTC1*$^{-/-}$ cells (Fig. 27). The presence of micronuclei containing whole chromosomes is an indicator of a failure during telophase to correctly integrate them into daughter nuclei. The most common cause of aneuploidy in tumour cells is not a SAC error per se, but rather lagging chromosomes during anaphase [267] (individual chromosomes that exhibit delayed segregation during anaphase). The cause of lagging chromosomes is the presence of a persistent merotelic kinetochore, a kinetochore that is attached to microtubules originating from both spindle poles [268] (Fig. 33). As kinetochore-spindle binding occurs stochastically, merotelic kinetochores are common during the early stages of mitosis but these are typically resolved by release and re-binding in the correct orientation [268]. Both increases in formation rates and decreases in resolution rates have been reported in different aneuploid cancers [269]. It has been reported that 80% of lagging chromo-

somes in HCT116 cells result in micronuclei formation [61]. The presence of micronuclei containing whole chromosomes in *CTC1*Δ HCT116 cells therefore suggests a defect in appropriate chromosome-spindle binding is present, perhaps due to increasing the rate of kinetochore-microtubule binding, or by stabilising the binding and inhibiting the resolution of inappropriately bound merotelic kinetochores.

An increase in $\geq$4N (tetraploid) cells has been detected after *CTC1* knockout [182], indicating some mitotic slippage has occurred. Mitotic slippage is the exit of cells from mitosis into G1 inappropriately. Often this means failure to complete telophase and cytokinesis, where the mitotic spindle collapses without segregation of chromosomes into two daughter cells, forming one multi-nucleated 4N cell. This happens after persistent SAC activation (the delay required before slippage occurs can range from 4 to 20+ hours), and involves the degradation of cyclin-B by the APC [270]. Typically merotelic kinetochores do not induce persistent SAC activation as the microtubule binding requirements of the checkpoint are satisfied [268]. However, syntelic attachment (where both chromosomes are attached to the same spindle pole and not the other) does cause SAC activation and mitotic arrest, possibly due to a lack of tension applied to the kinetochores [62]. A possible model that explains the increase in both $\geq$4N cells and micronuclei containing whole chromosomes by a single mechanism is that loss of CTC1 stabilises kinetochore-spindle binding. If merotelic or syntelic kinetochores are unable to release from the mitotic spindle then they will produce lagging chromosomes or persistent SAC arrest and mitotic slippage respectively (Fig. 33). Alternatively, the accumulation of $\geq$4N cells and the formation of whole-chromosome micronuclei observed after *CTC1* knockout may be due to two separate pathways. It has been reported that chromatin bridges can cause cytokinesis to fail, resulting in binucleated cells [271]. As reported here, loss of CTC1 induces chromatin bridge formation. Therefore the origin of $\geq$4N cells may be chromatin bridge-induced cytokinesis abortion, and not spindle collapse following syntelic kinetochore binding. Notably, 4N cells produced by cytokinesis abortion result in binucleated cells (as they have passed through telophase) and not mononucleated 4N cells (which would be produced following spindle collapse [272]). The proportion of mono vs multi-nucleated $\geq$4N *CTC1*$^{-/-}$ cells is not currently known. This could be assessed by fluorescent microscopy, staining for DNA and the cytoskeleton.

No role for the CST complex at the kinetochore and/or mitotic spindle has been reported previously, however there are a number of proteins that function at both the telomere and the kinetochore. For example, shelterin component TRF1 has been found at kinetochores, and is essential there for regulating Aurora-B and ensuring proper chromosome segregation [273][274][275]. Whilst TRF1 has not been demonstrated to interact with CTC1 directly, the co-purification of STN1 with TPP1 [276] indicates physical interaction between the CST complex and shelterin does occur. Evidence for a role of CTC1 in mitosis is so far more circumstantial than direct, but is worth following up.

The G2 arrest in *cdc13-1 S. cerevisiae* is mediated largely by the Chk1 kinase pathway.

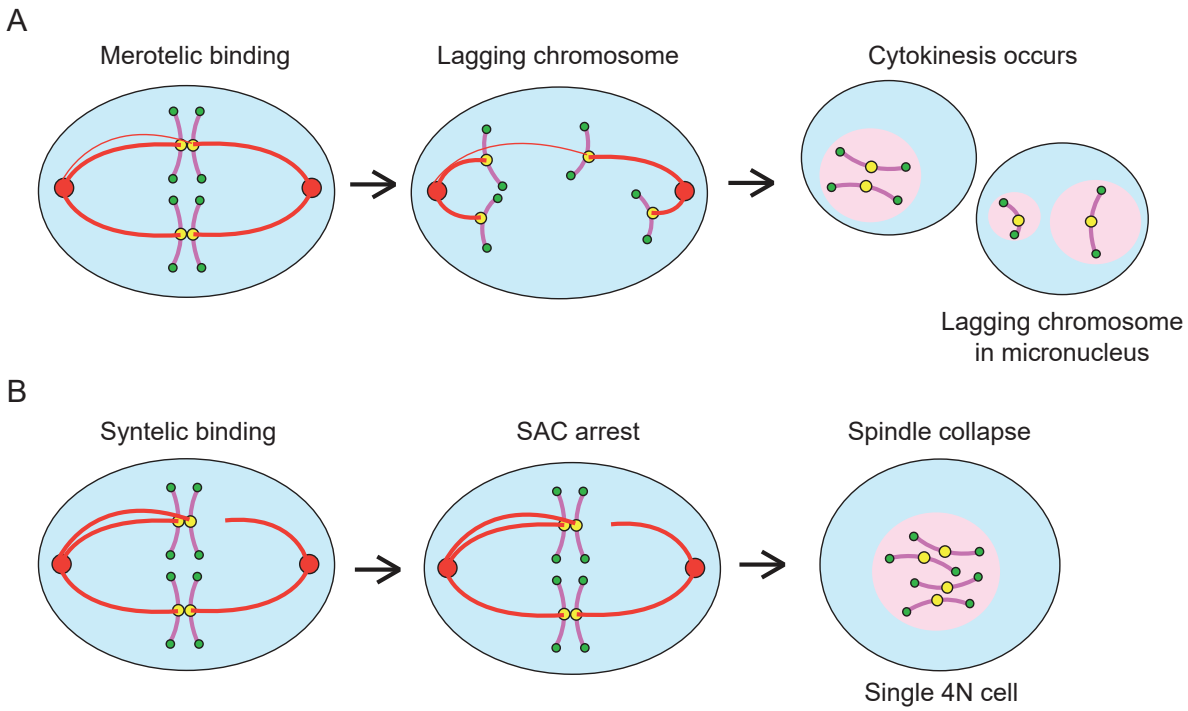

Figure 33. The effect of merotelic and syntelic kinetochores on chromosome segregation. (A) Merotelic kinetochores result in lagging chromosomes by resisting appropriate segregation towards one pole. Lagging chromosomes are frequently trapped outside the main nucleus in a micronucleus. (B) Syntelic kinetochores are thought to result in SAC activation due to a lack of tension applied to the kinetochore. Persistent SAC activation can eventually result in mitotic slippage and the generation of a single 4N cell in G_1.

Chk1 is phosphorylated and activated by Mec1 (The budding yeast homologue of ATR) and Chk1 [253]. Chk1 activated by DNA damage phosphorylates and stabilises Pds1 [277]. Subsequently Pds1 inhibits Esp1, a protease that cleaves cohesin and allows sister chromatid separation in anaphase [278]. Similar to budding yeast, the human CHK1 protein is activated through phosphorylation by ATR. RPA binds ssDNA, which recruits ATR as well as a multitude of repair factors [56]. The formation of this complex of proteins stimulates ATR to phosphorylate CHK1 at serines 317 and 345, which in turn induces CHK1 autophosphorylation of serine 296 [279]. Two of the downstream targets activated by CHK1 are the kinase WEE1 and the phosphatase CDC25C, both of which inhibit CDK1 and arrest the cell before the G2/M transition. As budding yeast *cdc13-1* triggers the activation of Chk1, and human *CTC1* knockout induces RPA accumulation at the telomere [182] (an event that typically occurs upstream of CHK1 activation), CHK1 presented the obvious candidate for mediating $CTC1^{-/-}$-induced cell cycle arrest. Instead, it appears the main pathway mediating the arrest is CHK1-independent p53/p21. p53 activation can occur downstream of CHK1 activation, but can also be induced by a multitude of other pathways including direct phosphorylation of p53 serines 15 and 37 by ATR [280]. Phosphorylation of p53 results in the stabilisation of p21, which is capable of inducing arrest in both G1 and G2 through CDK2/CDK4 or CDK1 inhibition [281][282].

The data in this chapter demonstrates the importance of CTC1 beyond the telomere in maintaining global genomic stability, and suggests a potential novel role in mitosis. This is not to downplay the clearly crucial role of CTC1 at the telomere; whilst global genomic instability is apparent from an early stage following *CTC1* knockout, the growth defect is minimal until the telomeric phenotypes become more advanced. On the other hand, the model HCT116 cell line is derived from a colorectal carcinoma and it is hard to extrapolate the tolerance of stresses to truly wild-type cells; different cell types may be more sensitive than others to the non-telomeric genomic instability induced by *CTC1* knockout.

Mutations in *CTC1* are associated with diseases such as Coats plus syndrome affecting the brain, bones, eyes, and gastrointestinal system [176]. It is possible that DSB repair or chromosome segregation errors play a role in CTC1-related disease development, potentially offering alternative avenues for the targeting of therapeutics.

6 The Regulation of *STN1* by Nonsense Mediated Decay

NMD was originally defined as a quality control pathway ensuring polypeptides are not produced from mRNA containing a PTC [283] (Fig. 18). However, NMD has also been demonstrated to degrade a fraction of 'normal' mRNAs that do not contain PTCs, in *S. cerevisiae* this is estimated to be approximately 10% of all genes [284][285]. One of the genes suppressed by the NMD mechanism in budding yeast is *STN1* [286] (*TEN1* appears to also be targeted by NMD, but not as strongly). NMD is targeted to *STN1* mRNA due to the presence of a overlapping-uORF; the 5′ UTR contains two uORFs, one of which overlaps with and terminates within the main *STN1* ORF. The stop codon of the overlapping-uORFs is interpreted as a PTC, inducing the degradation of the mRNA by NMD [231]. Human *STN1* mRNA also contains multiple uORFs, one of which overlaps with the main reading frame (Fig. 20). Luciferase expression assay data using part of the human *STN1* mRNA 5′ UTR (containing 2 of the 3 uORFs) suggests the *STN1* uORF sequence is capable of reducing expression of downstream transcripts in human cells [231]. The purpose of this chapter is to determine if human *STN1* is regulated by NMD.

6.1 U-2 OS Cell *STN1* mRNA Abundance is Affected by NMDI14, but *TEN1* and *CTC1* mRNA Abundance is Not

To determine if human *STN1* mRNA is degraded by NMD, U-2 OS cells were exposed to 5 μM NMD inhibitor NMDI14 for 3 days. The cell line and drug exposure conditions were chosen after testing the inhibitor for efficacy in PC-3, HCT116 and U2-OS cells. *ATF4* mRNA was used as a positive control for NMD inhibition as it is known to be degraded by NMD [287] (*ATF4* mRNA also contains an overlapping-uORF). The mRNA level of all three components of the human CST complex were assayed by qPCR after NMDI14 exposure. A >2-fold increase in *STN1* mRNA abundance was detected after inhibition of NMD activity (Fig. 34a). No significant change in either *TEN1* or *CTC1* mRNA abundance was detected. To determine if this change in mRNA abundance was reflected in the level of STN1 protein, whole-cell protein lysates were taken from U2-OS cells treated identically with NMDI14 as before and the level of STN1 was measured by Western blot. Consistent with the qPCR data, STN1 protein levels were increased on average 1.8-fold after NMD inhibition (Fig. 34b). Taken together, these data support the conclusion that human *STN1* is degraded by NMD.

A

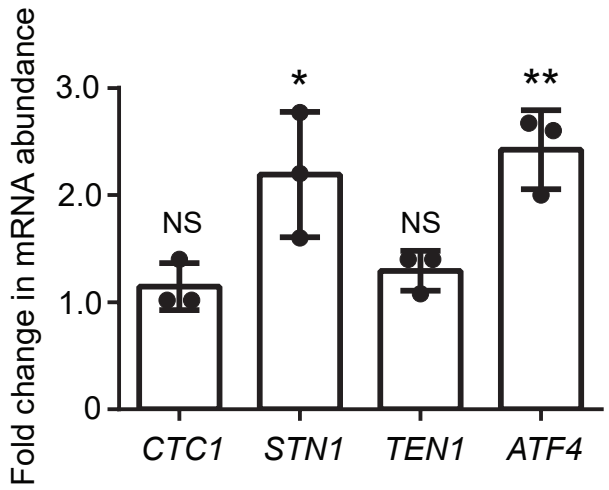

B

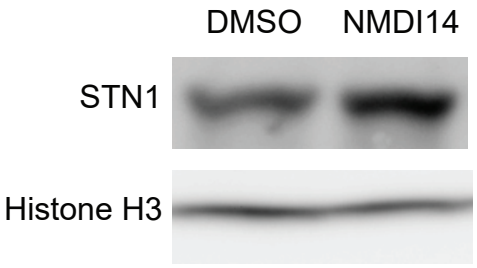

C

	Rep 1	Rep 2	Rep 3	Mean
STN1 fold change	1.8	1.6	2.2	1.8

Figure 34. Inhibiting Nonsense Mediated Decay raises *STN1* levels. U-2 OS cells were treated with 5 μM NMDI14 for 72 hours. (A) mRNA levels of the CST complex components *CTC1*, *STN1*, and *TEN1* were normalised to DMSO treated control samples. *ATF4* is a known NMD target and was used as a positive control for NMD inhibition, ribosomal 18S and RPL13A were used as reference genes. Bars represent standard deviation between three experimental repeats, Ct data were tested for statistical significance using One-Way Anova correcting for multiple comparisons (Sidak's method). (B) STN1 protein levels were assayed by Western blot following 5 μM NMDI14 treatment for 3 days. Blot is representative of 3 separately performed biological repeats. (C) Quantification of 3 Western blots assaying STN1 levels after 5 μM NMDI14 treatment for 3 days (Blot in (B) is replicate 1). Quantification was performed using the FIJI distribution of ImageJ.

6.2 Nonsense Mediated Decay Inhibition after Prolonged G_0 DNA Damage Stabilises *STN1* mRNA

NMD is down-regulated in response to a number of cellular stresses including endoplasmic reticulum stress, hypoxia and pathogen-induced stress [288]. It has recently been reported that one situation in which NMD is downregulated is when non-cycling cells experience prolonged DNA damage [237]. Nickless et al. (2017) grew RPE-1 cells to confluence in order to arrest their growth, exposed them to 63 μg/ml bleomycin for 24 hours, then removed the bleomycin and allowed the cells to recover for 96 hours. After the 96 hours (at which point significant DNA damage was still present) they reported the down-regulation of NMD in a MAPK14 (p38)-dependant manner, and the stabilisation of NMD targets.

To determine if *STN1* mRNA degradation was reduced under similar conditions as the above experiment was replicated, using *ATF4* as a positive control for degradation by NMD and *ORCL* as a negative control (as used by Martin et al. [289]). Following the 96 hour recovery period, the RPE-1 cells were exposed to 5 μM actinomycin-D in order to inhibit the production of new mRNAs by RNA polymerase II (Fig. 35a). Relative mRNA levels were compared from before and after transcriptional inhibition in order to determine how quickly each mRNA was being degraded. Relative mRNA levels after actinomycin-D treatments were assayed instead of just comparing absolute mRNA levels at day 4 in order to exclude any effect of changes at the transcriptional level. Ribosomal subunit 18S mRNA was used as a reference gene due to its high abundance and stability [237], but it should be noted that all degradation rates are relative to the degradation of 18S mRNA. The percentage of mRNA remaining in bleomycin treated cells after the 2 hours was compared to control cells that were not exposed to bleomycin. As expected, there was no change in the degradation rate of ORCL mRNA between bleomycin treated and untreated cells. The NMD target *ATF4* was degraded in untreated cells (approximately 75% of the *ATF4* mRNA remained after 2 hours) but this degradation was reduced in the bleomycin treated cells, from which the down-regulation of NMD can be inferred. In concordance with previous data indicating the degradation of *STN1* mRNA by NMD, *STN1* mRNA degradation was significantly reduced in the bleomycin treated cells (Fig. 35b).

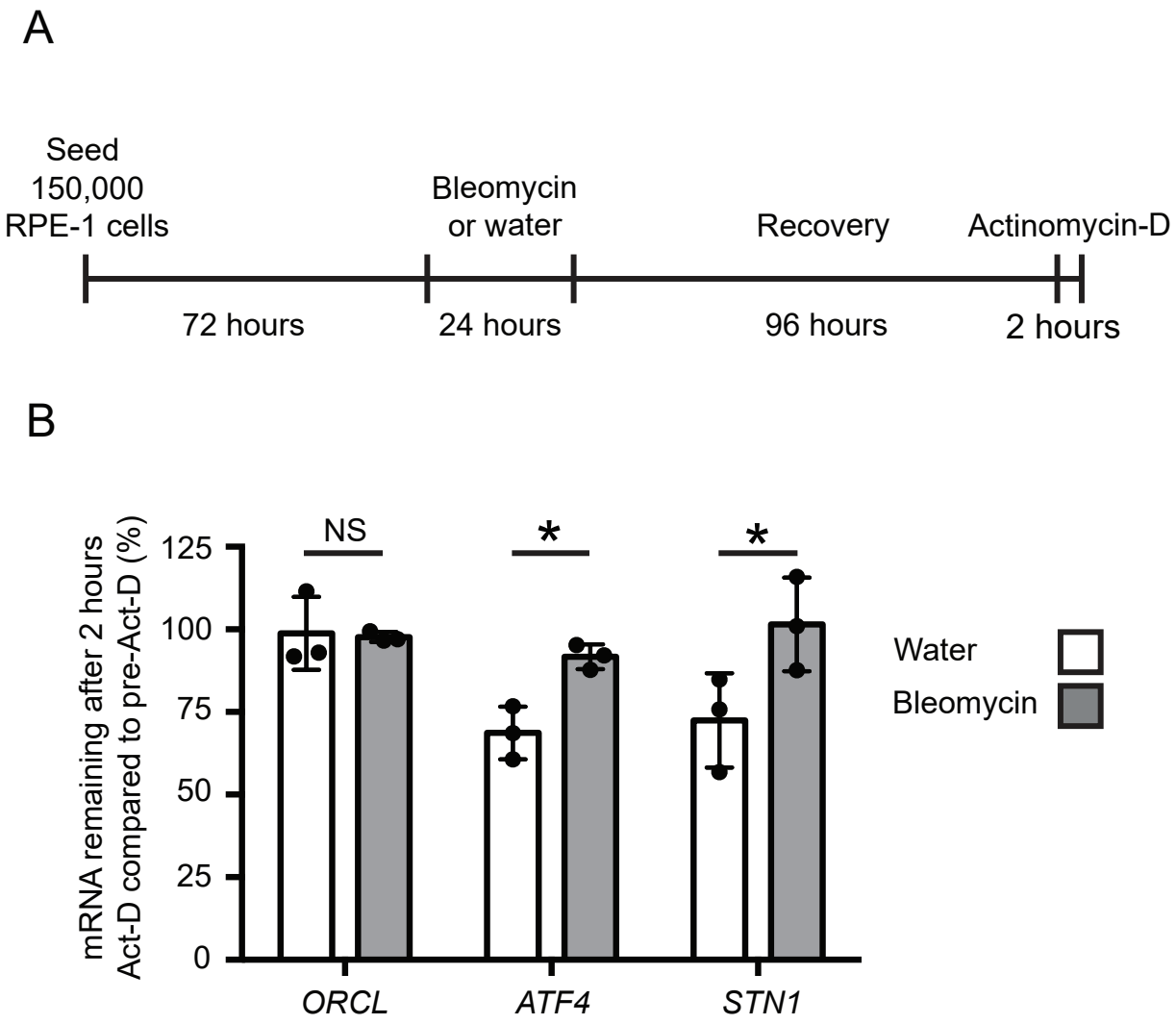

Figure 35. *STN1* mRNA degradation after prolonged DNA damage in non-cycling RPE-1 cells. (A) RPE-1 cells were grown to confluence over 72 hours in order to inhibit cell cycle progression before exposure to bleomycin (63 mg/ml) or water for 24 hours. Cells were allowed to recover for 96 hours before transcription was inhibited with 5 μM Actinomycin-D for two hours. mRNA abundance was then compared before and after transcription inhibition to determine mRNA decay rate. (B) qPCR data of relative mRNA levels in cells treated as described before and after transcription inhibition for two hours. *ATF4* was used as a positive control for degradation by NMD, and *ORCL* was used as a negative control. Ribosomal 18S was used as a reference gene due to its high abundance and stability . Bars are standard deviation between three experimental repeats, statistical significance was calculated by one way ANOVA using Sidak's multiple comparisons correction.

6.3 Discussion

S. cerevisiae up-frame suppressor (UPF) genes (key NMD components) have long been known to reduce Stn1 and Ten1 levels, and loss of these NMD genes induces telomere shortening that is indistinguishable from the shortening seen when Stn1 and Ten1 are over expressed [290]. More recently our lab reported that through inactivation of DDR and NMD pathways the requirement for Cdc13 could be efficiently suppressed [291]. This bypass was suggested to be due to the altered stoichiometry of CST complex components; raising Stn1 and Ten1 levels allowed them to bind to the telomere without Cdc13.

This chapter showed a significant increase in *STN1* mRNA after inhibition of NMD using the small-molecule inhibitor NMDI14. No significant change in *CTC1* or *TEN1* level was seen, but neither human *CTC1* or *TEN1* mRNA contain overlapping uORFs (*TEN1* mRNA contains a uORF but it does not overlap with the main *TEN1* ORF, terminating 93 nucleotides upstream). The increase in *STN1* mRNA level was approximately 2-fold, a similar magnitude change to the level of *ATF4*, a positive control gene with an overlapping uORF that is known to be targeted by NMD. The increase in STN1 protein levels was consistent with the increase in mRNA abundance. NMDI14 inhibits the phosphorylation of UPF1, a key step in the NMD pathway. It is unclear how efficient this inhibition is; if the inhibitor is only partially effective then natural inactivation of NMD could result in even higher levels of *STN1* and *ATF4* mRNA. However, *STN1* appears to be affected by NMDI14 to approximately the same degree as *ATF4*.

Artificial inhibitors are rarely without their drawbacks, however the literature supports NMDI14's effective inhibition of NMD with little-to-no cytotoxicity at working concentrations [289] (no cytotoxicity was observed at 5 μM). Assaying degradation of *STN1* mRNA following NMD down-regulation offered useful corroborative data; assessing mRNA degradation rate rather than single-time-point abundance ruled out the effect of other regulatory mechanisms (such as transcription factors).

The question remains however, what is the benefit to the cell of regulating wild-type *STN1* mRNA by NMD? One hypothesis is that it allows genes to be more highly transcribed without a necessarily high protein abundance. This could be beneficial for ensuring essential genes are rapidly transcribed and made available after periods when global transcription was inhibited such as during mitosis. Alternatively, it may be that high STN1 levels have a negative impact on cell viability under healthy/unstressed circumstances, but are necessary during situations when NMD is down-regulated. NMD is suppressed in response to a range of cellular stresses [288] including prolonged DNA damage in G_0 as discussed previously. To better understand why regulation of STN1 by NMD is important, the impact of high STN1 levels on the cell must be assessed.

7 The Influence of STN1 on Telomere Homeostasis and Genomic Stability

7.1 Generation of *STN1*-Overexpression HCT116 Cells with an Inducible *CTC1* Deletion

The degradation of human *STN1* by NMD suggests a possible negative impact of high *STN1* levels on the overall health of the cell. The goal of this chapter is to determine if a deleterious impact of high STN1 levels is indeed the case, and to understand what the specific impact might be. Further to this goal, HCT116 cells that stably overexpress *STN1* were produced. The mammalian expression vector pcDNA3 containing flag-tagged *STN1* cDNA under the constitutive cytomegalovirus (CMV) promoter was constructed and transfected into the *CTC1*$^{lox/lox}$ HCT116 cells and stable integration of the *STN1* expression cassette was selected for using G418 (STN1 cDNA was a kind gift from Carolyn Price). Clones were screened for overproduction of STN1 by Western blot approximately 30 days after initial transfection. A clone that expressed approximately 6-fold STN1 compared to wild-type cells and a clone that expressed approximately 3.5-fold STN1 compared to wild-type cells were identified (Fig. 36a). *STN1*-OE overexpression clone DTC15-S9 was assayed for STN1 overexpression 90 days after initial transfection and STN1 expression was still approximately 5 fold greater than wild-type (Fig. 36b). It is worth noting that HCT116 cells are triploid for the long arm of chromosome 10 which contains the *STN1* gene, and as such may already have higher STN1 levels than the average diploid cell line. The exogenous STN1 runs noticeably higher on an SDS-PAGE gel than the endogenous STN1 due to the flag tag. A parallel *CTC1*$^{lox/lox}$ HCT116 cell line was maintained during the generation of *STN1*-overexpression clones in order to have control cell lines of equivalent age.

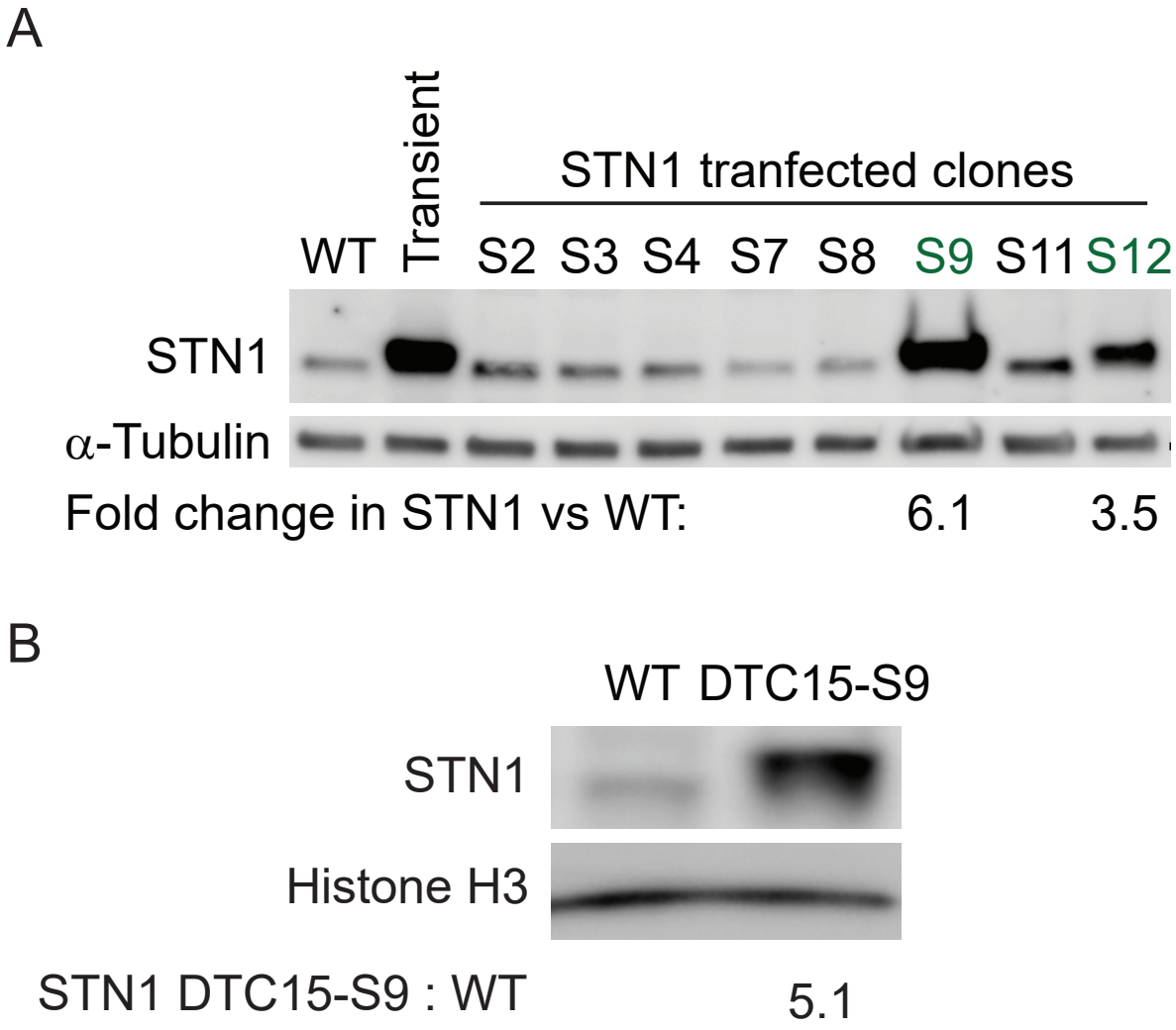

Figure 36. Stable overexpression of *STN1* in clonal HCT116 cells. (A) Following transfection with a *STN1* expression plasmid and selection for integration with G418, STN1 expression levels of clonal HCT116 cell populations were assayed (approximately 30 days post-transfection). Cells two days after transient transfection of the *STN1* expression cassette were used as a positive control for *STN1* overexpression. (B) STN1 expression level in DTC15-S9 overexpression clone 90 days after transfection. Relative STN1 signal intensity was measured using the FIJI distribution of ImageJ.

7.2 Increased Genomic Instability Markers in Cells that Overexpress *STN1*

The CST complex appears important in maintaining genomic stability (Fig. 26). It has been reported that overexpression of all three CST complex components simultaneously can improve HeLa cell viability following exposure to a range of DNA-damage inducing agents (although all agents tested generate cytotoxicity by blocking replication fork progression, the collapse of which can produce DSBs) [266]. Interestingly there is evidence in budding yeast that high levels of Stn1 can inhibit S-phase checkpoint activation in response to genome-wide stalled replication forks [292], and the increased viability of CST-overexpressing HeLa cells could be (at least partially) explained by checkpoint activation inhibition. The first step in assessing the effect of raising *STN1* levels on genomic stability was to score micronuclei frequency in otherwise unchallenged cells. Micronuclei were counted by staining fixed *STN1*-OE clones DTC15-S9 and DTC15-S12 with DAPI, and the frequency was compared to the control HCT116 cell line with only endogenous *STN1*. HCT116 cells have a relatively high frequency of micronuclei (Fig. 37) compared to non-cancerous cells [293], but they are derived from a colorectal carcinoma so the genomic instability is not necessarily surprising. The control cell line had a micronuclei frequency of approximately 5%, but micronuclei were more abundant in the *STN1*-OE clones DTC15-S9 and DTC15-S12 with a frequency of approximately 7% (Fig. 37a,b). In support of these data, average micronuclei abundance was significantly higher in HCT116 cells 3 days after transient transfection with the pcDNA3-*STN1* expression vector compared to control cells transfected with a *GFP* expression vector (Fig. 37c,d). This increase in micronuclei could be due to a number of factors, but serves as initial evidence that increasing STN1 levels can have negative effects in human cells and is perhaps why *STN1* is usually maintained at a low level by NMD.

When DNA is damaged, histone variant H2AX is phosphorylated by ATM or ATR kinases [294]. This phosphorylated histone (referred to as γH2AX) attracts DNA damage repair factors, and can be easily detected by immunofluorescence using a phosphorylation specific antibody. Whilst γH2AX phosphorylation spreads along chromatin [295], forming the strong signal that can be detected by immunofluorescence, the phosphorylation does remain localised enough to form individual foci which can be co-localised with other signals/structures. Given that *STN1*-OE appeared to exacerbate genomic instability in HCT116 cells (Fig. 37), the presence of γH2AX foci and their location might present some insight into the cause of the instability.

STN1-OE HCT116 clone DTC15-S9 cells were arrested in metaphase, centrifuged by cytospin, and fixed in formaldehyde to produce metaphase spreads. The cytospin step was optimised to ensure effective separation of individual chromosomes without compromising the chromosomes' structure by over-centrifugation. The metaphase spreads were probed with a primary antibody specific to γH2AX and an appropriate fluorophore-tagged sec-

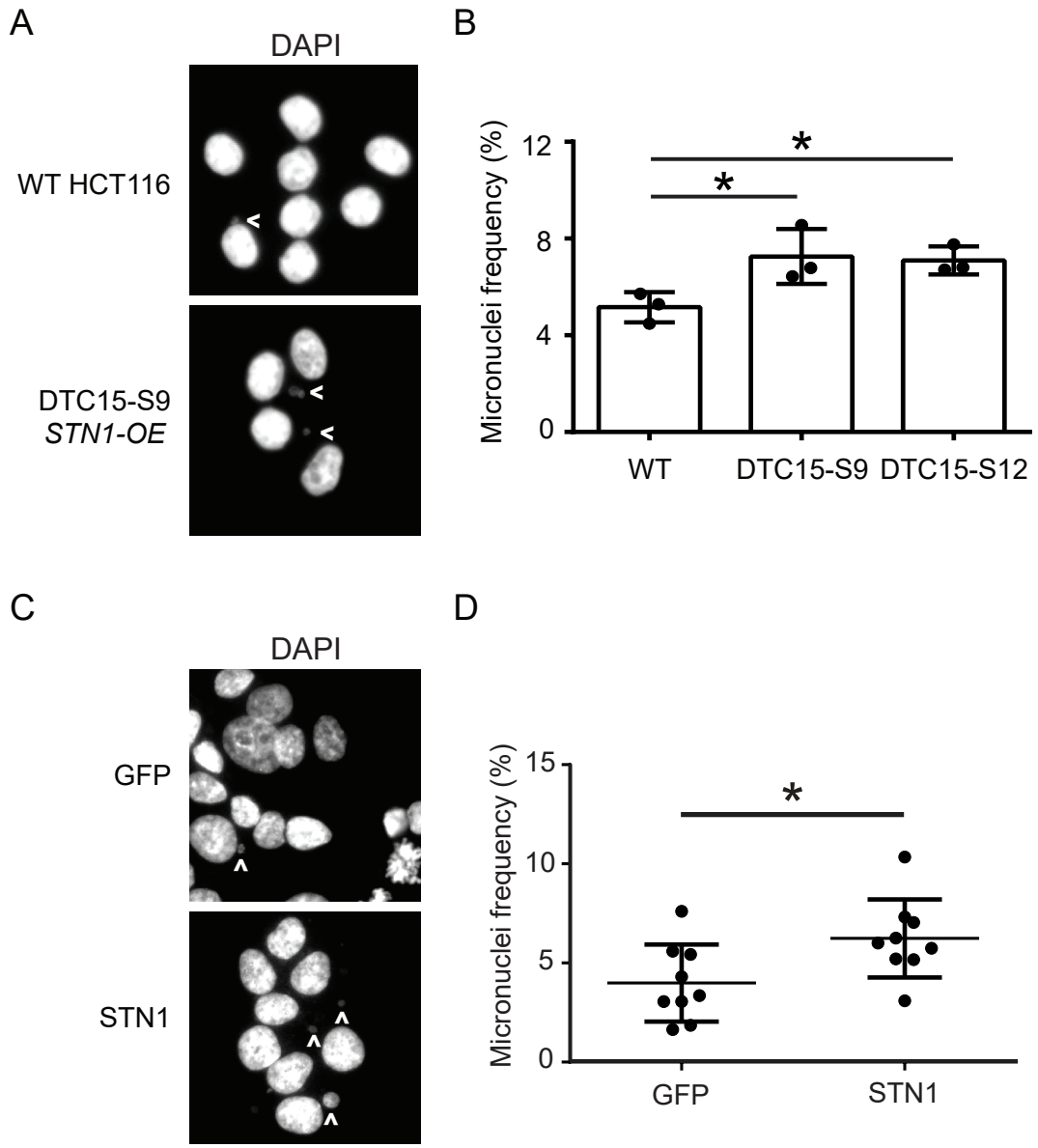

Figure 37. Micronuclei frequency in cells overexpressing *STN1*. Micronuclei frequency was assayed by fluorescent microscopy using the DAPI DNA stain. *STN1*-OE HCT116 cells were compared to HCT116 cells with wild-type levels of STN1 at an equivalent passage number. (A) A representative image of *STN1*-OE clone DTC15-S9 nuclei stained with DAPI and wild-type HCT116 cells. Micronuclei are indicated with white arrowheads. (B) Quantification of micronuclei frequency in *STN1*-OE clones DTC15-S9 and DTC15-S12 vs wild-type *STN1* HCT116 cells. Quantification was performed using the FIJI distribution of ImageJ. Bars represent standard deviation between 3 separate biological repeats. Statistical significance was calculated by one-way ANOVA and Dunnett's correction for multiple comparisons. (C) Representative images of HCT116 cell nuclei and micronuclei 3 days after transient transfection with a *GFP* expression vector or the pcDNA3-STN1 expression vector. Micronuclei indicated by white arrowhead. (D) Quantification of micronuclei in (C), Statistical significance calculated by student's t-test.

ondary antibody before hybridisation of telomere C-strand specific PNA probes. The spreads were then mounted with DAPI to counterstain for total DNA. The frequency of chromosomes with γH2AX was scored, differentiating between γH2AX foci that colocalised with telomeric signal and those that did not (Fig. 38a). The frequency of chromosomes with non-telomeric γH2AX in HCT116 cells with only endogenous *STN1* was approximately 6%, and this increased to 8% in *STN1*-OE DTC15-S9 cells (Fig. 38b). The frequency of telomeric γH2AX foci was unchanged by *STN1* overexpression (Fig. 38c). The increase in γH2AX foci further confirms that *STN1*-OE HCT116 cells have compromised genomic stability compared to wild-type cells, and that at any one time DNA damage is more abundant throughout their genome. The fact that there is no increase in γH2AX foci that colocalise with telomeric signal suggests that this instability is not due to replication fork stalling related defects that primarily effect the telomere.

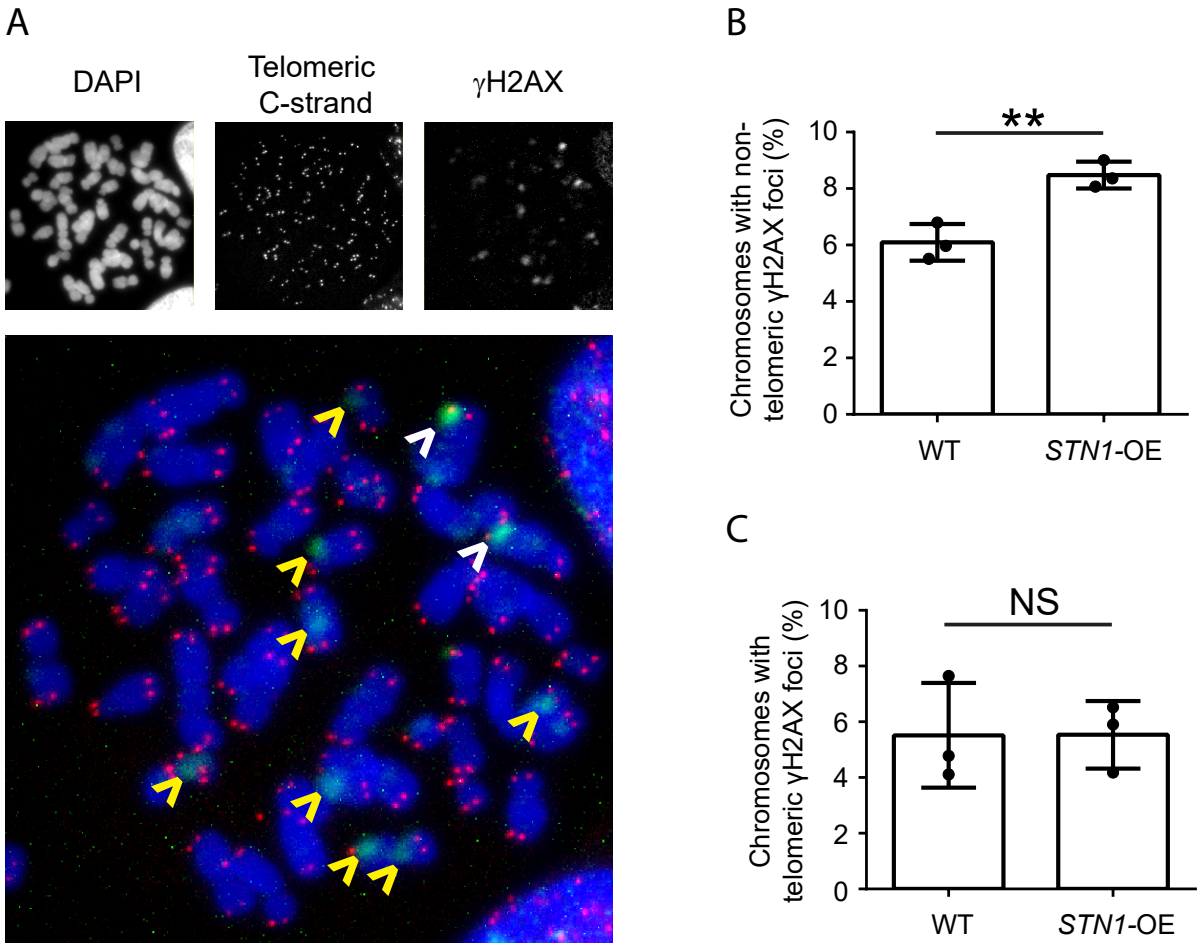

Figure 38. *STN1*-OE HCT116 DTC15-S9 cells have increased non-telomeric γH2AX foci. HCT116 cells with 5/6-fold raised levels of STN1 (DTC15-S9) were fixed in metaphase and stained with an anti-γH2AX antibody and a telomeric C-strand PNA probe. Fluorescent microscopy was used to score frequency of γH2AX foci and their colocalisation with the telomere. (A) Representative fluorescent images of *STN1*-OE HCT116 DTC15-S9 metaphase chromosome spread. Yellow arrowheads indicate non-telomeric γH2AX foci, white arrowheads indicate telomeric γH2AX foci. (B) Quantification of non-telomeric γH2AX foci in *STN1*-OE HCT116 DTC15-S9 cells. (C) Quantification of telomeric γH2AX foci in *STN1*-OE HCT116 DTC15-S9 cells. Bars represent standard deviation between three biological repeats. Significance calculated by student's t-test.

7.3 Overexpression of *STN1* Inhibits Homology Directed Repair

It is now known that the CST complex has a role in the fill-in of DSBs which might influence the repair pathway taken by the cell [189]. To generalise, there are two main pathways of DSB repair, HDR and NHEJ. HDR is a very accurate pathway that uses additional copies of the damaged locus as a template for repair, the restriction of this pathway is the requirement for easy access to template DNA which mostly limits HDR to the S and G2 phases of the cell cycle. HDR depends on the generation of a long overhang of ssDNA which is able to invade template dsDNA. At this point polymerases are able to replace the damaged locus using a strand of template DNA. The alternative pathway NHEJ does not require a template, blunt ends generated by DSBs are directly ligated together. NHEJ is less accurate than HDR and more frequently results in mutations, deletions, or the ligation of free ends that were not generated by the same DSB. However, NHEJ does have the benefit of being faster and can easily be performed at any stage of the cell cycle [296]. Which of the two pathways takes place ultimately depends on the protein factors that localise at the break and tip the balance in favour of one pathway over the other. For HDR to take place, the DNA is significantly resected to generate the long ssDNA overhang that is capable of invading the template strand [297]. NHEJ can take place without extensive resection.

The CST complex along with polymerase-α is recruited to DSBs by RIF1/Sheildin/53BP1, and promotes the filling back in of dsDNA at the ssDNA overhang. In this way the CST complex might inhibit HDR by eliminating the long ssDNA overhang HDR required [189][175]. It is possible that overexpression of *STN1* in otherwise HDR-competent cells is inhibiting HDR and promoting the NHEJ pathway through the activity of polymerase-α, a potential explanation of the reduced genomic stability of *STN1*-OE HCT116 cells. To determine if high levels of STN1 inhibit HDR the DRGFP system was used (Fig. 39). The DRGFP cassette works as a reporter for HDR activity by expressing an inactivated (non-fluorescent) copy of *GFP* that contains a restriction site for the endonuclease SceI. When the endonuclease is expressed (such as by transient transfection of an expression plasmid), the endonuclease generates a DSB within the inactivated *GFP* gene. The second part of the DRGFP cassette is a truncated version of wild-type *GFP* with no promoter and missing the $5'$ and $3'$ ends of the gene, but containing the correct genetic information where the upstream inactivated *GFP* carries the SceI restriction site. If the SceI-induced DSB is repaired by NHEJ then the break is simply re-ligated and the expressed GFP protein remains inactivated (and possibly even mutated further). If HDR is used to repair the break, the only template available is the downstream truncated *GFP* gene. Using the downstream *GFP* as a template will restore the fluorescence of the expressed GFP protein as the cut locus is repaired using the wild-type *GFP* DNA (Fig. 39). The pDRGFP plasmid was stably integrated into the genome of U-2 OS cells. A clone likely

to have integrated only have a single copy of the cassette (as determined by qPCR) was isolated.

Clonal U-2 OS DRGFP reporter cells were transfected with mammalian expression plasmids carrying *SceI*, *SceI* + *STN1*, or empty vector as a control. In all cases the cells were transfected with the same total amount of DNA, using empty vector DNA to make up the difference where applicable. 2 days after transfection, the cells were fixed and imaged by fluorescent microscopy in order to score GFP-positive cells (Fig. 40a). GFP-positive cells were present in the empty vector control population with a frequency of <0.1% (Fig. 40b)(this phenomenon of low-level GFP activation has been previously reported where random DSB recombination events within the cell are able to restore GFP function without SceI at a low frequency [245]). In contrast, when SceI was expressed in the reporter cells the frequency of GFP-positive cells after 2 days was >6%. This suggests the reporter cassette is functional, and that 6% of cells repaired cut *GFP* with HDR and restored GFP fluorescence. When an *STN1* expression cassette was co-transfected with SceI, the fraction of GFP-positive cells was reduced from >6% of cells to approximately 4%. These data indicate that high levels of STN1 are capable of inhibiting HDR, which possibly explains the increased genomic instability of HCT116 cells that constitutively overexpress *STN1*.

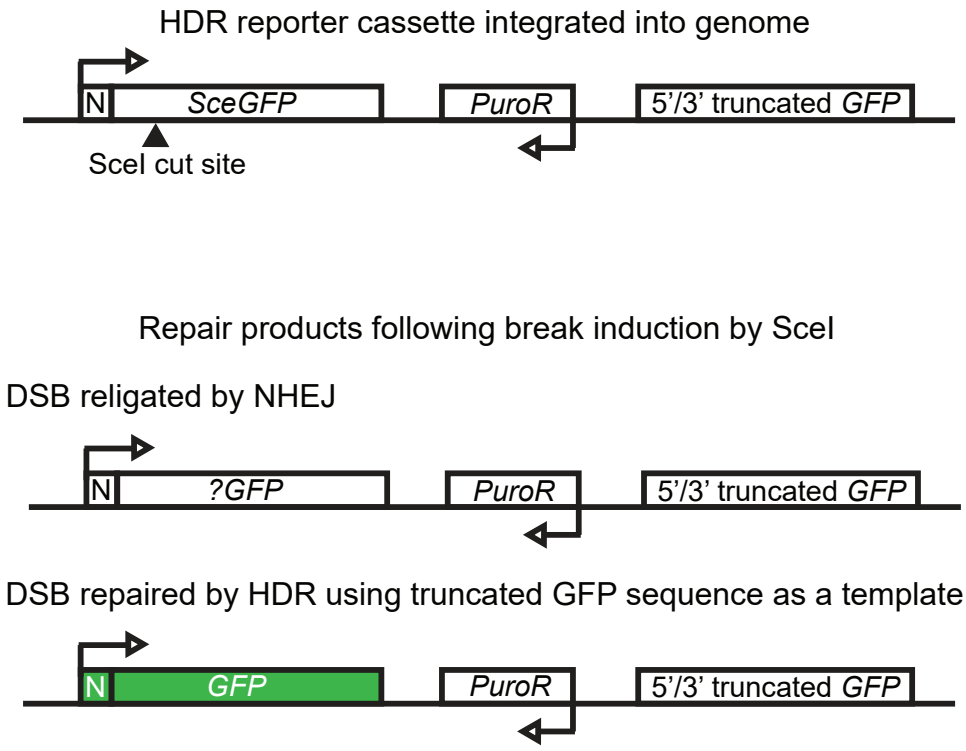

Figure 39. Detection of Homology-Directed Repair using the DRGFP reporter. The DRGFP reporter cassette contains a constitutively expressed mutated *GFP* gene fused to a nuclear localisation signal (N). The gene has been mutated in a manner that inactivates the fluorescent properties of GFP whilst also introducing an SceI restriction site). Downstream of the mutated *SceGFP* gene is the 5′ and 3′ truncated sequence of a non-mutated *GFP* gene. Expression of the endonuclease SceI induces a DNA double-strand break in the *SceGFP* locus. If this break is repaired by NHEJ, then the inactivated *SceGFP* will simply be re-ligated and it will not produce functional GFP. However, if the break is repaired by HDR using the downstream truncated *GFP* sequence as a template then GFP fluorescence will be restored.

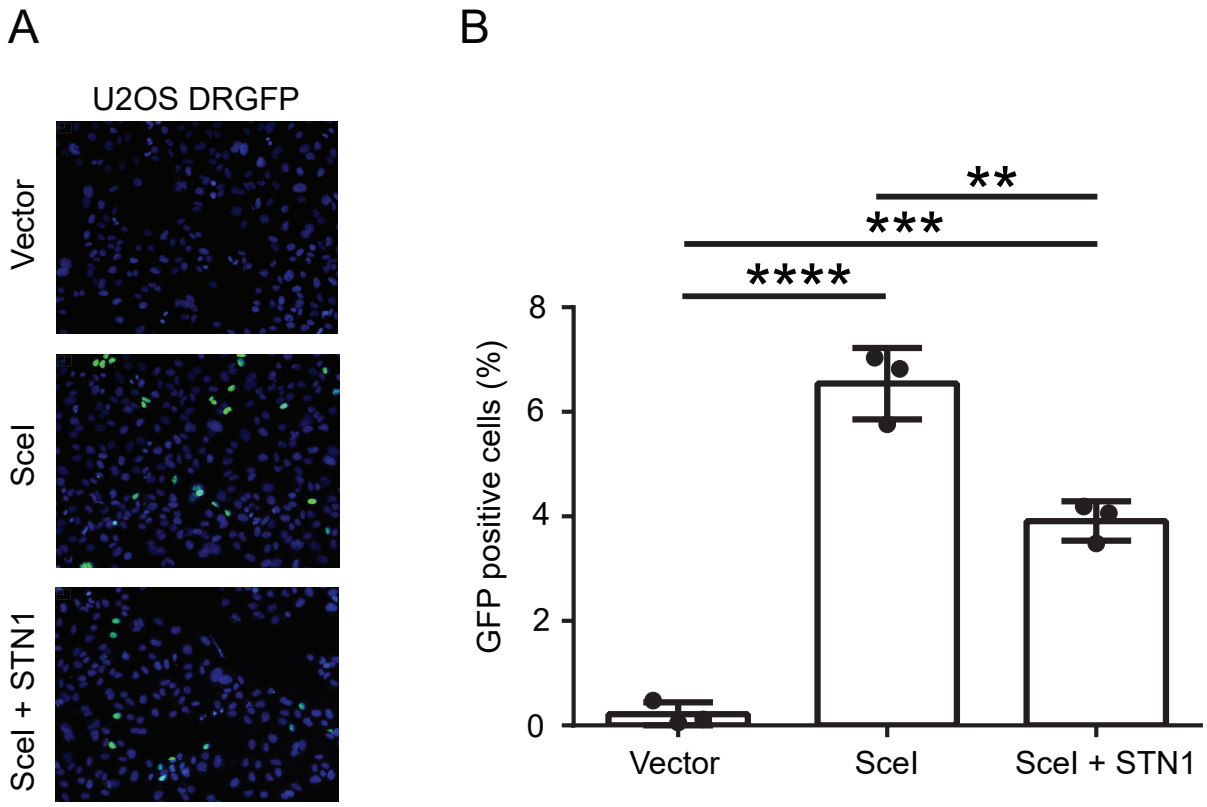

Figure 40. Overexpressing *STN1* inhibits Homology-Directed Repair. U-2 OS cells carrying 1-2 copies of the DRGFP reporter cassette were transfected with expression vectors carrying *SceI* and *STN1*. 48 hours later cells were assayed by fluorescent microscopy for GFP fluorescence. (A) Representative images of GFP fluorescence between samples transfected with empty vector, *SceI* and *SceI* + *STN1*. (B) Quantification of GFP fluorescence-positive cells. Bars represent standard deviation between three experimental repeats. Significance was calculated by one-way ANOVA correcting for multiple comparisons (Sidak's correction for multiple comparisons).

7.4 Overexpression of *STN1* Conveys Resistance to the Chemotherapeutic Agent Etoposide

It has been reported that overexpression of the CST complex is capable of conveying resistance to DNA damaging agents that introduce DNA single-strand breaks, lesions, or other forms of damage that become DSBs when they are met by a replication fork [266]. To determine if *STN1* overexpression affected the impact of replication fork-independent DSBs on genomic stability *STN1*-OE HCT116 DTC15-S9 cells were exposed to etoposide. Etoposide is a genotoxic agent that is used as a chemotherapeutic, it is a topoisomerase II poison that inhibits the re-ligation of DNA after a DSB is induced by the topoisomerase. The genotoxic DSB introduced is replication fork independent. HCT116 *STN1*-OE DTC15-S9 cells were exposed to 10 μM etoposide for 30 minutes to induce DSBs, then allowed to recover for 24 hours. The cells were fixed and probed with an anti-γH2AX antibody, counterstaining with DAPI. The abundance of γH2AX foci after the recovery period was used to assess how effectively the DSBs were repaired, and micronuclei/chromatin bridge frequency was used as a measure of the overall impact of etoposide on genomic stability.

24 hours after a 30 minute etoposide exposure, HCT116 cells with endogenous levels of STN1 exhibit a high frequency of micronuclei, nearly 30% of nuclei have adjacent micronuclei compared to approximately 5% of untreated endogenous-*STN1* cells (Fig. 41a/b). A roughly 6-fold increase in micronuclei, consistent with the ability of etoposide to rapidly induce DSB formation (by inducing a high frequency of DSBs the likelihood of repair errors that can result in micronuclei (Fig. 24b) also increases). *STN1*-OE HCT116 DTC15-S9 cells also exhibit a significant increase in micronuclei abundance after the 24 hour recovery period but this change is only 2-fold, in part due to the higher frequency of micronuclei in unchallenged cells, but also due to micronuclei frequency in etoposide treated cells being less than 20%. Chromatin bridge frequency followed a very similar pattern to micronuclei, increasing approximately 5-fold in endogenous *STN1* HCT116 cells after etoposide treatment, but only a 3-fold increase was seen in DTC15-S9 cells that overexpress *STN1* (Fig. 41c,d). When γH2AX foci were scored, the effect of high STN1 levels was even greater. Following the 24 hour recovery period, at which point etoposide-treated wild-type HCT116 cells have a 2-fold increase in γH2AX still (8% vs 4%), the difference in γH2AX foci between treated and untreated *STN1*-OE DTC15-S9 cells was insignificant (Fig. 41e,f). Together these data show DTC15-S9 HCT116 cells that overexpress *STN1* are able to recover from etoposide-induced DSBs with less genomic instability and residual damage compared to HCT116 cells with wild-type levels of STN1.

To assess if *STN1* overexpression is actually improving cell viability following etoposide exposure, wild-type and *STN1*-OE DTC15-S9 cells were exposed to a range of etoposide concentrations for 24 hours and relative population viability was measured by PrestoBlue assay. PrestoBlue is an MTT/MTS-like assay that measures mitochondrial activity, and

as such is an indirect measure of the number of live cells in culture. Population viability was assayed after 24 hours etoposide exposure and plotted relative to untreated cells (considered to have 100% viability). Both wild-type and *STN1*-OE DTC15-S9 cells have decreasing viabilities as etoposide concentration increases (Fig. 42), however the *STN1*-OE DTC15-S9 cells were significantly more viable than the wild-type cells at all concentrations of etoposide (up to 50 μM). This increase in viability is concordant with the micronuclei/chromatin bridge and γH2AX data, suggesting that highly abundant STN1 is beneficial to the cell when challenged with etoposide-induced DSBs. Whilst high STN1 levels may have a generally destabilising effect on genomic integrity (Fig. 37,38) in unchallenged cells, it appears there is at least one condition in which high STN1 levels are beneficial.

Figure 41 . *STN1*-OE HCT116 DTC15-S9 cells have reduced genomic instability 24 hours after etoposide exposure compared to wild type. 0.1% DMSO was used as a vector control. DTC15-S9 HCT116 cells overexpressing *STN1* were exposed to 10 μM etoposide for 30 minutes before being allowed to recover for 24 hours. Cells were fixed and stained for fluorescent microscopy. Bars represent standard deviation between three experimental repeats. Statistical significance was calculated by two-way ANOVA using Tukey's correction for multiple comparisons. (A) Representative images of DAPI stained micronuclei in HCT116 cells. Yellow arrowheads indicate micronuclei. (B) Quantification of micronuclei. (C) Representative images of DAPI-stained chromatin bridges in HCT116 cells. Yellow arrowheads indicate chromatin bridges. (D) Quantification of chromatin bridges in HCT116 cells. (E) Representative images of γH2AX foci in HCT116 cells. DAPI channel is greyscale and γH2AX channel is red. (F) Quantification of γH2AX foci in HCT116 cells.

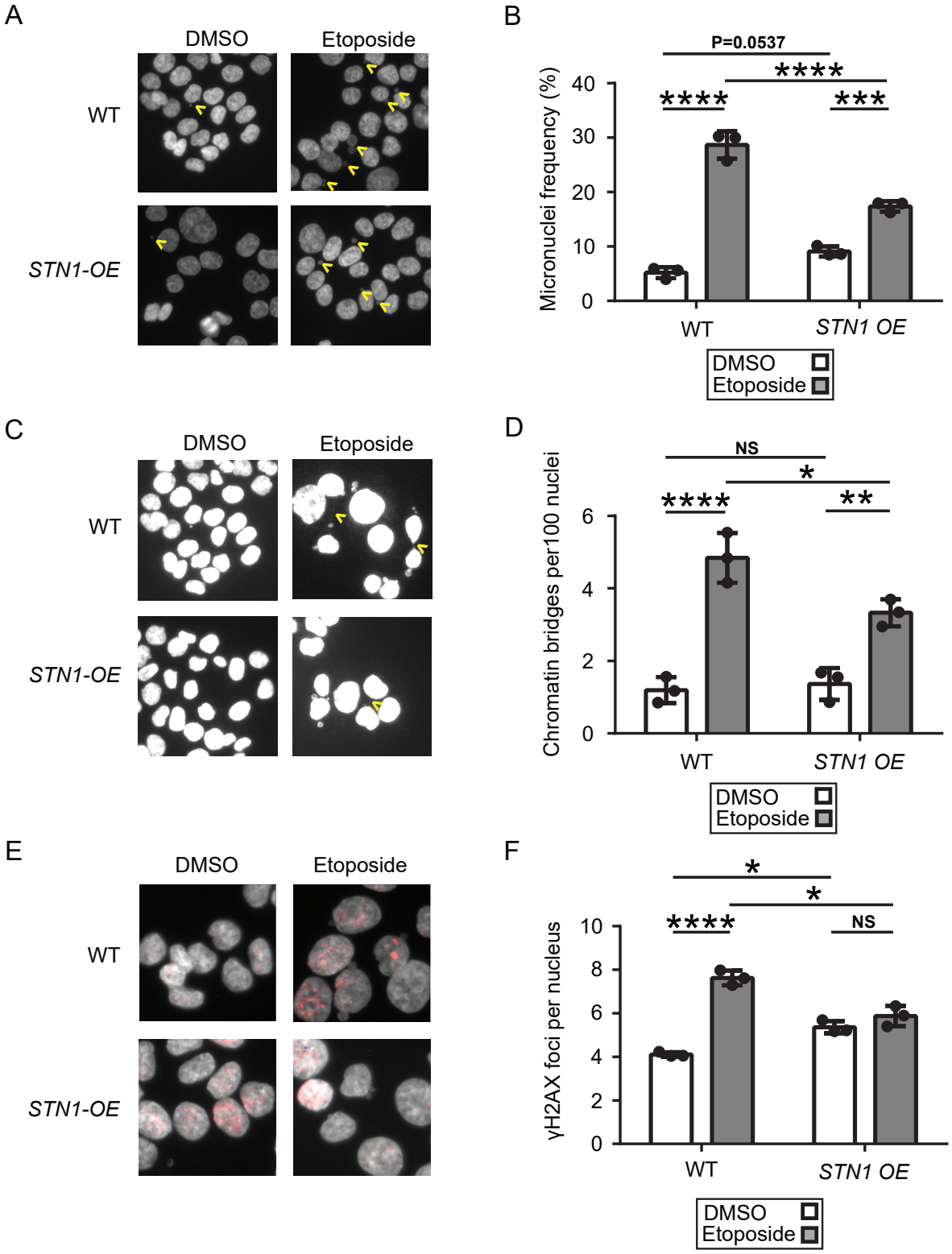
A
DMSO
Etoposide
WT
STN1-OE
B
P=0.0537
****
****
***
Micronuclei frequency (%)
40
30
20
10
0
WT
STN1 OE
DMSO
Etoposide
C
DMSO
Etoposide
WT
STN1-OE
D
NS
*
****
**
Chromatin bridges per100 nuclei
6
4
2
0
WT
STN1 OE
DMSO
Etoposide
E
DMSO
Etoposide
WT
STN1-OE
F
*
*
****
NS
γH2AX foci per nucleus
10
8
6
4
2
0
WT
STN1 OE
DMSO
Etoposide

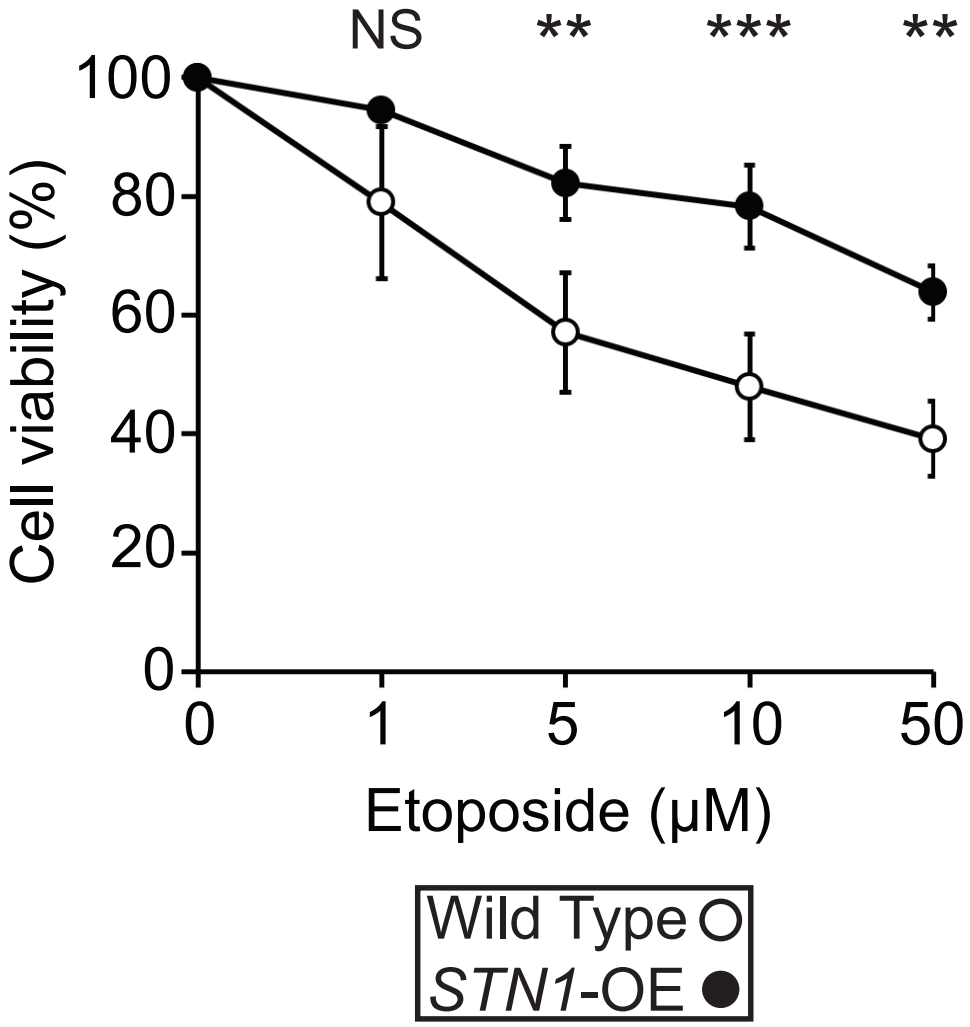

Figure 42. DTC15-S9 *STN1* overexpression promotes resistance to etoposide. Cells were exposed to a range of concentrations of etoposide for 24 hours. All samples were exposed to 0.5% DMSO. Relative viable cell count was measured by PrestoBlue MTT assay. 100% viability is that of untreated cells, to which all other viabilities are relative. Bars represent standard deviation between three biological repeats. Statistical significance calculated by two-way ANOVA, correcting for multiple comparisons using Sidak's method.

7.5 Overexpression of *STN1* Shortens the Telomere C-rich strands of HCT116 Cells and Increases the Frequency of Cellular Senescence

High *STN1* levels in budding yeast lead to telomere shortening, thought to be mediated by the CST complex's role as a telomerase inhibitor [290][298]. Overexpressing *STN1* in HCT116 cells did not appear to result in the activation of the DDR at the telomere (Fig. 44), but telomere length homoeostasis may still be affected. To investigate any impact on telomere C-strand length, DTC15-S9 and DTC15-S12 *STN1*-OE cells were grown for approximately 90 population doublings after transfection with the exogenous *STN1* cassette, before being fixed and probed with telomere C-strand specific PNA probes conjugated to a fluorophore. Probe signal was measured by fluorescent microscopy and used as an indicator of relative C-strand length. Telomere signal was compared to wild-type *STN1* HCT116 cells of equal age. Concordant with data from *S. cerevisiae*, DTC15-S9 and DTC15-S12 HCT116 cells overexpressing *STN1* had approximately 25% less telomeric C-strand signal than the equivalent age wild-type cells (Fig. 44). This assay does not address ssDNA overhang length, but indicates a loss of telomeric dsDNA.

A major trigger of cells entering G_0 and becoming senescent is telomere shortening. Telomeres function as a buffer of non-coding DNA that is gradually eroded as cells replicate. When this buffer becomes too short, cells become senescent in order to protect coding DNA from being lost. To determine if cells become senescent when *STN1* is overexpressed the β-galactosidase assay was used. DTC15-S9 HCT116 *STN1*-OE cells were fixed approximately 90 cell divisions after overexpression was induced by transfection, and the presence of senescence associated β-galactosidase activity was assayed. After incubating overnight with the β-galactosidase reporter buffers, cells were scored for blue colouration by visible light microscopy. Blue stained cells were considered to be senescent (Fig. 43a). Consistent with a decrease in average telomere length, the frequency of senescent cells in the HCT116 cell population increased from 2% in wild-type cells to >4% in *STN1*-OE DTC15-S9 cells (Fig. 43b). These data further support the hypothesis that low levels of STN1 are required for faithful and consistent cell replication.

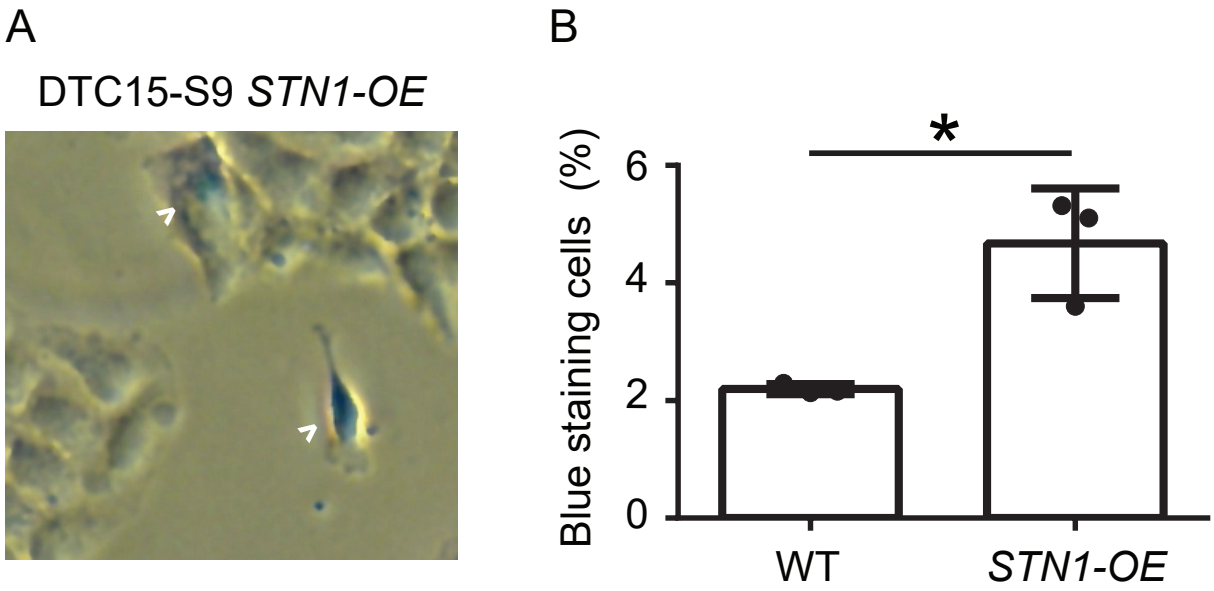

Figure 43. *STN1* overexpression increases the frequency of HCT116 cells entering senescence. DTC15-S9 HCT116 cells approximately 90 cell divisions after integration of an *STN1*-overexpression cassette were assayed for senescence and compared to identical aged wild-type HCT116 cells. Senescence was assayed by staining for senescence-associated β-galactosidase. (A) Representative visible light image of *STN1*-OE HCT116 cells stained for β-galactosidase. White arrowheads indicate blue staining (and therefore considered senescent) cells. (B) Quantification of blue stained cells. Bars represent standard deviation between three experimental repeats. Significance calculated by student's t-test.

7.6 *STN1*-Overexpression Can Partially Compensate for Loss of CTC1 at the Telomere but Enhances Non-Telomeric DNA Damage

The CST complex component STN1 was originally characterised in budding yeast as a protein capable of suppressing the *cdc13-1* temperature sensitive mutation of *CDC13* (the name *STN1* is derived from *Suppressor of cdc ThirteeN*) [299]. As the *STN1* overexpression cassette was integrated into the HCT116 cell-line with an inducible *CTC1* knockout, it was possible to determine if overexpression of *STN1* was capable of compensating for loss of *CTC1*.

CTC1 knockout was induced in wild-type and *STN1*-OE HCT116 cells, 10 days later relative telomere length was assayed as described previously using fluorophore-tagged PNA probes. Both *CTC1* knockout and *STN1*-OE induce telomeric C-strand shortening (Fig. 44), but simultaneous *CTC1* knockout and *STN1* overexpression appears to suppress the short telomere C-strand phenotype of those individual genotypes (Fig. 44). An explanation for what initially appears to be counter-intuitive telomere length data is that *CTC1* knockout cells lose C-strand signal as the CST complex is unable to promote polymerase-α C-strand fill-in; *STN1*-OE cells are able to fill in the C-strand, but the activity of telomerase is so effectively inhibited by STN1 that the G-rich overhang is not extended and the whole telomere is gradually eroded every replication cycle; and in the *CTC1* knockout *STN1*-OE cells telomerase inhibition by high STN1 is ineffective without CTC1, whilst C-strand erosion by nucleases is inhibited by excessive STN1 (Fig. 45). Alternatively, as the STN1-TEN1 complex has been demonstrated to retain some (albeit weak) binding ability without CTC1 [300], high STN1 levels could be compensating for a lack of CTC1 by promoting some polymerase-α activity on the C-strand.

Given the apparent ability of high STN1 levels to suppress *CTC1*-deletion-induced telomere C-strand length defects in HCT116 cells, it is possible that STN1 is also able to suppress the activation of the DDR at the telomere. *CTC1*$^{-/-}$ cells accumulate long ssDNA G-rich overhangs that are likely responsible for attracting DDR elements [182]. To determine if increased STN1 can suppress this telomeric DDR, metaphase spreads of *STN1*-OE HCT116 cells after *CTC1* knockout were probed for co-localisation of γH2AX foci and telomeres (Fig. 46a). As predicted, the percentage of chromosomes with telomeric γH2AX foci after *CTC1* knockout was approximately 22%, a >5-fold increase over the 5% of chromosomes in control cells (Fig. 46b). *CTC1* knockout in *STN1*-OE cells also significantly increased the frequency of telomeric γH2AX, but by only 3-fold compared to *CTC1*$^{+/+}$ cells (to approximately 15% of chromosomes) 46b). This statistically significant partial suppression indicates high STN1 levels are able to limit telomeric DDR activation after loss of *CTC1*. This could be due to *STN1*-OE limiting the ssDNA overhang produced in the absence of CTC1: overexpression of *STN1* could allow telomerase inhibition or Pol-α promotion in the absence of CTC1, both of which would limit the amount of ssDNA

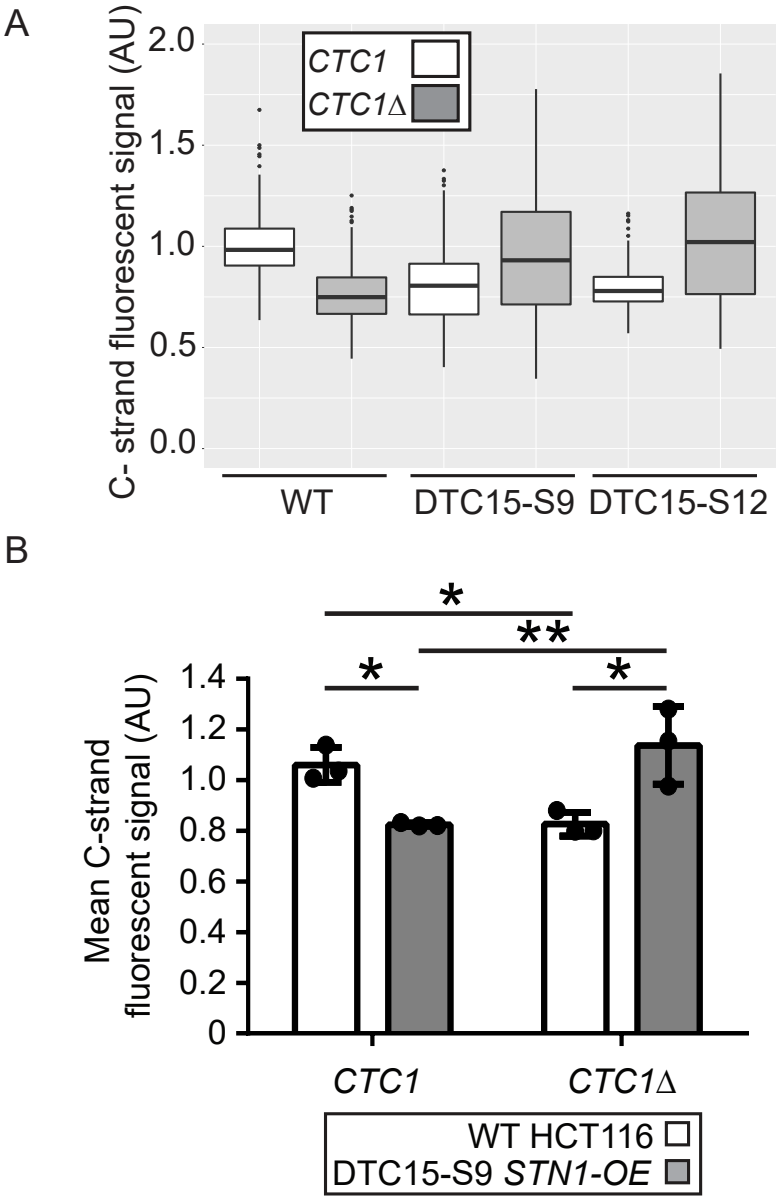

Figure 44. *STN1* overexpression can suppress the short telomere phenotype of HCT116 *CTC1*$^{-/-}$ cells. *CTC1* knockout was induced by addition of 10 nM tamoxifen to the culture media. Relative C-strand telomere length was measured by PNA probe fluorescence. (A) Box plot of WT HCT116, DTC15-S9 and DTC15-S12 cell telomere C-strand PNA-probe signal with and without *CTC1*. N > 600. Data was plotted in R using the ggplot2 package [301]. (B) Mean C-strand PNA probe signal in WT HCT116 or DTC15-S9 *STN1*-OE cells. Bars represent standard deviation between three experimental repeats. Statistical significance calculated by two-way ANOVA using Tukey's correction for multiple comparisons.

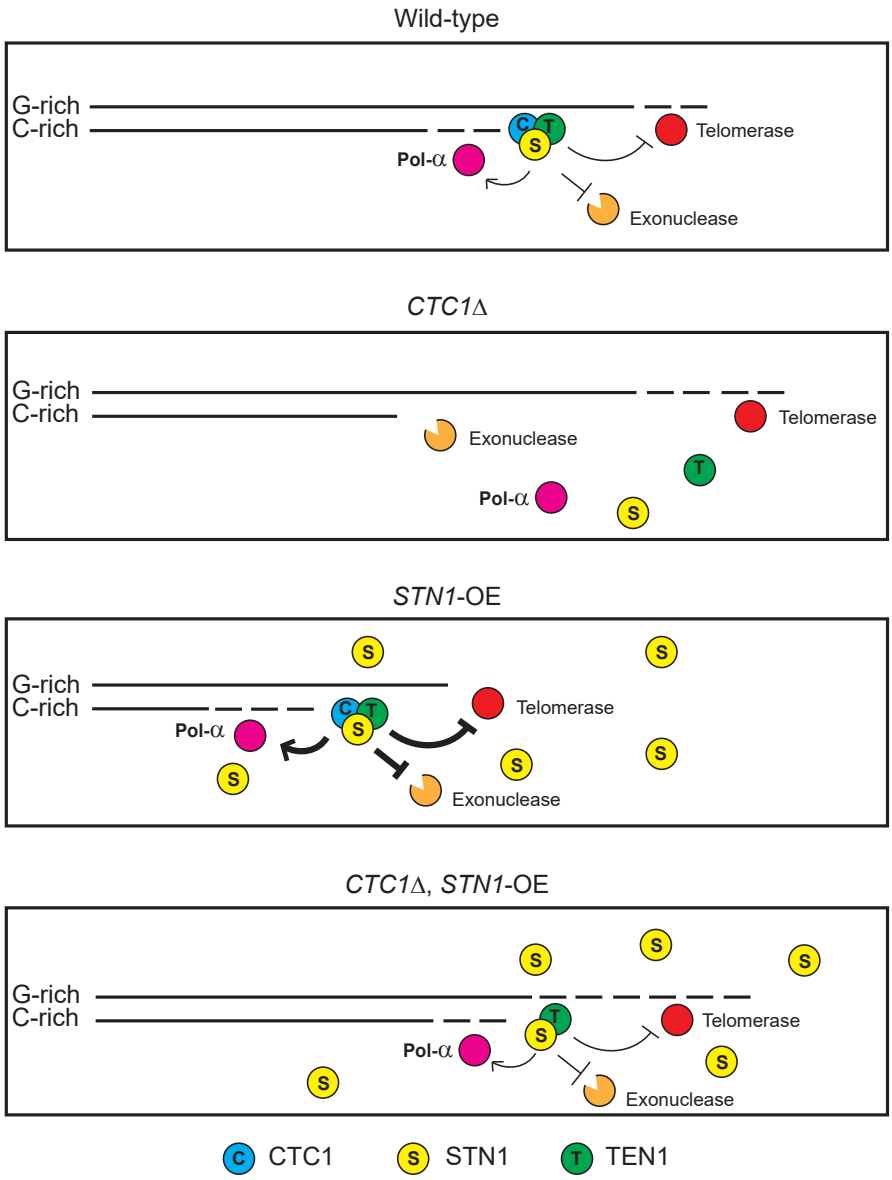

Figure 45. Model of telomere strand regulation in *CTC1*Δ,*STN1*-OE cells. In wild-type cells the CST complex functions as normal: inhibiting telomerase activity, promoting C-strand fill-in by Pol-α, and possibly inhibiting the action of exonucleases. In the *CTC1*Δ cells telomerase is no-longer inhibited which elongates the G-overhang, but the C-rich strand shortens as Pol-α is no-longer recruited to fill-in the strand. When *STN1* is overexpressed, telomerase inhibition is enhanced, and the gradual erosion of the telomere occurs as cells replicate (Pol-α recruitment may be enhanced, but the maximum possible length of the C-rich strand is limited by the shortening G-rich strand). In cells that lack *CTC1* and simultaneously overexpress *STN1*, telomerase extension of the G-rich overhang is not fully inhibited by STN1 as CTC1 is not present, whilst the high levels of STN1 may be able to inhibit resection of the C-rich strand or even promote Pol-α activity despite the absence of CTC1.

available (Fig. 45) to attract DDR elements such as RPA.

In contrast to the apparent suppression of *CTC1* knockout-induced telomeric γH2AX by *STN1*-OE, non-telomeric γH2AX appears significantly more abundant in *CTC1*$^{-/-}$ DTC15-S9 STN1-OE cells (Fig. 46c). Chromosomes with non-telomeric γH2AX foci were approximately 1.6-fold more common in *CTC1*$^{-/-}$ cells when *STN1* was overexpressed compared to *CTC1*$^{-/-}$ cells with wild-type *STN1*. This disparity supports the model of separate roles for STN1 at the telomere and in DSB repair genome-wide, and that high levels of STN1 can simultaneously have beneficial and deleterious effects on the cell.

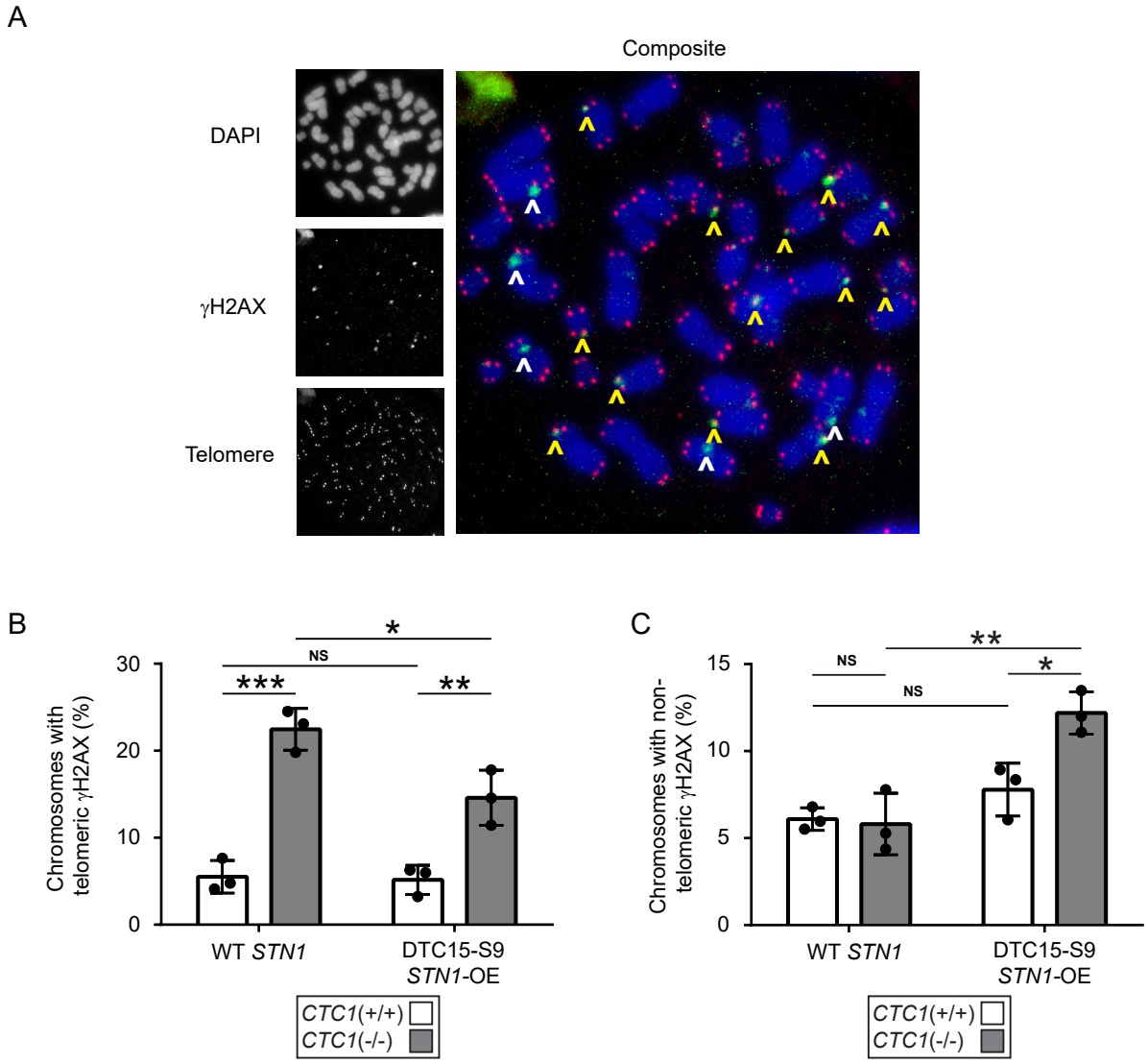

Figure 46. *STN1* overexpression can partially suppress telomeric γH2AX in *CTC1*$^{-/-}$ HCT116 cells, but enhances non-telomeric γH2AX. *CTC1* knockout was induced by addition of 10 nM tamoxifen to the culture media. 10 days later telomeric γH2AX localisation was measured by PNA probe FISH combined with immunofluorescence. (A) Representative fluorescent images of an *STN1*-OE *CTC1*$^{-/-}$ DTC15-S9 HCT116 metaphase chromosome spread. Yellow arrowheads indicate telomere signal and γH2AX signal co-localisation, white arrowheads indicate non-telomeric γH2AX. (B) Quantification of telomeric γH2AX frequency. (C) Quantification of non-telomeric γH2AX frequency. Bars represent standard deviation between three experimental repeats. Statistical significance calculated by two-way ANOVA using Tukey's correction for multiple comparisons.

7.7 Loss of *CTC1* Induces Cell Death in *STN1*-Overexpression HCT116 Cells

As *STN1* is capable of partially suppressing telomeric phenotypes of *CTC1* knockout cells, but enhances non-telomeric DNA damage, it remained unclear whether high STN1 levels would have a positive overall effect on cell viability. *CTC1* knockout induces a strong cell growth defect likely due to the activation of the DDR at the telomere, therefore the partial suppression of telomeric defects by STN1 might also result in a reduced growth defect. To address this, *CTC1* was knocked out of HCT116 cells with and without the *STN1* stable-overexpression cassette. Cells were counted and passaged every 2-3 days, and population doublings recorded. *STN1* overexpression had no significant effect on cell growth in the presence of *CTC1*. The deletion of *CTC1* induces the previously characterised gradual growth defect in wild-type *STN1* cells, however when *CTC1* is knocked out of DTC15-S9 or DTC15-S12 (HCT116 cells that overexpress *STN1*) the growth defect is significantly enhanced (Fig. 47). Whilst growth of $CTC1^{-/-}$ cells with endogenous levels of STN1 slowly declines from day 6 to day 12, the growth of the DTC15-S9 clone is reduced to near-zero 7 days after *CTC1* knockout induction. DTC15-S12 exhibited an intermediate enhancement of the $CTC1\Delta$ growth defect, concordant with its intermediate overexpression of *STN1*.

Whilst the growth defect of $CTC1^{-/-}$ cells is largely due to cellular senescence [182], the knockout of *CTC1* in *STN1*-OE cells appeared to be inducing a significant amount of cell death (based on observations of cell morphology made by eye during the population growth assay). To confirm and quantify this cell death, DTC15-S9 *STN1*-OE HCT116 cells were stained with trypan blue 10 days after *CTC1* knockout. Trypan blue is only capable of staining dead cells, as live cells are able to exclude the dye. At day 10 the *CTC1* knockout culture comprised approximately 6% dead cells, compared to 2% in the $CTC1^{+/+}$ population (Fig. 48). After knockout of *CTC1* in the *STN1*-OE cells, approximately 25% of cells in the culture were dead. These data suggest that when *STN1* is overexpressed, loss of *CTC1* has a significantly more catastrophic effect on cell viability. A possible explanation for this effect is that *STN1*-OE cells are HDR compromised. Loss of *CTC1* results in more replication fork stalling and collapse [185], events which HDR plays a key role in resolving. Additionally, Stn1 in budding yeast can suppress checkpoint activation by stalled replication forks [292]. If the same were true of human STN1, then the death of $CTC1^{-/-}$ *STN1*-OE cells may be due to entering mitosis with unresolved stalled replication forks.

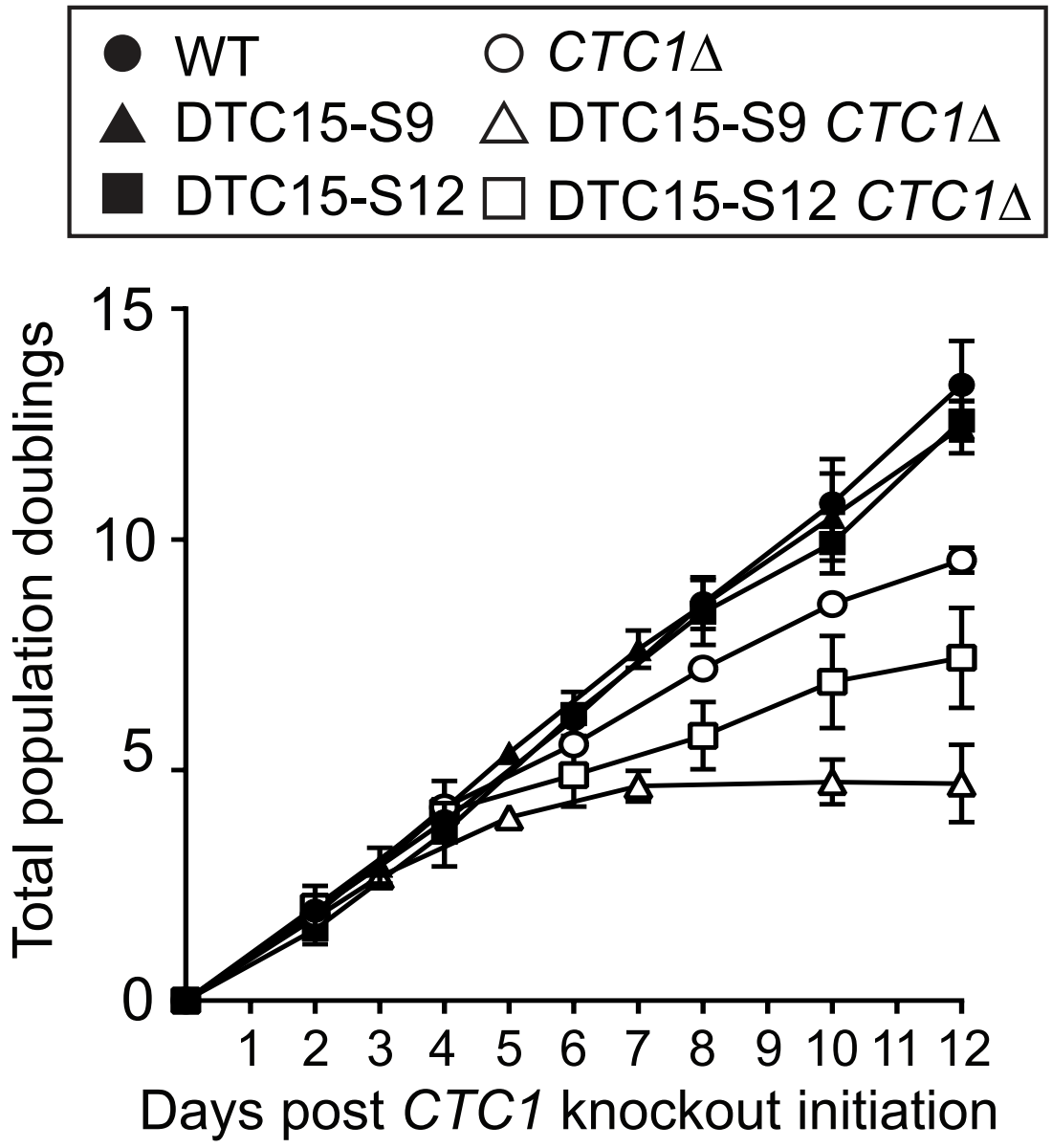

Figure 47. Growth of *STN1*-OE HCT116 cells after *CTC1* knockout. *CTC1* knockout was induced by addition of 10 nM tamoxifen to the culture media. Cells were counted every 2-3 days and population growth calculated. Bars represent standard deviation between 3 experimental repeats.

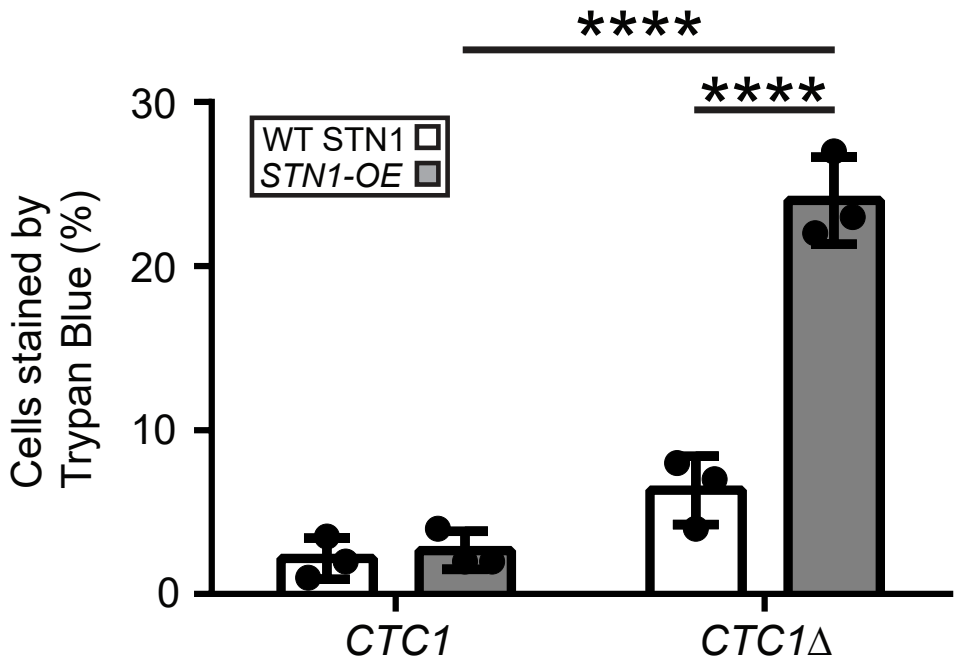

Figure 48. Cell death after *CTC1* knockout in DTC15-S9 HCT116 *STN1*-OE cells. *CTC1* knockout was induced by addition of 10 nM tamoxifen to the culture media. 10 days after knockout initiation cells were stained with trypan blue to score cell death. Bars represent standard deviation between three experimental repeats. Statistical significance was calculated by two-way ANOVA using Tukey's correction for multiple comparisons.

7.8 Discussion

The data in this chapter demonstrate the significant negative impact that raising STN1 levels has on genomic integrity. Overexpression of *STN1* induces short telomeres and appears to hinder the accurate repair of DNA damage.

HCT116 cells with high STN1 levels exhibited increased markers of genomic instability including micronuclei and (non-telomeric) γH2AX foci. HDR was significantly inhibited when STN1 was overexpressed, whilst NHEJ appeared to be supported (manifested in the resistance of *STN1*-overexpressing cells to etoposide). Additionally, high levels of STN1 appear able to partially compensate for loss of *CTC1* with regards to telomere length regulation, but exacerbated the overall genomic instability of *CTC1*Δ cells.

7.8.1 The Inhibition of HDR by STN1

The CST complex is recruited to resected DSBs by 53BP1/RIF1/Shieldin where it promotes the fill-in of dsDNA by Polymerase-α [189]. It has been previously demonstrated that loss of CST complex members could restore HDR in BRCA1-deficient cancers [175] as a lack of a functional CST complex allows hyper-resected ssDNA to persist and take part in HDR. We show here that as STN1 levels are raised above endogenous levels in cells with functional BRCA1 and HDR, HDR becomes significantly inhibited. Transient overexpression of *STN1* reduced HDR by approximately 40% when assayed using a DRGFP reporter system.

Inhibition of HDR could explain the increase in γH2AX foci frequency and chromatin bridges/micronuclei in cells overexpressing *STN1* via a number of pathways. Filling-in resected DSBs by Polymerase-α could increase the repair of DSBs by NHEJ, resulting in a higher frequency of chromosome fusions and dicentric chromosomes (as outlined in figure 25). Alternatively, it could be that when HDR is inhibited the cell is not able to use an alternative repair pathway and the damage remains unrepaired altogether. Additionally, overexpression of *STN1* in budding yeast overrides many aspects of the S-phase checkpoint response [292]. As the HDR pathway is key for repair of stalled replication forks [302], it is possible that high levels of STN1 are inhibiting the repair of collapsed replication forks in *STN1*-OE cells whilst simultaneously suppressing the cell cycle checkpoint that would be activated by said collapsed forks. This would result in cells entering mitosis with sister chromatids connected by DNA replication intermediates, which in turn become chromatin bridges and micronuclei as sister chromatids attempt to segregate into separate daughter cells [303].

7.8.2 STN1 Supports The Non-Homologous End Joining-Dependant DNA Damage Response Following Etoposide Treatment

HCT116 cells with raised STN1 levels are more viable following etoposide exposure than cells with endogenous levels of STN1 (Fig. 42). The *STN1*-OE cells also present fewer γH2AX foci and markers of genomic instability such as chromatin bridges and micronuclei (Fig. 37) following etoposide exposure. As etoposide-induced DSBs are repaired by the NHEJ pathway (after an initial processing by MRN-CtIP) [304], this implies that high levels of STN1 are capable of not only inhibiting HDR, but also actively promoting or supporting NHEJ.

Published evidence indicates that the CST complex is capable of promoting fill-in by Pol-α at resected DSBs. This DSB fill-in was hypothesised to be inhibiting HDR in BRCA1-deficient cancers, and that the purpose of CST-mediated Pol-α recruitment at DSBs in wild type cells was to inhibit hyper-resection and the mutagenic SSA pathway [175][189] (Fig. 14). It was hypothesised that the fill-in of the DSB could make it a substrate for Ku70/Ku80 binding and the initiation of NHEJ. Data presented here indicate that high STN1 levels in otherwise HDR-proficient cells can inhibit HDR, resulting in a switch to the less accurate NHEJ pathway (Fig. 49).

The promotion of the NHEJ DNA repair pathway by high levels of STN1 presents a possible reason for degradation of *STN1* mRNA by NMD. Data in this chapter demonstrate a negative impact on overall genomic stability by high levels of STN1, but for most genes low protein expression does not require NMD [305]. Many proteins exist in the cell at low levels due to transcriptional regulation, translational regulation, or by fast protein turnover. STN1 is one of a small fraction of proteins that is maintained at a low level by NMD. This could be because whilst it is important to maintain low levels of STN1 under most conditions, higher levels of STN1 are beneficial in the situations that NMD is downregulated. For example, NMD is downregulated when G_0 cells experience persistent DNA damage [237], and it is demonstrated in chapter 5 that this correlates with *STN1* mRNA stabilisation. Because HDR is dependant on readily available template DNA, cells in G_0 may have to rely on NHEJ to repair DNA damage. As *STN1* overexpression appears to promote or support the repair of DNA damage by NHEJ, NMD may be used as the pathway of *STN1* regulation so that last ditch efforts by non-cycling cells to repair persistent DNA damage get a supportive boost from higher STN1 levels.

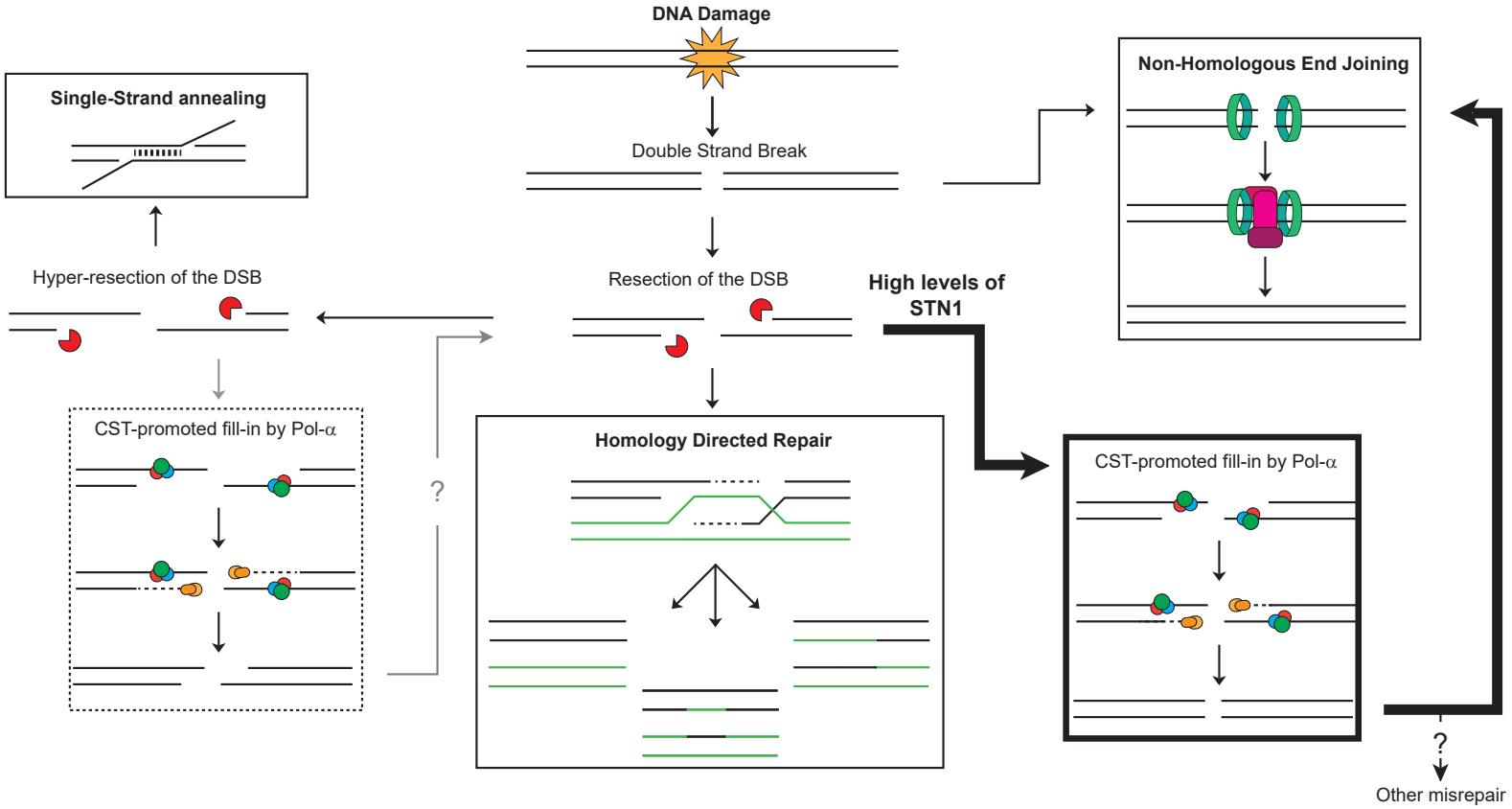

Figure 49. Proposed model of HDR inhibition and NHEJ promotion by high levels of STN1. HDR is dependent on resection of DSBs to produce ssDNA overhangs. The CST complex promotes the fill-in of these resected breaks. In cells with wild-type levels of STN1 this fill-in may be limited to hyper-resected DSBs as proposed by Barazas et al. (2018) [175]. However, high levels of STN1 appear capable of significantly inhibiting HDR in otherwise HDR-competent cells. As NHEJ appears to be supported by high STN1, it is proposed here that highly abundant STN1 inhibits the accurate HDR pathway and promotes the use of the inaccurate NHEJ pathway. It is also possible that some breaks are not repaired at all as a result of HDR inhibition.

7.8.3 High STN1 Levels Affect Telomere Length Regulation

Telomeres protect the integrity of the genome by providing a buffer of non-coding DNA at the end of chromosome. This DNA can be gradually eroded as cells progress through multiple replication cycles. If telomeres become critically short, cells risk losing genetic information so induce cell cycle-arrest. However, if the ssDNA overhang is overextended this can erroneously attract the DDR, inappropriate activity of nucleases and other DDR factors can result in chromosomal fusions and fragmentation. Maintaining the balance between under and over-extension of the telomeric G and C-rich strands is therefore important for the integrity of the chromosome. HCT116 cells that have overexpressed *STN1* for approximately 90 cell divisions have shorter telomeres than HCT116 cells of equivalent age and endogenous levels of STN1. This mirrors the short telomere phenotype of *STN1*-OE budding yeast [298]. The CST complex is a telomerase inhibitor, it is possible that high levels of STN1 alters the stoichiometry of the CST complex binding to the telomere, enhancing the inhibition of telomerase.

The majority of human cells do not have active telomerase, their telomeres gradually shorten until the cells become senescent, contributing to ageing and age-related diseases [306]. The long-term health impacts from higher than normal expression of *STN1* have not been investigated. Individuals with high levels of *STN1* expression may have earlier onset of cellular senescence and ageing-related diseases. Conversely, high STN1 levels (either naturally or artificially induced) may impact the ability of cancers to develop and proliferate indefinitely, as their ability to regenerate and maintain telomeric DNA is hindered.

7.8.4 The Partial Suppression of *CTC1*Δ by Overexpression of *STN1*

Knockout of *CTC1*, like *STN1* overexpression, induces telomere C-strand shortening. In *CTC1*Δ cells the G-rich overhang is also extended as telomerase inhibition is lost [171]. The *CTC1*Δ induced shortening of the C-strand is likely related to the role of the CST complex in recruiting Pol-α and promoting the fill-in of the C-strand [182]. Interestingly, when *CTC1* is knocked-out in *STN1*-OE HCT116 cells, the short telomere phenotype seen in both genotypes individually is suppressed. One model to explain this phenomenon is outlined in figure 45, when *CTC1* is lost in *STN1*-OE HCT116 the inhibition of telomerase is limited (returning it to near-normal levels), whilst the fill in of the C-strand (or the inhibition of its degradation by nucleases) is still possible due to the high STN1 levels compensating for *CTC1* loss (and the ability of STN1-TEN1 to weakly bind DNA still [300]). In support of this model, loss of *CTC1* also induces less telomeric γH2AX accumulation at the telomere of *STN1*-OE cells than it does in wild-type *STN1* cells (Fig. 46b). This is consistent with less ssDNA accumulation (which would attract RPA and trigger a DDR), due to either telomerase inhibition or recovery of C-Strand fill-in by Pol-α.

As *CTC1* knockout was induced in HCT116 cells that already overexpress *STN1* (and

therefore already have short telomeres), the near-normal telomere lengths after 10 days without CTC1 suggests that telomere length has not merely stabilised, but rather the C-rich strand of telomeres has been actively re-extended. It is not known if the telomeres had returned to a relatively static state of length homeostasis, or if they would have continued to extend were it not for the growth arrest and cell death of these *CTC1*Δ *STN1*-OE cells. Although the difference between the telomere C-strand lengths of wild-type HCT116 cells and *CTC1*Δ *STN1*-OE HCT116 cells was not significant, the mean length of the *CTC1*Δ *STN1*-OE telomere C-strands were slightly greater than in the WT. Furthermore, the standard deviation of the *CTC1*Δ *STN1*-OE telomere C-strand lengths was much greater than in the wild type. This variation in telomere length suggests the telomere length regulation is still far from perfect. Data in this chapter are consistent with the ability of Stn1 to partially compensate for telomere uncapping in *cdc13-1* budding yeast [299].

Whilst high levels of STN1 appear to make telomeres of HCT116 cells more tolerant of CTC1 loss, non-telomeric DNA damage is exacerbated, manifested in increased γH2AX foci. Unlike in wild-type *STN1* cells, loss of *CTC1* in *STN1*-OE HCT116 cells induces a strong cell-death response, likely related to the significant increase in non-telomeric DNA damage. A possible explanation of this increase in DNA damage is high levels of STN1 permitting entry of *CTC1*Δ cells from S-phase into G2 despite the presence of stalled replication forks (which has been reported in *S. cerevisiae* [292]). The result of which would be cells entering mitosis with double-strand breaks or unresolved replication intermediates, and the generation of ultra-fine bridge (UFB)s and DNA damage. However, in this model the increase in DNA damage would be expected to mostly occur at the telomere, as telomeric DNA is the most dependent on CTC1 and the CST complex for replication [185]. Alternatively, it may be that the collapsed replication forks induced by loss of *CTC1* cannot be repaired in the context of high STN1 (HDR plays a key role in the repair of collapsed replication forks [307], but high STN1 levels appear to inhibit HDR). Again however, if this is the case it is strange that the increase in γH2AX does not colocalise with the telomeres of these cells, as telomeric replication forks are particularly dependant on CTC1. Perhaps the explanation is simply that telomeric DNA is estimated to make up only 0.02% of the genome of HCT116 cells (based on an average telomere length of 7 kb [174] and a total genome size of 3235 mb), and as such non-telomeric damage has an overwhelming statistical likelihood over telomeric damage. Additionally the CST complex does support replication fork restart in non-telomeric regions of DNA as long as the region is GC-rich [185].

In summary, high levels of STN1 appear to inhibit HDR in human cells, compromising genomic stability. However, high levels of STN1 may be beneficial to the cell under certain conditions, such as when telomere homeostasis is compromised by loss of CTC1 function, or when NHEJ is the necessary repair pathway for DNA damage.

8 The role of *dna-2* in *Caenorhabditis elegans*

The nuclease/helicase Dna2 in *S. cerevisiae* has been demonstrated to resect elongated 5′ flaps of Okazaki fragments produced during lagging strand DNA synthesis [308]; DNA double strand breaks [309]; and telomeres uncapped by the loss of functional Cdc13 [310]. Recently reported data suggested an essential telomeric role for budding yeast Dna2 [311]: *dna2*Δ cells have telomere defects; Dna2 colocalises with RPA and Cdc13; and the temperature sensitive *dna2*Δ lethality can be suppressed by DNA damage checkpoint and telomeric helicase mutations (such as the 9-1-1 complex and Mph1 respectively). Suppression by knockout of DNA damage checkpoint genes implies an essential telomeric function of Dna2. When the telomere is somehow uncapped or accumulates ssDNA the DDR can identify the chromosome ends as deleterious breaks in DNA. Consequently the cell cycle is arrested by the DNA damage checkpoint. Therefore a key indicator of *Dna2* having an essential telomeric function is that its mutation lethality can be bypassed by deactivating the DNA damage checkpoint. Furthermore, suppression of this growth defect by knockout of the helicase *MPH1* supports the hypothesis of a telomeric role for Dna2 as Mph1 has been shown to unwind telomeric DNA [312]. Markiewicz-Potoczny et al. [311] proposed a function of Dna2 in cleaving the C-rich 5′ strand of partially unwound telomeres, limiting the activation of the DDR by exposed ssDNA (Fig. 50 I).

The goal of this chapter is to determine if this telomeric role of Dna2 could be conserved in higher eukaryotes. Like the budding yeast homologue, *C. elegans dna-2*Δ mutations are temperature sensitive, conveying embryonic lethality at 25°C. *dna-2*Δ also delays *C. elegans* embryo hatching at lower temperatures (observable at 20°C but strongest at 16°C). This presents a good opportunity for determining if DNA-2 has a telomeric role in a multicellular model organism, as knockout strains of both the telomeric helicase *fncm-1* (homologue of budding yeast *MPH1* and human *FANCM*) and the DNA damage checkpoint 9-1-1 complex component *mrt-2* (homologue of human *RAD1*) are available. Null mutations of both *MPH1* and 9-1-1 complex components in yeast are *dna2*Δ suppressors, supporting the hypothesis that Dna2 resects the 5′ strand of unwound telomeres (Fig. 50 I). If *fncm-1*Δ and *mrt-2*Δ are also able to suppress the *C. elegans dna-2*Δ embryonic lethality, that would suggest a telomeric role for Dna2 is conserved in higher eukaryotes. The delayed hatching of *dna-2*Δ worms at lower temperatures has be been hypothesised to be due to the role of *dna-2* in DNA synthesis which occurs less efficiently without DNA2 [313]. As such knockout of *mrt-2* or *fncm-1* might be expected to improve the viability of *dna-2*Δ embryos at 25°C without suppressing the slow development of embryos at 16 or 20°C. To address this, double-mutant worm strains were generated by crossing the *dna-2*(jh115) mutant strain with *fncm-1*(tm3148) or *mrt-2*(e2663) strains.

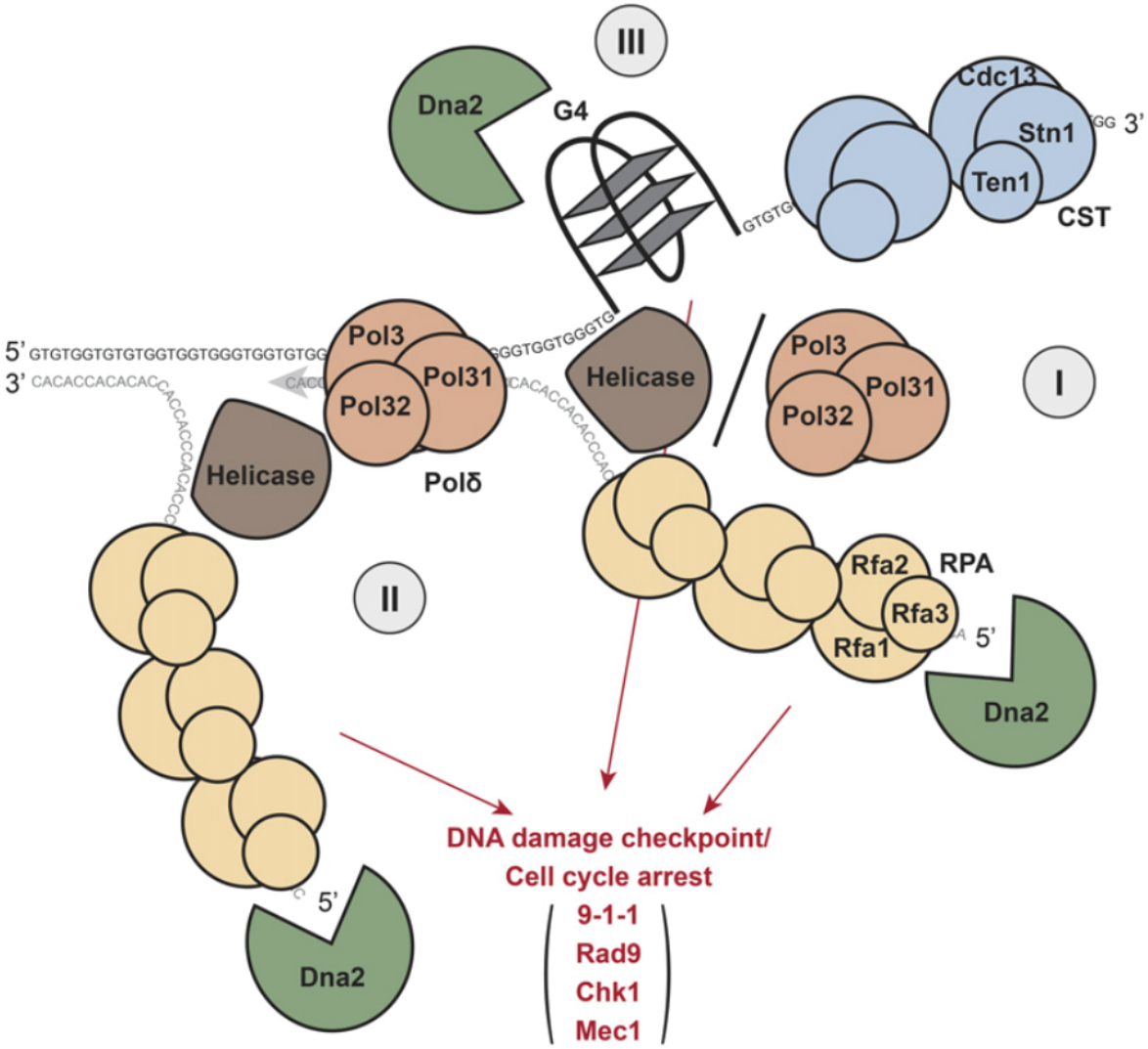

Figure 50. A proposed model of the telomeric role of *S. cerevisiae* Dna2. Markiewicz-Potoczny et al. proposed 3 potential functions of Dna2 at the telomere in budding yeast. (I) The primary proposed role of Dna2 at the telomere. Helicases/polymerases unwind 5′ telomeric DNA. RPA binds the ssDNA which is then cleaved by Dna2. (II) Long flaps of Okazaki fragments near the telomere are bound by RPA and cleaved by Dna2. (III) G-quadruplex structures that form on unwound telomeric DNA are unwound by Dna2. Figure from Markiewicz-Potoczny et al., 2018 [311].

8.1 *fncm-1*Δ and *mrt-2*Δ are Partial Suppressors of *dna-2*Δ Embryo Lethality

The budding yeast helicase Mph1 appears to be capable of remodelling telomeres, making them more accessible to nucleases [312]. The suppression of *dna2*Δ lethality by deletion of Mph1 [311] is therefore consistent with a telomeric role of Dna2. An explanation being that the need for Dna2 to resect telomeric ssDNA is reduced if Mph1 is no-longer unwinding telomeres and producing excessive ssDNA (Fig. 50 I).

*dna-2*Δ *C. elegans* embryos are >90% viable when grown at 20°C or lower (Fig. 51). However, when grown at 25°C less than 20% of embryos will hatch. The remaining embryos will die before hatching. At 25°C typically 100% of wild-type worm embryos will hatch, as will approximately 90% of *fncm-1*Δ (deletion of the *S. cerevisiae* homologue of *MPH1*) embryos. A *dna-2*Δ *fncm-1*Δ double-mutant worm was produced through crosses, and embryo hatching assessed. Consistent with the data from budding yeast [311], loss of *fncm-1* is capable of partially suppressing the embryo viability defect of *dna-2*Δ *C. elegans* embryos. At 25°C approximately 50% of eggs from *dna-2*Δ *fncm-1*Δ worms hatched, compared to less than 20% of *dna-2*Δ single-mutant worms (Fig. 51).

Deletion of the budding yeast 9-1-1 complex component *MEC3* was also capable of partially suppressing *dna2*Δ lethality [311]. The 9-1-1 complex is a key part of the DNA damage checkpoint. As suppression of mutation growth defects by inactivation of the DDR is a hallmark of telomere dysfunction, these data supported a telomeric role for Dna2.

A *C. elegans* strain with *hus-1* (homologue of *MEC3*) deleted was not readily available, however a strain with *mrt-2* (a different *C. elegans* 9-1-1 complex component) deleted was available and consequently used. As with *fncm-1*, the *mrt-2*Δ strain was crossed with the *dna-2*Δ mutant, and embryo hatching of the double-mutant was assessed. The absence of *mrt-2* results in a significant compromise to genomic stability due to the importance of the 9-1-1 complex in detecting and repairing real DNA damage. As such it is not surprising that after 36 hours less than 70% of *mrt-2*Δ embryos were viable (Fig. 51). Despite this significant viability defect, deletion of *mrt-2* in *C. elegans* appears to be capable of

---

Figure 51 . The *dna-2*(-/-) embryo hatching defect is partially suppressed by *fncm-1*(-/-) or *mrt-2*(-/-). Homozygous worms were grown from the L1 stage at 16°C, 20°C, or 25°C for 3-5 days (for strains carrying a *dna-2* mutation, these L1 worms were the *dna-2*$^{-/-}$ homozygous progeny of a *dna-2*(+/-) heterozygous parent). Adults were picked onto a fresh plate and allowed to lay eggs for 3 hours before being removed. The eggs were returned to 16/20/25°C and the percentage of hatched eggs was scored every 6 hours for 36 hours. Bars represent standard deviation between three separate experimental repeats.

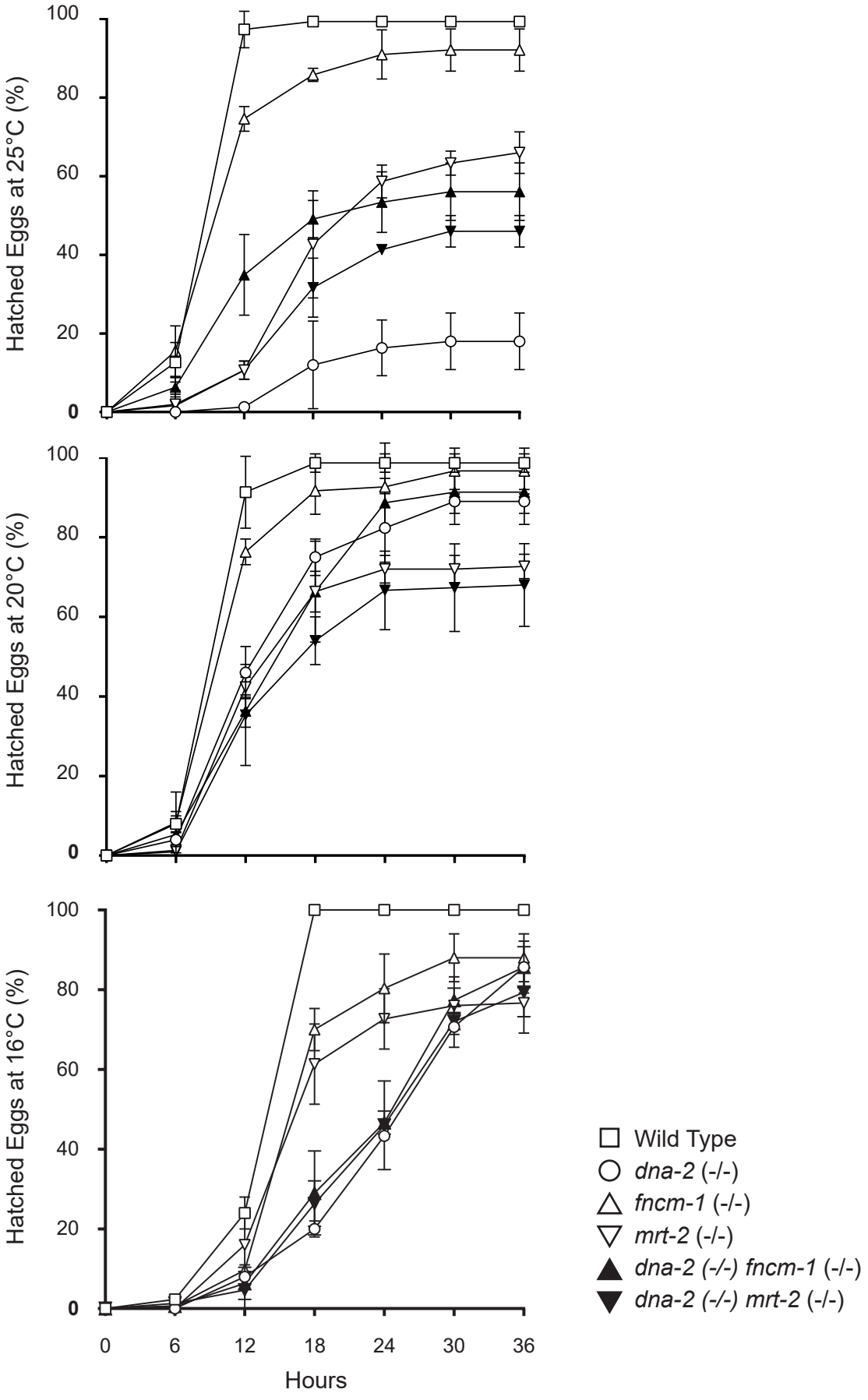
Hatched Eggs at 25°C (%)
Hatched Eggs at 20°C (%)
Hatched Eggs at 16°C (%)
100
80
60
40
20
0
0
6
12
18
24
30
36
Hours
Wild Type
dna-2 (-/-)
fncm-1 (-/-)
mrt-2 (-/-)
dna-2 (-/-) fncm-1 (-/-)
dna-2 (-/-) mrt-2 (-/-)

partially suppressing the embryonic viability defect of *dna-2*Δ worms (Fig. 51). After 36 hours more than 40% of *dna-2*Δ *mrt-2*Δ embryos at 25°C had hatched (compared to less than 20% of *dna-2*Δ single-mutant embryos).

8.2 *fncm-1*Δ and *mrt-2*Δ Do Not Suppress *dna-2*Δ Embryo Hatching Delay

Whilst *dna-2*Δ embryos are 80-90% viable at 20°C and 16°C, they exhibit a delayed development rate. Wild-type embryos typically complete hatching after 18 hours at 20°C and 16°C, but it takes *dna-2*Δ eggs 30-36 hours to reach 100% hatching of viable eggs. The cells of *C. elegans* embryos are dividing very rapidly, and as such any delay in DNA replication is likely to have a significant impact of development rate. The delay seen in *dna-2*Δ embryos was proposed to be due to its role in Okazaki fragment processing during DNA synthesis [313]. Unlike the embryonic viability defect at 25°C, neither deletion of *fncm-1* or *mrt-2* was able to suppress the slow development of *dna-2*Δ embryos at 20°C or 16°C (Fig. 51). This supports the hypothesis that the interaction of FNCM-1 and MRT-2 with DNA-2 is due to a role of DNA-2 that is separate to the known role of DNA-2 in DNA synthesis.

8.3 Discussion

The *C. elegans* data presented in this chapter are consistent with the proposed essential telomeric role of Dna2 in *S. cerevisiae*. The embryonic lethality at 25°C of the *dna-2*Δ worm can be significantly suppressed by inhibiting the DNA damage checkpoint or by knockout of a telomeric helicase. Whilst the CST complex binds G-rich ssDNA highly efficiently, it binds to C-rich ssDNA with less efficiency. This potentially leaves the C-rich strand exposed to the DDR. As Dna2 is capable of degrading RPA-bound ssDNA [35], the proposed role of Dna2 is the degradation of the 5′ C-rich strand should the dsDNA of the telomere become unwound. This degradation of the C-rich ssDNA would inhibit RPA-binding triggering the DDR (Fig. 50 I) [311].

In contrast to the embryo inviability, the slow rate of *dna-2*Δ embryo development at lower temperatures was unaffected by *mrt-2*Δ or *fncm-1*Δ. This suggests the slow embryo development is due to a different pathway than the low embryo viability of *dna-2* worms. A possible model is that the slow embryonic development is due to a role of *DNA-2* in Okazaki fragment long flap cleavage during DNA synthesis (which has been demonstrated in budding yeast [308]). Cleavage is necessary but performed redundantly by other nucleases, which means that in the absence of Dna2 DNA synthesis still occurs, but less efficiently. Less efficient DNA synthesis could translate into slower embryo development as it is the stage in the life cycle of the worm in which cell division is happening rapidly [313]. *MRT-2* and *FNCM-1* are not necessarily involved in the processing of Okazaki

fragment flaps which may be why their knockout would not suppress this developmental phenotype of *dna-2*Δ embryos.

An interesting consistency between *dna2*Δ *S. cerevisiae* and *dna-2*Δ *C. elegans* is the temperature sensitivity of the lethality, which is exacerbated at higher temperatures. This could be explained by temperature dependent telomere unwinding creating the 5′ ssDNA substrate for RPA binding and *DNA-2* cleavage.

The data in this chapter are congruent with an essential role of *DNA-2* in *C. elegans* in suppressing the activation of the DNA damage response to ssDNA at the telomere. This role is likely separate from a role in Okazaki fragment flap processing (Fig. 50 I). Nematodes and humans both belong to the kingdom animalia whilst budding yeast belongs to the fungi kingdom. Fungi and animalia diverged approximately 1.1 billion years ago, therefore if functions of Dna2 are conserved between *S. cerevisiae* and *C. elegans* then there is a good chance this essential telomeric function of *Dna2* is preserved in other metazoans such as humans.

9 Discussion

Following its discovery in 2009, the list of known roles the human CST complex plays in maintaining genomic integrity has continued to grow. In *S. cerevisiae* the CST complex is the main telomere capping complex, it is responsible for regulating and promoting the replication of the telomere. When the human homologues of *CDC13*, *STN1* and *TEN1* were discovered, evidence suggested they played a similar role in maintaining the integrity of the human telomere. CST does this by inhibiting the overextension of the G-rich 3′ overhang by telomerase [171], promoting the fill-in of the C-rich strand [182], and by supporting the replication of the telomere [184]. The ability of the human CST complex to aid replication fork restart during replication stress extends beyond the telomere however, this was the first piece of evidence pointing towards a role for the human CST complex outside of the telomere [173]. It is now known that the CST complex promotes the restart of stalled replication forks by recruiting RAD51 [185]. An additional non-telomeric role for the CST complex was recently discovered, the complex is capable of binding to resected DSBs and promoting the fill-in of duplex DNA [189][175]. Investigating how these newly discovered non-telomeric roles of the CST complex are regulated and how they impact genomic stability on a cellular level is important for understanding CST related disease pathogenesis.

9.1 Genomic Instability and Cell Cycle Arrest after Loss of CTC1

Here we confirm the role of CTC1 in maintaining the C-rich strand of the human telomere. C-strand erosion coincides with activation of the DNA damage response at the telomere, supporting the proposed role of CTC1 in promoting the fill-in of the C-rich strand by Pol-α and minimising the accumulation of ssDNA. The loss of telomere homeostasis observed correlates with a gradual growth arrest. Whilst these data closely mirror what is seen in *cdc13-1 S. cerevisiae* cells, the arrest of *CTC1*Δ human cells appears to be mediated by a separate pathway to that seen in budding yeast. Instead of being mediated by CHK1 (a DDR kinase that targets CDC25, inhibiting the formation of cyclin-dependant kinase complexes) the arrest of *CTC1*Δ cells is mediated by the p53/p21 pathway. The lack of CHK1 activation is surprising, as loss of CTC1 does result in γH2AX and RPA accumulation at the telomere, which is an upstream activator of CHK1. The apparent disconnect between telomeric RPA accumulation and the CHK1-independent cell cycle arrest might reflect the more complex role that the CST complex plays in human cells compared to budding yeast, and the importance of the complex's additional non-telomeric functions.

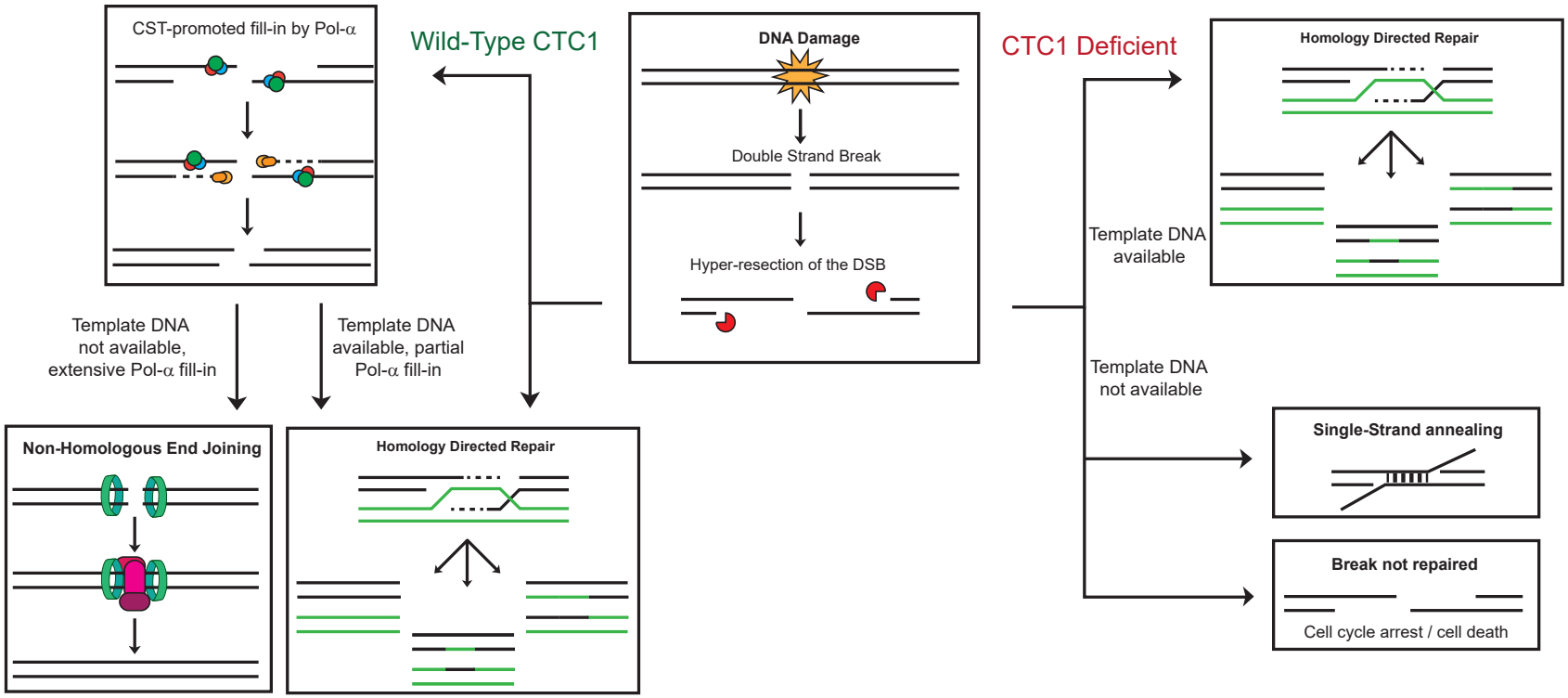

Figure 52. Proposed model of CTC1 influence on hyper-resected DSBs. In cells with functional CTC1 hyper-resection of DSBs is counteracted by Pol-α. If this fill-in is incomplete and a template strand is available the cell is capable of performing HDR. If a template strand is not available and fill-in has either completed or left only a short overhang then NHEJ could be used to repair the break. In CTC1Δ cells hyper-resected breaks can still be repaired by HDR if the template DNA is available. If no template DNA is available it is possible that the break may be repaired by SSA, but it may not be repaired at all, resulting in cell cycle arrest or death.

Perhaps related to the different (CHK1 independent) cell-cycle arrest pathway seen in *CTC1*Δ human cells, we report here a rapid onset of genomic instability after *CTC1* knockout that appears unrelated to telomere misregulation and is instead due to defective DNA repair. It was recently discovered that the CST complex can localise to resected DSBs and promote the fill-in of duplex DNA. When the CST complex is depleted, HDR (which is dependent on a long ssDNA overhang) is recovered in BRCA1-deficient cancers as the overhang is no-longer eliminated by Pol-α (which was recruited by CST). Whilst this loss of CST complex components was beneficial to BRCA1 deficient cells exposed to PARP inhibitors because it restored HDR functionality, it may be the cause of the genomic instability see in *CTC1*Δ HCT116 cells (Fig. 53b). HDR is dependant on the availability of template DNA in order to repair breaks. If a DSB is hyper-resected during the stages of the cell cycle when template DNA is not readily available, and the CST complex is not available to counteract the resection, then the repair process may stall, unable to use either HDR or NHEJ (Fig. 52). It is also possible that the persistence of hyper-resected DSBs as a result of CTC1 loss results in an increase in SSA which can result in the loss of long tracts of DNA and as such is highly mutagenic [175].

9.2 The Impact of High STN1 Levels on Genomic Stability

The negative impact of high STN1 levels on genomic stability and HDR reported here further underscores the importance of the CST complex in DDR regulation beyond the telomere. As previously discussed, the CST complex has been shown to promote the fill-in of hyper-resected DSBs [189]. Here we expand upon this discovery, demonstrating the ability of high levels of STN1 to inhibit HDR in cells that would otherwise be HDR competent. HDR inhibition is a possible explanation for the high levels of DNA damage in *STN1*-OE HCT116 cells (manifested in an increase in γH2AX foci and micronuclei). HDR is the more accurate pathway of DNA repair due to its use of a template sequence [314]. HDR is also crucial for the repair of stalled replication forks [315]. It is therefore important that the CST complex is not just expressed to any degree above a minimal level, but tightly regulated so as to not interfere with DNA repair pathways. Furthermore, high STN1 levels appear to convey resistance to the chemotherapeutic etoposide, which induces DSBs that rely on NHEJ for repair (after an initial processing by MRN-CtIP). A cancer tissue's STN1 level may therefore affect the efficacy of etoposide as a treatment option (Fig. 53c).

Additionally, high levels of STN1 resulted in shorter telomeres in HCT116 cells, likely due to the ability of the CST complex to inhibit telomerase [171]. This is consistent with what is seen in *S. cerevisiae* [298]. Stn1 was initially identified as a gene that suppressed the effects of the *cdc13-1* mutation in budding yeast. Whilst raising STN1 levels did appear to compensate for the loss of CTC1 at the telomere in human cells, the affect on genome-wide stability was significantly deleterious, resulting in cell death. The effect of STN1

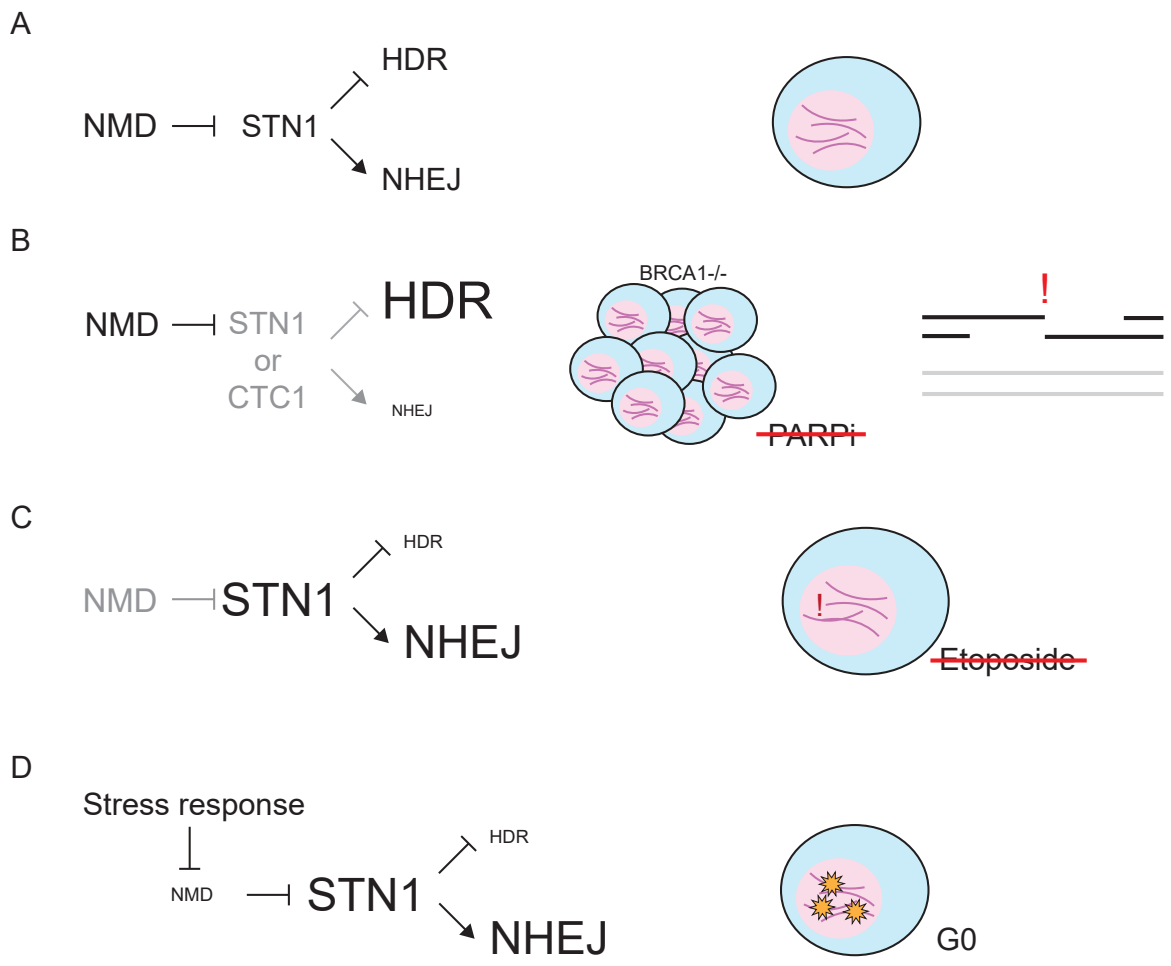

Figure 53. The regulation of CST complex components and their influence on DNA repair. (A) In a normal cell NMD suppresses STN1 levels, allowing the cell to use HDR and NHEJ as appropriate. (B) Loss of a CST complex component conveys PARP inhibitor resistance in BRCA1-deficient cancers by restoring HDR. Additionally loss of a CST component could inhibit any repair if a template strand for HDR is not available but the break has already been resected. (C) High STN1 levels convey resistance to etoposide, possibly by promoting NHEJ. Loss of NMD function may therefore correlate with cancer etoposide resistance. The promotion of NHEJ can however result in repair errors such as chromosome fusions. (D) NMD is inhibited as part of the stress response to prolonged DNA damage in G_0. This increases STN1 levels, which might act to support repair of the damage by NHEJ.

overexpression on *CTC1*Δ human cells highlights the importance of the extra-telomeric roles of the human CST complex, and further illustrates the importance of limiting STN1 levels.

9.3 Regulation of STN1 by Nonsense Mediated Decay

As tightly controlling STN1 levels appears necessary for maintaining genomic stability, it is important to understand the pathways that regulate STN1 abundance. Here we report evidence that like *STN1* in budding yeast [231], human *STN1* mRNA is degraded by NMD. When NMD was chemically inhibited the abundance of *STN1* mRNA and protein increased, and when NMD was down-regulated in RPE-1 cells the degradation rate of *STN1* mRNA was reduced. The question remains however, why is *STN1* regulated by NMD and not simply regulated at the transcriptional level? The answer may simply be that degradation of *STN1* by NMD enables a higher transcription rate, and the kinetics of *STN1* levels are therefore shifted to benefit the cell. The high transcription rate of *STN1* might be beneficial immediately after mitosis when transcription has been inhibited by the condensation of DNA. Having a high production and turnover rate could mean that newly divided daughter cells are more rapidly able to return *STN1* mRNA abundance to the desired level having been unable to transcribe it during mitosis. There are however other explanations for regulating *STN1* by NMD. High STN1 levels have been demonstrated here to be beneficial to the cell under specific circumstances, such as when challenged with DNA damage that needs to be repaired by NHEJ. Interestingly, it has been reported [237] (and replicated here) that NMD is down-regulated when non-cycling cells are challenged with persistent DNA damage (Fig. 53d). As these cells in G_0 will not have easy access to the template DNA necessary for HDR, NHEJ is particularly important. It may be that one reason *STN1* is regulated by NMD is so that high STN1 levels can promote and support NHEJ in a final effort to repair such damage.

9.4 CTC1 and Chromosome Segregation

An interesting impact loss of *CTC1* has that is unaddressed in the literature is the failure of the cell to ensure correct segregation of chromosomes during mitosis. Feng et al. [182] noted that knockout of *CTC1* resulted in an increase in ≥4N cells but did not speculate as to the cause or investigate the phenotype further. An increase in ≥4N cells indicates mitotic slippage could be occurring, this is when the SAC is activated for too long and consequently is deactivated despite failure to achieve appropriate binding and alignment of chromosomes at the spindle equator. As a result the spindle collapses, and (if the cell avoids an apoptotic response) the result is a single cell in G_1 with four copies of the genome (4N), instead of two daughter cells each with two copies [316]. Should the process of attempting replication but failing to segregate chromosomes happen again the genomic content is increased further, producing a >4N cell. Alternatively, these ≥4N

CTC1$^{-/-}$ cells may be bi/multi-nucleated cells produced as a result of chromatin bridges obstructing cytokinesis. Here we do observe an increase in chromatin bridges in CTC1$^{-/-}$ cells, suggesting the chromatin bridge-induced 4N cell model is very possible. Further investigation is necessary to determine the mechanism conclusively. Investigating whether the *CTC1*$^{-/-}$-induced $\geq$4N cells are mono or multi-nucleated may aid that determination.

In contrast, data presented here indicate that in some *CTC1*Δ cells anaphase, telophase and cytokinesis are performed unimpeded, but mis-segregation of chromosomes still occurs and daughter cells are left with whole chromosomes isolated in micronuclei. A potential novel role of CTC1 is hypothesised here to explain the combination of $\geq$4N cells and the presence of mis-segregated chromosomes in *CTC1*Δ HCT116 cells. It is possible that CTC1 allows kinetochores that are inappropriately bound to the mitotic spindle to release, and therefore have the opportunity to rebind correctly. If both kinetochores of a chromosome attach to the same spindle pole (syntelic binding) or if one kinetochore attached to both spindle poles (merotelic binding), and the kinetochores are unable to detach and correct due to a lack of CTC1, the observed occurrence of both $\geq$4N cells and whole-chromosome micronuclei would result (Fig. 33). Whilst this model fits the observed *CTC1*Δ phenotypes with a single mechanism, the evidence of a role for CTC1 at the kinetochore is indirect. Furthermore the $\geq$4N *CTC1*$^{-/-}$ cells may be due to chromatin bridge-induced cytokinesis abortion, and not lagging merotelic chromosomes. Whilst some of the chromosome segregation errors here could be explained by a role for the CST complex in mitosis, as of yet no members of the CST complex have been reported to localise to, or interact with, the kinetochore. However, the CST complex does interact and co-purify with Shelterin complex members [276], and depletion of TRF1 (a component of Shelterin) abolishes centromeric recruitment of Aurora-B [273]. As a result sister centromere cohesion is loosened, resulting in more merotelic kinetochores, lagging chromosomes, and micronuclei. It is possible that CTC1 is involved in this process, maintaining the integrity of mitosis, but further investigation is necessary to confirm it.

9.5 The Conservation of an Essential Role for Dna2 at The Telomere in Metazoans

Dna2 is a protein originally identified as having a role in DNA replication and the DDR that has only recently been proposed to have an essential function at the telomere [311]. An essential telomeric role of Dna2 was proposed in budding yeast based in part on its colocalisation with Cdc13 and the bypass of *dna2* mutation lethality by knocking out DNA damage checkpoint genes or helicases. As a nuclease/helicase Dna2 is hypothesised to resect unwound 5′ ssDNA at the telomere that the CST complex is unable to bind to. By resecting the 5′ DNA the strand no longer attracts RPA and subsequently does not activate the DDR (Fig. 50). Here we demonstrate the temperature sensitive embryonic

lethality of *dna-2*Δ *C. elegans* can be partially suppressed by knockout of either the 9-1-1 complex component (and DNA damage checkpoint gene) *mrt-2* or the telomeric helicase *fncm-1*. The fact that neither *fncm-1* or *mrt-2* knockout affected the reduced embryonic development rate of the *dna-2* mutants supports the notion that this essential role of *dna-2* is functionally separate from its role in Okazaki fragment processing during DNA synthesis. This is the first indication that the essential telomeric function of Dna2 is conserved in metazoans.

9.6 In Summary

In summary, the list of proteins with perhaps counter-intuitive roles in both supporting the DDR throughout the genome whilst simultaneously suppressing DDR activation at the telomere continues to grow. Data presented here underscore how important the regulation of these genes is in maintaining genomic stability. The data suggest a novel role for CTC1 in chromosome separation during mitosis, and demonstrates the crucial role of CTC1 and STN1 in DNA damage repair. The telomeric role of Dna2 appears conserved between *S. cerevisiae* and *C. elegans*, and is therefore likely to also be conserved in humans. *CTC1* and *STN1* mutations have been linked to Coats Plus syndrome [176][177] and antineoplastic resistance [175], whilst DNA2 mutations are associated with microcephalic primordial dwarfism [317]. By understanding the full range of roles these proteins play in the cell and how they are regulated we can gain significantly more insight into related disease pathogenesis.

10 References

[1] Martin, W.F., Garg, S., and Zimorski, V. Endosymbiotic theories for eukaryote origin. *Philosophical Transactions of the Royal Society B: Biological Sciences*, 370(1678), September 2015. ISSN 0962-8436. doi:10.1098/rstb.2014.0330.

[2] Olins, A.L. and Olins, D.E. Spheroid chromatin units (v bodies). *Science (New York, N.Y.)*, 183(4122):330–332, January 1974. ISSN 0036-8075. doi:10.1126/science.183.4122.330.

[3] Burki, F. The Eukaryotic Tree of Life from a Global Phylogenomic Perspective. *Cold Spring Harbor Perspectives in Biology*, 6(5):a016147, May 2014. ISSN , 1943-0264. doi:10.1101/cshperspect.a016147.

[4] Watson, J.D. and Crick, F.H.C. Molecular Structure of Nucleic Acids: A Structure for Deoxyribose Nucleic Acid. *Nature*, 171(4356):737–738, April 1953. ISSN 1476-4687. doi:10.1038/171737a0.

[5] Lander, E.S., Linton, L.M., Birren, B., Nusbaum, C., Zody, M.C., Baldwin, J., Devon, K., Dewar, K., Doyle, M., FitzHugh, W., Funke, R., Gage, D., Harris, K., Heaford, A., Howland, J., Kann, L., Lehoczky, J., LeVine, R., McEwan, P., McKernan, K., Meldrim, J., Mesirov, J.P., Miranda, C., Morris, W., Naylor, J., Raymond, C., Rosetti, M., Santos, R., Sheridan, A., Sougnez, C., Stange-Thomann, N., Stojanovic, N., Subramanian, A., Wyman, D., Rogers, J., Sulston, J., Ainscough, R., Beck, S., Bentley, D., Burton, J., Clee, C., Carter, N., Coulson, A., Deadman, R., Deloukas, P., Dunham, A., Dunham, I., Durbin, R., French, L., Grafham, D., Gregory, S., Hubbard, T., Humphray, S., Hunt, A., Jones, M., Lloyd, C., McMurray, A., Matthews, L., Mercer, S., Milne, S., Mullikin, J.C., Mungall, A., Plumb, R., Ross, M., Shownkeen, R., Sims, S., Waterston, R.H., Wilson, R.K., Hillier, L.W., McPherson, J.D., Marra, M.A., Mardis, E.R., Fulton, L.A., Chinwalla, A.T., Pepin, K.H., Gish, W.R., Chissoe, S.L., Wendl, M.C., Delehaunty, K.D., Miner, T.L., Delehaunty, A., Kramer, J.B., Cook, L.L., Fulton, R.S., Johnson, D.L., Minx, P.J., Clifton, S.W., Hawkins, T., Branscomb, E., Predki, P., Richardson, P., Wenning, S., Slezak, T., Doggett, N., Cheng, J.F., Olsen, A., Lucas, S., Elkin, C., Uberbacher, E., Frazier, M., Gibbs, R.A., Muzny, D.M., Scherer, S.E., Bouck, J.B., Sodergren, E.J., Worley, K.C., Rives, C.M., Gorrell, J.H., Metzker, M.L., Naylor, S.L., Kucherlapati, R.S., Nelson, D.L., Weinstock, G.M., Sakaki, Y., Fujiyama, A., Hattori, M., Yada, T., Toyoda, A., Itoh, T., Kawagoe, C., Watanabe, H., Totoki, Y., Taylor, T., Weissenbach, J., Heilig, R., Saurin, W., Artiguenave, F., Brottier, P., Bruls, T., Pelletier, E., Robert, C., Wincker, P., Rosenthal, A., Platzer, M., Nyakatura, G., Taudien, S., Rump, A., Smith, D.R., Doucette-Stamm, L., Rubenfield, M., Weinstock, K., Lee, H.M., Dubois, J., Yang, H., Yu, J., Wang, J., Huang,

G., Gu, J., Hood, L., Rowen, L., Madan, A., Qin, S., Davis, R.W., Federspiel, N.A., Abola, A.P., Proctor, M.J., Roe, B.A., Chen, F., Pan, H., Ramser, J., Lehrach, H., Reinhardt, R., McCombie, W.R., de la Bastide, M., Dedhia, N., Blöcker, H., Hornischer, K., Nordsiek, G., Agarwala, R., Aravind, L., Bailey, J.A., Bateman, A., Batzoglou, S., Birney, E., Bork, P., Brown, D.G., Burge, C.B., Cerutti, L., Chen, H.C., Church, D., Clamp, M., Copley, R.R., Doerks, T., Eddy, S.R., Eichler, E.E., Furey, T.S., Galagan, J., Gilbert, J.G.R., Harmon, C., Hayashizaki, Y., Haussler, D., Hermjakob, H., Hokamp, K., Jang, W., Johnson, L.S., Jones, T.A., Kasif, S., Kaspryzk, A., Kennedy, S., Kent, W.J., Kitts, P., Koonin, E.V., Korf, I., Kulp, D., Lancet, D., Lowe, T.M., McLysaght, A., Mikkelsen, T., Moran, J.V., Mulder, N., Pollara, V.J., Ponting, C.P., Schuler, G., Schultz, J., Slater, G., Smit, A.F.A., Stupka, E., Szustakowki, J., Thierry-Mieg, D., Thierry-Mieg, J., Wagner, L., Wallis, J., Wheeler, R., Williams, A., Wolf, Y.I., Wolfe, K.H., Yang, S.P., Yeh, R.F., Collins, F., Guyer, M.S., Peterson, J., Felsenfeld, A., Wetterstrand, K.A., Myers, R.M., Schmutz, J., Dickson, M., Grimwood, J., Cox, D.R., Olson, M.V., Kaul, R., Raymond, C., Shimizu, N., Kawasaki, K., Minoshima, S., Evans, G.A., Athanasiou, M., Schultz, R., Patrinos, A., Morgan, M.J., International Human Genome Sequencing Consortium, Whitehead Institute for Biomedical Research, C.f.G.R., The Sanger Centre:, Washington University Genome Sequencing Center, US DOE Joint Genome Institute:, Baylor College of Medicine Human Genome Sequencing Center:, RIKEN Genomic Sciences Center:, Genoscope and CNRS UMR-8030:, Department of Genome Analysis, I.o.M.B., GTC Sequencing Center:, Beijing Genomics Institute/Human Genome Center:, Multimegabase Sequencing Center, T.I.f.S.B., Stanford Genome Technology Center:, University of Oklahoma's Advanced Center for Genome Technology:, Max Planck Institute for Molecular Genetics:, Cold Spring Harbor Laboratory, L.A.H.G.C., GBF—German Research Centre for Biotechnology:, *Genome Analysis Group (listed in alphabetical order, a.i.i.l.u.o.h., Scientific management: National Human Genome Research Institute, U.N.I.o.H., Stanford Human Genome Center:, University of Washington Genome Center:, Department of Molecular Biology, K.U.S.o.M., University of Texas Southwestern Medical Center at Dallas:, Office of Science, U.D.o.E., and The Wellcome Trust:. Initial sequencing and analysis of the human genome. *Nature*, 409(6822):860–921, February 2001. ISSN 1476-4687. doi:10.1038/35057062.

[6] Pertea, M., Shumate, A., Pertea, G., Varabyou, A., Breitwieser, F.P., Chang, Y.C., Madugundu, A.K., Pandey, A., and Salzberg, S.L. CHESS: a new human gene catalog curated from thousands of large-scale RNA sequencing experiments reveals extensive transcriptional noise. *Genome Biology*, 19(1):208, November 2018. ISSN 1474-760X. doi:10.1186/s13059-018-1590-2.

[7] Kellis, M., Wold, B., Snyder, M.P., Bernstein, B.E., Kundaje, A., Marinov, G.K., Ward, L.D., Birney, E., Crawford, G.E., Dekker, J., Dunham, I., Elnitski, L.L.,

Farnham, P.J., Feingold, E.A., Gerstein, M., Giddings, M.C., Gilbert, D.M., Gingeras, T.R., Green, E.D., Guigo, R., Hubbard, T., Kent, J., Lieb, J.D., Myers, R.M., Pazin, M.J., Ren, B., Stamatoyannopoulos, J.A., Weng, Z., White, K.P., and Hardison, R.C. Defining functional DNA elements in the human genome. *Proceedings of the National Academy of Sciences of the United States of America*, 111(17):6131–6138, April 2014. ISSN 0027-8424. doi:10.1073/pnas.1318948111.

[8] Tjio, J.H. and Levan, A. The Chromosome Number of Man. *Hereditas*, 42(1-2):1–6, 1956. ISSN 1601-5223. doi:10.1111/j.1601-5223.1956.tb03010.x.

[9] Teif, V.B. and Bohinc, K. Condensed DNA: Condensing the concepts. *Progress in Biophysics and Molecular Biology*, 105(3):208–222, May 2011. ISSN 0079-6107. doi:10.1016/j.pbiomolbio.2010.07.002.

[10] Hillers, K.J., Jantsch, V., Martinez-Perez, E., and Yanowitz, J.L. Meiosis. *WormBook: The Online Review of C. Elegans Biology*, 2017:1–43, 2017. ISSN 1551-8507. doi:10.1895/wormbook.1.178.1.

[11] Wang, S., Zickler, D., Kleckner, N., and Zhang, L. Meiotic crossover patterns: Obligatory crossover, interference and homeostasis in a single process. *Cell Cycle*, 14(3):305–314, February 2015. ISSN 1538-4101. doi:10.4161/15384101.2014.991185.

[12] Stark, G.R. and Taylor, W.R. Analyzing the G2/M checkpoint. *Methods in Molecular Biology (Clifton, N.J.)*, 280:51–82, 2004. ISSN 1064-3745. doi:10.1385/1-59259-788-2:051.

[13] Malumbres, M. and Barbacid, M. Cell cycle, CDKs and cancer: a changing paradigm. *Nature Reviews Cancer*, 9(3):153–166, March 2009. ISSN 1474-1768. doi:10.1038/nrc2602.

[14] Evans, T., Rosenthal, E.T., Youngblom, J., Distel, D., and Hunt, T. Cyclin: A protein specified by maternal mRNA in sea urchin eggs that is destroyed at each cleavage division. *Cell*, 33(2):389–396, June 1983. ISSN 00928674. doi:10.1016/0092-8674(83)90420-8.

[15] van den Berg, J., G. Manjón, A., Kielbassa, K., Feringa, F.M., Freire, R., and Medema, R.H. A limited number of double-strand DNA breaks is sufficient to delay cell cycle progression. *Nucleic Acids Research*, 46(19):10132–10144, November 2018. ISSN 0305-1048. doi:10.1093/nar/gky786.

[16] Okazaki, R., Okazaki, T., Sakabe, K., Sugimoto, K., Kainuma, R., Sugino, A., and Iwatsuki, N. In Vivo Mechanism of DNA Chain Growth. *Cold Spring Harbor Symposia on Quantitative Biology*, 33:129–143, January 1968. doi:10.1101/SQB.1968.033.01.017.

[17] Burgers, P.M. and Kunkel, T.A. Eukaryotic DNA Replication Fork. *Annual Review of Biochemistry*, 86(1):417–438, June 2017. ISSN 0066-4154, 1545-4509. doi:10.1146/annurev-biochem-061516-044709.

[18] Deegan, T.D. and Diffley, J.F. MCM: one ring to rule them all. *Current Opinion in Structural Biology*, 37:145–151, April 2016. ISSN 0959-440X. doi:10.1016/j.sbi.2016.01.014.

[19] Muramatsu, S., Hirai, K., Tak, Y.S., Kamimura, Y., and Araki, H. CDK-dependent complex formation between replication proteins Dpb11, Sld2, Pol epsilon, and GINS in budding yeast. *Genes & Development*, 24(6):602–612, March 2010. ISSN 0890-9369. doi:10.1101/gad.1883410.

[20] Sengupta, S., van Deursen, F., de Piccoli, G., and Labib, K. Dpb2 Integrates the Leading-Strand DNA Polymerase into the Eukaryotic Replisome. *Current Biology*, 23(7):543–552, April 2013. ISSN 0960-9822. doi:10.1016/j.cub.2013.02.011.

[21] van Deursen, F., Sengupta, S., De Piccoli, G., Sanchez-Diaz, A., and Labib, K. Mcm10 associates with the loaded DNA helicase at replication origins and defines a novel step in its activation. *The EMBO Journal*, 31(9):2195–2206, May 2012. ISSN 0261-4189. doi:10.1038/emboj.2012.69.

[22] Perez-Arnaiz, P., Bruck, I., and Kaplan, D.L. Mcm10 coordinates the timely assembly and activation of the replication fork helicase. *Nucleic Acids Research*, 44(1):315–329, January 2016. ISSN 0305-1048. doi:10.1093/nar/gkv1260.

[23] Moyer, S.E., Lewis, P.W., and Botchan, M.R. Isolation of the Cdc45/Mcm2–7/GINS (CMG) complex, a candidate for the eukaryotic DNA replication fork helicase. *Proceedings of the National Academy of Sciences of the United States of America*, 103(27):10236–10241, July 2006. ISSN 0027-8424. doi:10.1073/pnas.0602400103.

[24] Fu, Y.V., Yardimci, H., Long, D.T., Ho, T.V., Guainazzi, A., Bermudez, V.P., Hurwitz, J., van Oijen, A., Schärer, O.D., and Walter, J.C. Selective bypass of a lagging strand roadblock by the eukaryotic replicative DNA helicase. *Cell*, 146(6):931–941, September 2011. ISSN 0092-8674. doi:10.1016/j.cell.2011.07.045.

[25] Samel, S.A., Fernández-Cid, A., Sun, J., Riera, A., Tognetti, S., Herrera, M.C., Li, H., and Speck, C. A unique DNA entry gate serves for regulated loading of the eukaryotic replicative helicase MCM2–7 onto DNA. *Genes & Development*, 28(15):1653–1666, August 2014. ISSN 0890-9369. doi:10.1101/gad.242404.114.

[26] Abid Ali, F., Renault, L., Gannon, J., Gahlon, H.L., Kotecha, A., Zhou, J.C., Rueda, D., and Costa, A. Cryo-EM structures of the eukaryotic replicative helicase bound to a translocation substrate. *Nature Communications*, 7, February 2016. ISSN 2041-1723. doi:10.1038/ncomms10708.

[27] Ohya, T., Kawasaki, Y., Hiraga, S.I., Kanbara, S., Nakajo, K., Nakashima, N., Suzuki, A., and Sugino, A. The DNA Polymerase Domain of pol epsilon Is Required for Rapid, Efficient, and Highly Accurate Chromosomal DNA Replication, Telomere Length Maintenance, and Normal Cell Senescence inSaccharomyces cerevisiae. *Journal of Biological Chemistry*, 277(31):28099–28108, August 2002. ISSN 0021-9258, 1083-351X. doi:10.1074/jbc.M111573200.

[28] Flood, C.L., Rodriguez, G.P., Bao, G., Shockley, A.H., Kow, Y.W., and Crouse, G.F. Replicative DNA Polymerase delta but Not epsilon Proofreads Errors in Cis and in Trans. *PLoS Genetics*, 11(3), March 2015. ISSN 1553-7390. doi:10.1371/journal.pgen.1005049.

[29] Nethanel, T., Reisfeld, S., Dinter-Gottlieb, G., and Kaufmann, G. An Okazaki piece of simian virus 40 may be synthesized by ligation of shorter precursor chains. *Journal of Virology*, 62(8):2867–2873, August 1988. ISSN 0022-538X.

[30] Tsurimoto, T. and Stillman, B. Replication factors required for SV40 DNA replication in vitro. II. Switching of DNA polymerase alpha and delta during initiation of leading and lagging strand synthesis. *Journal of Biological Chemistry*, 266(3):1961–1968, January 1991. ISSN 0021-9258, 1083-351X.

[31] Yuzhakov, A., Kelman, Z., Hurwitz, J., and O'Donnell, M. Multiple competition reactions for RPA order the assembly of the DNA polymerase delta holoenzyme. *The EMBO Journal*, 18(21):6189–6199, November 1999. ISSN 0261-4189. doi:10.1093/emboj/18.21.6189.

[32] Stodola, J.L. and Burgers, P.M. Resolving individual steps of Okazaki fragment maturation at msec time-scale. *Nature structural & molecular biology*, 23(5):402–408, May 2016. ISSN 1545-9993. doi:10.1038/nsmb.3207.

[33] Burgers, P.M.J. Polymerase Dynamics at the Eukaryotic DNA Replication Fork. *The Journal of Biological Chemistry*, 284(7):4041–4045, February 2009. ISSN 0021-9258. doi:10.1074/jbc.R800062200.

[34] Balakrishnan, L. and Bambara, R.A. Flap Endonuclease 1. *Annual Review of Biochemistry*, 82(1):119–138, June 2013. ISSN 0066-4154, 1545-4509. doi:10.1146/annurev-biochem-072511-122603.

[35] Kang, Y.H., Lee, C.H., and Seo, Y.S. Dna2 on the road to Okazaki fragment processing and genome stability in eukaryotes. *Critical Reviews in Biochemistry and Molecular Biology*, 45(2):71–96, April 2010. ISSN 1040-9238. doi:10.3109/10409230903578593.

[36] Johnston, L.H. and Nasmyth, K.A. Saccharomyces cerevisiae cell cycle mutant cdc9 is defective in DNA ligase. *Nature*, 274(5674):891–893, August 1978. ISSN 0028-0836. doi:10.1038/274891a0.

[37] Schellhaus, A.K., De Magistris, P., and Antonin, W. Nuclear Reformation at the End of Mitosis. *Journal of Molecular Biology*, 428(10, Part A):1962–1985, May 2016. ISSN 0022-2836. doi:10.1016/j.jmb.2015.09.016.

[38] Thadani, R., Uhlmann, F., and Heeger, S. Condensin, Chromatin Crossbarring and Chromosome Condensation. *Current Biology*, 22(23):R1012–R1021, December 2012. ISSN 0960-9822. doi:10.1016/j.cub.2012.10.023.

[39] Martínez-Balbás, M.A., Dey, A., Rabindran, S.K., Ozato, K., and Wu, C. Displacement of sequence-specific transcription factors from mitotic chromatin. *Cell*, 83(1):29–38, October 1995. ISSN 00928674. doi:10.1016/0092-8674(95)90231-7.

[40] Steinhardt, R.A. and Alderton, J. Intracellular free calcium rise triggers nuclear envelope breakdown in the sea urchin embryo. *Nature*, 332(6162):364–366, March 1988. ISSN 1476-4687. doi:10.1038/332364a0.

[41] Vandré, D.D., Davis, F.M., Rao, P.N., and Borisy, G.G. Distribution of cytoskeletal proteins sharing a conserved phosphorylated epitope. *European Journal of Cell Biology*, 41(1):72–81, June 1986. ISSN 0171-9335.

[42] Cheeseman, I.M. The Kinetochore. *Cold Spring Harbor Perspectives in Biology*, 6(7), July 2014. ISSN 1943-0264. doi:10.1101/cshperspect.a015826.

[43] Kirschner, M. and Mitchison, T. Beyond self-assembly: from microtubules to morphogenesis. *Cell*, 45(3):329–342, May 1986. ISSN 0092-8674. doi:10.1016/0092-8674(86)90318-1.

[44] Bakhoum, S.F., Silkworth, W.T., Nardi, I.K., Nicholson, J.M., Compton, D.A., and Cimini, D. The mitotic origin of chromosomal instability. *Current biology : CB*, 24(4):R148–R149, February 2014. ISSN 0960-9822. doi:10.1016/j.cub.2014.01.019.

[45] Joglekar, A.P. and Aravamudhan, P. How the kinetochore switches off the spindle assembly checkpoint. *Cell Cycle*, 15(1):7–8, December 2015. ISSN 1538-4101. doi:10.1080/15384101.2015.1112695.

[46] Uhlmann, F. Chromosome cohesion and segregation in mitosis and meiosis. *Current Opinion in Cell Biology*, 13(6):754–761, December 2001. ISSN 0955-0674. doi:10.1016/S0955-0674(00)00279-9.

[47] Mitchison, T., Evans, L., Schulze, E., and Kirschner, M. Sites of microtubule assembly and disassembly in the mitotic spindle. *Cell*, 45(4):515–527, May 1986. ISSN 0092-8674, 1097-4172. doi:10.1016/0092-8674(86)90283-7.

[48] Maddox, P., Desai, A., Oegema, K., Mitchison, T.J., and Salmon, E.D. Poleward Microtubule Flux Is a Major Component of Spindle Dynamics and Anaphase A in Mitotic Drosophila Embryos. *Current Biology*, 12(19):1670–1674, October 2002. ISSN 0960-9822. doi:10.1016/S0960-9822(02)01183-1.

[49] Scholey, J.M., Civelekoglu-Scholey, G., and Brust-Mascher, I. Anaphase B. *Biology*, 5(4), December 2016. ISSN 2079-7737. doi:10.3390/biology5040051.

[50] Renshaw, M.J., Ward, J.J., Kanemaki, M., Natsume, K., Nédélec, F.J., and Tanaka, T.U. Condensins Promote Chromosome Recoiling during Early Anaphase to Complete Sister Chromatid Separation. *Developmental Cell*, 19(2):232–244, August 2010. ISSN 1534-5807. doi:10.1016/j.devcel.2010.07.013.

[51] Green, R.A., Paluch, E., and Oegema, K. Cytokinesis in Animal Cells. *Annual Review of Cell and Developmental Biology*, 28(1):29–58, November 2012. ISSN 1081-0706, 1530-8995. doi:10.1146/annurev-cellbio-101011-155718.

[52] Massagué, J. G1 cell-cycle control and cancer. *Nature*, 432(7015):298–306, November 2004. ISSN 1476-4687. doi:10.1038/nature03094.

[53] Hochegger, H., Sonoda, E., and Takeda, S. Post-replication repair in DT40 cells: translesion polymerases versus recombinases. *BioEssays*, 26(2):151–158, February 2004. ISSN 1521-1878. doi:10.1002/bies.10403.

[54] Satyanarayana, A. and Kaldis, P. Mammalian cell-cycle regulation: several Cdks, numerous cyclins and diverse compensatory mechanisms. *Oncogene*, 28(33):2925–2939, August 2009. ISSN 1476-5594. doi:10.1038/onc.2009.170.

[55] Lavin, M.F. and Kozlov, S. ATM Activation and DNA Damage Response. *Cell Cycle*, April 2007. doi:10.4161/cc.6.8.4180.

[56] Cimprich, K.A. and Cortez, D. ATR: An Essential Regulator of Genome Integrity. *Nature reviews. Molecular cell biology*, 9(8):616–627, August 2008. ISSN 1471-0072. doi:10.1038/nrm2450.

[57] Iyer, D.R. and Rhind, N. The Intra-S Checkpoint Responses to DNA Damage. *Genes*, 8(2), February 2017. ISSN 2073-4425. doi:10.3390/genes8020074.

[58] O'Connell, M.J., Raleigh, J.M., Verkade, H.M., and Nurse, P. Chk1 is a wee1 kinase in the G2 DNA damage checkpoint inhibiting cdc2 by Y15 phosphorylation. *The EMBO Journal*, 16(3):545–554, February 1997. ISSN 1460-2075. doi:10.1093/emboj/16.3.545.

[59] Shaltiel, I.A., Krenning, L., Bruinsma, W., and Medema, R.H. The same, only different – DNA damage checkpoints and their reversal throughout the cell cycle.

Journal of Cell Science, 128(4):607–620, February 2015. ISSN 0021-9533, 1477-9137. doi:10.1242/jcs.163766.

[60] Allard, C.A.H., Opalko, H.E., Liu, K.W., Medoh, U., and Moseley, J.B. Cell size–dependent regulation of Wee1 localization by Cdr2 cortical nodes. *The Journal of Cell Biology*, 217(5):1589–1599, May 2018. ISSN 0021-9525, 1540-8140. doi: 10.1083/jcb.201709171.

[61] Thompson, S.L. and Compton, D.A. Chromosome missegregation in human cells arises through specific types of kinetochore–microtubule attachment errors. *Proceedings of the National Academy of Sciences*, 108(44):17974–17978, November 2011. ISSN 0027-8424, 1091-6490. doi:10.1073/pnas.1109720108.

[62] Magidson, V., He, J., Ault, J.G., O'Connell, C.B., Yang, N., Tikhonenko, I., McEwen, B.F., Sui, H., and Khodjakov, A. Unattached kinetochores rather than intrakinetochore tension arrest mitosis in taxol-treated cells. *The Journal of Cell Biology*, 212(3):307–319, February 2016. ISSN 0021-9525, 1540-8140. doi: 10.1083/jcb.201412139.

[63] Lara-Gonzalez, P., Westhorpe, F.G., and Taylor, S.S. The Spindle Assembly Checkpoint. *Current Biology*, 22(22):R966–R980, November 2012. ISSN 0960-9822. doi: 10.1016/j.cub.2012.10.006.

[64] Caydasi, A.K., Ibrahim, B., and Pereira, G. Monitoring spindle orientation: Spindle position checkpoint in charge. *Cell Division*, 5(1):28, December 2010. ISSN 1747-1028. doi:10.1186/1747-1028-5-28.

[65] Zhang, Y., Shim, E.Y., Davis, M., and Lee, S.E. Regulation of Repair Choice. *DNA repair*, 8(10):1235–1241, October 2009. ISSN 1568-7864. doi:10.1016/j.dnarep.2009.07.007.

[66] Mimitou, E.P. and Symington, L.S. Ku prevents Exo1 and Sgs1-dependent resection of DNA ends in the absence of a functional MRX complex or Sae2. *The EMBO Journal*, 29(19):3358–3369, October 2010. ISSN 0261-4189. doi:10.1038/emboj.2010.193.

[67] Garcia, V., Phelps, S.E.L., Gray, S., and Neale, M.J. Bidirectional resection of DNA double-strand breaks by Mre11 and Exo1. *Nature*, 479(7372):241–244, October 2011. ISSN 0028-0836. doi:10.1038/nature10515.

[68] Moynahan, M.E., Chiu, J.W., Koller, B.H., and Jasin, M. Brca1 Controls Homology-Directed DNA Repair. *Molecular Cell*, 4(4):511–518, October 1999. ISSN 1097-2765. doi:10.1016/S1097-2765(00)80202-6.

[69] Bothmer, A., Robbiani, D.F., Feldhahn, N., Gazumyan, A., Nussenzweig, A., and Nussenzweig, M.C. 53bp1 regulates DNA resection and the choice between classical and alternative end joining during class switch recombination. *The Journal of Experimental Medicine*, 207(4):855–865, April 2010. ISSN 0022-1007. doi: 10.1084/jem.20100244.

[70] Bouwman, P., Aly, A., Escandell, J.M., Pieterse, M., Bartkova, J., van der Gulden, H., Hiddingh, S., Thanasoula, M., Kulkarni, A., Yang, Q., Haffty, B.G., Tommiska, J., Blomqvist, C., Drapkin, R., Adams, D.J., Nevanlinna, H., Bartek, J., Tarsounas, M., Ganesan, S., and Jonkers, J. 53bp1 loss rescues BRCA1 deficiency and is associated with triple-negative and BRCA-mutated breast cancers. *Nature structural & molecular biology*, 17(6):688–695, June 2010. ISSN 1545-9993. doi: 10.1038/nsmb.1831.

[71] Mari, P.O., Florea, B.I., Persengiev, S.P., Verkaik, N.S., Brüggenwirth, H.T., Modesti, M., Giglia-Mari, G., Bezstarosti, K., Demmers, J.A.A., Luider, T.M., Houtsmuller, A.B., and van Gent, D.C. Dynamic assembly of end-joining complexes requires interaction between Ku70/80 and XRCC4. *Proceedings of the National Academy of Sciences of the United States of America*, 103(49):18597–18602, December 2006. ISSN 0027-8424. doi:10.1073/pnas.0609061103.

[72] Walker, J.R., Corpina, R.A., and Goldberg, J. Structure of the Ku heterodimer bound to DNA and its implications for double-strand break repair. *Nature*, 412(6847):607–614, August 2001. ISSN 1476-4687. doi:10.1038/35088000.

[73] Nick McElhinny, S.A., Snowden, C.M., McCarville, J., and Ramsden, D.A. Ku Recruits the XRCC4-Ligase IV Complex to DNA Ends. *Molecular and Cellular Biology*, 20(9):2996–3003, May 2000. ISSN 0270-7306.

[74] Uematsu, N., Weterings, E., Yano, K.i., Morotomi-Yano, K., Jakob, B., Taucher-Scholz, G., Mari, P.O., van Gent, D.C., Chen, B.P.C., and Chen, D.J. Autophosphorylation of DNA-PKCS regulates its dynamics at DNA double-strand breaks. *The Journal of Cell Biology*, 177(2):219–229, April 2007. ISSN 0021-9525. doi: 10.1083/jcb.200608077.

[75] Yano, K.i., Morotomi-Yano, K., Wang, S.Y., Uematsu, N., Lee, K.J., Asaithamby, A., Weterings, E., and Chen, D.J. Ku recruits XLF to DNA double-strand breaks. *EMBO Reports*, 9(1):91–96, January 2008. ISSN 1469-221X. doi:10.1038/sj.embor.7401137.

[76] Grundy, G.J., Rulten, S.L., Zeng, Z., Arribas-Bosacoma, R., Iles, N., Manley, K., Oliver, A., and Caldecott, K.W. APLF promotes the assembly and activity of non-homologous end joining protein complexes. *The EMBO Journal*, 32(1):112–125, January 2013. ISSN 0261-4189. doi:10.1038/emboj.2012.304.

[77] Mahajan, K.N., Nick McElhinny, S.A., Mitchell, B.S., and Ramsden, D.A. Association of DNA Polymerasemu with Ku and Ligase IV: Role for pol mu in End-Joining Double-Strand Break Repair. *Molecular and Cellular Biology*, 22(14):5194–5202, July 2002. ISSN 0270-7306. doi:10.1128/MCB.22.14.5194-5202.2002.

[78] Cooper, M.P., Machwe, A., Orren, D.K., Brosh, R.M., Ramsden, D., and Bohr, V.A. Ku complex interacts with and stimulates the Werner protein. *Genes & Development*, 14(8):907–912, April 2000. ISSN 0890-9369.

[79] Pang, D., Yoo, S., Dynan, W.S., Jung, M., and Dritschilo, A. Ku Proteins Join DNA Fragments as Shown by Atomic Force Microscopy. *Cancer Research*, 57(8):1412–1415, April 1997. ISSN 0008-5472, 1538-7445.

[80] Cary, R.B., Peterson, S.R., Wang, J., Bear, D.G., Bradbury, E.M., and Chen, D.J. DNA looping by Ku and the DNA-dependent protein kinase. *Proceedings of the National Academy of Sciences of the United States of America*, 94(9):4267–4272, April 1997. ISSN 0027-8424.

[81] Andres, S.N., Vergnes, A., Ristic, D., Wyman, C., Modesti, M., and Junop, M. A human XRCC4–XLF complex bridges DNA. *Nucleic Acids Research*, 40(4):1868–1878, February 2012. ISSN 0305-1048. doi:10.1093/nar/gks022.

[82] Bernstein, N.K., Williams, R.S., Rakovszky, M.L., Cui, D., Green, R., Karimi-Busheri, F., Mani, R.S., Galicia, S., Koch, C.A., Cass, C.E., Durocher, D., Weinfeld, M., and Glover, J.N.M. The Molecular Architecture of the Mammalian DNA Repair Enzyme, Polynucleotide Kinase. *Molecular Cell*, 17(5):657–670, March 2005. ISSN 1097-2765. doi:10.1016/j.molcel.2005.02.012.

[83] Ahel, I., Rass, U., El-Khamisy, S.F., Katyal, S., Clements, P.M., McKinnon, P.J., Caldecott, K.W., and West, S.C. The neurodegenerative disease protein aprataxin resolves abortive DNA ligation intermediates. *Nature*, 443(7112):713–716, October 2006. ISSN 1476-4687. doi:10.1038/nature05164.

[84] Ma, Y., Pannicke, U., Schwarz, K., and Lieber, M.R. Hairpin Opening and Overhang Processing by an Artemis/DNA-Dependent Protein Kinase Complex in Nonhomologous End Joining and V(D)J Recombination. *Cell*, 108(6):781–794, March 2002. ISSN 0092-8674, 1097-4172. doi:10.1016/S0092-8674(02)00671-2.

[85] Perry, J.J.P., Yannone, S.M., Holden, L.G., Hitomi, C., Asaithamby, A., Han, S., Cooper, P.K., Chen, D.J., and Tainer, J.A. WRN exonuclease structure and molecular mechanism imply an editing role in DNA end processing. *Nature Structural & Molecular Biology*, 13(5):414–422, May 2006. ISSN 1545-9985. doi:10.1038/nsmb1088.

[86] Kanno, S.i., Kuzuoka, H., Sasao, S., Hong, Z., Lan, L., Nakajima, S., and Yasui, A. A novel human AP endonuclease with conserved zinc-finger-like motifs involved in DNA strand break responses. *The EMBO Journal*, 26(8):2094–2103, April 2007. ISSN 0261-4189. doi:10.1038/sj.emboj.7601663.

[87] Grawunder, U., Wilm, M., Wu, X., Kulesza, P., Wilson, T.E., Mann, M., and Lieber, M.R. Activity of DNA ligase IV stimulated by complex formation with XRCC4 protein in mammalian cells. *Nature*, 388(6641):492–495, July 1997. ISSN 1476-4687. doi:10.1038/41358.

[88] Gu, J., Lu, H., Tippin, B., Shimazaki, N., Goodman, M.F., and Lieber, M.R. XRCC4:DNA ligase IV can ligate incompatible DNA ends and can ligate across gaps. *The EMBO Journal*, 26(4):1010–1023, February 2007. ISSN 0261-4189. doi: 10.1038/sj.emboj.7601559.

[89] Hammel, M., Yu, Y., Mahaney, B.L., Cai, B., Ye, R., Phipps, B.M., Rambo, R.P., Hura, G.L., Pelikan, M., So, S., Abolfath, R.M., Chen, D.J., Lees-Miller, S.P., and Tainer, J.A. Ku and DNA-Dependant Protein Kinase Dynamic Conformations and Assembly Regulate DNA Binding and the Initial Non-homologous End Joining Complex. *The Journal of Biological Chemistry*, 285(2):1414–1423, January 2010. ISSN 0021-9258. doi:10.1074/jbc.M109.065615.

[90] Postow, L., Ghenoiu, C., Woo, E.M., Krutchinsky, A.N., Chait, B.T., and Funabiki, H. Ku80 removal from DNA through double strand break–induced ubiquitylation. *The Journal of Cell Biology*, 182(3):467–479, August 2008. ISSN 0021-9525. doi: 10.1083/jcb.200802146.

[91] Sartori, A.A., Lukas, C., Coates, J., Mistrik, M., Fu, S., Bartek, J., Baer, R., Lukas, J., and Jackson, S.P. Human CtIP promotes DNA end resection. *Nature*, 450(7169):509–514, November 2007. ISSN 0028-0836. doi:10.1038/nature06337.

[92] Zhu, Z., Chung, W.H., Shim, E.Y., Lee, S.E., and Ira, G. Sgs1 helicase and two nucleases Dna2 and Exo1 resect DNA double strand break ends. *Cell*, 134(6):981–994, September 2008. ISSN 0092-8674. doi:10.1016/j.cell.2008.08.037.

[93] Stark, J.M., Pierce, A.J., Oh, J., Pastink, A., and Jasin, M. Genetic Steps of Mammalian Homologous Repair with Distinct Mutagenic Consequences. *Molecular and Cellular Biology*, 24(21):9305–9316, November 2004. ISSN 0270-7306. doi: 10.1128/MCB.24.21.9305-9316.2004.

[94] Tutt, A., Bertwistle, D., Valentine, J., Gabriel, A., Swift, S., Ross, G., Griffin, C., Thacker, J., and Ashworth, A. Mutation in Brca2 stimulates error-prone homology-directed repair of DNA double-strand breaks occurring between repeated sequences. *The EMBO Journal*, 20(17):4704–4716, September 2001. ISSN 0261-4189. doi: 10.1093/emboj/20.17.4704.

[95] Moynahan, M.E. and Jasin, M. Mitotic homologous recombination maintains genomic stability and suppresses tumorigenesis. *Nature Reviews. Molecular Cell Biology*, 11(3):196–207, March 2010. ISSN 1471-0072. doi:10.1038/nrm2851.

[96] Zhang, F., Ma, J., Wu, J., Ye, L., Cai, H., Xia, B., and Yu, X. PALB2 Links BRCA1 and BRCA2 in the DNA-Damage Response. *Current biology : CB*, 19(6):524–529, March 2009. ISSN 0960-9822. doi:10.1016/j.cub.2009.02.018.

[97] Klein, H.L. and Symington, L.S. Sgs1—The Maestro of Recombination. *Cell*, 149(2):257–259, April 2012. ISSN 0092-8674, 1097-4172. doi:10.1016/j.cell.2012.03.020.

[98] LaRocque, J.R., Stark, J.M., Oh, J., Bojilova, E., Yusa, K., Horie, K., Takeda, J., and Jasin, M. Interhomolog recombination and loss of heterozygosity in wild-type and Bloom syndrome helicase (BLM)-deficient mammalian cells. *Proceedings of the National Academy of Sciences of the United States of America*, 108(29):11971–11976, July 2011. ISSN 0027-8424. doi:10.1073/pnas.1104421108.

[99] Jasin, M. and Rothstein, R. Repair of Strand Breaks by Homologous Recombination. *Cold Spring Harbor Perspectives in Biology*, 5(11), November 2013. ISSN 1943-0264. doi:10.1101/cshperspect.a012740.

[100] Symington, L.S. and Gautier, J. Double-Strand Break End Resection and Repair Pathway Choice. *Annual Review of Genetics*, 45(1):247–271, December 2011. ISSN 0066-4197, 1545-2948. doi:10.1146/annurev-genet-110410-132435.

[101] Bakkenist, C.J. and Kastan, M.B. DNA damage activates ATM through intermolecular autophosphorylation and dimer dissociation. *Nature*, 421(6922):499–506, January 2003. ISSN 0028-0836. doi:10.1038/nature01368.

[102] Stracker, T.H. and Petrini, J.H.J. The MRE11 complex: starting from the ends. *Nature reviews. Molecular cell biology*, 12(2):90–103, February 2011. ISSN 1471-0072. doi:10.1038/nrm3047.

[103] Ciccia, A. and Elledge, S.J. The DNA Damage Response: Making it safe to play with knives. *Molecular cell*, 40(2):179–204, October 2010. ISSN 1097-2765. doi:10.1016/j.molcel.2010.09.019.

[104] Chaturvedi, P., Eng, W.K., Zhu, Y., Mattern, M.R., Mishra, R., Hurle, M.R., Zhang, X., Annan, R.S., Lu, Q., Faucette, L.F., Scott, G.F., Li, X., Carr, S.A., Johnson, R.K., Winkler, J.D., and Zhou, B.B. Mammalian Chk2 is a downstream effector of the ATM-dependent DNA damage checkpoint pathway. *Oncogene*, 18(28):4047–4054, July 1999. ISSN 0950-9232. doi:10.1038/sj.onc.1202925.

[105] Shiloh, Y. and Ziv, Y. The ATM protein kinase: regulating the cellular response to genotoxic stress, and more. *Nature Reviews. Molecular Cell Biology*, 14(4):197–210, April 2013. ISSN 1471-0080.

[106] Cai, Z., Chehab, N.H., and Pavletich, N.P. Structure and Activation Mechanism of the CHK2 DNA Damage Checkpoint Kinase. *Molecular Cell*, 35(6):818–829, September 2009. ISSN 1097-2765. doi:10.1016/j.molcel.2009.09.007.

[107] Chen, Y.H., Jones, M.J.K., Yin, Y., Crist, S.B., Colnaghi, L., Sims, R.J., Rothenberg, E., Jallepalli, P.V., and Huang, T.T. ATR-mediated phosphorylation of FANCI regulates dormant origin firing in response to replication stress. *Molecular cell*, 58(2):323–338, April 2015. ISSN 1097-2765. doi:10.1016/j.molcel.2015.02.031.

[108] Liu, Q., Guntuku, S., Cui, X.S., Matsuoka, S., Cortez, D., Tamai, K., Luo, G., Carattini-Rivera, S., DeMayo, F., Bradley, A., Donehower, L.A., and Elledge, S.J. Chk1 is an essential kinase that is regulated by Atr and required for the G2/M DNA damage checkpoint. *Genes & Development*, 14(12):1448–1459, June 2000. ISSN 0890-9369, 1549-5477. doi:10.1101/gad.14.12.1448.

[109] Zhao, H. and Piwnica-Worms, H. ATR-Mediated Checkpoint Pathways Regulate Phosphorylation and Activation of Human Chk1. *Molecular and Cellular Biology*, 21(13):4129–4139, July 2001. ISSN 0270-7306, 1098-5549. doi:10.1128/MCB.21.13.4129-4139.2001.

[110] Segurado, M. and Diffley, J.F.X. Separate roles for the DNA damage checkpoint protein kinases in stabilizing DNA replication forks. *Genes & Development*, 22(13):1816–1827, July 2008. ISSN 0890-9369, 1549-5477. doi:10.1101/gad.477208.

[111] Shiotani, B. and Zou, L. Single-Stranded DNA Orchestrates an ATM-to-ATR Switch at DNA Breaks. *Molecular cell*, 33(5):547–558, March 2009. ISSN 1097-2765. doi:10.1016/j.molcel.2009.01.024.

[112] Sanchez, Y., Wong, C., Thoma, R.S., Richman, R., Wu, Z., Piwnica-Worms, H., and Elledge, S.J. Conservation of the Chk1 Checkpoint Pathway in Mammals: Linkage of DNA Damage to Cdk Regulation Through Cdc25. *Science*, 277(5331):1497–1501, September 1997. ISSN 0036-8075, 1095-9203. doi:10.1126/science.277.5331.1497.

[113] Mailand, N., Podtelejnikov, A.V., Groth, A., Mann, M., Bartek, J., and Lukas, J. Regulation of G2/M events by Cdc25a through phosphorylation-dependent modulation of its stability. *The EMBO Journal*, 21(21):5911–5920, November 2002. ISSN 0261-4189. doi:10.1093/emboj/cdf567.

[114] Okuda, K., Bardeguez, A., Gardner, J.P., Rodriguez, P., Ganesh, V., Kimura, M., Skurnick, J., Awad, G., and Aviv, A. Telomere Length in the New-

born. *Pediatric Research*, 52(3):377–381, September 2002. ISSN 1530-0447. doi: 10.1203/00006450-200209000-00012.

[115] Arai, Y., Martin-Ruiz, C.M., Takayama, M., Abe, Y., Takebayashi, T., Koyasu, S., Suematsu, M., Hirose, N., and Zglinicki, T.v. Inflammation, But Not Telomere Length, Predicts Successful Ageing at Extreme Old Age: A Longitudinal Study of Semi-supercentenarians. *EBioMedicine*, 2(10):1549–1558, October 2015. ISSN 2352-3964. doi:10.1016/j.ebiom.2015.07.029.

[116] Makarov, V.L., Hirose, Y., and Langmore, J.P. Long G Tails at Both Ends of Human Chromosomes Suggest a C Strand Degradation Mechanism for Telomere Shortening. *Cell*, 88(5):657–666, March 1997. ISSN 0092-8674. doi:10.1016/S0092-8674(00) 81908-X.

[117] Griffith, J.D., Comeau, L., Rosenfield, S., Stansel, R.M., Bianchi, A., Moss, H., and de Lange, T. Mammalian Telomeres End in a Large Duplex Loop. *Cell*, 97(4):503–514, May 1999. ISSN 0092-8674. doi:10.1016/S0092-8674(00)80760-6.

[118] Lange, T.d. Shelterin: the protein complex that shapes and safeguards human telomeres. *Genes & Development*, 19(18):2100–2110, September 2005. ISSN 0890-9369, 1549-5477. doi:10.1101/gad.1346005.

[119] Surovtseva, Y.V., Churikov, D., Boltz, K.A., Song, X., Lamb, J.C., Warrington, R., Leehy, K., Heacock, M., Price, C.M., and Shippen, D.E. Conserved Telomere Maintenance Component 1 Interacts with STN1 and Maintains Chromosome Ends in Higher Eukaryotes. *Molecular Cell*, 36(2):207–218, October 2009. ISSN 1097-2765. doi:10.1016/j.molcel.2009.09.017.

[120] Sakabe, K. and Okazaki, R. A unique property of the replicating region of chromosomal DNA. *Biochimica et Biophysica Acta (BBA) - Nucleic Acids and Protein Synthesis*, 129(3):651–654, December 1966. ISSN 0005-2787. doi:10.1016/0005-2787(66) 90088-8.

[121] Kratz, K. and de Lange, T. Both Protection of Telomeres 1 proteins POT1a and POT1b can repress ATR signaling by RPA exclusion but binding to CST limits ATR repression by POT1b. *The Journal of Biological Chemistry*, August 2018. ISSN 1083-351X. doi:10.1074/jbc.RA118.004598.

[122] Amiard, S., Doudeau, M., Pinte, S., Poulet, A., Lenain, C., Faivre-Moskalenko, C., Angelov, D., Hug, N., Vindigni, A., Bouvet, P., Paoletti, J., Gilson, E., and Giraud-Panis, M.J. A topological mechanism for TRF2-enhanced strand invasion. *Nature Structural & Molecular Biology*, 14(2):147–154, February 2007. ISSN 1545-9993. doi:10.1038/nsmb1192.

[123] Doksani, Y., Wu, J.Y., de Lange, T., and Zhuang, X. Super-resolution fluorescence imaging of telomeres reveals TRF2-dependent T-loop formation. *Cell*, 155(2):345–356, October 2013. ISSN 1097-4172. doi:10.1016/j.cell.2013.09.048.

[124] Okamoto, K., Bartocci, C., Ouzounov, I., Diedrich, J.K., Yates, J.R., and Denchi, E.L. A two-step mechanism for TRF2-mediated chromosome end protection. *Nature*, 494(7438):502–505, February 2013. ISSN 0028-0836. doi:10.1038/nature11873.

[125] Hewitt, G., Jurk, D., Marques, F.D.M., Correia-Melo, C., Hardy, T., Gackowska, A., Anderson, R., Taschuk, M., Mann, J., and Passos, J.F. Telomeres are favoured targets of a persistent DNA damage response in ageing and stress-induced senescence. *Nature Communications*, 3:708, February 2012. ISSN 2041-1723. doi: 10.1038/ncomms1708.

[126] Konishi, A. and Lange, T.d. Cell cycle control of telomere protection and NHEJ revealed by a ts mutation in the DNA-binding domain of TRF2. *Genes & Development*, 22(9):1221–1230, May 2008. ISSN 0890-9369, 1549-5477. doi: 10.1101/gad.1634008.

[127] Wang, F., Podell, E.R., Zaug, A.J., Yang, Y., Baciu, P., Cech, T.R., and Lei, M. The POT1-TPP1 telomere complex is a telomerase processivity factor. *Nature*, 445(7127):506–510, February 2007. ISSN 1476-4687. doi:10.1038/nature05454.

[128] Miyake, Y., Nakamura, M., Nabetani, A., Shimamura, S., Tamura, M., Yonehara, S., Saito, M., and Ishikawa, F. RPA-like Mammalian Ctc1-Stn1-Ten1 Complex Binds to Single-Stranded DNA and Protects Telomeres Independently of the Pot1 Pathway. *Molecular Cell*, 36(2):193–206, October 2009. ISSN 1097-2765. doi: 10.1016/j.molcel.2009.08.009.

[129] de Lange, T. Shelterin-Mediated Telomere Protection. *Annual Review of Genetics*, 52(1):223–247, November 2018. ISSN 0066-4197, 1545-2948. doi:10.1146/annurev-genet-032918-021921.

[130] Raghuraman, M.K., Winzeler, E.A., Collingwood, D., Hunt, S., Wodicka, L., Conway, A., Lockhart, D.J., Davis, R.W., Brewer, B.J., and Fangman, W.L. Replication dynamics of the yeast genome. *Science (New York, N.Y.)*, 294(5540):115–121, October 2001. ISSN 0036-8075. doi:10.1126/science.294.5540.115.

[131] Arnoult, N., Schluth-Bolard, C., Letessier, A., Drascovic, I., Bouarich-Bourimi, R., Campisi, J., Kim, S.h., Boussouar, A., Ottaviani, A., Magdinier, F., Gilson, E., and Londoño-Vallejo, A. Replication Timing of Human Telomeres Is Chromosome Arm–Specific, Influenced by Subtelomeric Structures and Connected to Nuclear Localization. *PLoS Genetics*, 6(4), April 2010. ISSN 1553-7390. doi:10.1371/journal.pgen.1000920.

[132] Hayano, M., Kanoh, Y., Matsumoto, S., Renard-Guillet, C., Shirahige, K., and Masai, H. Rif1 is a global regulator of timing of replication origin firing in fission yeast. *Genes & Development*, 26(2):137–150, January 2012. ISSN 0890-9369. doi: 10.1101/gad.178491.111.

[133] Makovets, S., Herskowitz, I., and Blackburn, E.H. Anatomy and Dynamics of DNA Replication Fork Movement in Yeast Telomeric Regions. *Molecular and Cellular Biology*, 24(9):4019–4031, May 2004. ISSN 0270-7306. doi:10.1128/MCB.24.9.4019-4031.2004.

[134] Maestroni, L., Matmati, S., and Coulon, S. Solving the Telomere Replication Problem. *Genes*, 8(2), January 2017. ISSN 2073-4425. doi:10.3390/genes8020055.

[135] Sfeir, A., Kosiyatrakul, S.T., Hockemeyer, D., MacRae, S.L., Karlseder, J., Schildkraut, C.L., and de Lange, T. Mammalian telomeres resemble fragile sites and require TRF1 for efficient replication. *Cell*, 138(1):90–103, July 2009. ISSN 0092-8674. doi:10.1016/j.cell.2009.06.021.

[136] Williamson, J.R., Raghuraman, M.K., and Cech, T.R. Monovalent cation-induced structure of telomeric DNA: The G-quartet model. *Cell*, 59(5):871–880, December 1989. ISSN 0092-8674. doi:10.1016/0092-8674(89)90610-7.

[137] Balk, B., Maicher, A., Dees, M., Klermund, J., Luke-Glaser, S., Bender, K., and Luke, B. Telomeric RNA-DNA hybrids affect telomere-length dynamics and senescence. *Nature Structural & Molecular Biology*, 20(10):1199–1205, October 2013. ISSN 1545-9985. doi:10.1038/nsmb.2662.

[138] Vannier, J.B., Pavicic-Kaltenbrunner, V., Petalcorin, M.I.R., Ding, H., and Boulton, S.J. RTEL1 dismantles T loops and counteracts telomeric G4-DNA to maintain telomere integrity. *Cell*, 149(4):795–806, May 2012. ISSN 1097-4172. doi:10.1016/j.cell.2012.03.030.

[139] Ye, J., Lenain, C., Bauwens, S., Rizzo, A., Saint-Léger, A., Poulet, A., Benarroch, D., Magdinier, F., Morere, J., Amiard, S., Verhoeyen, E., Britton, S., Calsou, P., Salles, B., Bizard, A., Nadal, M., Salvati, E., Sabatier, L., Wu, Y., Biroccio, A., Londoño-Vallejo, A., Giraud-Panis, M.J., and Gilson, E. TRF2 and apollo cooperate with topoisomerase 2alpha to protect human telomeres from replicative damage. *Cell*, 142(2):230–242, July 2010. ISSN 1097-4172. doi:10.1016/j.cell.2010.05.032.

[140] Wang, Q., Liu, J.q., Chen, Z., Zheng, K.w., Chen, C.y., Hao, Y.h., and Tan, Z. G-quadruplex formation at the 3-prime end of telomere DNA inhibits its extension by telomerase, polymerase and unwinding by helicase. *Nucleic Acids Research*, 39(14):6229–6237, August 2011. ISSN 0305-1048. doi:10.1093/nar/gkr164.

[141] Yanez, G.H., Khan, S.J., Locovei, A.M., Pedroso, I.M., and Fletcher, T.M. DNA structure-dependent recruitment of telomeric proteins to single-stranded/double-stranded DNA junctions. *Biochemical and Biophysical Research Communications*, 328(1):49–56, March 2005. ISSN 0006-291X. doi:10.1016/j.bbrc.2004.12.134.

[142] Mohaghegh, P., Karow, J.K., Jr, R.M.B., Bohr, V.A., and Hickson, I.D. The Bloom's and Werner's syndrome proteins are DNA structure-specific helicases. *Nucleic Acids Research*, 29(13):2843, July 2001. doi:10.1093/nar/29.13.2843.

[143] Sun, H., Karow, J.K., Hickson, I.D., and Maizels, N. The Bloom's Syndrome Helicase Unwinds G4 DNA. *Journal of Biological Chemistry*, 273(42):27587–27592, October 1998. ISSN 0021-9258, 1083-351X. doi:10.1074/jbc.273.42.27587.

[144] Crabbe, L., Verdun, R.E., Haggblom, C.I., and Karlseder, J. Defective Telomere Lagging Strand Synthesis in Cells Lacking WRN Helicase Activity. *Science*, 306(5703):1951–1953, December 2004. ISSN 0036-8075, 1095-9203. doi:10.1126/science.1103619.

[145] Vannier, J.B., Sandhu, S., Petalcorin, M.I., Wu, X., Nabi, Z., Ding, H., and Boulton, S.J. RTEL1 Is a Replisome-Associated Helicase That Promotes Telomere and Genome-Wide Replication. *Science*, 342(6155):239–242, October 2013. ISSN 0036-8075, 1095-9203. doi:10.1126/science.1241779.

[146] Sarek, G., Vannier, J.B., Panier, S., Petrini, J.H.J., and Boulton, S.J. TRF2 Recruits RTEL1 to Telomeres in S Phase to Promote T-Loop Unwinding. *Molecular Cell*, 57(4):622, February 2015. doi:10.1016/j.molcel.2014.12.024.

[147] Opresko, P.L., Otterlei, M., Graakjær, J., Bruheim, P., Dawut, L., Kølvraa, S., May, A., Seidman, M.M., and Bohr, V.A. The Werner Syndrome Helicase and Exonuclease Cooperate to Resolve Telomeric D Loops in a Manner Regulated by TRF1 and TRF2. *Molecular Cell*, 14(6):763–774, June 2004. ISSN 1097-2765. doi:10.1016/j.molcel.2004.05.023.

[148] Lillard-Wetherell, K., Machwe, A., Langland, G.T., Combs, K.A., Behbehani, G.K., Schonberg, S.A., German, J., Turchi, J.J., Orren, D.K., and Groden, J. Association and regulation of the BLM helicase by the telomere proteins TRF1 and TRF2. *Human Molecular Genetics*, 13(17):1919–1932, September 2004. ISSN 0964-6906. doi:10.1093/hmg/ddh193.

[149] Azzalin, C.M., Reichenbach, P., Khoriauli, L., Giulotto, E., and Lingner, J. Telomeric Repeat–Containing RNA and RNA Surveillance Factors at Mammalian Chromosome Ends. *Science*, 318(5851):798–801, November 2007. ISSN 0036-8075, 1095-9203. doi:10.1126/science.1147182.

[150] Costantino, L. and Koshland, D. The Yin and Yang of R-loop Biology. *Current opinion in cell biology*, 34:39–45, June 2015. ISSN 0955-0674. doi:10.1016/j.ceb.2015.04.008.

[151] Arora, R., Lee, Y., Wischnewski, H., Brun, C.M., Schwarz, T., and Azzalin, C.M. RNaseH1 regulates TERRA-telomeric DNA hybrids and telomere maintenance in ALT tumour cells. *Nature Communications*, 5, October 2014. ISSN 2041-1723. doi:10.1038/ncomms6220.

[152] Flynn, R.L., Cox, K.E., Jeitany, M., Wakimoto, H., Bryll, A.R., Ganem, N.J., Bersani, F., Pineda, J.R., Suvà, M.L., Benes, C.H., Haber, D.A., Boussin, F.D., and Zou, L. Alternative lengthening of telomeres renders cancer cells hypersensitive to ATR inhibitors. *Science (New York, N.Y.)*, 347(6219):273–277, January 2015. ISSN 1095-9203. doi:10.1126/science.1257216.

[153] Zhang, D.H., Zhou, B., Huang, Y., Xu, L.X., and Zhou, J.Q. The human Pif1 helicase, a potential Escherichia coli RecD homologue, inhibits telomerase activity. *Nucleic Acids Research*, 34(5):1393–1404, 2006. ISSN 1362-4962. doi:10.1093/nar/gkl029.

[154] Bandaria, J.N., Qin, P., Berk, V., Chu, S., and Yildiz, A. Shelterin Protects Chromosome Ends by Compacting Telomeric Chromatin. *Cell*, 164(4):735–746, February 2016. ISSN 0092-8674. doi:10.1016/j.cell.2016.01.036.

[155] Benarroch-Popivker, D., Pisano, S., Mendez-Bermudez, A., Lototska, L., Kaur, P., Bauwens, S., Djerbi, N., Latrick, C.M., Fraisier, V., Pei, B., Gay, A., Jaune, E., Foucher, K., Cherfils-Vicini, J., Aeby, E., Miron, S., Londoño-Vallejo, A., Ye, J., Le Du, M.H., Wang, H., Gilson, E., and Giraud-Panis, M.J. TRF2-Mediated Control of Telomere DNA Topology as a Mechanism for Chromosome-End Protection. *Molecular cell*, 61(2):274–286, January 2016. ISSN 1097-2765. doi:10.1016/j.molcel.2015.12.009.

[156] Ludérus, M.E., van Steensel, B., Chong, L., Sibon, O.C., Cremers, F.F., and de Lange, T. Structure, subnuclear distribution, and nuclear matrix association of the mammalian telomeric complex. *The Journal of Cell Biology*, 135(4):867–881, November 1996. ISSN 0021-9525. doi:10.1083/jcb.135.4.867.

[157] Morin, G.B. The human telomere terminal transferase enzyme is a ribonucleoprotein that synthesizes TTAGGG repeats. *Cell*, 59(3):521–529, November 1989. ISSN 0092-8674. doi:10.1016/0092-8674(89)90035-4.

[158] Greider, C.W. and Blackburn, E.H. Identification of a specific telomere terminal transferase activity in tetrahymena extracts. *Cell*, 43(2, Part 1):405–413, December 1985. ISSN 0092-8674. doi:10.1016/0092-8674(85)90170-9.

[159] Hiyama, E. and Hiyama, K. Telomere and telomerase in stem cells. *British Journal of Cancer*, 96(7):1020–1024, April 2007. ISSN 1532-1827. doi:10.1038/sj.bjc.6603671.

[160] Shay, J.W. Role of Telomeres and Telomerase in Aging and Cancer. *Cancer Discovery*, 6(6):584–593, June 2016. ISSN 2159-8274, 2159-8290. doi:10.1158/2159-8290.CD-16-0062.

[161] Cohen, S.B., Graham, M.E., Lovrecz, G.O., Bache, N., Robinson, P.J., and Reddel, R.R. Protein Composition of Catalytically Active Human Telomerase from Immortal Cells. *Science*, 315(5820):1850–1853, March 2007. ISSN 0036-8075, 1095-9203. doi:10.1126/science.1138596.

[162] Kim, N.W., Piatyszek, M.A., Prowse, K.R., Harley, C.B., West, M.D., Ho, P.L., Coviello, G.M., Wright, W.E., Weinrich, S.L., and Shay, J.W. Specific association of human telomerase activity with immortal cells and cancer. *Science*, 266(5193):2011–2015, December 1994. ISSN 0036-8075, 1095-9203. doi:10.1126/science.7605428.

[163] Bryan, T.M., Englezou, A., Dalla-Pozza, L., Dunham, M.A., and Reddel, R.R. Evidence for an alternative mechanism for maintaining telomere length in human tumors and tumor-derived cell lines. *Nature Medicine*, 3(11):1271–1274, November 1997. ISSN 1078-8956. doi:10.1038/nm1197-1271.

[164] Dunham, M.A., Neumann, A.A., Fasching, C.L., and Reddel, R.R. Telomere maintenance by recombination in human cells. *Nature Genetics*, 26(4):447–450, December 2000. ISSN 1061-4036. doi:10.1038/82586.

[165] Cesare, A.J. and Griffith, J.D. Telomeric DNA in ALT Cells Is Characterized by Free Telomeric Circles and Heterogeneous t-Loops. *Molecular and Cellular Biology*, 24(22):9948–9957, November 2004. ISSN 0270-7306. doi:10.1128/MCB.24.22.9948-9957.2004.

[166] Bechter, O.E., Zou, Y., Shay, J.W., and Wright, W.E. Homologous recombination in human telomerase-positive and ALT cells occurs with the same frequency. *EMBO Reports*, 4(12):1138–1143, December 2003. ISSN 1469-221X. doi:10.1038/sj.embor.7400027.

[167] Zhang, J.M., Yadav, T., Ouyang, J., Lan, L., and Zou, L. Alternative Lengthening of Telomeres through Two Distinct Break-Induced Replication Pathways. *Cell Reports*, 26(4):955–968.e3, January 2019. ISSN 22111247. doi:10.1016/j.celrep.2018.12.102.

[168] Jensen, R.B., Carreira, A., and Kowalczykowski, S.C. Purified human BRCA2 stimulates RAD51-mediated recombination. *Nature*, 467(7316):678–683, October 2010. ISSN 1476-4687. doi:10.1038/nature09399.

[169] Liu, J., Doty, T., Gibson, B., and Heyer, W.D. Human BRCA2 protein promotes RAD51 filament formation on RPA-covered single-stranded DNA. *Nature Structural & Molecular Biology*, 17(10):1260–1262, October 2010. ISSN 1545-9985. doi:10.1038/nsmb.1904.

[170] Bianchi, A. and Shore, D. How Telomerase Reaches Its End: Mechanism of Telomerase Regulation by the Telomeric Complex. *Molecular Cell*, 31(2):153–165, July 2008. ISSN 1097-2765. doi:10.1016/j.molcel.2008.06.013.

[171] Chen, L.Y., Redon, S., and Lingner, J. The human CST complex is a terminator of telomerase activity. *Nature*, 488(7412):540–544, August 2012. ISSN 0028-0836. doi:10.1038/nature11269.

[172] Wu, P., Takai, H., and de Lange, T. Telomeric 3-prime Overhangs Derive from Resection by Exo1 and Apollo and Fill-In by POT1b-Associated CST. *Cell*, 150(1):39–52, July 2012. ISSN 0092-8674. doi:10.1016/j.cell.2012.05.026.

[173] Stewart, J.A., Wang, F., Chaiken, M.F., Kasbek, C., Chastain, P.D., Wright, W.E., and Price, C.M. Human CST promotes telomere duplex replication and general replication restart after fork stalling. *The EMBO Journal*, 31(17):3537–3549, August 2012. ISSN 0261-4189. doi:10.1038/emboj.2012.215.

[174] Kasbek, C., Wang, F., and Price, C.M. Human TEN1 Maintains Telomere Integrity and Functions in Genome-wide Replication Restart. *Journal of Biological Chemistry*, 288(42):30139–30150, October 2013. ISSN 0021-9258, 1083-351X. doi:10.1074/jbc.M113.493478.

[175] Barazas, M., Annunziato, S., Pettitt, S.J., de Krijger, I., Ghezraoui, H., Roobol, S.J., Lutz, C., Frankum, J., Song, F.F., Brough, R., Evers, B., Gogola, E., Bhin, J., van de Ven, M., van Gent, D.C., Jacobs, J.J.L., Chapman, R., Lord, C.J., Jonkers, J., and Rottenberg, S. The CST Complex Mediates End Protection at Double-Strand Breaks and Promotes PARP Inhibitor Sensitivity in BRCA1-Deficient Cells. *Cell Reports*, 23(7):2107–2118, May 2018. ISSN 2211-1247. doi:10.1016/j.celrep.2018.04.046.

[176] Anderson, B.H., Kasher, P.R., Mayer, J., Szynkiewicz, M., Jenkinson, E.M., Bhaskar, S.S., Urquhart, J.E., Daly, S.B., Dickerson, J.E., O'Sullivan, J., Leibundgut, E.O., Muter, J., Abdel-Salem, G.M.H., Babul-Hirji, R., Baxter, P., Berger, A., Bonafé, L., Brunstom-Hernandez, J.E., Buckard, J.A., Chitayat, D., Chong, W.K., Cordelli, D.M., Ferreira, P., Fluss, J., Forrest, E.H., Franzoni, E., Garone, C., Hammans, S.R., Houge, G., Hughes, I., Jacquemont, S., Jeannet, P.Y., Jefferson, R.J., Kumar, R., Kutschke, G., Lundberg, S., Lourenço, C.M., Mehta, R., Naidu, S., Nischal, K.K., Nunes, L., Õunap, K., Philippart, M., Prabhakar, P., Risen, S.R., Schiffmann, R., Soh, C., Stephenson, J.B.P., Stewart, H., Stone, J., Tolmie, J.L.,

van der Knaap, M.S., Vieira, J.P., Vilain, C.N., Wakeling, E.L., Wermenbol, V., Whitney, A., Lovell, S.C., Meyer, S., Livingston, J.H., Baerlocher, G.M., Black, G.C.M., Rice, G.I., and Crow, Y.J. Mutations in CTC1, encoding conserved telomere maintenance component 1, cause Coats plus. *Nature Genetics*, 44(3):338–342, March 2012. ISSN 1061-4036. doi:10.1038/ng.1084.

[177] Simon, A.J., Lev, A., Zhang, Y., Weiss, B., Rylova, A., Eyal, E., Kol, N., Barel, O., Cesarkas, K., Soudack, M., Greenberg-Kushnir, N., Rhodes, M., Wiest, D.L., Schiby, G., Barshack, I., Katz, S., Pras, E., Poran, H., Reznik-Wolf, H., Ribakovsky, E., Simon, C., Hazou, W., Sidi, Y., Lahad, A., Katzir, H., Sagie, S., Aqeilan, H.A., Glousker, G., Amariglio, N., Tzfati, Y., Selig, S., Rechavi, G., and Somech, R. Mutations in STN1 cause Coats plus syndrome and are associated with genomic and telomere defects. *The Journal of Experimental Medicine*, 213(8):1429–1440, July 2016. ISSN 0022-1007. doi:10.1084/jem.20151618.

[178] Broccoli, D., Young, J.W., and de Lange, T. Telomerase activity in normal and malignant hematopoietic cells. *Proceedings of the National Academy of Sciences of the United States of America*, 92(20):9082–9086, September 1995. ISSN 0027-8424.

[179] Counter, C.M., Gupta, J., Harley, C.B., Leber, B., and Bacchetti, S. Telomerase activity in normal leukocytes and in hematologic malignancies. *Blood*, 85(9):2315–2320, May 1995. ISSN 0006-4971, 1528-0020.

[180] Cifuentes-Rojas, C. and Shippen, D.E. Telomerase Regulation. *Mutation Research*, 730(1-2):20–27, February 2012. ISSN 0027-5107. doi:10.1016/j.mrfmmm.2011.10.003.

[181] Latrick, C.M. and Cech, T.R. POT1–TPP1 enhances telomerase processivity by slowing primer dissociation and aiding translocation. *The EMBO Journal*, 29(5):924–933, March 2010. ISSN 1460-2075. doi:10.1038/emboj.2009.409.

[182] Feng, X., Hsu, S.J., Kasbek, C., Chaiken, M., and Price, C.M. CTC1-mediated C-strand fill-in is an essential step in telomere length maintenance. *Nucleic Acids Research*, 45(8):4281–4293, 2017. ISSN 1362-4962. doi:10.1093/nar/gkx125.

[183] Goulian, M., Heard, C.J., and Grimm, S.L. Purification and properties of an accessory protein for DNA polymerase alpha/primase. *Journal of Biological Chemistry*, 265(22):13221–13230, August 1990. ISSN 0021-9258, 1083-351X.

[184] Wang, F., Stewart, J.A., Kasbek, C., Zhao, Y., Wright, W.E., and Price, C.M. Human CST Has Independent Functions during Telomere Duplex Replication and C-Strand Fill-In. *Cell Reports*, 2(5):1096–1103, November 2012. ISSN 2211-1247. doi:10.1016/j.celrep.2012.10.007.

[185] Chastain, M., Zhou, Q., Shiva, O., Whitmore, L., Jia, P., Dai, X., Huang, C., Fadri-Moskwik, M., Ye, P., and Chai, W. Human CST Facilitates Genome-wide RAD51 Recruitment to GC-Rich Repetitive Sequences in Response to Replication Stress. *Cell Reports*, 16(5):1300–1314, August 2016. ISSN 2211-1247. doi:10.1016/j.celrep.2016.06.077.

[186] Hashimoto, Y., Ray Chaudhuri, A., Lopes, M., and Costanzo, V. Rad51 protects nascent DNA from Mre11-dependent degradation and promotes continuous DNA synthesis. *Nature Structural & Molecular Biology*, 17(11):1305–1311, November 2010. ISSN 1545-9985. doi:10.1038/nsmb.1927.

[187] Sirbu, B.M., McDonald, W.H., Dungrawala, H., Badu-Nkansah, A., Kavanaugh, G.M., Chen, Y., Tabb, D.L., and Cortez, D. Identification of Proteins at Active, Stalled, and Collapsed Replication Forks Using Isolation of Proteins on Nascent DNA (iPOND) Coupled with Mass Spectrometry. *Journal of Biological Chemistry*, 288(44):31458–31467, November 2013. ISSN 0021-9258, 1083-351X. doi:10.1074/jbc.M113.511337.

[188] Jaspers, J.E., Kersbergen, A., Boon, U., Sol, W., Deemter, L.v., Zander, S.A., Drost, R., Wientjens, E., Ji, J., Aly, A., Doroshow, J.H., Cranston, A., Martin, N.M.B., Lau, A., O'Connor, M.J., Ganesan, S., Borst, P., Jonkers, J., and Rottenberg, S. Loss of 53bp1 Causes PARP Inhibitor Resistance in Brca1-Mutated Mouse Mammary Tumors. *Cancer Discovery*, 3(1):68–81, January 2013. ISSN 2159-8274, 2159-8290. doi:10.1158/2159-8290.CD-12-0049.

[189] Mirman, Z., Lottersberger, F., Takai, H., Kibe, T., Gong, Y., Takai, K., Bianchi, A., Zimmermann, M., Durocher, D., and de Lange, T. 53bp1/Rif1/Shieldin counteract DSB resection through CST/Pol alpha-dependent fill-in. *Nature*, 560(7716):112–116, August 2018. ISSN 0028-0836. doi:10.1038/s41586-018-0324-7.

[190] Thomas, M.C. and Chiang, C.M. The General Transcription Machinery and General Cofactors. *Critical Reviews in Biochemistry and Molecular Biology*, 41(3):105–178, January 2006. ISSN 1040-9238. doi:10.1080/10409230600648736.

[191] Lemon, B. and Tjian, R. Orchestrated response: a symphony of transcription factors for gene control. *Genes & Development*, 14(20):2551–2569, October 2000. ISSN 0890-9369. doi:10.1101/gad.831000.

[192] Li, Y., Flanagan, P.M., Tschochner, H., and Kornberg, R.D. RNA polymerase II initiation factor interactions and transcription start site selection. *Science (New York, N.Y.)*, 263(5148):805–807, February 1994. ISSN 0036-8075. doi:10.1126/science.8303296.

[193] Bushnell, D.A. and Kornberg, R.D. Complete, 12-subunit RNA polymerase II at 4.1-A resolution: implications for the initiation of transcription. *Proceedings of the*

National Academy of Sciences of the United States of America, 100(12):6969–6973, June 2003. ISSN 0027-8424. doi:10.1073/pnas.1130601100.

[194] Flores, O., Lu, H., Killeen, M., Greenblatt, J., Burton, Z.F., and Reinberg, D. The small subunit of transcription factor IIF recruits RNA polymerase II into the preinitiation complex. *Proceedings of the National Academy of Sciences of the United States of America*, 88(22):9999–10003, November 1991. ISSN 0027-8424.

[195] Gnatt, A.L., Cramer, P., Fu, J., Bushnell, D.A., and Kornberg, R.D. Structural basis of transcription: an RNA polymerase II elongation complex at 3.3 A resolution. *Science (New York, N.Y.)*, 292(5523):1876–1882, June 2001. ISSN 0036-8075. doi: 10.1126/science.1059495.

[196] Hahn, S. Structure and mechanism of the RNA polymerase II transcription machinery. *Nature Structural & Molecular Biology*, 11(5):394–403, May 2004. ISSN 1545-9993. doi:10.1038/nsmb763.

[197] Shuman, S. Structure, mechanism, and evolution of the mRNA capping apparatus. In *Progress in Nucleic Acid Research and Molecular Biology*, volume 66, pages 1–40. Academic Press, January 2000. doi:10.1016/S0079-6603(00)66025-7.

[198] Buratowski, S. Progression through the RNA polymerase II CTD cycle. *Molecular cell*, 36(4):541–546, November 2009. ISSN 1097-2765. doi:10.1016/j.molcel.2009.10.019.

[199] Kim, S.J. and Martinson, H.G. Poly(A)-dependent transcription termination: continued communication of the poly(A) signal with the polymerase is required long after extrusion in vivo. *The Journal of Biological Chemistry*, 278(43):41691–41701, October 2003. ISSN 0021-9258. doi:10.1074/jbc.M306304200.

[200] Glover-Cutter, K., Larochelle, S., Erickson, B., Zhang, C., Shokat, K., Fisher, R.P., and Bentley, D.L. TFIIH-associated Cdk7 kinase functions in phosphorylation of C-terminal domain Ser7 residues, promoter-proximal pausing, and termination by RNA polymerase II. *Molecular and Cellular Biology*, 29(20):5455–5464, October 2009. ISSN 1098-5549. doi:10.1128/MCB.00637-09.

[201] Jo, B.S. and Choi, S.S. Introns: The Functional Benefits of Introns in Genomes. *Genomics & Informatics*, 13(4):112–118, December 2015. ISSN 1598-866X. doi: 10.5808/GI.2015.13.4.112.

[202] Merkin, J., Russell, C., Chen, P., and Burge, C.B. Evolutionary Dynamics of Gene and Isoform Regulation in Mammalian Tissues. *Science*, 338(6114):1593–1599, December 2012. ISSN 0036-8075, 1095-9203. doi:10.1126/science.1228186.

[203] Görnemann, J., Kotovic, K.M., Hujer, K., and Neugebauer, K.M. Cotranscriptional Spliceosome Assembly Occurs in a Stepwise Fashion and Requires the Cap Binding Complex. *Molecular Cell*, 19(1):53–63, July 2005. ISSN 1097-2765. doi:10.1016/j.molcel.2005.05.007.

[204] Montecucco, A. and Biamonti, G. Pre-mRNA processing factors meet the DNA damage response. *Frontiers in Genetics*, 4, 2013. ISSN 1664-8021. doi:10.3389/fgene.2013.00102.

[205] Black, D.L. Mechanisms of alternative pre-messenger RNA splicing. *Annual Review of Biochemistry*, 72:291–336, 2003. ISSN 0066-4154. doi:10.1146/annurev.biochem.72.121801.161720.

[206] Wahl, M.C., Will, C.L., and Lührmann, R. The Spliceosome: Design Principles of a Dynamic RNP Machine. *Cell*, 136(4):701–718, February 2009. ISSN 0092-8674, 1097-4172. doi:10.1016/j.cell.2009.02.009.

[207] Lee, Y. and Rio, D.C. Mechanisms and Regulation of Alternative Pre-mRNA Splicing. *Annual Review of Biochemistry*, 84(1):291–323, June 2015. ISSN 0066-4154, 1545-4509. doi:10.1146/annurev-biochem-060614-034316.

[208] Tange, T.., Nott, A., and Moore, M.J. The ever-increasing complexities of the exon junction complex. *Current Opinion in Cell Biology*, 16(3):279–284, June 2004. ISSN 0955-0674. doi:10.1016/j.ceb.2004.03.012.

[209] Ramakrishnan, V. Ribosome Structure and the Mechanism of Translation. *Cell*, 108(4):557–572, February 2002. ISSN 0092-8674, 1097-4172. doi:10.1016/S0092-8674(02)00619-0.

[210] Rabl, J., Leibundgut, M., Ataide, S.F., Haag, A., and Ban, N. Crystal Structure of the Eukaryotic 40s Ribosomal Subunit in Complex with Initiation Factor 1. *Science*, 331(6018):730–736, February 2011. ISSN 0036-8075, 1095-9203. doi:10.1126/science.1198308.

[211] Ben-Shem, A., Loubresse, N.G.d., Melnikov, S., Jenner, L., Yusupova, G., and Yusupov, M. The Structure of the Eukaryotic Ribosome at 3.0 Å Resolution. *Science*, 334(6062):1524–1529, December 2011. ISSN 0036-8075, 1095-9203. doi:10.1126/science.1212642.

[212] Kozak, M. Point mutations define a sequence flanking the AUG initiator codon that modulates translation by eukaryotic ribosomes. *Cell*, 44(2):283–292, January 1986. ISSN 0092-8674, 1097-4172. doi:10.1016/0092-8674(86)90762-2.

[213] Rodnina, M.V., Beringer, M., and Wintermeyer, W. How ribosomes make peptide bonds. *Trends in Biochemical Sciences*, 32(1):20–26, January 2007. ISSN 0968-0004. doi:10.1016/j.tibs.2006.11.007.

[214] Banerjee, D. and Sanyal, S. Protein Folding Activity of the Ribosome (PFAR) — A Target for Antiprion Compounds. *Viruses*, 6(10):3907–3924, October 2014. ISSN 1999-4915. doi:10.3390/v6103907.

[215] Gunišová, S., Hronová, V., Mohammad, M.P., Hinnebusch, A.G., and Valášek, L.S. Please do not recycle! Translation reinitiation in microbes and higher eukaryotes. *FEMS Microbiology Reviews*, 42(2):165–192, March 2018. ISSN 0168-6445. doi: 10.1093/femsre/fux059.

[216] Thermann, R., Neu-Yilik, G., Deters, A., Frede, U., Wehr, K., Hagemeier, C., Hentze, M.W., and Kulozik, A.E. Binary specification of nonsense codons by splicing and cytoplasmic translation. *The EMBO Journal*, 17(12):3484–3494, June 1998. ISSN 0261-4189. doi:10.1093/emboj/17.12.3484.

[217] Zhang, J., Sun, X., Qian, Y., and Maquat, L.E. Intron function in the nonsense-mediated decay of beta-globin mRNA: indications that pre-mRNA splicing in the nucleus can influence mRNA translation in the cytoplasm. *RNA*, 4(7):801–815, July 1998. ISSN 1355-8382.

[218] Amrani, N., Ganesan, R., Kervestin, S., Mangus, D.A., Ghosh, S., and Jacobson, A. A faux 3 prime-UTR promotes aberrant termination and triggers nonsense-mediated mRNA decay. *Nature*, 432(7013):112–118, November 2004. ISSN 1476-4687. doi: 10.1038/nature03060.

[219] Gehring, N.H., Lamprinaki, S., Kulozik, A.E., and Hentze, M.W. Disassembly of exon junction complexes by PYM. *Cell*, 137(3):536–548, May 2009. ISSN 1097-4172. doi:10.1016/j.cell.2009.02.042.

[220] Schweingruber, C., Rufener, S.C., Zünd, D., Yamashita, A., and Mühlemann, O. Nonsense-mediated mRNA decay - mechanisms of substrate mRNA recognition and degradation in mammalian cells. *Biochimica Et Biophysica Acta*, 1829(6-7):612–623, July 2013. ISSN 0006-3002. doi:10.1016/j.bbagrm.2013.02.005.

[221] Hug, N., Longman, D., and Cáceres, J.F. Mechanism and regulation of the nonsense-mediated decay pathway. *Nucleic Acids Research*, 44(4):1483–1495, February 2016. ISSN 0305-1048. doi:10.1093/nar/gkw010.

[222] Yamashita, A., Ohnishi, T., Kashima, I., Taya, Y., and Ohno, S. Human SMG-1, a novel phosphatidylinositol 3-kinase-related protein kinase, associates with components of the mRNA surveillance complex and is involved in the regulation of nonsense-mediated mRNA decay. *Genes & Development*, 15(17):2215–2228, September 2001. ISSN 0890-9369. doi:10.1101/gad.913001.

[223] Chamieh, H., Ballut, L., Bonneau, F., and Le Hir, H. NMD factors UPF2 and UPF3 bridge UPF1 to the exon junction complex and stimulate its RNA helicase

activity. *Nature Structural & Molecular Biology*, 15(1):85–93, January 2008. ISSN 1545-9985. doi:10.1038/nsmb1330.

[224] Eberle, A.B., Lykke-Andersen, S., Mühlemann, O., and Jensen, T.H. SMG6 promotes endonucleolytic cleavage of nonsense mRNA in human cells. *Nature Structural & Molecular Biology*, 16(1):49–55, January 2009. ISSN 1545-9985. doi: 10.1038/nsmb.1530.

[225] Loh, B., Jonas, S., and Izaurralde, E. The SMG5-SMG7 heterodimer directly recruits the CCR4-NOT deadenylase complex to mRNAs containing nonsense codons via interaction with POP2. *Genes & Development*, 27(19):2125–2138, October 2013. ISSN 1549-5477. doi:10.1101/gad.226951.113.

[226] Unterholzner, L. and Izaurralde, E. SMG7 acts as a molecular link between mRNA surveillance and mRNA decay. *Molecular Cell*, 16(4):587–596, November 2004. ISSN 1097-2765. doi:10.1016/j.molcel.2004.10.013.

[227] Singh, G., Rebbapragada, I., and Lykke-Andersen, J. A Competition between Stimulators and Antagonists of Upf Complex Recruitment Governs Human Nonsense-Mediated mRNA Decay. *PLOS Biology*, 6(4):e111, April 2008. ISSN 1545-7885. doi:10.1371/journal.pbio.0060111.

[228] Peccarelli, M. and Kebaara, B.W. Regulation of Natural mRNAs by the Nonsense-Mediated mRNA Decay Pathway. *Eukaryotic Cell*, 13(9):1126–1135, September 2014. ISSN 1535-9778. doi:10.1128/EC.00090-14.

[229] Davies, W.L., Vandenberg, J.I., Sayeed, R.A., and Trezise, A.E.O. Post-transcriptional regulation of the cystic fibrosis gene in cardiac development and hypertrophy. *Biochemical and Biophysical Research Communications*, 319(2):410–418, June 2004. ISSN 0006-291X. doi:10.1016/j.bbrc.2004.05.008.

[230] Yepiskoposyan, H., Aeschimann, F., Nilsson, D., Okoniewski, M., and Mühlemann, O. Autoregulation of the nonsense-mediated mRNA decay pathway in human cells. *RNA*, 17(12):2108–2118, December 2011. ISSN 1355-8382, 1469-9001. doi:10.1261/rna.030247.111.

[231] Torrance, V. and Lydall, D. Overlapping open reading frames strongly reduce human and yeast STN1 gene expression and affect telomere function. *PLOS Genetics*, 14(8):e1007523, August 2018. ISSN 1553-7404. doi:10.1371/journal.pgen.1007523.

[232] Viegas, M.H., Gehring, N.H., Breit, S., Hentze, M.W., and Kulozik, A.E. The abundance of RNPS1, a protein component of the exon junction complex, can determine the variability in efficiency of the Nonsense Mediated Decay pathway. *Nucleic Acids Research*, 35(13):4542–4551, 2007. ISSN 1362-4962. doi:10.1093/nar/gkm461.

[233] Huang, L. and Wilkinson, M.F. Regulation of nonsense-mediated mRNA decay. *Wiley interdisciplinary reviews. RNA*, 3(6):807–828, December 2012. ISSN 1757-7012. doi:10.1002/wrna.1137.

[234] Gardner, L.B. Nonsense mediated RNA decay regulation by cellular stress; implications for tumorigenesis. *Molecular cancer research : MCR*, 8(3):295–308, March 2010. ISSN 1541-7786. doi:10.1158/1541-7786.MCR-09-0502.

[235] Wang, D., Zavadil, J., Martin, L., Parisi, F., Friedman, E., Levy, D., Harding, H., Ron, D., and Gardner, L.B. Inhibition of Nonsense-Mediated RNA Decay by the Tumor Microenvironment Promotes Tumorigenesis. *Molecular and Cellular Biology*, 31(17):3670–3680, September 2011. ISSN 0270-7306. doi:10.1128/MCB.05704-11.

[236] Gardner, L.B. Hypoxic inhibition of nonsense-mediated RNA decay regulates gene expression and the integrated stress response. *Molecular and Cellular Biology*, 28(11):3729–3741, June 2008. ISSN 1098-5549. doi:10.1128/MCB.02284-07.

[237] Nickless, A., Cheruiyot, A., Flanagan, K.C., Piwnica-Worms, D., Stewart, S.A., and You, Z. p38 MAPK inhibits nonsense-mediated RNA decay in response to persistent DNA damage in noncycling cells. *The Journal of Biological Chemistry*, 292(37):15266–15276, 2017. ISSN 1083-351X. doi:10.1074/jbc.M117.787846.

[238] ATCC. HCT 116 Homo sapiens colon colorectal carcin. `https://www.lgcstandards-atcc.org/products/all/CCL-247.aspx`. Accessed: 2019-07-07.

[239] ATCC. U-2 OS Homo sapiens bone osteosarcoma. `https://www.lgcstandards-atcc.org/products/all/HTB-96.aspx`. Accessed: 2019-07-07.

[240] ATCC. hTERT RPE-1 Homo sapiens Retina, eye; pigm. `https://www.lgcstandards-atcc.org/products/all/CRL-4000.aspx`. Accessed: 2019-07-07.

[241] Sauer, B. and Henderson, N. Site-specific DNA recombination in mammalian cells by the Cre recombinase of bacteriophage P1. *Proceedings of the National Academy of Sciences of the United States of America*, 85(14):5166–5170, July 1988. ISSN 0027-8424.

[242] Metzger, D. and Chambon, P. Site- and Time-Specific Gene Targeting in the Mouse. *Methods*, 24(1):71–80, May 2001. ISSN 1046-2023. doi:10.1006/meth.2001.1159.

[243] Schneider, C.A., Rasband, W.S., and Eliceiri, K.W. NIH Image to ImageJ: 25 years of image analysis. *Nature Methods*, 9(7):671–675, July 2012. ISSN 1548-7105. doi:10.1038/nmeth.2089.

[244] Ferreira, T. Filename Randomizer. `https://imagej.nih.gov/ij/macros/Filename_Randomizer.txt`, April 2009.

[245] Pierce, A.J., Johnson, R.D., Thompson, L.H., and Jasin, M. XRCC3 promotes homology-directed repair of DNA damage in mammalian cells. *Genes & Development*, 13(20):2633–2638, October 1999. ISSN 0890-9369.

[246] Arai, N., Ström, A., Rafter, J.J., and Gustafsson, J.A. Estrogen receptor beta mRNA in colon cancer cells: growth effects of estrogen and genistein. *Biochemical and Biophysical Research Communications*, 270(2):425–431, April 2000. ISSN 0006-291X. doi:10.1006/bbrc.2000.2444.

[247] Casteel, D.E., Zhuang, S., Zeng, Y., Perrino, F.W., Boss, G.R., Goulian, M., and Pilz, R.B. A DNA Polymerase-alpha·Primase Cofactor with Homology to Replication Protein A-32 Regulates DNA Replication in Mammalian Cells. *Journal of Biological Chemistry*, 284(9):5807–5818, February 2009. ISSN 0021-9258, 1083-351X. doi:10.1074/jbc.M807593200.

[248] Amiard, S., Olivier, M., Allain, E., Choi, K., Smith-Unna, R., Henderson, I.R., White, C.I., and Gallego, M.E. Telomere stability and development of ctc1 mutants are rescued by inhibition of EJ recombination pathways in a telomerase-dependent manner. *Nucleic Acids Research*, 42(19):11979–11991, October 2014. ISSN 0305-1048, 1362-4962. doi:10.1093/nar/gku897.

[249] Jdey, W., Thierry, S., Popova, T., Stern, M.H., and Dutreix, M. Micronuclei Frequency in Tumors Is a Predictive Biomarker for Genetic Instability and Sensitivity to the DNA Repair Inhibitor AsiDNA. *Cancer Research*, 77(16):4207–4216, August 2017. ISSN 0008-5472, 1538-7445. doi:10.1158/0008-5472.CAN-16-2693.

[250] Fenech, M., Kirsch-Volders, M., Natarajan, A.T., Surralles, J., Crott, J.W., Parry, J., Norppa, H., Eastmond, D.A., Tucker, J.D., and Thomas, P. Molecular mechanisms of micronucleus, nucleoplasmic bridge and nuclear bud formation in mammalian and human cells. *Mutagenesis*, 26(1):125–132, January 2011. ISSN 0267-8357. doi:10.1093/mutage/geq052.

[251] Pang, T.L., Wang, C.Y., Hsu, C.L., Chen, M.Y., and Lin, J.J. Exposure of Single-stranded Telomeric DNA Causes G2/M Cell Cycle Arrest in Saccharomyces cerevisiae. *Journal of Biological Chemistry*, 278(11):9318–9321, March 2003. ISSN 0021-9258, 1083-351X. doi:10.1074/jbc.M208347200.

[252] Sanchez, Y., Bachant, J., Wang, H., Hu, F., Liu, D., Tetzlaff, M., and Elledge, S.J. Control of the DNA Damage Checkpoint by Chk1 and Rad53 Protein Kinases Through Distinct Mechanisms. *Science*, 286(5442):1166–1171, November 1999. ISSN 0036-8075, 1095-9203. doi:10.1126/science.286.5442.1166.

[253] Blankley, R.T. and Lydall, D. A domain of Rad9 specifically required for activation of Chk1 in budding yeast. *Journal of Cell Science*, 117(4):601–608, February 2004. ISSN 0021-9533, 1477-9137. doi:10.1242/jcs.00907.

[254] Gardner, R., Putnam, C.W., and Weinert, T. RAD53, DUN1 and PDS1 define two parallel G2/M checkpoint pathways in budding yeast. *The EMBO Journal*, 18(11):3173–3185, June 1999. ISSN 0261-4189, 1460-2075. doi:10.1093/emboj/18.11.3173.

[255] Jia, X., Weinert, T., and Lydall, D. Mec1 and Rad53 inhibit formation of single-stranded DNA at telomeres of Saccharomyces cerevisiae cdc13-1 mutants. *Genetics*, 166(2):753–764, February 2004. ISSN 0016-6731.

[256] Liu, Y., Vidanes, G., Lin, Y.C., Mori, S., and Siede, W. Characterization of a Saccharomyces cerevisiae homologue of Schizosaccharomyces pombe Chk1 involved in DNA-damage-induced M-phase arrest. *Molecular and General Genetics MGG*, 262(6):1132–1146, January 2000. ISSN 1432-1874. doi:10.1007/PL00008656.

[257] Chen, M.S., Ryan, C.E., and Piwnica-Worms, H. Chk1 Kinase Negatively Regulates Mitotic Function of Cdc25a Phosphatase through 14-3-3 Binding. *Molecular and Cellular Biology*, 23(21):7488–7497, November 2003. ISSN 0270-7306, 1098-5549. doi:10.1128/MCB.23.21.7488-7497.2003.

[258] Walton, M.I., Eve, P.D., Hayes, A., Henley, A.T., Valenti, M.R., De Haven Brandon, A.K., Box, G., Boxall, K.J., Tall, M., Swales, K., Matthews, T.P., McHardy, T., Lainchbury, M., Osborne, J., Hunter, J.E., Perkins, N.D., Aherne, G.W., Reader, J.C., Raynaud, F.I., Eccles, S.A., Collins, I., and Garrett, M.D. The clinical development candidate CCT245737 is an orally active CHK1 inhibitor with preclinical activity in RAS mutant NSCLC and E-MYC driven B-cell lymphoma. *Oncotarget*, 7(3):2329–2342, July 2015. ISSN 1949-2553. doi:10.18632/oncotarget.4919.

[259] Wilsker, D., Petermann, E., Helleday, T., and Bunz, F. Essential function of Chk1 can be uncoupled from DNA damage checkpoint and replication control. *Proceedings of the National Academy of Sciences*, 105(52):20752–20757, December 2008. ISSN 0027-8424, 1091-6490. doi:10.1073/pnas.0806917106.

[260] Koniaras, K., Cuddihy, A.R., Christopoulos, H., Hogg, A., and O'Connell, M.J. Inhibition of Chk1-dependent G2 DNA damage checkpoint radiosensitizes p53 mutant human cells. *Oncogene*, 20(51):7453, November 2001. ISSN 1476-5594. doi:10.1038/sj.onc.1204942.

[261] Agarwal, M.L., Agarwal, A., Taylor, W.R., and Stark, G.R. p53 controls both the G2/M and the G1 cell cycle checkpoints and mediates reversible growth arrest in human fibroblasts. *Proceedings of the National Academy of Sciences of the United States of America*, 92(18):8493–8497, August 1995. ISSN 0027-8424.

[262] Xiong, Y., Hannon, G.J., Zhang, H., Casso, D., Kobayashi, R., and Beach, D. p21 is a universal inhibitor of cyclin kinases. *Nature*, 366(6456):701, December 1993. ISSN 1476-4687. doi:10.1038/366701a0.

[263] Georgakilas, A.G., Martin, O.A., and Bonner, W.M. p21: A Two-Faced Genome Guardian. *Trends in Molecular Medicine*, 23(4):310–319, April 2017. ISSN 1471-4914. doi:10.1016/j.molmed.2017.02.001.

[264] Rhodes, D. and Lipps, H.J. G-quadruplexes and their regulatory roles in biology. *Nucleic Acids Research*, 43(18):8627–8637, October 2015. ISSN 0305-1048. doi: 10.1093/nar/gkv862.

[265] Henderson, A., Wu, Y., Huang, Y.C., Chavez, E.A., Platt, J., Johnson, F.B., Brosh, R.M., Sen, D., and Lansdorp, P.M. Detection of G-quadruplex DNA in mammalian cells. *Nucleic Acids Research*, 42(2):860–869, January 2014. ISSN 1362-4962. doi: 10.1093/nar/gkt957.

[266] Wang, F., Stewart, J., and Price, C.M. Human CST abundance determines recovery from diverse forms of DNA damage and replication stress. *Cell Cycle*, 13(22):3488–3498, October 2014. ISSN 1538-4101. doi:10.4161/15384101.2014.964100.

[267] Thompson, S.L. and Compton, D.A. Examining the link between chromosomal instability and aneuploidy in human cells. *The Journal of Cell Biology*, 180(4):665–672, February 2008. ISSN 0021-9525. doi:10.1083/jcb.200712029.

[268] Cimini, D., Howell, B., Maddox, P., Khodjakov, A., Degrassi, F., and Salmon, E.D. Merotelic kinetochore orientation is a major mechanism of aneuploidy in mitotic mammalian tissue cells. *The Journal of Cell Biology*, 153(3):517–527, April 2001. ISSN 0021-9525. doi:10.1083/jcb.153.3.517.

[269] Thompson, S.L., Bakhoum, S.F., and Compton, D.A. Mechanisms of Chromosomal Instability. *Current biology : CB*, 20(6):R285–R295, March 2010. ISSN 0960-9822. doi:10.1016/j.cub.2010.01.034.

[270] Cheng, B. and Crasta, K. Consequences of mitotic slippage for antimicrotubule drug therapy. *Endocrine-Related Cancer*, 24(9):T97–T106, September 2017. ISSN 1351-0088, 1479-6821. doi:10.1530/ERC-17-0147.

[271] Pampalona, J., Frías, C., Genescà, A., and Tusell, L. Progressive Telomere Dysfunction Causes Cytokinesis Failure and Leads to the Accumulation of Polyploid Cells. *PLoS Genetics*, 8(4), April 2012. ISSN 1553-7390. doi:10.1371/journal.pgen.1002679.

[272] Balachandran, R.S. and Kipreos, E.T. Addressing a weakness of anticancer therapy with mitosis inhibitors: Mitotic slippage. *Molecular & Cellular Oncology*, 4(2), January 2017. ISSN 2372-3556. doi:10.1080/23723556.2016.1277293.

[273] Ohishi, T., Muramatsu, Y., Yoshida, H., and Seimiya, H. TRF1 ensures the centromeric function of Aurora-B and proper chromosome segregation. *Molec-*

ular and Cellular Biology, 34(13):2464–2478, July 2014. ISSN 1098-5549. doi: 10.1128/MCB.00161-14.

[274] Ohishi, T., Hirota, T., Tsuruo, T., and Seimiya, H. TRF1 mediates mitotic abnormalities induced by Aurora-A overexpression. *Cancer Research*, 70(5):2041–2052, March 2010. ISSN 1538-7445. doi:10.1158/0008-5472.CAN-09-2008.

[275] Prime, G. and Markie, D. The telomere repeat binding protein Trf1 interacts with the spindle checkpoint protein Mad1 and Nek2 mitotic kinase. *Cell Cycle (Georgetown, Tex.)*, 4(1):121–124, January 2005. ISSN 1551-4005. doi:10.4161/cc.4.1.1351.

[276] Wan, M., Qin, J., Songyang, Z., and Liu, D. OB Fold-containing Protein 1 (OBFC1), a Human Homolog of Yeast Stn1, Associates with TPP1 and Is Implicated in Telomere Length Regulation. *Journal of Biological Chemistry*, 284(39):26725–26731, September 2009. ISSN 0021-9258, 1083-351X. doi:10.1074/jbc.M109.021105.

[277] Wang, H., Liu, D., Wang, Y., Qin, J., and Elledge, S.J. Pds1 phosphorylation in response to DNA damage is essential for its DNA damage checkpoint function. *Genes & Development*, 15(11):1361–1372, June 2001. ISSN 0890-9369. doi:10.1101/gad.893201.

[278] Ciosk, R., Zachariae, W., Michaelis, C., Shevchenko, A., Mann, M., and Nasmyth, K. An ESP1/PDS1 Complex Regulates Loss of Sister Chromatid Cohesion at the Metaphase to Anaphase Transition in Yeast. *Cell*, 93(6):1067–1076, June 1998. ISSN 0092-8674. doi:10.1016/S0092-8674(00)81211-8.

[279] Okita, N., Minato, S., Ohmi, E., Tanuma, S.i., and Higami, Y. DNA damage-induced CHK1 autophosphorylation at Ser296 is regulated by an intramolecular mechanism. *FEBS Letters*, 586(22):3974–3979, 2012. ISSN 1873-3468. doi:10.1016/j.febslet.2012.09.048.

[280] Tibbetts, R.S., Brumbaugh, K.M., Williams, J.M., Sarkaria, J.N., Cliby, W.A., Shieh, S.Y., Taya, Y., Prives, C., and Abraham, R.T. A role for ATR in the DNA damage-induced phosphorylation of p53. *Genes & Development*, 13(2):152–157, January 1999. ISSN 0890-9369, 1549-5477.

[281] Wade Harper, J., Adami, G.R., Wei, N., Keyomarsi, K., and Elledge, S.J. The p21 Cdk-interacting protein Cip1 is a potent inhibitor of G1 cyclin-dependent kinases. *Cell*, 75(4):805–816, November 1993. ISSN 0092-8674. doi:10.1016/0092-8674(93)90499-G.

[282] Baus, F., Gire, V., Fisher, D., Piette, J., and Dulić, V. Permanent cell cycle exit in G2 phase after DNA damage in normal human fibroblasts. *The EMBO Journal*, 22(15):3992–4002, August 2003. ISSN 0261-4189. doi:10.1093/emboj/cdg387.

[283] Isken, O. and Maquat, L.E. The multiple lives of NMD factors: balancing roles in gene and genome regulation. *Nature reviews. Genetics*, 9(9):699–712, September 2008. ISSN 1471-0056. doi:10.1038/nrg2402.

[284] Lelivelt, M.J. and Culbertson, M.R. Yeast Upf Proteins Required for RNA Surveillance Affect Global Expression of the Yeast Transcriptome. *Molecular and Cellular Biology*, 19(10):6710–6719, October 1999. ISSN 0270-7306.

[285] He, F., Li, X., Spatrick, P., Casillo, R., Dong, S., and Jacobson, A. Genome-Wide Analysis of mRNAs Regulated by the Nonsense-Mediated and 5-prime to 3-prime mRNA Decay Pathways in Yeast. *Molecular Cell*, 12(6):1439–1452, December 2003. ISSN 1097-2765. doi:10.1016/S1097-2765(03)00446-5.

[286] Addinall, S.G., Holstein, E.M., Lawless, C., Yu, M., Chapman, K., Banks, A.P., Ngo, H.P., Maringele, L., Taschuk, M., Young, A., Ciesiolka, A., Lister, A.L., Wipat, A., Wilkinson, D.J., and Lydall, D. Quantitative Fitness Analysis Shows That NMD Proteins and Many Other Protein Complexes Suppress or Enhance Distinct Telomere Cap Defects. *PLOS Genetics*, 7(4):e1001362, April 2011. ISSN 1553-7404. doi:10.1371/journal.pgen.1001362.

[287] Wengrod, J., Martin, L., Wang, D., Frischmeyer-Guerrerio, P., Dietz, H.C., and Gardner, L.B. Inhibition of Nonsense-Mediated RNA Decay Activates Autophagy. *Molecular and Cellular Biology*, 33(11):2128–2135, June 2013. ISSN 0270-7306. doi:10.1128/MCB.00174-13.

[288] Goetz, A.E. and Wilkinson, M. Stress and the nonsense-mediated RNA decay pathway. *Cellular and molecular life sciences : CMLS*, 74(19):3509–3531, October 2017. ISSN 1420-682X. doi:10.1007/s00018-017-2537-6.

[289] Martin, L., Grigoryan, A., Wang, D., Wang, J., Breda, L., Rivella, S., Cardozo, T., and Gardner, L.B. Identification and characterization of small molecules that inhibit nonsense mediated RNA decay and suppress nonsense p53 mutations. *Cancer research*, 74(11):3104–3113, June 2014. ISSN 0008-5472. doi:10.1158/0008-5472.CAN-13-2235.

[290] Dahlseid, J.N., Lew-Smith, J., Lelivelt, M.J., Enomoto, S., Ford, A., Desruisseaux, M., McClellan, M., Lue, N., Culbertson, M.R., and Berman, J. mRNAs Encoding Telomerase Components and Regulators Are Controlled by UPF Genes in Saccharomyces cerevisiae. *Eukaryotic Cell*, 2(1):134–142, February 2003. ISSN 1535-9778, 1535-9786. doi:10.1128/EC.2.1.134-142.2003.

[291] Holstein, E.M., Clark, K.R., and Lydall, D. Interplay between Nonsense-Mediated mRNA Decay and DNA Damage Response Pathways Reveals that Stn1 and Ten1 Are the Key CST Telomere-Cap Components. *Cell Reports*, 7(4):1259–1269, May 2014. ISSN 22111247. doi:10.1016/j.celrep.2014.04.017.

[292] Gasparyan, H.J., Xu, L., Petreaca, R.C., Rex, A.E., Small, V.Y., Bhogal, N.S., Julius, J.A., Warsi, T.H., Bachant, J., Aparicio, O.M., and Nugent, C.I. Yeast telomere capping protein Stn1 overrides DNA replication control through the S phase checkpoint. *Proceedings of the National Academy of Sciences*, 106(7):2206–2211, February 2009. ISSN 0027-8424, 1091-6490. doi:10.1073/pnas.0812605106.

[293] Sangle, V.A., Bijjaragi, S., Shah, N., Kangane, S., Ghule, H.M., and Rani, S.A. Comparative study of frequency of micronuclei in normal, potentially malignant diseases and oral squamous cell carcinoma. *Journal of Natural Science, Biology, and Medicine*, 7(1):33–38, 2016. ISSN 0976-9668. doi:10.4103/0976-9668.175049.

[294] Podhorecka, M., Skladanowski, A., and Bozko, P. H2ax Phosphorylation: Its Role in DNA Damage Response and Cancer Therapy. *Journal of Nucleic Acids*, 2010:e920161, August 2010. doi:10.4061/2010/920161.

[295] Firsanov, D.V., Solovjeva, L.V., and Svetlova, M.P. H2ax phosphorylation at the sites of DNA double-strand breaks in cultivated mammalian cells and tissues. *Clinical Epigenetics*, 2(2):283–297, June 2011. ISSN 1868-7075. doi:10.1007/s13148-011-0044-4.

[296] Mao, Z., Bozzella, M., Seluanov, A., and Gorbunova, V. Comparison of nonhomologous end joining and homologous recombination in human cells. *DNA repair*, 7(10):1765–1771, October 2008. ISSN 1568-7864. doi:10.1016/j.dnarep.2008.06.018.

[297] Symington, L.S. End Resection at Double-Strand Breaks: Mechanism and Regulation. *Cold Spring Harbor Perspectives in Biology*, 6(8):a016436, August 2014. ISSN , 1943-0264. doi:10.1101/cshperspect.a016436.

[298] Puglisi, A., Bianchi, A., Lemmens, L., Damay, P., and Shore, D. Distinct roles for yeast Stn1 in telomere capping and telomerase inhibition. *The EMBO Journal*, 27(17):2328–2339, September 2008. ISSN 0261-4189, 1460-2075. doi:10.1038/emboj.2008.158.

[299] Grandin, N., Reed, S.I., and Charbonneau, M. Stn1, a new Saccharomyces cerevisiae protein, is implicated in telomere size regulation in association with Cdc13. *Genes & Development*, 11(4):512–527, February 1997. ISSN 0890-9369, 1549-5477. doi:10.1101/gad.11.4.512.

[300] Bryan, C., Rice, C., Harkisheimer, M., Schultz, D.C., and Skordalakes, E. Structure of the Human Telomeric Stn1-Ten1 Capping Complex. *PLoS ONE*, 8(6), June 2013. ISSN 1932-6203. doi:10.1371/journal.pone.0066756.

[301] Wickham, H. *Ggplot2: Elegant Graphics for Data Analysis*. Springer Publishing Company, Incorporated, 2nd edition, 2009. ISBN 978-0-387-98140-6.

[302] Lundin, C., Erixon, K., Arnaudeau, C., Schultz, N., Jenssen, D., Meuth, M., and Helleday, T. Different roles for nonhomologous end joining and homologous recombination following replication arrest in mammalian cells. *Molecular and Cellular Biology*, 22(16):5869–5878, August 2002. ISSN 0270-7306.

[303] Chan, K.L., Palmai-Pallag, T., Ying, S., and Hickson, I.D. Replication stress induces sister-chromatid bridging at fragile site loci in mitosis. *Nature Cell Biology*, 11(6):753–760, June 2009. ISSN 1476-4679. doi:10.1038/ncb1882.

[304] Quennet, V., Beucher, A., Barton, O., Takeda, S., and Löbrich, M. CtIP and MRN promote non-homologous end-joining of etoposide-induced DNA double-strand breaks in G1. *Nucleic Acids Research*, 39(6):2144–2152, March 2011. ISSN 1362-4962. doi:10.1093/nar/gkq1175.

[305] Mendell, J.T., Sharifi, N.A., Meyers, J.L., Martinez-Murillo, F., and Dietz, H.C. Nonsense surveillance regulates expression of diverse classes of mammalian transcripts and mutes genomic noise. *Nature Genetics*, 36(10):1073–1078, October 2004. ISSN 1061-4036, 1546-1718. doi:10.1038/ng1429.

[306] Childs, B.G., Durik, M., Baker, D.J., and van Deursen, J.M. Cellular senescence in aging and age-related disease: from mechanisms to therapy. *Nature medicine*, 21(12):1424–1435, December 2015. ISSN 1078-8956. doi:10.1038/nm.4000.

[307] Costes, A. and Lambert, S.A.E. Homologous Recombination as a Replication Fork Escort: Fork-Protection and Recovery. *Biomolecules*, 3(1):39–71, December 2012. ISSN 2218-273X. doi:10.3390/biom3010039.

[308] Rossi, S.E., Foiani, M., and Giannattasio, M. Dna2 processes behind the fork long ssDNA flaps generated by Pif1 and replication-dependent strand displacement. *Nature Communications*, 9(1):1–11, November 2018. ISSN 2041-1723. doi:10.1038/s41467-018-07378-5.

[309] Ngo, G.H.P. and Lydall, D. The 9-1-1 checkpoint clamp coordinates resection at DNA double strand breaks. *Nucleic Acids Research*, 43(10):5017–5032, May 2015. ISSN 0305-1048. doi:10.1093/nar/gkv409.

[310] Ngo, G.H.P., Balakrishnan, L., Dubarry, M., Campbell, J.L., and Lydall, D. The 9-1-1 checkpoint clamp stimulates DNA resection by Dna2-Sgs1 and Exo1. *Nucleic Acids Research*, 42(16):10516–10528, September 2014. ISSN 0305-1048, 1362-4962. doi:10.1093/nar/gku746.

[311] Markiewicz-Potoczny, M., Lisby, M., and Lydall, D. A Critical Role for Dna2 at Unwound Telomeres. *Genetics*, 209(1):129–141, May 2018. ISSN 0016-6731. doi:10.1534/genetics.118.300809.

[312] Luke-Glaser, S. and Luke, B. The Mph1 Helicase Can Promote Telomere Uncapping and Premature Senescence in Budding Yeast. *PLOS ONE*, 7(7):e42028, July 2012. ISSN 1932-6203. doi:10.1371/journal.pone.0042028.

[313] Lee, M.H., Hollis, S.E., Yoo, B.H., and Nykamp, K. Caenorhabditis elegans DNA-2 helicase/endonuclease plays a vital role in maintaining genome stability, morphogenesis, and life span. *Biochemical and Biophysical Research Communications*, 407(3):495–500, April 2011. ISSN 0006-291X. doi:10.1016/j.bbrc.2011.03.045.

[314] Liang, F., Han, M., Romanienko, P.J., and Jasin, M. Homology-directed repair is a major double-strand break repair pathway in mammalian cells. *Proceedings of the National Academy of Sciences of the United States of America*, 95(9):5172–5177, April 1998. ISSN 0027-8424.

[315] Ait Saada, A., Lambert, S.A.E., and Carr, A.M. Preserving replication fork integrity and competence via the homologous recombination pathway. *DNA Repair*, 71:135–147, November 2018. ISSN 1568-7864. doi:10.1016/j.dnarep.2018.08.017.

[316] Sinha, D., Duijf, P.H.G., and Khanna, K.K. Mitotic slippage: an old tale with a new twist. *Cell Cycle*, 18(1):7–15, January 2019. ISSN 1538-4101. doi:10.1080/15384101.2018.1559557.

[317] Tarnauskaitė, y., Bicknell, L.S., Marsh, J.A., Murray, J.E., Parry, D.A., Logan, C.V., Bober, M.B., Silva, D.C.d., Duker, A.L., Sillence, D., Wise, C., Jackson, A.P., Murina, O., and Reijns, M.A.M. Biallelic variants in DNA2 cause microcephalic primordial dwarfism. *Human Mutation*, 40(8):1063–1070, 2019. ISSN 1098-1004. doi:10.1002/humu.23776.